Study of the aquatic dissolved organic matter from the Seine River catchment (France) by optical spectroscopy combined to asymmetrical flow field-flow fractionation

Phuong Thanh Nguyen

université de BORDEAUX

A THESIS SUBMITTED IN CONFORMITY WITH THE REQUIREMENTS

FOR THE DEGREE OF

DOCTOR

UNIVERSITY OF BORDEAUX

DOCTORAL SCHOOL OF CHEMICAL SCIENCES

SPECIALITY: Analytical and Environmental Chemistry

by Phuong Thanh NGUYEN

Study of the aquatic dissolved organic matter from the Seine River catchment (France) by optical spectroscopy combined to asymmetrical flow field-flow fractionation

Supervised by: Edith PARLANTI

Defense on Thursday 6 November, 2014

Members of jury:

Ms LESPES Gaëtane, Professor, University of Pau and Pays de l'Adour	Reviewer
Mr MOUNIER Stéphane, Lecturer, University of Sud Toulon-Var	Reviewer
Mr VARRAULT Gilles, Professor, University of Paris-Est Créteil	Examiner
Mr ORANGE Didier, Researcher, IRD - iEES-Paris	Examiner
Mr MAZELLIER Patrick, Professor, University of Bordeaux	Examiner
Ms PARLANTI Edith, Researcher, University of Bordeaux	Director of thesis

université de BORDEAUX

THÈSE PRÉSENTÉE

POUR OBTENIR LE GRADE DE

DOCTEUR DE

L'UNIVERSITÉ DE BORDEAUX

ÉCOLE DOCTORALE SCIENCES CHIMIQUES

SPÉCIALITÉ : Chimie Analytique et Environnementale

Par Phuong Thanh NGUYEN

Étude de la matière organique dissoute aquatique dans le bassin versant de la Seine (France) par spectroscopie optique combinée au fractionnement par couplage flux/force avec flux asymétrique

Sous la direction de : Edith PARLANTI

Soutenue le 6 Novembre 2014

Membres du jury :

Mme LESPES Gaëtane, Professeur, Université de Pau et des Pays de l'Adour	Rapporteur
M. MOUNIER Stéphane, Maître de Conférences, Université du Sud Toulon-Var	Rapporteur
M. VARRAULT Gilles, Professeur, Université Paris-Est Créteil	Examinateur
M. ORANGE Didier, Chargé de Recherche, IRD - iEES-Paris	Examinateur
M. MAZELLIER Patrick, Professeur, Université de Bordeaux	Examinateur
Mme PARLANTI Edith, Chargée de Recherche, Université de Bordeaux	Directrice de thèse

Dedicated to

My parents

My husband

My lovely son

ABSTRACT OF THESIS

Title: Study of the aquatic dissolved organic matter from the Seine River catchment (France) by optical spectroscopy combined to asymmetrical flow field-flow fractionation.

Abstract: The main goal of this thesis was to investigate the characteristics of dissolved organic matter (DOM) within the Seine River catchment in the Northern part of France. This PhD thesis was performed within the framework of the PIREN-Seine research program. The application of UV/visible absorbance and EEM fluorescence spectroscopy combined to PARAFAC and PCA analyses allowed us to identify different sources of DOM and highlighted spatial and temporal variations of DOM properties. The Seine River was characterized by the strongest biological activity. DOM from the Oise basin seemed to have more "humic" characteristics, while the Marne basin was characterized by a third specific type of DOM. For samples collected during low-water periods, the distributions of the 7 components determined by PARAFAC treatment varied between the studied sub-basins, highlighting different organic materials in each zone. A homogeneous distribution of the components was obtained for the samples collected in period of flood.

Then, a semi-quantitative asymmetrical flow field-flow fractionation (AF4) methodology was developed to fractionate DOM. The following optimized parameters were determined: a cross-flow rate of 2 ml min^{-1} during the focus step with a focusing time of 2 min and an exponential gradient of cross-flow from 3.5 to 0.2 ml min^{-1} during the elution step. The fluorescence properties of various size-based fractions of DOM were evaluated by applying the optimized AF4 methodology to fractionate 13 samples, selected from the three sub-basins. The fluorescence properties of these fractions were analysed, allowing us to discriminate between the terrestrial or autochthonous origin of DOM.

Keywords: *dissolved organic matter (DOM); colloids; freshwater aquatic ecosystems; asymmetrical flow field-flow fractionation (AF4); EEM fluorescence spectroscopy; UV–Visible absorbance; parallel factor analysis (PARAFAC); principal component analysis (PCA); Seine River catchment.*

UMR CNRS 5805 EPOC – Oceanic and Continental Environments et Paleoenvironments
LPTC group – Laboratory of environmental and toxicological chemistry
University of Bordeaux - 351 cours de la Libération - 33405 Talence cedex – France

RESUME DE LA THESE

Titre : Étude de la matière organique dissoute aquatique dans le bassin versant de la Seine (France) par spectroscopie optique combinée au fractionnement par couplage flux/force avec flux asymétrique.

Résumé : Le but principal de cette thèse était d'étudier les caractéristiques de la matière organique dissoute (MOD) dans le bassin versant de la Seine. Ce travail a été réalisé dans le cadre du programme de recherche PIREN-Seine. Les travaux présentés ici visaient plus particulièrement à identifier les sources de MOD et à suivre son évolution dans les zones d'étude. L'analyse des propriétés optiques (UV-Visible, fluorescence) de la MOD, couplée aux traitements PARAFAC et ACP, a permis de discriminer différentes sources de MOD et de mettre en évidence des variations spatio-temporelles de ses propriétés. L'axe Seine, en aval de Paris, a notamment été caractérisé par l'activité biologique la plus forte. La MOD du bassin de l'Oise a montré des caractéristiques plus "humiques", tandis que le bassin de la Marne a été caractérisé par un troisième type spécifique de MOD. Il a d'autre part été mis en évidence la présence de MODs spécifiques dans chaque zone pour les échantillons prélevés en périodes d'étiage, alors qu'une distribution homogène des composants a été obtenue pour l'ensemble des échantillons prélevés en période de crue.

Le rôle environnemental des colloïdes naturels étant étroitement lié à leur taille, il a d'autre part été développé une technique analytique/séparative originale pour l'étude de ce matériel complexe, un fractionnement par couplage flux/force avec flux asymétrique (AF4). Le fractionnement par AF4 des échantillons a confirmé la variabilité spatio-temporelle en composition et en taille de la MOD d'un site de prélèvement à un autre et a permis de distinguer différentes sources de MOD colloïdale confirmant les résultats de l'étude de ses propriété optiques.

Mots Clés : *matière organique dissoute (MOD) ; colloïdes ; écosystèmes aquatiques d'eau douce ; fractionnement par flux/force avec flux asymétrique (AF4) ; spectroscopie de fluorescence EEM ; absorbance UV-Visible ; analyse factorielle parallèle (PARAFAC) ; analyse des composantes principales (ACP) ; Bassin versant de la Seine*

UMR CNRS 5805 EPOC - Environnements et Paléoenvironnements Océaniques et Continentaux
Equipe LPTC – Laboratoire de Physico et ToxicoChimie de l'environnement
Université de Bordeaux - 351 cours de la Libération - 33405 Talence cedex

1. Contexte des travaux de recherche

La matière organique dissoute (MOD) joue un rôle important pour la biogéochimie des micropolluants influençant potentiellement leur spéciation et leur biodisponibilité. La MOD est un mélange de composés de propriétés chimiques variées et d'origines diverses. Elle est principalement constituée de colloïdes naturels qui sont des macromolécules et nanoparticules ayant une taille variant de 1 nm à 1 µm. De nature très complexe et dynamique, la MOD est un acteur clé dans la dispersion des éléments traces, le transport des contaminants, le cycle du carbone organique et la biodisponibilité des micronutriments et des contaminants.

Le changement climatique exprimé en termes de précipitations, productivité primaire, rayonnement solaire et température entraînera des changements de la qualité et de la concentration en MOD impliquant des modifications du piégeage et de la biodisponibilité des contaminants. Les facteurs contrôlant la qualité et la quantité de la MOD ne sont toujours pas bien compris. Une connaissance plus approfondie de ces processus est nécessaire pour prédire au mieux les changements de la MOD et de ses interactions avec les contaminants. Malgré son importance majeure dans l'environnement sur le devenir des contaminants, les cycles et la composition chimique de la MOD restent mal compris. Il y a, cependant, un réel besoin d'une caractérisation chimique détaillée de la MOD et il est nécessaire d'évaluer l'influence de la variabilité chimique de la MOD sur les processus environnementaux. Le rôle environnemental des colloïdes naturels est d'autre part étroitement lié à leur taille. Néanmoins, le rôle de la taille de la MOD sur ses propriétés d'interaction avec les contaminants est encore méconnu.

Le but principal de cette thèse était d'étudier les caractéristiques de la MOD dans le bassin versant de la Seine. Ce travail a été réalisé dans le cadre du programme de recherche PIREN-Seine (Programme Interdisciplinaire de Recherche sur l'ENvironnement de la Seine - http://www.sisyphe.upmc.fr/piren/) qui est conjointement financé depuis 1989 par le CNRS et les acteurs publics et privés de la gestion de l'eau du bassin de Seine-Normandie. Ce groupement de recherche a pour objectif de développer, à partir de mesures de terrain et de modélisations, une vision d'ensemble du fonctionnement du système formé par le réseau hydrographique de la Seine, son bassin versant et la société humaine qui l'investit. Le bassin de la Seine, 12% du territoire national, supporte le quart de la population de la France, un tiers de sa production agricole et industrielle, et plus de la moitié de son trafic fluvial. Le fonctionnement écologique de l'ensemble du système fluvial et sa modélisation, depuis les bactéries jusqu'aux poissons, sont basés sur l'étude fine des processus physiques, chimiques et biologiques des milieux. Les modèles développés par le PIREN-Seine simulent les variations

écologiques et biochimiques de l'hydrosystème, depuis les ruisseaux jusqu'à l'entrée de l'estuaire.

Dans le cadre du bloc « Matière organique » du thème Biogéochimie de l'axe fluvial du programme PIREN-Seine, il était prévu d'étudier spécifiquement la matière organique (MO) dans le bassin versant de la Seine. Le but principal de cette thèse était d'étudier les caractéristiques de la MOD et plus particulièrement d'identifier ses sources et de suivre son évolution dans cet écosystème. Les sources de matière organique dissoute peuvent être multiples :

- Autochtone naturelle : provenant du biote présent dans le milieu (algues, bactéries, macrophytes) ;
- Allochtone naturelle : issue des sols ;
- Allochtone anthropique : rejets urbains domestiques et industriels, rejets liés à l'agriculture.

2. Matériel et méthodes

Afin d'identifier ces sources de matière organique, des campagnes « snapshot » ont été menées dans le bassin de la Seine en basses eaux, à deux saisons différentes (automne 2011 et été 2012), et en période de crue (hiver 2013), au cours desquelles 23, 39 et 40 échantillons respectivement ont été prélevés. Ces sites d'échantillonnage étaient répartis sur le bassin de l'Oise, le bassin de la Marne et sur la Seine.

Les deux campagnes de basses eaux ont été menées en novembre 2011 et en août/septembre 2012 à des conditions de débits similaires (environ 100 $m^3.s^{-1}$ à Austerlitz). Le débit restitué par les grands lacs de Seine contribue à environ 50% en août/septembre 2012 contre seulement 20% en novembre 2011 (soutien étiage tardif). La campagne de hautes eaux s'est déroulée en février 2013 avec des débits de 280 m^3s^{-1} pour l'Oise à Creil, de à 700 m^3s^{-1} pour la Seine à Alfortville et de 350 m^3s^{-1} pour la Marne à Gournay.

Les échantillons ont été filtrés immédiatement après le prélèvement sur des filtres en fibre de verre (GF/F 0.7µm; Whatman) préalablement pyrolysés à 450°. Ils ont ensuite été stockés au frais (4°C) et à l'abri de la lumière avant analyses.

La matière organique contenue dans ces échantillons a été caractérisée dans le cadre de cette thèse par les techniques présentées succinctement ci-dessous.

2.1. La spectroscopie d'absorption UV-visible

Le spectrophotomètre UV-visible utilisé (Jasco V-560) est équipé d'un tube à décharge au deutérium (190 à 350 nm) et d'une lampe à incandescence à filament de tungstène (330 à 900 nm), d'un double monochromateur (réseau plan) pour la sélection des longueurs d'onde et d'un photomultiplicateur (qui permet de transformer l'intensité lumineuse reçue en un signal électrique) comme détecteur. Bien que l'appareil fonctionne en mode double faisceau, il a été utilisé en mode simple faisceau : le signal de référence (cuve + solvant) n'est pas acquis simultanément avec l'échantillon mais avant l'échantillon et soustrait manuellement afin d'utiliser exactement la même cuve dans les deux acquisitions.

L'une des principales caractéristiques que le spectre d'absorption peut permettre de déterminer est l'aromaticité de la matière organique contenue dans l'échantillon. Deux paramètres sont généralement utilisés pour caractériser l'aromaticité d'un échantillon :

- *l'indice SUVA*

$$\mathrm{SUVA} = \frac{\mathrm{Abs}_{254}}{[\mathrm{COD}]} \times 100$$

où Abs254 est l'absorbance à 254 nm et [COD] est la concentration en COD en mg/l.

- *le pourcentage d'aromaticité*

Il a été calculé à partir de l'absorbance à 280 nm

$$\text{aromaticité}(\%) = 0{,}05 \times \frac{\mathrm{Abs}_{280}}{[\mathrm{COD}]} + 6{,}74$$

où Abs280 est l'absorbance à 280 nm et [COD] est la concentration en COD en mol/l.

- *le rapport de pentes spectrales S_R*

Le rapport de pentes spectrales S_R (pente 275–295 nm / pente 350–400 nm) calculé à partir des spectres d'absorbance UV-Visible permet également d'estimer la variation du poids moléculaire de la MOD. Quand S_R augmente le poids moléculaire diminue.

2.2. La spectrofluorimétrie

Les spectres de fluorescence ont été enregistrés à l'aide d'un spectrofluorimètre Fluorolog SPEX Jobin-Yvon FL3-22, équipé de doubles monochromateurs à l'excitation et à l'émission. Les échantillons ont été placés dans des cuves en quartz de 1cm de trajet optique, thermostatées à 20°C. Les spectres de fluorescence 3D ont été générés par l'enregistrement successif de 17 spectres d'émission (260-700nm) à des longueurs d'ondes d'excitation prises

tous les 10nm entre 250 et 410 nm. Les spectres 3D des échantillons ont été obtenus par soustraction du spectre 3D d'un blanc d'eau ultrapure (Millipore, Milli-Q).

Les propriétés de fluorescence de la MOD permettent d'obtenir des informations sur la structure et les propriétés générales des macromolécules. La fluorescence est une technique très sensible qui permet de caractériser la MOD à partir d'un échantillon aqueux de faible volume sans nécessité de concentration ou d'extraction. Pour caractériser la MOD, la fluorescence tridimensionnelle (3D ou EEM pour excitation-émission-matrice) est généralement utilisée. Cette technique consiste à accumuler les spectres d'émission acquis pour plusieurs longueurs d'onde d'excitation. Les données quantitatives et qualitatives à prendre en compte sont l'intensité et la position des maxima de fluorescence qui varient en fonction de la nature et de l'origine des échantillons et dépendent des espèces moléculaires fluorescentes qu'ils contiennent.

Le spectre EEM obtenu est interprété par la présence de pics et de rapports d'intensité caractéristiques. Les principales bandes généralement observées pour les eaux naturelles sont mentionnées dans le Tableau ci-dessous.

Pics	Longueur d'onde d'excitation (nm)	Longueur d'onde d'émission (nm)	Type de composés
α	330 - 350	420 - 480	Substances type humiques
α'	250 - 260	380 - 480	Substances humiques + matériel plus récent
β	310 - 320	380 - 420	Matériel récent, composante biologique
γ	270 - 280	300 - 320	Tyrosine, tryptophane ou protéines + activité bactérienne

Les indices de fluorescence HIX et BIX ont également été déterminés afin d'estimer les sources et le degré de maturation de la MOD fluorescente.

La détermination de l'indice d'humification HIX est basée sur le fait que l'avancement des processus d'humification conduit à une augmentation du rapport C/H, i.e. à une augmentation de l'aromaticité de la MOD. Cette augmentation entraîne un déplacement du spectre de fluorescence vers les plus grandes longueurs d'onde d'émission. L'indice HIX est calculé en réalisant le rapport des deux aires définies respectivement par l'intervalle L: 300-345 nm et H: 435-480 nm pour une longueur d'onde d'excitation de 250 nm. L'indice d'humification HIX est alors donné par le rapport H/L.

Lorsque le degré d'aromaticité de la matière organique augmente, l'indice HIX augmente. En d'autres termes, de fortes valeurs de HIX indiquent la présence d'un matériel organique humifié. Les valeurs de HIX diminuent lorsque la fluorescence de la MOD est déplacée vers les courtes longueurs d'onde, i.e. pour des composés présentant un degré d'aromaticité moins important et des masses moléculaires plus faibles.

L'indice BIX est calculé à partir du spectre d'émission à 310 nm en divisant l'intensité de fluorescence émise à 380 nm, qui correspond au maximum d'intensité de fluorescence de la bande β quand elle est isolée, par celle émise à 430 nm, qui correspond au maximum de la bande α. Une augmentation de l'indice BIX est liée à une présence plus marquée du fluorophore β dans les échantillons d'eaux naturelles. Puisque le fluorophore β est lié à l'activité biologique autochtone, l'indice BIX permet de juger de la production de matière organique dissoute due à cette activité. Les fortes valeurs de cet indice traduisent une origine autochtone prépondérante de la MOD et la présence de matière organique fraîchement produite dans le milieu.

- *PARAFAC*

Un algorithme trilinéaire de décomposition nommé PARAFAC (Parallel Factor Analysis) a été utilisé sous le logiciel Matlab (DOMFluor toolbox). PARAFAC est une procédure multidimensionnelle qui permet de traiter un jeu de donnée à 3 dimensions dans sa globalité. C'est une méthode d'analyse de données consistant à construire un modèle linéaire, en estimant les spectres d'excitation et d'émission de F fluorophores et le coefficient appliqué à chacune de ces matrices, afin de pouvoir recomposer le cube de données.

On analyse ainsi un ensemble d'échantillons dans lequel chaque matrice d'excitation et d'émission est un mélange de F composants fluorescents différents.

On considère :

- $x_{i,j,k}$ comme l'intensité de fluorescence d'un échantillon i donné, mesuré au couple de longueurs d'onde d'excitation-émission (j, k),
- $a_{i,f}$ comme facteur de fluorescence (produit de la concentration et du rendement quantique) du fluorophore f (f variant de 1 à F) dans l'échantillon i (variant de 1 à I)
- $b_{i,f}$ comme valeur du spectre d'absorption du fluorophore f à la longueur d'onde j
- $c_{i,f}$ comme valeur du spectre d'émission du fluorophore f à la longueur d'onde k
- $\varepsilon_{i,j,k}$ comme résidus (bruit et autres variations non expliquées par le modèle)

La loi de Beer–Lambert donne :

$$\forall i,j,k \qquad x_{i,j,k} = \Sigma^{F}_{f=1}\, a_{i,f}\, b_{i,f}\, c_{i,f} + \varepsilon_{i,j,k}$$

Ainsi à partir d'un jeu d'échantillons comprenant autant de matrices d'excitation et d'émission de fluorescence, les trois inconnues a, b et c sont estimées par PARAFAC en fonction du nombre de fluorophores F fixé et validé pour le modèle le plus approprié, c'est à dire celui présentant des résidus minimum tout en conservant un maximum d'information sans que celle-ci soit répétée. Le modèle a été contraint à la non-négativité des valeurs et le mode « split half analysis » a été utilisé pour valider les composants identifiés.

Il convient d'avoir un nombre élevé d'échantillons pour que l'analyse soit plus précise et le modèle plus fiable.

2.3. Le Fractionnement par couplage Flux/Force avec Flux Asymétrique (AF4)

Aujourd'hui, parmi les techniques de séparation en ligne, les systèmes de fractionnement par couplage flux-force (FFF) présentent un grand intérêt pour séparer les différentes fractions colloïdales, car ils possèdent de nombreux avantages par rapport aux techniques chromatographiques, notamment une grande résolution et une large gamme de distribution en taille (de 1 nm à quelques 10 µm). Récemment, de nombreux travaux ont été réalisés grâce au système de fractionnement par couplage flux/force avec flux asymétrique (Asymmetric-Flow Field-Flow Fractionation – AF4), une technique de FFF qui est apparue très prometteuse en terme de pouvoir séparatif et de possibilités de couplage avec des détecteurs variés. Cette technique offre de nouvelles perspectives dans la caractérisation et la séparation des biopolymères, des macromolécules colloïdales et des nanoparticules. C'est une technique qui permet de séparer le matériel colloïdal en fonction de sa taille et représente une alternative aux dispositifs de chromatographie sur colonne. La séparation a lieu dans un canal sans phase stationnaire et permet de déterminer non seulement la taille mais également l'état de dispersion et la forme des colloïdes.

Le système AF4 utilisé est un Eclipse 3 de Wyatt Technology Europe. Il est équipé d'un détecteur UV (HP1200 series, Agilent) et d'un détecteur à diffusion de lumière statique multi-angulaire (3 angles de mesure - miniDAWN TREOS, Wyatt Technology Europe). L'AF4 est équipé d'un canal de séparation court Eclipse avec un espaceur de 490 µm d'épaisseur et d'une membrane Pall Omega en polyethersulfone de seuil de coupure 1 kDa.

Les paramètres du fractionnement suivants ont été optimisés dans ce travail : le débit au détecteur, les volumes et temps d'injection, les débits et temps de focus, le type de flux croisé appliqué pendant la phase d'élution. Les conditions opératoires optimales retenues ont été les suivantes :

Le débit au détecteur est maintenu constant à 0,5 ml/min. Après équilibre du débit pendant 2 min, 1 ml d'échantillon est injecté à un débit de 0,2 ml/min pendant 6 min avec un flux de focus de 2 ml/min. Le temps de relaxation optimal a été déterminé à 2 min avec un flux de focus de 2 ml/min. Différents programmes de flux croisé pour l'élution ont été testés (constant, gradient linéaire, gradient exponentiel). Les conditions optimales qui ont été retenues pour l'élution sont un flux croisé constant à 3,5 ml/min pendant 15 min, suivi d'un gradient exponentiel de flux croisé de 3,5 ml/min à 0,2 ml/min en 28min.

3. Résultats

3.1. Fluorescence EEM

L'ensemble des échantillons des campagnes « snapshot » de novembre 2011, août/septembre 2012 et février 2013 ont été analysés par fluorescence 3D.

Les concentrations en carbone organique fluorescent en août/septembre 2012 et février 2013 sont plus faibles qu'en novembre 2011. Les échantillons de Seine sont caractérisés par une plus forte proportion de composés de type protéique, notamment pour les échantillons en aval de Paris, traduisant une plus forte activité biologique dans ces eaux.

D'un point de vue qualitatif, l'examen des rapports d'intensités des principales bandes de fluorescence caractéristiques d'un matériel récent et d'origine plutôt autochtone (α', β et γ) sur la bande α spécifique du matériel le plus humifié, donc plus ancien, est intéressant car il permet d'estimer les contributions relatives des différentes composantes de la MOD et le type de matériel en présence. Les distributions de ces rapports d'intensités des principales bandes de fluorescence en fonction de la teneur en COD ont permis d'observer des variations très nettes de la qualité de la MOD entre les 3 périodes de prélèvement pour les bassins de la Marne et de la Seine alors que les résultats sont moins discriminants pour le bassin de l'Oise.

Les valeurs de ces rapports sont majoritairement plus élevées pour les échantillons de la campagne « snapshot » de 2012. Ceci tend à montrer la présence d'un matériel organique fluorescent plus récent et une plus forte contribution biologique en septembre 2012.

Les indices de fluorescence HIX et BIX ont également montré des variations spatiales de la qualité de la MOD. Les plus fortes valeurs de l'indice HIX, traduisant le matériel organique

le plus mature et aromatique, ont été observées dans le bassin de l'Oise et, de façon logique, les maximales en zones forestières (O1 et RF). L'ensemble des échantillons a globalement été caractérisé par une activité biologique en moyenne relativement élevée (BIX>0.6), les plus fortes valeurs étant observées en Seine en 2011 et 2012 et dans le bassin de la Marne en 2012.

La période de crue (2013) s'est distinguée par de fortes valeurs de HIX alors que les plus faibles valeurs ont été observées en période d'étiage (2012) et majoritairement associées à de fortes valeurs de BIX, traduisant une forte activité biologique pour ces échantillons.

Les matrices d'excitation et d'émission de fluorescence de l'ensemble des 102 échantillons des trois campagnes « snapshot » ont été traitées par PARAFAC. Un modèle à 7 composants a ainsi pu être déterminé, expliquant 99,8 % de la variabilité du jeu de données.

Le composant 4 est similaire au fluorophore β et le composant 6 correspond au matériel de type protéique (fluorophore γ). Les composants 1, 2 et 3, quant à eux, s'apparentent à du matériel de type humique (fluorophores α' et α).

Les variations de ces 7 composants pour l'ensemble des échantillons ont montré des intensités des composants plus fortes en 2011 traduisant des concentrations en matériel fluorescent plus élevées. Pour 2011 et 2012 nous avons observé des distributions de ces 7 composants très différentes d'un bassin versant à l'autre mettant en évidence des caractéristiques de matériel organique différentes et spécifiques pour chaque bassin. Au contraire, pour la campagne de crue de 2013, la distribution des 7 composants était beaucoup plus homogène avec le composant 1 dominant pour l'ensemble des échantillons et des caractéristiques plus humiques traduisant la présence d'un matériel organique majoritaire certainement d'origine terrigène.

L'analyse statistique des données a montré une variation temporelle de la distribution des 7 composants représentatifs de la MOD avec un composant 7 bien plus représenté en 2011. Une variation des caractéristiques de la MOD en fonction des sites de prélèvement et une différenciation des sous-bassins étudiés a également été mise en évidence.

Ces variations spatio-temporelles ont notamment montrées des distributions des 7 composants dominées par le composant 1 pour l'année 2013 mais également pour le bassin de l'Oise quelque soit la campagne de prélèvement. Le composant 7 semblerait caractériser le sous-bassin de la Marne. Les échantillons de la Seine (2011 et 2012) se sont singularisés avec une signature particulière prédominée par les composants 3, 4 et 5.

3.2. Absorbance UV – Visible

L'indice SUVA est apparu globalement plus élevé pour les échantillons de la campagne « snapshot » de novembre 2011 sauf pour les échantillons de la Marne et pour S6 où les plus fortes valeurs ont été obtenues en 2013.

L'étude de la variation des rapports des pentes spectrales S_R pour l'ensemble des sites et des campagnes de prélèvement a montré que les échantillons de la Marne (2011 et 2012) étaient caractérisés par le matériel organique de plus faible poids moléculaire. Les échantillons de la Seine en 2012 ont également été caractérisés par une MOD de faible poids moléculaire. Le matériel de plus haut poids moléculaire a été observé pour les échantillons de Grand Morin et les échantillons des trois bassins en 2013. Il n'a pas pu être observé de relations entre poids moléculaire et indice d'humification ou pourcentage d'aromaticité.

3.3. Analyse en composantes principales des données spectroscopiques

Une analyse en composantes principales (ACP) a été réalisée en utilisant comme variables les 7 composants déterminés par l'analyse PARAFAC, les indices d'absorbance (S_R, % aromaticité et SUVA), les indices de fluorescence (HIX, BIX, Iα'/Iα, Iβ/Iα et Iγ/Iα) et les intensités de fluorescence (Iα', Iα, Iβ et Iγ) / COD.

Cette ACP a montré que les composants 4, 5, 6 et 7 apparaissent plutôt liés à l'activité biologique. Le composant 4 apparait, comme déjà mentionné, similaire au fluorophore β. Les composants 1, 2 et 3, quant à eux, seraient plutôt liés à l'aromaticité et au matériel de type humique.

L'analyse ACP a permis de différencier les bassins de la Seine, de l'Oise et de la Marne. Les échantillons du sous-bassin de l'Oise sont apparus caractérisés par une MOD plus mature, aromatique alors que ceux des sous-bassins de la Seine et de la Marne présenterait une MOD majoritairement liée à une forte activité biologique.

L'analyse ACP a également permis de différencier les 3 campagnes de prélèvement, faisant à nouveau ressortir le caractère plus mature, aromatique de la MOD de l'ensemble des échantillons prélevés en période de crue. Les échantillons de 2011 et 2012 étaient quant à eux caractéristiques d'une forte activité biologique, les échantillons de 2012 se différenciant par de plus faibles poids moléculaires et un caractère plus récent de la MOD.

L'analyse des propriétés optiques de la MOD a donc permis de discriminer différentes sources de matières organiques et de mettre en évidence des variations tant qualitatives que quantitatives de cette MOD. Ces variations sont apparues à la fois liées aux conditions hydro-

logiques (crue, étiage) et aux spécificités des sites géographiques (différenciation des 3 sous-bassins).

3.4. Fractionnement par couplage Flux/Force avec Flux Asymétrique (AF4)

Tous les échantillons des campagnes « snapshot » ont été fractionnés par AF4.

Le bassin de la Marne a été caractérisé par une MOD majoritairement constituée de molécules de petites tailles en bon accord avec les résultats de l'analyse de la variation des rapports des pentes spectrales S_R. Une seconde population de molécules de taille supérieure est observée en moindre proportion. Les échantillons du bassin de l'Oise ont montré globalement une population majoritaire de molécules de taille intermédiaire si l'on compare avec celles observées pour le bassin de la Marne. Dans le bassin de la Seine on a observé une distribution avec deux populations en proportions similaires (S6 et S7), les deux de tailles légèrement supérieures par rapport aux échantillons de la Marne. On a retrouvé cette distribution pour les échantillons G2 et G3 du bassin du Grand Morin. Les distributions observées pour les échantillons S5', S8 et S9 du bassin de la Seine s'apparentent plus aux distributions en taille de molécules des échantillons du bassin de l'Oise de même que pour l'échantillon G1 du bassin du Grand Morin. L'échantillon G4 de ce dernier bassin présentait une distribution en taille similaire à celles déterminées pour les échantillons du bassin de la Marne.

On a ainsi observé globalement trois types de distributions en bon accord avec la discrimination mise en évidence par l'analyse ACP et les résultats de l'analyse de la variation des rapports des pentes spectrales S_R. Un premier type est caractérisé par une prédominance de petites molécules et d'une autre population de taille supérieure (par exemple M7). Le second type serait caractérisé par deux populations en proportions similaires et de tailles légèrement supérieures à celles du type 1 (par exemple S6). La troisième catégorie est constituée d'une seule population de molécules de taille intermédiaire (par exemple Se).

L'étude de la distribution en taille des constituants de la MOD a montré qu'ils étaient globalement de relativement petite taille avec néanmoins une gamme de tailles moléculaires montrant l'hétérogénéité du matériel organique. Les plus hautes valeurs ont été observées pour les échantillons en 2011, et plus particulièrement pour les échantillons de Grand Morin. Ces résultats étaient en bon accord avec ceux relatifs à la variation du rapport de pentes spectrales S_R.

Des échantillons ont été choisis sur la base de leurs propriétés optiques et de leurs distributions en taille observée par AF4 en veillant à leur représentativité des sites des 3 sous-bassins et des différentes périodes d'échantillonnage. Les échantillons qui ont été sélectionnés sont : G1 (2011 et 2013) - Grand Morin ; M7 (2011, 2012 et 2013) - Marne ; O1 (2011, 2012 et 2013) - Oise, zone forestière ; S5 (2012 et 2013) et S6 (2011, 2012 et 2013) - Seine en aval de Paris. Pour ces 13 échantillons 8 à 9 fractions ont été séparées et collectées pour être analysées par fluorescence.

Les valeurs les plus basses de BIX ont été systématiquement déterminées pour la 3ème fraction, indépendamment des échantillons considérés, suggérant ainsi la présence dans cette fraction des constituants de MOD d'origine principalement terrestre. Pour tous les échantillons considérés, les valeurs les plus fortes de BIX n'ont pas été observées seulement pour les petites tailles moléculaires, montrant que les constituants d'origine autochtone de la MOD peuvent être caractérisés à la fois par des bas ou des hauts poids moléculaires. Des fluorophores caractéristiques de pigments ont pu être détectés dans quelques fractions des sous-bassins de l'Oise et de la Marne.

Le fractionnement par AF4 des échantillons a ainsi confirmé la variabilité spatiale et temporelle en composition et en taille de la MOD et a permis de distinguer différents types de matière organique colloïdale.

4. Conclusion et perspectives

L'AF4 a été utilisé pour fractionner dans un continuum de tailles colloïdales les constituants de la MOD d'échantillons d'eau de surface. La combinaison de l'AF4 avec des techniques de spectroscopie optique (absorbance UV/Visible et fluorescence) couplée à PARAFAC et à des analyses statistiques, nous a permis de distinguer différentes sources de matière organique dissoute dans le bassin versant de la Seine et a mis en évidence des variations spatiales et temporelles significatives de la MOD ainsi que des typologies de MOD spécifiques des différents sites d'échantillonnage.

La fluorescence EEM couplée à l'AF4 semble ainsi être un outil puissant pour l'étude de la MOD dans l'environnement aquatique et offre de nouvelles perspectives dans la caractérisation et la séparation de la MOD colloïdale.

Il serait intéressant de poursuivre l'observation des variations spatio-temporelles des caractéristiques de la MOD dans le bassin versant de la Seine. En effet, bien que la MOD joue un rôle clé dans les processus environnementaux, il y a clairement un manque de connaissances concernant sa caractérisation et un manque de suivi à long terme. Une connaissance plus détaillée des caractéristiques de la MOD est en effet nécessaire si l'on veut d'une part, pouvoir comprendre ses cycles biogéochimiques et les processus mis en jeu dans l'environnement et notamment concernant les interactions MOD/contaminants et, d'autre part, prédire l'impact des changements globaux sur ces processus.

En ce qui concerne le système AF4, il serait intéressant de continuer l'optimisation des paramètres expérimentaux. Il parait particulièrement essentiel en effet de minimiser la perte d'échantillon en testant différents matériaux de membrane ainsi que des seuils de coupure plus petits. De plus, il serait aussi nécessaire d'étudier l'effet de la force ionique de la phase éluante sur l'efficacité de la séparation des macromolécules naturelles.

Il serait de plus important, pour pouvoir étudier les interactions de la MOD avec les contaminants, de coupler la spectrométrie de masse au système de fractionnement par flux/force avec flux asymétrique. D'un point de vue général, compte tenu de la complexité de la matière organique, des écosystèmes environnementaux et des processus d'interactions MOD/contaminants, une approche par détection multidimensionnelle semble essentielle.

ACKNOWLEDGEMENTS

It is my pleasure to write these acknowledgements

I would like to acknowledge the financial support of the Program PIREN-Seine *(http://www.piren-seine.fr)*. All the members involved in the "Organic Matter" part of PIREN Seine project are acknowledged for their help in collecting samples from the Seine River catchment. Especially, I would like to extend my thanks to the members in Laboratory of Water Geochemistry (LGE), Institute of Geophysics (IPGP), Université Paris Diderot, Sorbonne Paris Cité and Laboratory Sisyphe, University Pierre and Marie Curie, Paris, France for providing me with the DOC analysis for all samples collected in the Seine River catchment.

I would like to acknowledge the Vietnamese and French Governments (Embassy of France in Hanoi) for my PhD grant. I am also grateful to the University of Science and Technology of Hanoi for their recruiting of PhD scholars to study in France.

I would like to thank **Ms. Gaëtane LESPES** and **Mr. Stéphane MOUNIER** who agreed to be reviewers of my thesis for their insightful comments. I want to thank **Mr. Gilles VARRAULT, Mr. Didier ORANGE** and **Mr. Patrick MAZELLIER** for participating in my committee.

I wish to express my deepest gratitude to my supervisor, **Dr. Edith PARLANTI**, for her guidance, encouragement, and patience during these extended years, especially during the finalizing of this thesis and for not giving up on me. Her expertise in the field of dissolved organic matter improved my research skills and prepared me for future challenges.

I especially want to thank **Dr. Hélène BUDZINSKI**, the director of the Laboratory of Physical and Toxicological chemistry of the environment, for giving me the opportunity to work in her lab.

I would like to thank all former and current members of the Laboratory of Physical and Toxicological chemistry of the environment. I truly thank **Van Hoi BUI** for introducing me about our lab, for all his help throughout my years here in Bordeaux. I am greatly indebted to **Marie-Ange CORDIER** for her technical advice and her training on lab equipment. **Jérémie PAROT**, thank you for discussing my data, bringing laughter to me. I am proud to know both you and Marie-Ange. Thanks to **Yuzhe GUO** for teaching me how to run PARAFAC model in MATLAB. Thanks to **Julien GIGAULT** for helping with important knowleadge and experience about AF4. I would like to extend my thanks to **Maylis SAINT-HUBERT** and her mother for all their help. Thanks to **Laurène LECUYER, Camille LOPEZ, Stéphanie CUENOT-WOLFF, Jean FROMENT** for everyday life in the lab.

I wish to express my sincere thanks to **Prof. Céline GUEGUEN** (department of chemistry, Trent University, Canada) for giving me the beginning knowledge about AF4.

Thanks to my Vietnamese friends in Bordeaux, **anh Minh-Ngoc, anh Dao, chi Hai-Hong, chi Nga, chi Hang, chi Van, chi Trang, chi Huong, anh Tung, ban Dung, ban Tung, em Ha, em Luan, em My Anh, em Truong, em Xuan-Hong, em Lien, em Thanh, em Thao**…, who have helped me pass to difficulties in my life when I am here. My special thanks go to my best friend, **Minh Thao QUACH**, you are the first person to bring a tear to my eye in writing these acknowledgements. You helped me to understand what I was truly meant to do and what truly makes me happiest in life. I cannot stop smiling, I love sharing my life with you. And to my friends in the laBRI, **Lorijn, Claire, Nesrine, Omessaad**…, thank you for your friendship. I feel lucky to meet all of you in Bordeaux.

Last but not least, the biggest thanks go to my family. Words cannot express my gratitude thanks to my parents, my husband, my brother and my lovely son for all the love and the encouragement they offered me. I dedicate this thesis to them.

TABLE OF CONTENTS

ABSTRACT OF THESIS i
RESUME DE LA THESE iii
ACKNOWLEDGEMENTS xvii
TABLE OF CONTENTS xix
LIST OF ACRONYMS xxiii
LIST OF TABLES xxv
LIST OF FIGURES xxvii
GENERAL INTRODUCTION 1
CHAPTER I: BIBLIOGRAPHIC SYNTHESIS 5
1.1. Overview about natural organic matter 7
1.2. Source of DOM in aquatic environment 8
1.3. Composition of DOM 10
1.3.1. Humic substances 10
1.3.2. Non-humic substances 13
1.4. The optical properties of DOM 15
1.4.1. The absorbance properties of DOM 15
1.4.2. The fluorescence properties of DOM 18
1.5. The fractionation techniques of DOM in aquatic environment 24
1.5.1. Fractionation by tangential ultrafiltration 25
1.5.2. Fractionation by size exclusion chromatography (SEC) 27
1.5.3. Fractionation by flow field flow fractionation 29
1.6. Conclusions 38
1.7. Objectives 38
CHAPTER II: MATERIALS AND METHODS 41
2.1 Study area 43
2.2 Different methods for characterisation and fractionation of DOM 46
2.2.1 DOC measurement 46
2.2.2 UV-visible absorption spectroscopy 46
2.2.3 Fluorescence spectroscopy 51
2.2.4 The asymmetrical flow field flow fractionation 58
2.2.5. AF4 detectors 66
2.3 Data processing and statistical analysis 68
2.3.1 Parallel Factor Analysis modelling 68
2.3.2 Principal component analysis (PCA) 69

2.3.3 Statistical analysis 69
CHAPTER III: CHARACTERIZATION OF DISSOLVED ORGANIC MATTER (DOM) IN THE SEINE RIVER CATCHMENT 71
3.1. Dissolved organic carbon concentrations 73
3.2. Absorbance spectroscopy 75
3.3. Fluorescence spectroscopy 79
3.3.1. Fluorescence intensities 80
3.3.2. Fluorescence indices 85
3.4. EEM-PARAFAC modeling 90
3.4.1. EEM-PARAFAC components of DOM 90
3.4.2. Spatial distribution of EEM-PARAFAC components 94
3.4.3. Correlations between EEM-PARAFAC components 99
3.4.4. Correlation between ratios of EEM-PARAFAC components with fluorescence indices 104
3.5. Principal component analysis 105
3.6 Conclusion 108
CHAPTER IV: DEVELOPMENT OF ASYMMETRICAL FLOW FIELD-FLOW FRACTIONATION TO CHARACTERIZE DISSOLVED ORGANIC MATTER IN NATURAL FRESHWATER ENVIRONMENTS 111
4.1 Introduction 113
4.2 Material and methods 114
4.2.1 Sampling site 114
4.2.2 DOC measurements 115
4.2.3 Fluorescence measurements 115
4.2.4 Asymmetrical flow field-flow fractionation setup 116
4.3 Results and discussion 116
4.3.1 Optimization of cross-flow rate/cross flow mode 116
4.3.2 Optimization of relaxation time 120
4.4 Applicability 122
4.5 Conclusion 123
CHAPTER V: ASYMMETRICAL FLOW FIELD-FLOW FRACTIONATION COMBINED TO OPTICAL SPECTROSCOPY FOR THE CHARACTERIZATION OF AQUATIC DISSOLVED ORGANIC MATTER FROM THE SEINE RIVER CATCHMENT (FRANCE) 127
5.1. Molecular weight calibration 129
5.2. Characterization of organic matter fractions 131
5.2. Fluorescence properties of DOM fractions 140
5.2.1. Oise River 141
5.2.2. Grand Morin River 147

5.2.3. Marne River 151
5.2.4. Seine River 156
5.3. Conclusions 165
GENERAL CONCLUSIONS AND PERSPECTIVES 167
APPENDICES 175
REFERENCES 187

LIST OF ACRONYMS

a :	absorption coefficient (m^{-1})
AsFFFF or AF4 :	Asymmetric flow field-flow fractionation
BIX :	biological autochthonous input index
CDOM :	coloured or chromophoric dissolved organic matter
CF :	cross-flow rate during elution time (ml/min)
DBPs :	disinfection byproducts
DF :	Detector or channel flow (ml/min)
DLS :	dynamic light scattering
DOC :	Dissolved Organic Carbon
DOM :	dissolved organic matter
EEM :	excitation-emission matrix
EEMs :	excitation-emission matrix spectral
ETM :	estuarine turbidity maximum
FDOM :	fluorescent dissolved organic matter
FF :	cross-flow rate during focusing time (ml/min)
FFF :	field flow fractionation
FIFO	frit inlet/frit outlet–flow field-flow fractionation
FlFFF :	flow field flow fractionation
FTIR :	Fourier Transform InfraRed
HAAs :	haloacetic acids
HIX :	humification index
HMW :	high molecular weight
HPIA :	Hydrophilic acid fraction
HPIA :	Hydrophilic acid fraction
HPIN :	Hydrophilic neutral fraction
HPLC :	high performance liquid chromatography
HPOA :	Hydrophobic acid fraction
HPOB :	Hydrophobic base fraction
HPON :	Hydrophobic neutral fraction
HPSEC :	High pressure size exclusion chromatography
HSs :	humic substances
ICP-MS :	inductively coupled plasma mass spectroscopy
IHSS :	International Humic Substances Society
LMW :	low molecular weight
MALLS :	laser light scattering
M_n :	number-average
MP :	mobile phase composition
MS :	mass spectrometry
M_w :	weight-average
MW :	molecular weight

MWCO :	molecular weight cut off
NDIR :	non dispersive infrared detector
NMR :	Nuclear Magnetic Resonance
NOM :	natural organic matter
NPOC	non-purgeable organic carbon
PAHs :	polycyclic aromatic hydrocarbons
PARAFAC :	parallel factor analysis
PCA :	Principal component analysis
PDI :	polydispersity index
PES :	polyethersulfone
PSS :	polystyrenesulfonate
R :	retention ratio
RC :	regenerated cellulose
r_{gw} :	weight-average radius of gyration
RI :	differential refractive index
RMM :	relative molar mass
S :	spectral slope
SEC :	size exclusion chromatography
S_R :	spectral slope ratio
SRFA :	Suwannee River fulvic acid
SRHA :	Suwannee River humic acid
SUVA :	specific ultraviolet absorption
t_f :	relaxation or focus time (min)
THMs :	trihalomethanes
t_o :	void time (min)
TOC :	total dissolved organic carbon
t_R :	retention time (min)
UV :	Ultraviolet
UV-Vis :	Ultraviolet visible
XOM :	xenobiotic organic matter

LIST OF TABLES

Table 1.1 Compositions of NOM fractions and chemical groups

Table 1.2 Main fluorescence bands for natural waters

Table 1.3 Summary of FlFFF operational conditions and main conclusions of DOM studies

Table 2.1 List of sampling sites and their codes

Table 2.2 DOM characteristics associated with the range of values obtained for the HIX and BIX indices from estuarine and seawater samples

Table 3.1 UV–Visible absorbance parameters of surface water samples in the Seine River catchment

Table 3.2 Spearman coefficients of correlation ($P<0.01$, $n=102$) between ratios of fluorescent intensities to DOC concentration

Table 3.3 Spatial Mann-Whitney U-test analysis for comparison of HIX values during the three sampling events

Table 3.4 Spatial Mann-Whitney U-test analysis for comparison of BIX values during the three sampling events

Table 3.5 Characteristics of the seven component model determined by PARAFAC in this work compared to previous studies

Table 3.6 Regression analysis of logarithmic correlation between EEM-PARAFAC components

Table 3.7 Correlation coefficients between ratios of intensities of EEM-PARAFAC components with fluorescence indices

Table 5.1 Number-average (M_n), weight-average (M_w), peak (M_p) molecular weights and polydispersity index (PDI) of lower-molecular weight fraction determined at 280 nm using UV detection

Table 5.2 EEM contour plots (intensity scales different) of the bulk samples and the nine AF4 fractions isolated for O1 (2011, 2012 and 2013) in the Oise River

Table 5.3 EEM contour plots (intensity scales different) of the bulk samples and the eight AF4 fractions isolated for G1 (2011 and 2013) in the Grand Morin tributary

Table 5.4 EEM contour plots (intensity scales different) of the bulk samples and the nine AF4 fractions isolated for M7 (2011, 2012 and 2013) in the Marne River

Table 5.5 EEM contour plots (intensity scales different) of the bulk samples and the nine AF4 fractions isolated for S5 (2012 and 2013) in the Seine River
Table 5.6 EEM contour plots (intensity scales different) of the bulk samples and the nine AF4 fractions isolated for S6 (2011, 2012 and 2013) in the Seine River

LIST OF FIGURES

Figure 1.1 The continual size of natural organic matter in the aquatic environment

Figure 1.2 Two proposed models of molecular structure of humic substances

Figure 1.3 Normalized emission spectra (at excitation wavelength 310 nm) of samples in the Gironde Estuary in a range of variable salinity (S = 0 to 34.3)

Figure 1.4 Basic separation principle of flow field flow fractionation

Figure 2.1 Location of sampling sites in 2011 in the Seine River catchment, France

Figure 2.2 Location of sampling sites in 2012 (low-water) in the Seine River catchment, France

Figure 2.3 Location of sampling sites in 2013 (flood) in the Seine River catchment, France

Figure 2.4 Perrin–Jablonski diagram and illustration of the relative positions of absorption, fluorescence and phosphorescence spectra

Figure 2.5 UV-visible absorption spectrum (sample Mery/ Seine-S1, 2012)

Figure 2.6 Emission spectrum at the excitation wavelength 370 nm to calculate the f_{450}/f_{500} index (sample Mery/ Seine-S1, 2012)

Figure 2.7 Emission spectrum at the excitation wavelength 254 nm to calculate the HIX index

Figure 2.8 Emission spectrum at the excitation wavelength 310 nm to calculate the BIX index

Figure 2.9 Two main types of FlFFF

Figure 2.10 Principle of the separation of macromolecules by FlFFF

Figure 2.11 Field flow fractionation fractogram

Figure 3.1 DOC concentrations for samples collected in November 2011

Figure 3.2 DOC concentrations for samples collected in 2012

Figure 3.3 DOC concentrations for samples collected in 2013

Figure 3.4 Variations of relationship between $SUVA_{254}$ and Aromaticity in the Seine River catchment

Figure 3.5 Variations of specific ultraviolet absorbance ($SUVA_{254}$) ($L.m^{-1}.mg^{-1}C^{)}$ in the three studied basins

Figure 3.6 Variation of the spectral slope ratio S_R in the Seine River catchment during the three sampling periods

Figure 3.7 Variations of (a) spectral slope ratio S_R and (b) $SUVA_{254}$ as a function of DOC concentration

Figure 3.8 Variations of fluorescence intensities of (a) α'; (b) α; (c) β and (d) γ bands as a function of DOC concentrations in the Seine River catchment during the three campaign periods

Figure 3.9 Box plots of fluorescence intensities normalized to DOC concentration

Figure 3.10 Distribution of $I_{\alpha'}/I_{\alpha}$ ratio as a function of DOC concentration in the Marne (a), Oise (b) and Seine (c) basins during the three snapshot campaigns

Figure 3.11 Distribution of I_{β}/I_{α} ratio as a function of DOC concentration in the Marne (a), Oise (b) and Seine (c) basins during the three snapshot campaigns

Figure 3.12 Distribution of I_γ/I_α ratios as a function of DOC concentration in the Marne (a), Oise (b) and Seine (c) basins during the three snapshot campaigns

Figure 3.13 Variations of the f_{450}/f_{500} index as a function of DOC concentration

Figure 3.14 Variations of HIX and BIX for samples in the Marne (a), Oise (b) and Seine (c) basins during the three snapshot campaigns

Figure 3.15 Variations of HIX (a) and BIX (b) indices as a function of DOC concentration

Figure 3.16 Variations of BIX index (a) and spectral slope ratio S_R (b) as a function of HIX index

Figure 3.17 (a) Contour plots of the seven components identified by PARAFAC analysis, and (b) Excitation (solid lines) and Emission loadings (dotted lines) of each component

Figure 3.18 Examples of measured (a-d), modeled (e-h) and residual (i-l) EEMs for different DOM in the catchment. Fluorescence emission is in Raman units

Figure 3.19 Distribution of the fluorescence intensity normalized to DOC of the 7 components identified by PARAFAC in the three studied basins in (a) 2011; (b) 2012 and (c) 2013

Figure 3.20 Relative percentage distributions of the 7 components identified by PARAFAC in the three studied basins in (a) 2011; (b) 2012 and (c) 2013

Figure 3.21 Distribution of the 7 components identified by PARAFAC by river basin and among periods of sampling.

Figure 3.22 Ratios of the average fluorescence maximum of each component to the fluorescence maximum of C2 during the three sampling times

Figure 3.23 Variations of relationships between fluorescence maximum of pairs of components in the Seine River catchment

Figure 3.24 Variations of relationships between fluorescence maximum of pairs of components in the Seine River catchment

Figure 3.25 Principal component score plot of the total variance from data set

Figure 4.1 Location of six sampling sites in 2012 in the Seine River catchment, France

Figure 4.2 Correlation between cross-flow rate (V_c) and the retention time (t_R) of small fractions of DOM macromolecules of sample Beaumont (O5) collected in 2012

Figure 4.3 Cross-flow rate during different phases of a programmed cross-flow separation

Figure 4.4 Effect of different cross-flow program form on the separation of DOM macromolecules of sample Mery (S1) collected in 2012

Figure 4.5 Fractograms of small fractions of DOM obtained by UV detector as a function of focus time.

Figure 4.6 EEM spectra of (a) bulk sample Mery (S1- 2012), (b) fraction collected for t_f =0 min, (c) fraction collected for t_f =2 min

Figure 4.7 Fractograms for 6 samples from the Seine River catchment in the optimized conditions obtained by (a) UV and (b) MALLS detectors

Figure 5.1 (a) UV fractogram of standards, and (b) UV calibration curve obtained between molecular weight and retention time of standards

Figure 5.2 MALLS fractograms of samples collected in the Seine River catchment in

2013
Figure 5.3 UV fractograms of samples collected in (a) Marne River and (b) Grand Morin tributary in 2011
Figure 5.4 UV fractograms of samples collected in (a) Oise River and (b) its tributaries in 2011
Figure 5.5 UV fractograms of samples collected in Seine River in 2011
Figure 5.6 Variations of Mp in the four basins
Figure 5.7 Comparison of M_p and S_R for all the samples collected in 2011
Figure 5.8 Distributions of (a) DOC, (b) PDI, (c) HIX, (d) SUVA, (e) Mp, (f) SR, (g) BIX and (h) I_γ/I_α for the 13 samples selected for fractionation
Figure 5.9 AF4 fractograms of the samples M7 collected both in 2011, 2012 and 2013
Figure 5.10 AF4 fractograms of the samples G1 collected both in 2011 and 2013
Figure 5.11 AF4 fractograms of the samples O1 collected both in 2011, 2012 and 2013
Figure 5.12 AF4 fractograms of samples S5 (a) and S6 (b) fractionated for the Seine River
Figure 5.13 Examples of EEM spectra of DOM in the Seine River catchment
Figure 5.14 Positions of all fluorescence intensity maxima identified within EEM spectra for all fractions of samples O1 collected in the Oise River (a) in 2011 (b) in 2012 and (c) in 2013
Figure 5.15 Emission spectra of nine fractions from sample O1 collected in 2011 at E_x = 310 nm
Figure 5.16 Variations of the fluorescence intensity of the bands α', α and β between the nine fractions and the three sampling dates for O1 in the Oise River
Figure 5.17 Variations of BIX between fractions compared to bulk samples for site O1 in 2011, 2012 and 2013
Figure 5.18 Positions of all fluorescence intensity maxima identified within EEM spectra for all fractions of samples G1 collected in the Grand Morin River (a) in 2011 and (b) in 2013
Figure 5.19 Variations of the fluorescence intensity of the bands α', α and β between the eight fractions and the sampling dates 2011 and 2013 for sample G1
Figure 5.20 Positions of all fluorescence intensity maxima identified within EEM spectra for all fractions of samples M7 collected in the Marne River (a) in 2011, (b) in 2012 and (c) in 2013
Figure 5.21 Variations of the fluorescence intensity of the bands α', α and β between the nine fractions and the three sampling dates for M7 in the Marne River
Figure 5.22 Variations of BIX between fractions compared to bulk samples for site M7 in 2011, 2012 and 2013
Figure 5.23 Positions of all fluorescence intensity maxima identified within EEM spectra for all fractions of samples S5 collected in the Seine River (a) in 2012 and (b) in 2013
Figure 5.24 Variations of the fluorescence intensity of the bands α', α and β between the nine fractions isolated by AF4 for samples S5 collected in 2012 and in 2013 in the Seine River
Figure 5.25 Positions of all fluorescence intensity maxima within EEM, identified in all fractions of sample S6 collected in the Seine River (a) in 2012, (b) in 2012

and (c) in 2013

Figure 5.26 Variations of the fluorescence intensity of the bands α', α and β between the nine fractions and the three sampling dates for S6 collected in the Seine River

Figure 5.27 Variations of BIX between fractions compared to bulk samples for the sites (a) S5 (2011 and 2012) and (b) S6 (2011, 2012 and 2013) in the Seine River

GENERAL INTRODUCTION

The PIREN-Seine research program (Programme Interdisciplinaire de Recherche sur l'ENvironnement de la Seine), a large interdisciplinary research program on the Seine River System jointly financed since 1989 by the French CNRS (National Center for Scientific Research) and the public and private actors of the management of the water of the Seine-Normandy basin, accompanied and contributed to the recent progress in the aquatic science. The aim of the program was to understand the biogeochemical and ecological functioning of the Seine River system at the level of its whole drainage network (from headwaters to the coastal zone), in relation to land use and the environmental management in the watershed (Billen et al., 2007).

For its 6th phase, the PIREN-Seine program suggested structuring its works around 5 main areas of research:

- ✓ What agriculture for tomorrow?
- ✓ Interfaces between ground water and river
- ✓ Biogeochemistry of the River
- ✓ The determinants of the ecological quality of the aquatic ecosystem
- ✓ Contaminations during long term period

They were drawn to answer the majority of the questionings of the partners, in coherence with the current stakes identified for the Seine basin by its main actors.

The study of the organic matter is a part of the 3rd section "Biogeochemistry of the River", which main objective is to study the characteristics of dissolved organic matter (DOM) with the aim of identifying its sources and tracing its evolution and behavior in the Seine River catchment.

DOM in aquatic environments represents one of the largest reservoirs of carbon. It plays an important environmental role not only in the biogeochemical cycles of carbon but also in the transport, stability, speciation, bioavailability and toxicity of pollutants. Generally, DOM originated from three major sources (Mostofa et al., 2013):

1. Allochthonous origins from soils

2. Autochthonous origins from the degradation of algae or phytoplankton
3. Anthropogenic origins mainly from agricultural, industrial and sewage effluents as well as human activities

Moreover, colloids constitute the bulk of the dissolved organic matter (DOM) in aquatic environments and also play a crucial role in many physical, chemical and biological processes in the ecosystem (Dubascoux et al., 2008). To better understand the composition of environmental colloids as well as their interactions with pollutants, it is necessary to separate these substances according to their properties, especially in terms of their size.

This PhD thesis aims to develop an analytical technique (asymmetrical flow field-flow fractionation) in order to partition DOM into different size fractions whose fluorescence properties will be evaluated.

The results of these works reported in this manuscript thesis which is divided into five chapters.

- ✓ The first chapter provides a literature review on dissolved organic matter and the common analytical techniques utilized to fractionate DOM are also reviewed.
- ✓ The second chapter describes the study sites within the Seine River catchment and the various analytical techniques as well as the statistical tools which were implementedto characterize and fractionate DOM. Forty-five sites were thus sampled along three sub-basins within the Seine River catchment including the Marne River and its tributary (Grand Morin River) the Oise River and the Seine River.
- ✓ The third chapter presents the optical properties of the surface water samples collected during three sampling campaigns.
- ✓ The fourth chapter deals with the optimization of a methodology suitable for DOM fractionation.
- ✓ Finally, the fifth chapter presents the molecular weight distribution of DOM for the various samples collected from the Seine river catchment and the investigation of fluorescence properties of the isolated DOM fractions for selected samples.

CHAPTER I: BIBLIOGRAPHIC SYNTHESIS

1.1. Overview about natural organic matter

Natural organic matter (NOM) is a highly complex mixture of organic compounds composed of the decay of living organisms in aquatic and terrestrial environments. NOM is ubiquitous in water (Chen M.et al., 2010; Chin et al., 1998; Lam et al., 2007; Penru et al., 2013; Repeta et al., 2002; Rosario-Ortiz et al., 2007; Shon et al., 2006; Thomas, 1997), soil (Akagi et al., 2007; Fellman et al., 2008b; Semenov et al., 2013) and sediments (Burdige, 2005, 2001; Mayer et al., 2006; Wang and Mulligan, 2006). NOM in aquatic ecosystem can be divided into two categories: dissolved and particulate phases. There is no natural cut-off existing between these two fractions and this is still an operational distinction. These two fractions are traditionally separated on the rather arbitrary criteria of filter pore sizes typically in the range of 0.1 to 0.8µm (Asmala et al., 2013). The continuum size of organic matter in aquatic environments is shown in Figure 1.1.

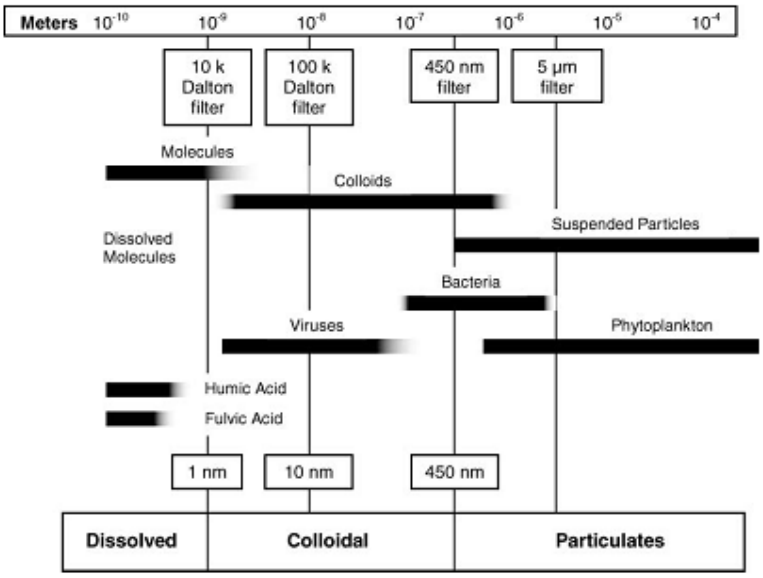

Figure 1.1 The continual size of natural organic matter in the aquatic environment (Aiken et al., 2011)

Of the two categories, dissolved phase, named dissolved organic matter (DOM), plays an essential role in shaping aquatic ecosystems because of the number of processes in which it becomes involved.

Firstly, DOM has been recognized as an important reservoir of oceanic organic carbon with a pool size of roughly 685 $\times 10^{15}$ C (Hansell, 2001). The total transport of organic carbon to the ocean is estimated in the range of 0.4 to 0.9 x 10^{15} g $year^{-1}$ (Griffith et al., 2012; Jahnke, 1996; Schlesinger and Melack, 1981). Changes in the production or consumption of DOM could lead to significant perturbations of the global carbon cycle.
Secondly, DOM could interact with a large number of organic and inorganic pollutants in aquatic environment such as metals, pesticides, polycyclic aromatic hydrocarbons (PAHs) (Backhus et al., 2003; Guéguen et al., 2004; Koukal et al., 2003) and therefore influence their speciation, solubility, toxicity, transport and bioavailability.

In addition, DOM is also involved in aqueous photochemical reactions, nutrients cycling and availability (Bormann and Likens, 1967). It plays a role as the major light absorbing material in aquatic ecosystems where it absorbs biologically harmful UV light and protects corals and other light-sensitive organism from UV radiation (Anderson et al., 2001; Cory et al., 2004). Furthermore, DOM exerts a strong control in the formation of disinfection byproducts (DBPs), for example, trihalomethanes (THMs) and haloacetic acids (HAAs), during the drinking water supply treatments with disinfectants (Kraus et al., 2008; Pifer and Fairey, 2012).

Taking into account all the factors above, it is essential for us to study about DOM in order to better understand the nature and properties of dissolved organic matter in the aquatic ecosystem.

1.2. Source of DOM in aquatic environment

DOM present in the aquatic system originates from three major sources: autochthonous, allochthonous and anthropogenic sources (McKnight and Aiken, 1998; Mostofa et al., 2009). The autochthonous inputs are derived from the degradation and excretion of algal biomass, submerged aquatic vegetation, seagrass, bacteria, macrophytes and phytoplankton (Boyd and Osburn, 2004; Henderson et al., 2008; McKnight et al., 1998; Wada et al., 2007; Wang et al., 2007; Wu and Tanoue, 2002; Yamashita and Tanoue, 2004; Zhang Yunlin et al., 2009). Photoinduced respiration and microbial respiration or assimilation of algae or phytoplankton and bacteria are two key processes to produce and release new DOM into natural water (Mostofa et al., 2013a). It has been estimated that more than 97% of autochthonous DOM in

fresh water lakes and wetlands originated from macrophytes, while phytoplankton is the basic source of DOM in large lakes and oceanic systems (Søndergaard et al., 2004). There are a number of factors influencing the release process of DOM in water by algae, phytoplankton and bacteria such as: occurrence of the phytoplankton species or microbes, water quality, water temperature, the presence of nutrients, metabolic abilities or inabilities and so on (Gobler et al., 2004; Keller and Hood, 2011; Pete et al., 2010; Puddu et al., 2003; Rochelle-Newall et al., 2011).

On the other hand, the main allochthonous inputs are derived from terrestrial soil organic matter and the degradation of plant in the surrounding watershed (McKnight et al., 2001). DOM from terrestrial ecosystem has a high content of humic material and very complex chemistry (Søndergaard et al., 2004). Terrestrial humic substances (fulvic and humic acids) are known as the dominant DOM fractions in river environments (Malcolm, 1985).
Allochthonous DOM originating from plant materials or particulate detrital pool is significantly different in various regions (tropical, temperate and boreal) due to some factors such as: physical and chemical parameters as well as microbial processes (Mostofa et al., 2013a). The origin of allochthonous DOM from microbial processes can be estimated from significant fluctuation in respired organic carbon in different soil environments. Furthermore, a small proportion of allochthonous aquatic DOM originates from wind-blown material, direct precipitation and leaf fall. Allochthonous DOM differs from autochthonous DOM in several optical (McKnight et al., 1994) and chemical characteristics (Benner, 2002).

The anthropogenic source of DOM typically comes from agricultural, industrial and sewerage effluents as well as human activities (Mostofa et al., 2010). These anthropogenic and human activities released a large number of organic contaminants such as fluorescence whitening agents, phenols, pesticides, PAHs, pharmaceuticals and so on in natural waters (Huang et al., 2010; Kramer et al., 1996; Meng et al., 2013; Morvan et al., 2006; Mostofa et al., 2013; Parinos et al., 2013; Rawn et al., 2001; Yamaji et al., 2010). These organic pollutants could be assimilated by littoral benthos and this is an important pathway for transfer of anthropogenic-associated contaminants to fish or directly to microorganisms (Fu et al., 2010).

1.3. Composition of DOM

Organic matter is composed of a variety of substances, which vary in time and space and is a function of temperature, pH and ionic strength as well as photolytic and microbial processes (Leenheer and Croué, 2003). Dissolved organic carbon can be separated into hydrophobic and hydrophilic constituents. Further, each constituent is divided into acid, base, and neutral fractions (Leenheer and Noyes, 1984). Dissolved organic matter (DOM) can be divided into two major groups: humic and non-humic substances. The humic substances are more hydrophobic in character and are composed of humic and fulvic acids. On the other hand, the non-humic substances are less hydrophobic in character and consist of hydrophilic acids, proteins, amino acids and carbohydrates (Owen et al., 1995). It is relatively difficult to separate humic substances from non-humic materials because the first ones can be bound covalently to the second ones (Peuravuori, 1992). The proposed compositions of different NOM fractions and the chemical groups involved are summarised in Table 1.1.

Table 1.1 Compositions of NOM fractions and chemical groups (Edzwald, 1993 cited in Matilainen, 2007)

Fraction	Chemical group
Hydrophobic	
Acids	
Strong	Fulvic acid, humic acid, high molecular weight alkyl monocarboxylic acids (≥ C9), dicarboxylic acids (≥C12), aromatic acids
Weak	Tannins, phenols, intermediate molecular weight alkyl monocarboxylic acids (C5-C8), dicarboxylic acids (C8-C11)
Bases	Amphoteric, proteins, aromatic amines, hight molecular weight alkyl amines (≥C12), alkyl pyridines
Neutrals	Hydrocarbons, aldehydes, high molecular weight methyl ketones (C6); furans, most ethers, high molecular weight alkyl alcohols (≥C5), lactones, pyrrole
Hydrophilic	
Acids	Hydroxyl acids, sugars, sulfonics, low molecular weight alkyl monocarboxylic acids (C1-C4), and dicarboxylic acids (C2-C7)
Bases	Amino acids, low molecular weight alkyl amines (C1-C11), purines, pyridine, hydroxyl pyridines
Neutrals	Polysaccharides, low molecular weight alkyl alcohols, aldehydes, ketones, polyketones, amides

1.3.1. Humic substances

Humic substances are a heterogeneous mixture of aliphatic and aromatic molecules with a broad range of chemical compositions and molecular sizes (Matilainen, 2007) and are the

major constituents of NOM in soils and continental aquatic ecosystems (Abbt-Braun et al., 2004; Sutton and Sposito, 2005). The humic substances are also called refractory organic matter, due to their low (but nonzero) biodegradability (Duursma and Dawson, 1981). The acid-base properties of humic substances play a vital role in the acid-base balance in natural waters. Humic substances in soils comprise humic acids, fulvic acids and humin (Aiken et al., 1985).

Humic substances account for 25% of the total organic carbon on the earth and represents 50-75% of the dissolved organic carbon in the waters (Hertkorn et al., 2002). They are non-volatile compounds having a molecular weight in the range of 500-5000 Da and their elemental composition includes roughly 50% carbon, 4-5% hydrogen, 35-40% oxygen, 1-2% nitrogen, and less than 1% sulphur plus phosphorus (Thurman, 1985a). Humic substances are characterized by a wide variety of functional groups including carboxylic acid, phenolic hydroxyl, carbonyl and hydroxyl groups. According to the IHSS (International Humic Substances Society), aquatic humic substances can be divided into two broad categories: fulvic and humic acids. The hypothetical structure of humic acid contains free and bound phenolic OH groups, quinine structures, nitrogen and oxygen as bridge units and COOH groups as shown in figure 1.2. The hypothetical model structure of fulvic acid (Alvarez-Puebla et al., 2006) contains aromatic and aliphatic structures as well as extensively substituted with oxygen-containing functional groups as shown in figure 1.2. In aquatic environments, humic substances are mainly represented by fulvic acids. In seawater, the composition of humic substances include approximately 85% fulvic acids and 15% humic acids and originated from the decomposition of phytoplankton (Thurman, 1985a). In streams and rivers, the contributions of humic substances account for 20-85% of total DOM (15-80% of fulvic acids and 5-29% of humic acids). The ratio of fulvic acid to humic acid is more or less 4:1 for higher stream DOC, while this ratio is about 9:1 for lower stream (Mostofa et al., 2013a). Humic substances in rivers and streams are typically originated from soil and plant matter. In lakes, the contribution of humic substances is 14-90%, with fulvic and humic acids accounting for 14-70% and 0-22%, respectively.

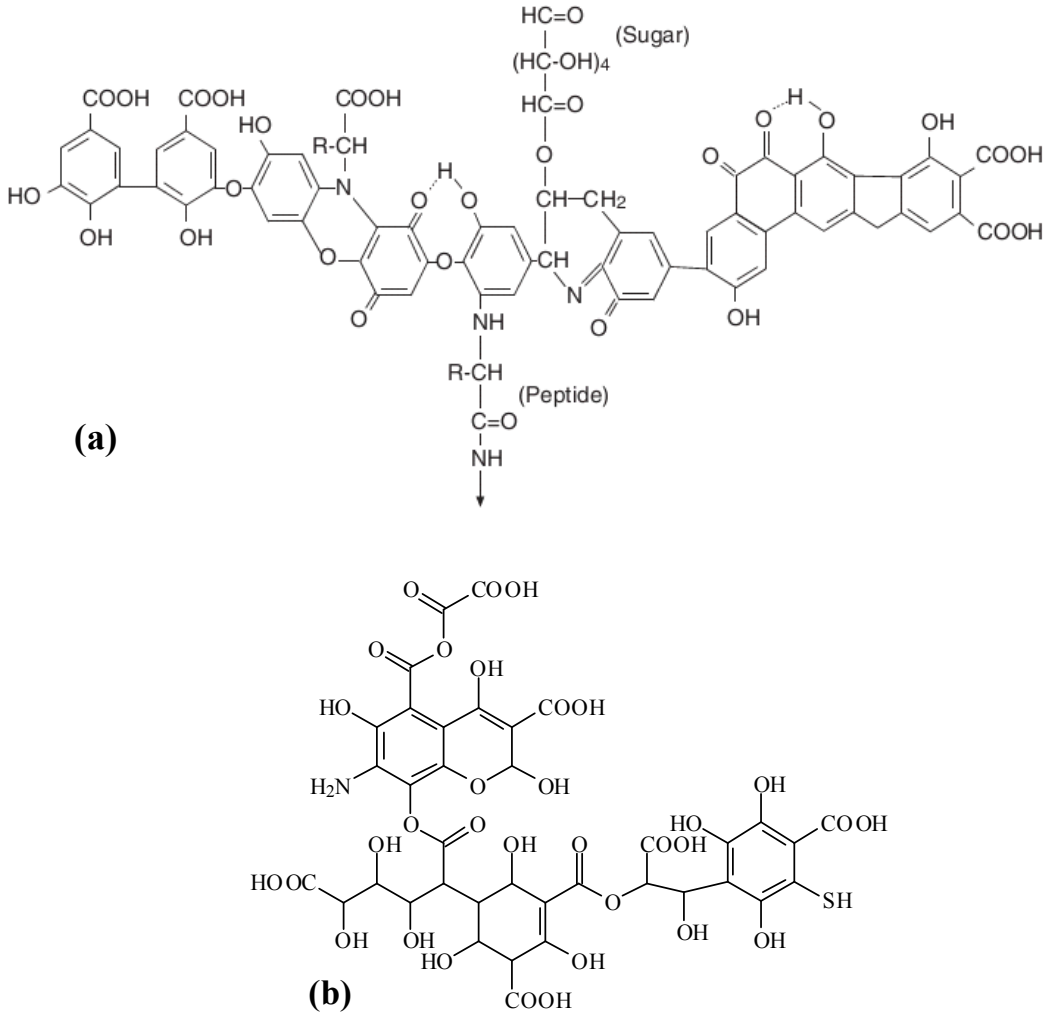

Figure 1.2 Two proposed models of molecular structure of humic substances: (a) humic acid (Stevenson, 1982 cited in Aiken et al., 1985) and (b) fulvic acid (Alvarez-Puebla et al., 2006)

Generally, humic acids have higher molecular mass and higher aromaticity but low charge density than fulvic acids (Aiken, 1985). Moreover, in comparison with fulvic acids, humic acids are enriched in basic, hydroxy-, sulphur-containing and aromatic amino acids (Thurman and Malcolm, 1981). However, fulvic acids have a greater proportion of carboxyl groups than humic acids. Both components are generally removed from water by acidifying to pH 2.8-3.0 and adsorbed on a suitable resin column. Acrylic-ester copolymer (XAD-8 or DAX8) resin was considered to adsorb and elute aquatic humic substances most efficiently (Aiken, 1985; Thurman and Malcolm, 1981). A strong base is often used to extract humic acids and fulvic acids from resins. The pH is then adjusted to 2 in order to precipitate the humic acids. The

humic substances are adsorbed on the resins, while the non-humic substances (amino acids, peptides, sugar…) pass through the column without being retained.

Piccolo (2001) proposed that the conformational nature of humic substances was seen as supramolecular associations of self-assembling heterogeneous and relatively small molecules deriving from the degradation and decomposition of dead biological material. Humic superstructures of relatively small molecules are stabilized predominantly by weak dispersive forces such as dispersive hydrophobic interactions (van der Waals, π-π, and CH-π bondings) and hydrogen bonds, instead of covalent bonds (Piccolo, 2001). By considering the supramolecular concept, the humic acids may be associated with hydrophobic compounds which are stabilized at neutral pH by hydrophobic dispersive forces, while fulvis acids may be composed by small hydrophilic molecules with acidic functional groups to keep fulvic clusters dispersed in solution at any pH.

1.3.2. Non-humic substances

Non-humic substances are the fractions of organic matter that are not retained on the XAD-8 resin column(Leenheer, 1981; Lenheer and Huffman, 1976; Thurman and Malcolm, 1981). However, the non-humic fractions of NOM exhibit some of properties typically observed for humic fractions (Barrett Sylvia E. et al., 2000). The humic substances are most readily removed by conventional treatment, which consists of flocculation, sedimentation, and filtration, while the non-humic substances are more difficult to remove. Compared to fulvic acids, non-humic substances had lower molecular mass, greater carbohydrate content and greater content of acidic functional groups (McKnight et al., 1985). The composition of the non-humic fraction includes hydrophilic acids, proteins, amino acids, amino sugars and carbohydrates (Baghoth, 2012). The carbohydrate and amino sugars dominate the carbon distribution of the non-humic fraction in fresh water (Croué, 2004).

Carbohydrates

Carbohydrates serve as one of the most frequently used substrates by bacteria for energy and growth in aquatic environments (Hedges et al., 1994) and control the bioavailability of iron in the ocean (Hassler et al., 2011). The composition of carbohydrates in aquatic systems has been intensively studied for many years (Cowie and Hedges, 1984; Guggenberger and Zech, 1994;

Macko et al., 1991; Senior and Chevolot, 1991). Carbohydrates in marine systems originated primarily from phytoplankton (Romankevich, 1984). They represent a significant fraction (10–30%) of the DOC pool in the riverine, coastal, and marine waters (Benner et al., 1992; Pakulski and Benner, 1994). 74% of the carbohydrates in the non-humic fraction is arabinose and mannose (McKnight et al., 1985).

Carbohydrates are the primary products of photosynthesis which can be transformed into other essential components such as proteins, lipids and nucleic acids (Zhang Yanping et al., 2009).

Amino acids

Amino acids are the major forms of nitrogen and important compositions of organic carbon in most marine organisms (Cowie and Hedges, 1992; Ittekkot and Zhang, 1989). They occur in aquatic environments in a free status, likely as dissolved free individual compounds, as part of natural polymers such as peptides and proteins (Münster, 1999). Total dissolved amino acids contribute to about 2 to 5% of the DOC in surface waters (Thurman, 1985b). The major amino acids found in surface waters are glutamic acids, glycine, serine and aspartic acid (Hedges et al., 1994; Lara et al., 1998; Thurman, 1985b). Duan and Bianchi (2007) reported that the dominant amino acids in the lower Mississippi and Pearl Rivers are glycine, alanine, glutamic acid, aspartic acid, serine, valine and leucine, accounting for over 60% of the total amino acids. Amino acids are derived into aquatic environments from bacterial enzymatic degradation of particulate and dissolved proteinaceous material and excretion by a variety of planktonic organisms such as algae, higher water plants, bacteria (Münster and Chróst, 1990; Münster, 1999).

Generally, dissolved amino acids originate directly from algal release via autolysis and extracellular excretion, or are indirectly released during feeding by grazers, microbial degradation of detritus, viral or bacterial lyses of phytoplankton cells and can be inherited by continuous release and physical transport of terrestrial material (Zhang Yanping et al., 2009).

Amino sugars are biochemical constituents of natural organic matter and account for 0.6% to 2.5% of organic carbon in the dissolved phase (<0.1 μm) of organic matter (Benner and Kaiser, 2003).

1.4. The optical properties of DOM

The optical properties of DOM supply information on either the amount of material present or the chemical properties of the bulk sample, which undergo alteration due to chemical, biological, and physical processes (Coble, 2007). The optical properties of DOM can be altered for waters impacted by forests, wetlands, urbanization, sewage effluent, agricultural practices, local biology and groundwater discharges. Thus, the optical properties of this material, and especially their absorbance and fluorescence properties, can be used as tracers of water masses. There is an increasing interest in advanced applications of UV and fluorescence spectroscopy to characterize and identify the properties of DOM in aquatic systems because of their qualitative and quantitative reliabilities. The discussed parameters include absorption coefficients, aromaticity, spectral slopes (Blough et al., 1993), fluorescence intensities and the fluorescence intensity ratios (Conmy et al., 2004; McKnight et al., 2001), positions of fluorescence maxima (Coble, 1996), and apparent fluorescence efficiencies. All of them have been used to distinguish compositional characteristics and to discriminate DOM sources between autochthonous and allochthonous as well as to observe DOM transformations through ecosystems (Blough and Del Vecchio, 2002; Coble, 1996; Conmy, 2008).

1.4.1. The absorbance properties of DOM

Aquatic DOM strongly absorbs energy in the ultra violet-visible (UV-Vis) wavelength range, thus UV-Vis absorbance spectroscopy is considered as a useful method for characterizing DOM (Weishaar et al., 2003; Helms et al. 2008). Although it may not be used for refined characterization of organic matter, it remains useful as a quick, cheap and reliable method of estimating DOM quantity and describing its quality and is thus a commonly used technique.

The optically active components of bulk DOM that absorbs light over a broad range of ultra-violet (UV) and visible wavelengths (200-800nm), is named coloured or chromophoric dissolved organic matter (CDOM) (Arrigo and Brown, 1996; Blough et al., 1993; Coble, 2007; Korshin et al., 1997; Rochelle-Newall and Fisher, 2002; Vähätalo and Wetzel, 2004; Zhang Yunlin et al., 2009). CDOM in natural waters absorbs mainly in the blue spectral region and its UV-visible absorption spectrum increases approximately exponentially with decreasing wavelengths (Twardowski et al., 2004). In order to extract information about CDOM properties

from the absorbance spectra, some parameters have been examined such as absorption ratios (Chen et al., 2002; Minero et al., 2007; Thomsen et al., 2002; You et al., 1999), aromaticity (Yu-Ping. Chin et al., 1994; Lepane et al., 2004; Schwede-Thomas et al., 2005; Thomsen et al., 2002), SUVA (specific ultraviolet absorption) (Akkanen et al., 2005; Fellman et al., 2008a; Henderson et al., 2008; Hood et al., 2006; Weishaar et al., 2003; Matilainen et al., 2011; Vidon et al., 2008; Westerhoff et al., 1999), absorption spectral slopes (Asmala et al., 2013; Fichot and Benner, 2012, 2011; Franke et al., 2012; Stolpe et al., 2013), and spectral slope ratios (Chen H. et al., 2010; Guéguen and Cuss, 2011; Helms et al., 2008).

Several authors (De Haan and De Boer, 1987; Peuravuori and Pihlaja, 1997) applied the absorption ratio E_2/E_3 (Abs_{250nm}/Abs_{365nm}) to track changes in the relative size of DOM molecules and indicated that molecular size decreased when E_2/E_3 ratio increased as a result of stronger light absorption by high-molecular-weight CDOM at longer wavelengths. Some authors (Chin et al., 1994; Summers et al., 1987) reported that the absorption ratio E_4/E_6 (Abs_{465nm}/Abs_{665nm}) was inversely related to CDOM aromaticity. On the other hand, other authors (Chen et al., 1977; Senesi et al., 1989) showed that the E_4/E_6 ratio was better correlated with molecular size than to aromaticity and, therefore, was better suited as a general tracer of humification. In fact, the E_4/E_6 ratio was found to increase with decreasing average molecular weight and increasing oxygen content, and the E_2/E_3 ratio increased with a decrease in aromaticity (Thomsen et al., 2002).

UV absorption at 254 nm when normalized to DOC concentration, named specific UV absorbance ($SUVA_{254}$), had a strong correlation with percentage of DOM aromaticity as determined by ^{13}C NMR for a large number of organic matter isolates obtained from a variety of aquatic environments (Weishaar et al., 2003). Thus, $SUVA_{254}$ is considered as an indicator of aromaticity and chemical reactivity for aquatic organic matter samples from various origins. In addition, this index describes the nature of DOM in the water in terms of hydrophobicity and hydrophilicity, higher SUVA values (SUVA>4) showed mainly hydrophobic and especially aromatic material while lower SUVA values (SUVA<3) mainly characterized hydrophilic material (Edzwald and Tobiason, 1999; Matilainen et al., 2011).

In addition to absorption ratios and SUVA, the spectral slopes (S, nm^{-1}) have been based on CDOM absorption spectra by fitting the absorption data to the equation:

$$a_{\lambda} = a_{\lambda_{ref}} e^{-S\left(\lambda - \lambda_{ref}\right)} \quad (*)$$

with a, the absorption coefficient (m^{-1}); λ, the wavelength (nm); and λ_{ref}, the reference wavelength (nm) (Helms et al., 2008; Twardowski et al., 2004).

The spectral slopes were obtained by fitting a linear equation to the log-transformed of the expression (*) or by fitting an exponential function to the expression (*). Spectral slopes supplied further insights into the average characteristics (chemistry, source, diagenesis) of CDOM compared with absorption values alone and like the E_2/E_3 and E_4/E_6 ratios, they are largely independent of CDOM concentration (Helms et al., 2008). The spectral slope ratio (S_R) is defined as the ratio of shorter wavelength region (275-295 nm) to that of the longer wavelength region (350-400 nm). Both these spectra slopes and slope ratio had a relationship to DOM molecular weight and to photochemically induced shifts in molecular weight. In fact, the S_R ratio was reported to be negatively correlated with molecular weight of CDOM in humic substances fractionated by size exclusion chromatography (SEC) (Helms et al., 2008). These authors also indicated that the S_R ratio depends on the origin of CDOM. For example, S_R is higher than 1 for CDOM from marine waters (around 1.7 for coastal waters and about 4.6 for remote samples) and smaller than 1 for CDOM of terrestrial origin (Helms et al., 2008).

The S_R, SUVA and E_2/E_3 ratios have been used to characterized DOM in surface water and soil pore water samples from a cypress-tupelo wetland near Winyah Bay, South Carolina (Chow et al., 2013). Lower SUVA, higher S_R and E_2/E_3 ratios of DOM, were noticed at the end of the flooding season in comparison with the initial flooding, showing that the wetland system changes from high aromatic and large DOM molecules into smaller and hydrophilic fractions possibly through photochemical oxidation.

There is a clear potential of the application of absorption measurements to characterize DOM and to determine DOC fluxes in aquatic environments. Absorption measurements allow to increase spatial and temporal resolutions of DOM dynamics and thus to improve the understanding of the role of DOM in the ecosystem. They also lead to more accurate flux estimates (Spencer et al., 2009).

CDOM absorption properties are substantially influenced by several factors: DOM content and its chemical nature (Ishiwatari, 1973; Lawrence, 1980; Minero et al., 2007; Singh et al., 2010a, 2010b; Zanardi-Lamardo et al., 2004; Zepp et al., 1981), photoinduced and microbial processes in aquatic environments (Boehme and Coble, 2000; Hernes, 2003; Moran et al., 2000), occurrence and types of suspended particulate matter (Dupouy et al., 2010; Zhang Yunlin et al., 2009), and salinity (Blough and Del Vecchio, 2002; Hernes, 2003).

1.4.2. The fluorescence properties of DOM

Fluorescence spectroscopy is a rapid, sensitive and non-destructive method which is particularly suitable to study the physico-chemical properties of DOM. Generally, this method requires only a small volume of low-concentration sample, whilst other techniques require larger volumes of samples in order to isolate and concentrate sufficient amounts of DOM for further characterization steps (Huguet, 2007).

The fluorescence properties of organic matter have been widely studied for many years. The pioneering studies carried out by Kalle (1949) and Duursma (1974) utilized the fluorescence of terrestrial humic substances to trace soil organic matter in freshwater and seawater ecosystems (Mostofa et al., 2013a). Humic substances have been considered as the main cause for the fluorescence of organic matter (Ewald et al., 1983; Laane and Kramer, 1990). The fluorescence properties of humic substances have been used to discriminate the mixing of river water with seawater and to trace the sources of these materials (Almgren et al., 1975; De Souza Sierra et al., 1994; Murphy et al., 2008; Sierra et al., 2005).

The three-dimensional fluorescence or excitation-emission matrix (EEM) spectroscopy has been firstly applied to distinguish between the humic-like and protein-like fluorescence peaks of marine fluorescent dissolved organic matter (FDOM) in seawater (Coble et al., 1990). These EEM spectra are also used to obtain information on the number, on the type as well as on the relative concentration of the fluorophores present in complex mixtures. The different wavelength ranges or fluorescence bands, associated to each type of compounds constituting DOM, are summarized in Table 1.2.

Table 1.2 Main fluorescence bands for natural waters (Hudson et al., 2007)

Fluorophore Name (Coble, 1996)	Fluorophore Name (Parlanti et al., 2000)	Fluorophore Name (Marhaba and Lippincott, 2000; Marhaba et al., 2000)	Fluorophore type	Ex/Em wavelength (nm) at max fluorescence intensity	Author
A	α'	Hydrophobic acid fraction (HPOA)	Humic-like	237-260/400-500	
C	α		Humic-like	300-370/400-500	
M	β		Autochthonous production	310-320/380-400	
B	γ	Hydrophobic neutral fraction (HPON)	Protein-like (Tyrosine-like)	225-237/309-321 and 275/310	
T	δ	Hydrophobic base fraction (HPOB)	Protein-like (Trytophan-like)	225-237/340-381 and 275/340	
		Hydrophilic acid fraction (HPIA)			
		Hydrophilic acid fraction (HPIA)			
		Hydrophilic neutral fraction (HPIN)			
Chlorophyll a				431/670	(Moberg et al., 2001)
Chlorophyll b				435/659	(Moberg et al., 2001)
Naphthalene			XOM-landfill leachate	220-230/340-370	(Baker and Curry, 2004)
			Fluorescent whitening agent	260/430 260/540 400/460	(Westerhoff et al., 2001)

The α and α' bands

The α band accounts for the excitation-emission wavelength range at E_x/E_m = 330-350/420-480 nm, which is associated with humic substances, combination between humic and fulvic acids. The α' band accounts for the shorter excitation wavelength and this band represents the wavelength region at E_x/E_m = 250-260/380-480 nm, which is attributed to humic-like material, but also related to more recent organic matter. Several studies (Baker and Spencer, 2004; Mounier et al., 1999) attempted to ascribe α and α' bands to compounds of humic and fulvic types, respectively. Nevertheless, these two bands are always present together in all spectra of humic acids or fulvic acids extracted from soil or water samples (Vacher, 2004; Sierra et al., 2005). These fluorophores are common to both humic and fulvic acids groups, and their relative concentrations (intensities of α and α' bands) vary independently and depend on the nature and origin of the samples (Vacher, 2004; Huguet et al., 2009). In natural waters, the ratio of the fluorescence intensity of α' versus the fluorescence intensity of α bands was utilized to discriminate terrestrial organic matter in marine system, based on the fact that the fluorescence intensity of the α band is greatly reduced in the marine environment (Huguet, 2007). Thus, the higher values of α'/α ratio are mainly observed in seawater (Coble, 1996).

The β band

In contrast to α and α' fluorophores, the β fluorophore is slightly blue shifted. It is observed in the spectrum area from 310 nm to 320 nm for excitation wavelength and from 380 nm to 400 nm for emission wavelength (Figure 1.3) and was initially attributed to humic-like material of marine origin (Coble et al., 1990). This band generally appears as a shoulder on the α band. It was later demonstrated that its presence was related to recent autochthonous production in coastal marine environments (Parlanti et al., 2000), but also in freshwaters (Huguet et al., 2010). With regard to the origin of the β fluorophore, Parlanti et al. (2000) carried out to analyze the degradation of green macro-algae in pure and natural waters and indicated that this band could be associated with recently produced organic material related to biological activity in coastal marine environments.

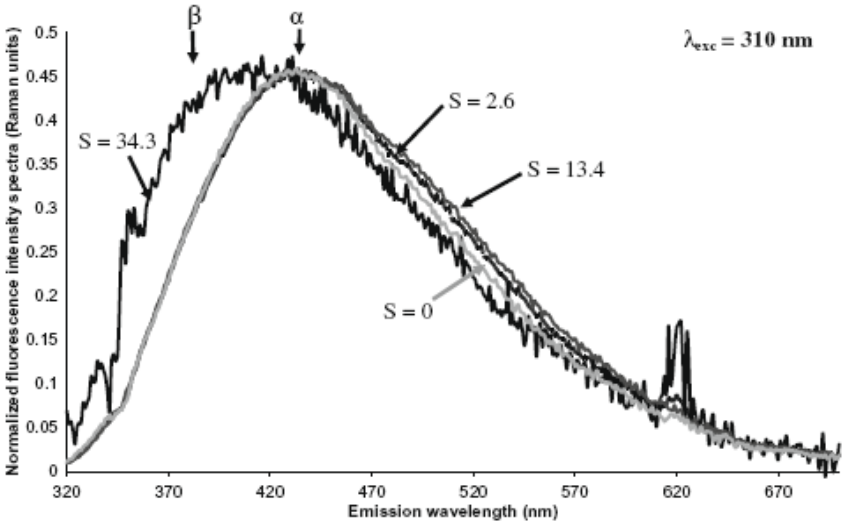

Figure 1.3 Normalized emission spectra (at excitation wavelength 310 nm) of samples in the Gironde Estuary in a range of variable salinity (S = 0 to 34.3) (Huguet et al., 2009)

The γ band

The γ band is observed in the position of the excitation wavelength from 270 nm to 280 nm and attributed to protein-like compounds, which have structures similar to the aromatic amino acids such as tyrosine or tryptophan. The position of the emission wavelength for the tyrosine is in the range 300-320 nm and that for the tryptophan ranges from 320 nm to 350 nm. It is difficult to discern between these two bands due to overlapping and a potential interference with the fluorescence of humic substances. These protein-like fluorophores have a recent algal or bacterial origin and correspond to a labile fraction of DOM (Determann et al., 1998). It has also been shown that the fluorescence intensity of protein-type compounds may be used as marker of anthropogenic DOM sources (Baker and Inverarity, 2004; Baker et al., 2003; Meng et al., 2013).

Observations of the protein-like band have been used to establish the dynamics of DOM in relation to its biological reactivity (Yamashita and Tanoue, 2003). These fluorophores have been noticed in samples not only from seawater, but also from freshwater and sediment pore waters (Baker et al., 2004, 2003; Burdige et al., 2004).

The fluorescence properties of FDOM are substantially influenced by several factors in natural waters: origin of FDOM (Aoki et al., 2008; Cammack et al., 2004), photodegradation of FDOM (Brooks et al., 2007; Miller et al., 2009; Moran et al., 2000), microbial degradation of FDOM

(Ma and Green, 2004; Moran et al., 2000; Mostofa et al., 2007), complex formation of FDOM with trace elements (Fu et al., 2007; Wu et al., 2004a, 2004, 2004b), salinity (Coble, 1996; Determann et al., 1996; Laane and Kramer, 1990), pH (Baker et al., 2007; Henderson et al., 2009; Spencer et al., 2007; Zhang et al., 2010), and temperature (Henderson et al., 2009).

To find out more useful information in EEM spectra, parallel factor analysis (PARAFAC), a statistical modeling approach, has been successfully applied to decompose EEMs of complex mixtures in aqueous solution into their individual fluorescent components (Bro, 1999, 1997; JiJi et al., 2000; Stedmon and Bro, 2008; Stedmon et al., 2003). The combination between EEM and PARAFAC is widely applied to determine the fluorescent DOM components in rivers and freshwaters (Baghoth et al., 2011; Chen et al., 2013; Chen M. et al., 2010; Fellman et al., 2009; Holbrook et al., 2006; Hood et al., 2005; Stedmon et al., 2011), lakes (Borisover et al., 2009; Cory and McKnight, 2005; Hua et al., 2010; Kothawala et al., 2012; Zhang et al., 2011), wetlands (Fellman et al., 2008a; Holbrook et al., 2006), estuaries (Dalzell et al., 2009; Guo et al., 2011; Stedmon et al., 2003; Yamashita et al., 2008), coastal and marine waters (Cawley et al., 2012; Chari et al., 2012; Guéguen et al., 2011; Jiang et al., 2008; Kowalczuk et al., 2010; Murphy et al., 2008; Stedmon et al., 2007b; Yamashita et al., 2010), wastewaters (Baghoth et al., 2011; Guo et al., 2010, 2012; Jiang et al., 2008), and soil (Banaitis et al., 2006; Fellman et al., 2009, 2008b).

Stedmon et al. (2003) were the first authors who combined EEM spectroscopy with PARAFAC to characterize the fluorescent fraction of DOM in aquatic environments. In that study, five different fluorescent DOM components, including three components associated with UV humic-like material, one protein-like component associated with phytoplankton productivity and one unidentified component, were identified from 90 samples collected in August, 2001 in the catchment of a Danish estuary. This study showed a good agreement between the model components and previously identified peaks and suggested that PARAFAC modeling was an efficient method for the characterization of DOM with EEMs. However, this analysis was limited by the number of samples in the data set and this most likely resulted in the merger of two or more different fluorophore groups into one group. Thus, a much larger data set (1,276 samples) from the same region over a one year period was applied by the same techniques in order to characterize the DOM fluorescence in a more detailed manner (Stedmon and Markager, 2005a). Eight fluorescent components were then determined by the PARAFAC

modeling of a larger data set accounting for seasonal variability: four biogenic terrestrial, two anthropogenic, and two protein-like components were identified.

The PARAFAC model was also applied to South Atlantic Bight samples to identify six distinct components in the DOM fluorescence excitation emission spectra , including three terrestrial humic-like components, one marine humic-like component and two protein-like components (Kowalczuk et al., 2009). In this study the humic-like components dominated the EEMs composition of estuarine waters, while protein-like components were predominant in the Gulf Stream waters. The EEMs composition of coastal areas fringed by extensive salt marsh ecosystems is a mixture of terrestrial humic-like components and protein-like components, indicating significant microbial reprocessing and local production of DOM (Kowalczuk et al., 2009).

In another study, three PARAFAC components were validated for a dataset of 63 surface samples collected in Hudson Bay and Hudson Strait (Guéguen et al., 2011). The component C1 was present as a terrestrial humic-like component and it has been associated with high molecular weight and aromatic terrestrial organic matter. The component C2 was similar to the component 4 identified by Stedmon et al. (2003) and was attributed to microbially processed phytoplankton degradation or marine-like humic component. The component C3 was similar to the fluorescent protein-like component identified as component 5 in Stedmon et al. (2003) and as component 7 in Stedmon and Markager (2005a).

The PARAFAC analysis of DOM fluorescence was used to distinguish between the autochthonous and allochthonous origins of DOM (Chen et al., 2013; Chen M. et al., 2010; Murphy et al., 2008; Stedmon et al., 2007b; Zhang Yunlin et al., 2009). Stedmon et al. (2007b) applied fluorescence spectroscopy combined with PARAFAC analysis to study the nature of DOM within the sea ice compared with the underlying and source waters. This study suggested that DOM is composed of a mixture of material originated from biological activity within the ice and terrestrial material from the source waters from which the ice formed and that autochthonous material represented by protein-like fluorescent component dominated the fluorescence characteristics of the sea ice DOM. Zhang Yunlin et al. (2009) applied the PARAFAC analysis for 34 EEM spectra collected during a phytoplankton degradation

experiment and identified four distinct components, among which two marine-humic components originate from microbially processed phytoplankton degradation products.

PARAFAC can also be used to trace biological and photochemical production or degradation of DOM components (Cory and McKnight, 2005; Cory et al., 2007; Fellman et al., 2008b; Jacobson, 2012; Stedmon and Markager, 2005b; Stedmon et al., 2007a). Stedmon and Markager (2005b) used fluorescence spectroscopy combined with PARAFAC analysis to trace the production and removal of different DOM fractions produced during an experimental algal bloom. Seven independent fluorescent fractions, including five different humic-like fractions, two proteinaceous fractions, indicated differences in their spectral characteristic, production rates, and sensitivity to photochemical and microbial degradation processes. All humic fractions were derived from the subsequent microbial processing of algae-derived DOM, with the greatest production occurring under combined Si- and P-limiting conditions, while the two proteinaceous fractions were derived from the exponential growth of phytoplankton, irrespective of biomass composition. These authors concluded that fluorescenct autochthonous DOM is either derived directly from algae exudation or the subsequent microbial processing if algae-derived DOM and that photodegradation was an important sink for components identified from PARAFAC model (Stedmon and Markager, 2005b).

In addition, PARAFAC analysis of EEMs also allowed tracing DOM in relation to water quality parameters (Baghoth et al., 2011), in the studies of interactions between trace metals and DOM (Wu et al., 2011; Yamashita and Jaffé, 2008), in the identification of changes in the fulvic acid redox state (Cory and McKnight, 2005), in the study of pH effects on DOM (Chen and Kenny, 2007).

1.5. The fractionation techniques of DOM in aquatic environment

The properties of DOM in aquatic environment have been indicated to be unevenly distributed among different molecular size fractions owing to the heterogeneous nature of DOM. Piccolo indicated that shows an alternative understanding of the conformational nature of humic substances, which should be regarded as supramolecular associations of self-assembling heterogeneous and relatively small molecules deriving from the degradation and decomposition of dead biological material. A major aspect of the humic supramolecular conformation is that it

is stabilized predominantly by weak dispersive forces instead of covalent linkages (Piccolo, 2012).

Studies about the molecular size distribution of DOM help in better understanding the physical and chemical characteristics of DOM in aquatic ecosystems. A number of analytical techniques have been utilized to fractionate DOM based on solubility (solvent extraction and freeze-drying), size (ultracentrifugation, ultrafiltration, size-exclusion chromatography, and field flow fractionation), hydrophobicity and so on. In this chapter, we briefly focus on describing three popular techniques commonly used to determine the size distribution of DOM in the aquatic environments: ultrafiltration (Amon and Benner, 1996; Huguet et al., 2010; Tadanier et al., 2000; Yoshioka et al., 2007; Zhao et al., 2006), size-exclusion chromatography (Her et al., 2003; Hongve et al., 1996; Lanxiu et al., 2004; Peuravuori and Pihlaja, 1997; Schäfer et al., 2002; Swietlik and Sikorska, 2006) and field flow fractionation (Alasonati et al., 2010; Assemi et al., 2004; Beckett et al., 1987; Cuss and Guéguen, 2012; Chin et al., 1994; Guéguen and Cuss, 2011; Lyvén et al., 1997; Moon et al., 2006; Reszat and Hendry, 2005; Sharma et al., 1993; Yohannes et al., 2005).

1.5.1. Fractionation by tangential ultrafiltration

Tangential ultrafiltration or cross-flow ultrafiltration is an effective technique largely applied to separate the constituents of DOM according to their molecular size without using solvent or buffer. This technique does not require any changes in pH of the sample. The DOM constituents are separated into two fractions, retentate and permeate, under the effect of the pressure. Molecules having molecular weights larger than the pore size of the used membrane are retained and concentrated in the retentate fraction. Conversely, molecules with molecular weight smaller than the pore size of the membrane pass through the membrane in the filtrate or permeate.

Guéguen et al. (2002) used tangential flow filtration with the regenerated cellulose membrane of 1 kDa molecular weight cut-off to study size fractionation of natural dissolved organic matter in the water samples from the central part of Lake Geneva (Switzerland-France), the Vistula River (downstream from Cracow, Southern Poland) and the Adour estuary (Basque Country, south-western France). The tangential flow filtration performance in the separation of

humic substances was evaluated by absorbance, fluorescence and DOC measurements. Fluorescence measurements indicated that the ultrafiltration correctly isolated the smaller compounds in permeate and the higher ones in retentate. Furthermore, the authors concluded that high ionic strength and high DOC contents did not enhance membrane fouling and that the natural organic colloids fractionations by tangential flow filtration were reliable and efficient in aquatic systems (Guéguen et al., 2002).

Tangential ultrafiltration was also applied to investigate the molecular size distributions of DOM in the Lake Biwa and Lake Baikal watersheds, Japan (Yoshioka et al., 2007). The results indicated that the relative contribution of the <5 kDa fraction accounted for 58%-68% and 44%-56% of DOM in Lake Biwa and Lake Baikal watersheds, respectively. The fraction of 5 kDa-0.1 μm contributed to 21%-40% DOM for the former watershed and to 43%-56% for the latter one. The relative contribution of the 0.1 μm-GF/F fraction to DOM concentration was roughly 2% in both watersheds. In the combination with three-dimensional fluorescence measurements, protein-like substances were shown to be associated with the 0.1 μm-GF/F fraction of DOM, while humic-like components were found in two remained fractions. However, the humic-like fluorescence peak position of the <5 kDa fraction was observed at the shorter wavelength region compared with that of the 5 kDa-0.1 μm fraction.

In previous studies, the size distribution of fluorescent dissolved organic matter (FDOM) was investigated by Huguet et al. (2010) in estuarine waters on the French Atlantic coast. Three membranes of smaller molecular weight cut off (MWCO) points were used (3 kDa, 1 kDa and 0.5 kDa) and the results were compared to the work of Yoshioka et al. (2007). DOM was dominated by the high molecular weight compounds (> 1 kDa) in the estuarine turbidity maximum (ETM) and in the upstream part of the Seine Estuary, while a high DOC proportion was observed in the smallest size fraction (< 0.5 kDa) in the Gironde Estuary. These differences were explained by the fact that the Seine Estuary was subjected to the impact of human activities in big cities and to fluvial inputs from the eutrophic Seine River while the Gironde Estuary is one of the less human-impacted estuaries in Europe. The combination of cross-flow ultrafiltration and EEM spectroscopy supplied more information about DOM properties in these areas. Indeed, the smallest size fraction (< 0.5 kDa) of non-marine samples was characterised by a lower aromaticity and higher autochthonous DOM components,

whereas the higher molecular fractions of fresh and brackish water samples were dominated by humic-like fluorescence signature.

One of the main advantages of ultrafiltration technique is that it is based on physical criteria and it does not involve chemical reagents, thus avoiding any change in the structure of organic molecules (Matar, 2012). However, the apparent molecular weight distributions determined by ultrafiltration fractionation of DOM may be influenced by a number of parameters (Leenheer and Croué, 2003). These parameters include pH, ionic strength or membrane types. In addition, although ultrafiltration allows large quantities of size-fractionated DOM to be isolated for structural, elemental or isotopic analyses, only discrete fractions of materials can be isolated using this method (Guéguen and Cuss, 2011).

1.5.2. Fractionation by size exclusion chromatography (SEC)

Size exclusion chromatography (SEC) is a chromatographic technique in which molecules in solution are separated on the basis of their molecular sizes and it has been applied to fractionate large molecules or macromolecular complexes. The separation by SEC is based on differential permeation of molecules of various sizes into a porous matrix. When the sample is injected into the column, the larger compounds permeate the matrix pores to a less degree than the small components and are retained shorter. Thus, the larger components will be eluted first and the smallest one will be eluted last.

High pressure size exclusion chromatography (HPSEC) has been commonly used to determine the molecular weight distribution of DOM in both aquatic and terrestrial environments (Alasonati et al., 2010; Hongve et al., 1996; Swietlik and Sikorska, 2006). This method is non-destructive, relatively fast and requires small amounts of samples and no sample pre-treatment (Matilainen, 2007).

Hongve et al. (1996) applied HPSEC technique for molecular size characterization of humic substances in surface waters from southern Norway. Two different kinds of SEC columns, silica and polymer-based columns, were used to characterize humic substances according to their molecular size distributions and optimal conditions of mobile phase correlated with each column were investigated in order to reduce unwanted interactions with the support material.

Using 0.02 M phosphate buffer, pH 6.5 and 0.02 M neutral salt solution were recommended for the silica and polymer-based columns, respectively. With the polymer-based column, the neutral salts were used as mobile phase in order to avoid corrosion and degradation of the support material. Adjusting the pH of the mobile phase and natural water samples was not necessary. Moreover, calibration curves for molecular weights of humic substances were constructed by using polystyrene sulfonates of known molecular weight (Hongve et al., 1996).

Peuravuori and Pihlaja (1997) used HPSEC to study the molecular size distribution of DOM from two lakes: Lake Savojärvi and Lake Mekkojärvi, Finland. These authors indicated that applying sodium acetate as an eluent on a TSK G3000SW high-speed column provided illustrative information about the nature of DOM that was not available with phosphate buffer and that aquatic humic substances contained some very large-sized through minor constituents, leading to a fairly polydisperse mixture. In comparison with the results obtained from vapor-pressure osmometry, averaged molecular weights obtained by using HPSEC system were 4-5 times greater.

High pressure size exclusion chromatography combined with specific UV absorbance and total luminescence spectroscopy were used to study the composition of the six NOM fractions isolated on XAD resins (Swietlik and Sikorska, 2006). These are humic acids, hydrophobic acids, hydrophobic neutrals, hydrophilic acids, bases and neutrals. The results showed that humic acids and hydrophobic acids comprised high content of complex, aromatic, high molecular weight subunits, while hydrophobic neutrals and hydrophilic acids and bases were characterized by components with lower molecular sizes and lower degree of condensed aromatic moieties. The results also indicated that hydrophilic neutrals were constituted by non-humic, more aliphatic and low molecular weight compounds and that hydrophilic acids and neutrals as well as hydrophobic neutrals contained protein-like constituents.

Her et al. (2003) applied high performance liquid chromatography (HPLC)-size exclusion chromatography (SEC) combined with sequential on-line detectors consisting of UV, fluorescence, and quantitative DOC measurement to investigate the composition of DOM according to apparent molecular weight in three types of samples: ground water (Irvine Ranch), surface water (Barr Lake) and wastewater secondary effluent (Hawaii). Five different molecular size fractions were identified for each sample based on the DOC chromatograms.

Among all fractions, the DOM fraction in the medium apparent molecular weight range (5000-1000 g mol^{-1}) presented the highest aromaticity for all samples. The DOM fraction in the low apparent molecular weight range (below 680 g mol^{-1}) comprised additional aliphatic organic matter for Irvine Ranch ground water and protein-like substances for Barr Lake surface water. The results also indicated that DOM fraction correlated to the high apparent molecular weight range (over 10,000 g mol^{-1}) was composed of polysaccharide-like compounds for Irvine Ranch ground water and a mixture of polysaccharide-like/protein-like substances for Barr Lake surface water and wastewater secondary effluent and that there was a small amount of fulvic-like substances found in the wastewater secondary effluent sample.

1.5.3. Fractionation by flow field flow fractionation

Field flow fractionation (FFF) was first proposed in 1966 by Giddings as an analytical separation method for macromolecules, colloids, and particulates. It is a versatile technique, capable of fractionating and characterizing materials in a wide range of size distribution extending from roughly 2 nm to 100 μm (Nilsson, 2013).

FFF is a family of chromatography-like elution techniques in which the separation is achieved within a very thin, flat channel. A separation field (flow field, thermal field, gravitational field, sedimentation field, electromagnetic field…) is applied perpendicularly to the direction of the mobile phase flow to bring analytes close to the bottom of the channel wall (accumulation wall), and a diffusion field separates them against the accumulation wall according to their size: larger size analytes will move close to the accumulation wall while smaller size analytes migrate farther away. As a result, and due to the parabolic flow profile, the smallest size analytes will be eluted earlier, while the largest ones will be eluted last (Figure 1.4). The more detail information of size-different analytes will be obtained by on-line hyphenating to a wide range of detectors or collecting sample fractions for further off-line analysis. Typically, the most commonly utilized detectors with flow field flow fractionation (FlFFF) are UV-Vis and fluorescence detectors, laser light scattering (MALLS), dynamic light scattering (DLS), and differential refractive index (RI).

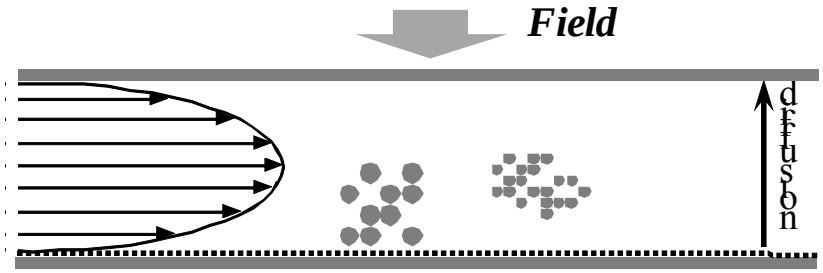

Figure 1.4 Basic separation principle of flow field flow fractionation

There are some important variables with FlFFF used for separation of DOM – the mobile phase composition (MP), the cross-flow rate (CF), the channel dimensions, the quantity of analyte injected, the relaxation time (focus time), the membrane (material and pore size cut-off).

Studies carried out using FlFFF for the analysis of DOM are summarized in Table 1.3.

Table 1.3 Summary of FlFFF operational conditions and main conclusions of DOM studies. Note: AF4 asymmetric flow field flow fractionation; FIFO–FlFFF, frit inlet/frit outlet–flow field-flow fractionation; MP, mobile phase; DF, detector flow rate; FF, cross-flow rate during focusing time; CF, cross-flow rate during elution time

Aim of study	Sample types and location	System	FFF parameters	Main conclusions and comments	References
Determination of the molecular weight distribution of humic substances	Terrestrial and freshwater samples (rivers, soil, peat bog, and lignite coal)	FlFFF UV_{254} 10 kDa PES	MP: 0.05 M Triss, 0.0268 M HNO3, 0.00308 M NaN3; pH 7.9 PSS standards	Aquatic humic substances were smaller than those found in soils. Fulvic acids were smaller than humic acids.	(Beckett et al., 1987)
Optimization of FlFFF technique to determine the size distributions of low molecular weight colloidal material	A marine surface sample from the central Baltic Sea A freshwater sample from a small creek, Delsjöbäcken	FlFFF UV_{270} 1 and 10 kDa RC 1 kDa PES 0.5 kDa YC05	Spacer 350 µm focus time 6 min MP: 10 mM borate with 20 mM NaCl or 25 mM Tris with 20 mM NaCl DF: 0.5 ml min^{-1} FF: 1.2 ml min^{-1} CF: 3.8 ml min^{-1} PSS standards	The optimized conditions for focus time, flow rates, carrier solution and membrane type. Two different mobile phases based on Tris and borate buffers were evaluated with respect to analyte loss rate. The results indicated a decrease in loss rates as well as in plate height when increasing the ionic strength of mobile phase by adding NaCl. The detection limits were 0.09 µmol L^{-1} and 9 µmol carbon L^{-1} for 1430 M_w PSS and natural samples, respectively.	(Lyvén et al., 1997)
Studying the behavior of humic acids when varying the pH and the ionic strength of the solution	Soil along the coast of North Carolina Sand trap in the water treatment plant in Denver, Colorado Sphagnum peat in Thoreau's Bog near Boston, Massachusetts	AF4 UV_{280} UF-C-5 membrane	Spacer 245 µm MP: $CaCl_2$ solution DF: 0.10 ml min^{-1} CF: 3.90 ml min^{-1} PSS standards	When the MP concentration increased, the size distributions of humic acids broaden and became multimodal. The humic acids aggregated severely at pH < 4.	(Schimpf and Wahlund, 1997)

Aim of study	Sample types and location	System	FFF parameters	Main conclusions and comments	References
Determination of the size and molecular weight distributions of various aquatic humic acids of different origins	Groundwater from the Gorleben aquifer and the Boom clay	FlFFF UV_{254} 5 and 10kDa RC 2 and 4 kDa PES	MP: 5 mM Tris, pH 9.1 DF: 1 ml min^{-1} CF: 2 ml min^{-1}PSS standards	Humic substance recovery decrease dramatically with increasing cross flow, increasing ionic strength and decreasing pH. Better recovery (less adsorption) with RC membrane than with PES membrane. Low ionic-strength carrier gave overloading with PSS, but not with humic substances	(Ngo et al., 2001)
Characterization of CDOM in river and coastal waters	River and coastal waters from Florida	FIFO-FlFFF UV-Vis DAD, EEM 3 kDa RC	MP: 0.005% FL-70; 0.05 M Tris and 0.029 M HCl; pH 8 DF: 1.4 ml min^{-1} CF: 4.0 ml min^{-1} PSS standards	FIFO increased sensitivity by an order of magnitude and presented a wide dynamic range of molecular weights and concentrations of CDOM. Low recovery rates (35–65% for fresh waters and 5.7–8.1% for marine waters). ~98% of CDOM were found in 2kDa fraction and ~2% in a larger 13 kDa size fraction.	(Zanardi-Lamardo et al., 2001)
Determination of the size continuum of colloidal CDOM in coastal waters	The Birdfoot region of the Mississippi River delta and the adjacent Atachafalya River	FlFFF UV_{254} 1 kDa RC	Spacer 254 µm DF: 0.4 ml min^{-1} FF: 5.0 ml min^{-1} CF: 4.0 ml min^{-1} PSS standards	Recoveries of the small-sized matter were roughly 35% owing to the fact that the smallest colloidal matter was forced through the 1 kDa membrane under the flow conditions used. Colloidal size distributions in nearshore surface waters contained a mixture of features observed in offshore waters, plume waters, and in phytoplankton cultures. Plume waters had a high abundance of larger colloidal phases but continued dilution with coastal waters led to preferential losses of mid-sized colloidal matter. Size fractogram of colloidal CDOM in offshore waters of the the Gulf of Mexico during spring and in estuarine waters after the spring bloom were similar.	(Wells, 2004)

Aim of study	Sample types and location	System	FFF parameters	Main conclusions and comments	References
Determination of relative molar mass (RMM) distributions of both UV absorbing and fluorescent CDOM	the Baltic proper, Kattegatt and Skagerrak seas	FlFFF UV_{270}, E_x/E_m=350/450nm 1 kDa RC	Spacer 225 µm MP: borate 10 mM and NaCl 190 mM (pH 8.2) PSS standards	The RMM for fluorescence decreased from the brackish to the marine surface waters while the RMM of UV absorbance increased. The integrated detector signals of both UV and fluorescence decreased with increasing salinity but the fluorescence to UV ratios in surface water were lower than in Baltic, Kattegatt and Skagerrak deep waters. There was a reverse relation between salinity and the RMM distribution derived from UV detection, whilst the relation between salinity and the RMM distribution derived from fluorescence was parallel. The specific UV absorbance taken as a proxy of the aromaticity of the chromophoric organic material showed decreasing trend with both increasing salinity and increasing UV derived weight average relative molar mass.	(Hassellöv, 2005)
Optimizing a conventional total organic carbon (TOC) analyzer for use with a FFF-UV system to characterize DOC. Comparison between the FFF-DOC and FFF-UV results	Groundwater samples in Saskatchewan, Canada Surface water samples in a boreal forest in central Alberta, Canada Suwannee River (SW) humic standards	AF4 DOC, UV_{254} 1 kDa RC	Spacer 225 µm MP: 0.005 M Na_2SO_4, 0.003 M NaN_3 DF: 1.5 ml min^{-1} CF: 3.5 ml min^{-1} PSS standards	Compared to results derived from UV analysis, molecular weight determinations in the samples and standards derived from DOC analysis were 6-30% lower. DOC detection may be a more accurate method to characterize molecular weight of the DOC than UV detection Differences in the relative amounts of aromatic and aliphatic carbon in DOC were distinguished by using a normalized intensity comparison method to compare the two detector (UV and TOC) responses.	(Reszat and Hendry, 2005)

Aim of study	Sample types and location	System	FFF parameters	Main conclusions and comments	References
Investigation of the influence of pH, ionic strength of the buffer, and the binding of PAHs on the particle sizes of **humic substances**	Water samples from the Vantaa and Mätäjoki rivers in the Helsinki area and seawater from Finnish territorial waters	AF4 UV_{254} 10 kDa RC	Spacer 500 µm MP: 0.02% NaN_3, NaCl with 0.1% Fl 70 at pH 10.0; or 20 mM Tris at pH 9.1 and pH 8.0; or 20 mM phosphate at pH 6.5 and 3.8 PSS standards	Particle sizes of HSs in acidic medium with phosphate buffer were greater than in alkaline medium or in acidic medium with acetate buffer, The total particle size of HS did not change when HS were associated with PAH. Particle sizes in river water and seawater were mostly similar to the standards HSs. Some larger particles (30–70 nm) were also found in natural waters.	(Yohannes et al., 2005)
Investigation of the size distribution of marine CDOM and its optical variability as a function of phytoplankton bloom dynamic	Water samples from the Damariscotta River Estuary (Walpole, Maine)	FlFFF UV_{254}, EEM 1 kDa	Spacer 200 µm PSS standards	Two size fractions of CDOM were identified, corresponding to materials 1-5 kDa and 13-150 kDa. A protein-like peak dominates the small colloidal fraction, while a humic-like fluorescence signature was identified in the larger fractions. The humic-like fluorophore in the large colloidal matter was blue shifted with decreasing colloid size. This size-related blue shift reflected in-situ degradation or the release of new matter rather than the presence of terrestrially derived colloidal matter. Marine CDOM comprised subcomponents that could exist physically distinctly from other constituents. The changes in the contributions of DOM fractions will be the key to predict insights to marine CDOM behaviour.	(Boehme and Wells, 2006)

Aim of study	Sample types and location	System	FFF parameters	Main conclusions and comments	References
Investigation of the continuous colloidal size spectra of CDOM, humic-type and protein-type fluorescent organic matter Tracing elements in three rivers with different water chemistries	The lower Mississippi River, the Atchafalaya River and the Pearl River in the northern Gulf of Mexico	FlFFF UV_{254}; ICP-MS $Fluo_{350/48}$ $Fluo_{350/4500}$ $Fluo_{310/420}$ $Fluo_{275/340}$ 1kDa PES	MP: 15 mM NH_4Cl, pH 8 for river samples 55 mM NH_4Cl, pH 8 for seawater samples DF: 0.5 ml min^{-1} CF: 3.0 ml min^{-1} FF: 4.5 ml min^{-1} PSS standards	3-4 colloid populations were presented as follows. 0.5-4 nm CDOM-colloids binds most elements. 3-8 nm protein-like colloids bind P in seawater. 5-40 nm Fe-rich colloids bind P, Mn, Zn, and Pb. The >40 nm fraction contained largely protein-like colloidal matter, Fe, P, Mn and Pb. The CDOM-colloids represent terrestrial fulvic acid; and the protein-like colloids mostly originate from in situ biological production; while the iron-rich colloids are largely inorganic and contain Fe(III)-hydroxide/oxyhydroxide. The colloidal concentrations were generally much higher in the Pearl River than in the the Mississippi and the Atchafalaya Rivers. They decrease seaward in the Gulf of Mexico. In comparison with the Pearl River, the Mississippi and Atchafalaya Rivers presented the largest size distribution of protein-like organic matter, Fe-rich colloids and associated elements.	(Stolpe et al., 2010)

Aim of study	Sample types and location	System	FFF parameters	Main conclusions and comments	References
Investigation of the role of the spatial and temporal variability of the fluvial system on the size and molar mass of colloidal organic matter.	Colloidal samples in the Amazon River basin (Brazil)	AF4 UV, MALLS 1 kDa; 10 kDa RC	MP: 10 mM $NaNO_3$; pH 5.7 For 1 kDa membrane: DF: 1 ml min^{-1} FF: 3.09 ml min^{-1} CF: 3 ml min^{-1} For 10 kDa membrane: DF: 1 ml min^{-1} FF: 4.09 ml min^{-1} CF: 0.25 ml min^{-1} PSS standards	There was a decrease in size of the colloidal matter when passing from first order streams to higher order rivers. There were no significant changes in sizes of samples collected during the low and high flow stages at the same site, while the average molar mass was found to be weakly shifted towards higher values in samples acquired during the high-flow period. The colloidal organic matter average molar masses reduced around 40%, when passing from small to large watercourses. Sample pre-treatments with ultrafiltration and reverse osmosis did not influence significantly the size characteristics of samples.	(Alasonati et al., 2010)
Analysis of the fine scale distribution of size-based optical properties of aquatic DOM	freshwater samples from the Athabasca and Otonabee rivers, Canada	AF4 UV-Vis DAD $Fluo_{270/460}$ $Fluo_{355/460}$ 0.3 kDa PES	Spacer 500 µm MP: 58 ppm NaCl DF: 0.3 ml min^{-1} FF: 3.3 ml min^{-1} CF: 3.5 ml min^{-1} Standards: rhodamine B, Trypan blue, vitamin B12, bovine heart cytochrome C, hen egg white lysozyme and bovine serum albumin	A red-shift in emission and excitation wavelength maxima associated with lower spectral slope ratios was related to higher MW DOM. There was a significant difference in optical properties of DOM derived from different origins at similar MW. Freshwater DOM is not a uniform matrix of organic molecules, but rather consists of a range of constituents that have different molecular sizes and optical properties.	(Guéguen and Cuss, 2011)

Aim of study	Sample types and location	System	FFF parameters	Main conclusions and comments	References
Study of physicochemical properties of CDOM in unperturbed freshwaters, sampled weekly at three depths from a drinking water treatment plant reservoir	the Beaver Lake Reservoir on the White River in northwest Arkansas	AF4, PARAFAC UV_{254}, EEM 0.3 kDa PES	Spacer 410 µm MP: 1 mM NaCl DF: 0.3 ml min^{-1} FF: 4.0 ml min^{-1} CF: 4.0 ml min^{-1} PSS standards	The intensities and SUVA values of 10-m depth samples were higher than those of the 3- and 18-m depth samples. The Beaver Lake water CDOM was comprised of relatively low molecular weight aromatic carbon-containing molecules with no measured colloidal fraction (3000–100,000 Da). Five principal components were identified by PARAFAC analysis, including three humic-like components, a protein-like component and a component which was attributed to instrument noise and discarded. The Beaver Lake water CDOM and type of fluorophores were stratified by depth.	(Pifer et al., 2011)
Assessing the MW properties of PARAFAC components in DOM	Leaf litter from red maple, bur oak and white spruce	AF4 UV_{254}, EEM PARAFAC 0.3 kDa PES	MP: pH 6 and conductivity 120 µS cm^{-1} (adjusted by NaOH and NaCl) DF: 0.4 ml min^{-1} CF: 2.5 ml min^{-1}	Tyrosine/polyphenol-like fluorescence was significantly correlated with the smallest size group (relative molecular weight = 310 ± 10 Da), microbial humic-like and terrestrial visible humic-like fluorescence with the intermediate size group (1600 ± 150 Da), and terrestrial humic/fulvic-like and tryptophan/polyphenol-like fluorescence with the largest size group (4300 ± 660Da).	(Cuss and Guéguen, 2012)

The FlFFF technique has the following main advantages: (i) separating a wide range of NOM sizes continuously (1 nm to 100 μm), (ii) fractionation of DOM by FlFFF based on its diffusion coefficient which is a key parameter relating to DOM behavior in aquatic systems, (iii) no stationary phase is required so reducing the interactions between the sample and the stationary phase (iv) no upper molar mass size limit in opposite to SEC (Wahlund, 2013), and (v) coupled either on-line or off-line to a wide range of detectors. However, like any techniques, the FlFFF technique also has drawbacks, the most important are: (i) sample dilution, (ii) loss of material through the membrane or by interaction or adsorption of sample on the membrane surface.

1.6. Conclusions

To sum up, dissolved organic matter is a heterogeneous, complex mixture of compounds with wide ranging chemical properties and diverse origins. It is well known to interact with pollutants and to affect their transport and their fate in aquatic environment, and plays a vital role in the global cycling of carbon. Thus, the study of dissolved organic matter is of major environmental interest in order to trace variability of DOM properties as well as to identify its sources in the aquatic environment. As we have emphasized throughout this chapter, the properties of DOM in aquatic ecosystems have been implicated to be unevenly distributed among different molecular size fractions owing to the heterogeneous nature of DOM. Studies about the molecular size distribution of DOM will help in better understanding the physical and chemical characteristics of DOM in aquatic environments. Several techniques of DOM fractionation were mentioned in this chapter. Among them, flow field-flow fractionation (FlFFF), a size-fractionation technique, has been used to fractionate DOM across the size continuum.

1.7. Objectives

DOM plays a key role for the fate of organic and inorganic contaminants in the aquatic environment, influencing their speciation and their bioavailability. It plays also a vital role in the global cycling of carbon and is a key parameter related to drinking water treatment.

This PhD thesis was performed within the framework of the PIREN-Seine research program. The primary aim of this work was to investigate the characteristics of DOM within the Seine

River catchment in the Northern part of France. In order to achieve this aim, the objectives of this work are as follows:

The first objective was the investigation of the optical properties of DOM within the Seine River catchment. UV/visible absorbance and excitation emission matrix (EEM) fluorescence spectroscopy, combined with Parallel Factor Analysis (PARAFAC) and Principal Component Analysis (PCA), have been used to characterize colloidal DOM in this river watershed in order to estimate DOM sources as well as spatial and temporal variability of DOM properties. The assessment of both quantitative and qualitative variations of DOM optical properties is the object of chapter III.

Another objective of this study was to develop an asymmetrical flow field-flow fractionation technique (AsFlFFF or AF4) for determining the size distribution of DOM from natural waters without pre-concentration before injecting into the AF4 separation channel. The chapter IV concerns the optimization of the operating parameters for the AF4 system, such as focus or relaxation time, cross flow rate and cross flow mode.

In chapter V, the size distribution of DOM was investigated in the Seine River catchment. The characterization of the weight averaged molecular weight (M_w), number-averaged molecular weight (M_n), molecular weight at the peak maximum (M_p) and polydispersity (M_w/M_n) of DOM were determined by using online UV detector hyphenated to AF4. The characterization of the different DOM fractions isolated was investigated by using off-line EEM fluorescence spectroscopy.

CHAPTER II: MATERIALS AND METHODS

2.1 Study area

The Seine River catchment (75,000 km^2) in the Northern part of France is characterised by a high population of some 16 million inhabitants (28% of the total French population), mainly present in the urban area of Paris (Even et al., 2007). It represents an important example of regional territory strongly influenced by anthropogenic activity (Billen et al., 2007). Figures 2.1; 2.2 and 2.3 show the catchment together with locations for water samples that were collected from 23, 39 and 40 sites in November 2011, September 2012 (low-water) and February 2013 (flood) respectively. The full description of all samples and their codes are listed in Table 2.1. After collection, all samples were immediately filtered through a pre-combusted glass fibre filter (GF/F 0.7µm; Whatman) and stored in the dark at 4°C until analyses.

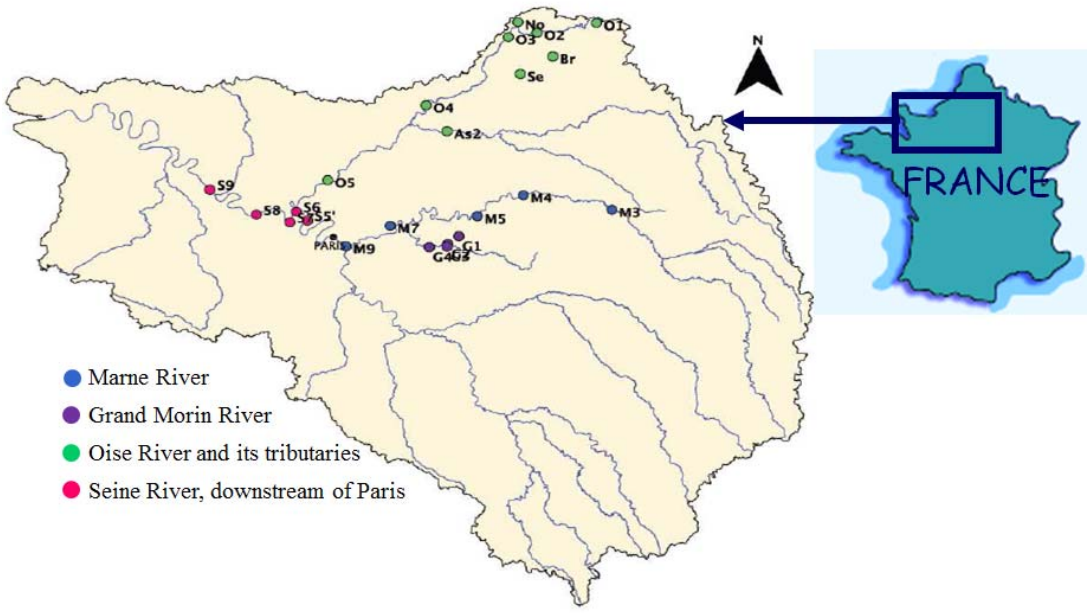

Figure 2.1 Location of sampling sites in 2011 in the Seine River catchment, France (Varrault et al., 2013)

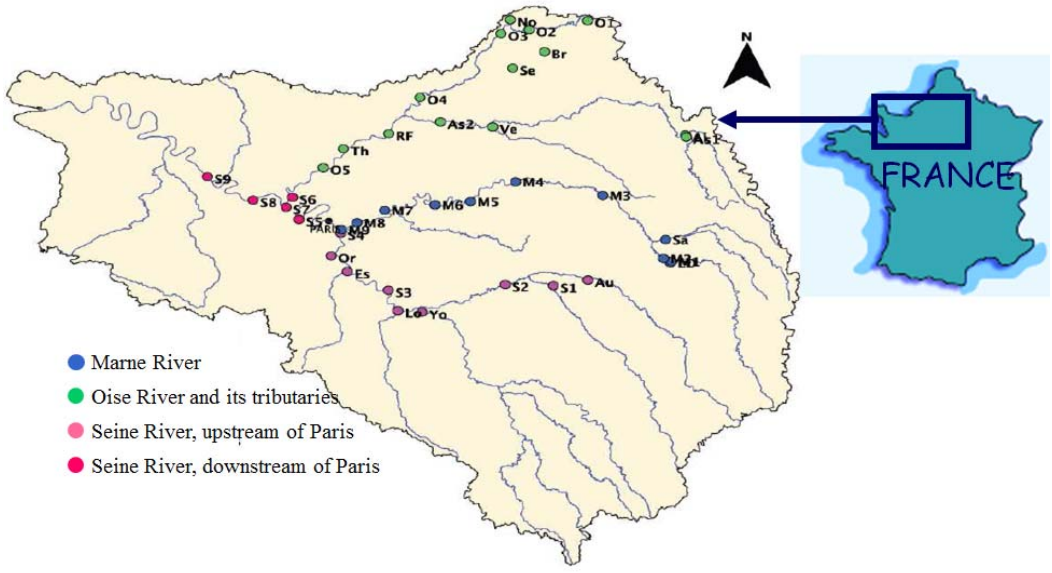

Figure 2.2 Location of sampling sites in 2012 (low-water) in the Seine River catchment, France (Varrault et al., 2013)

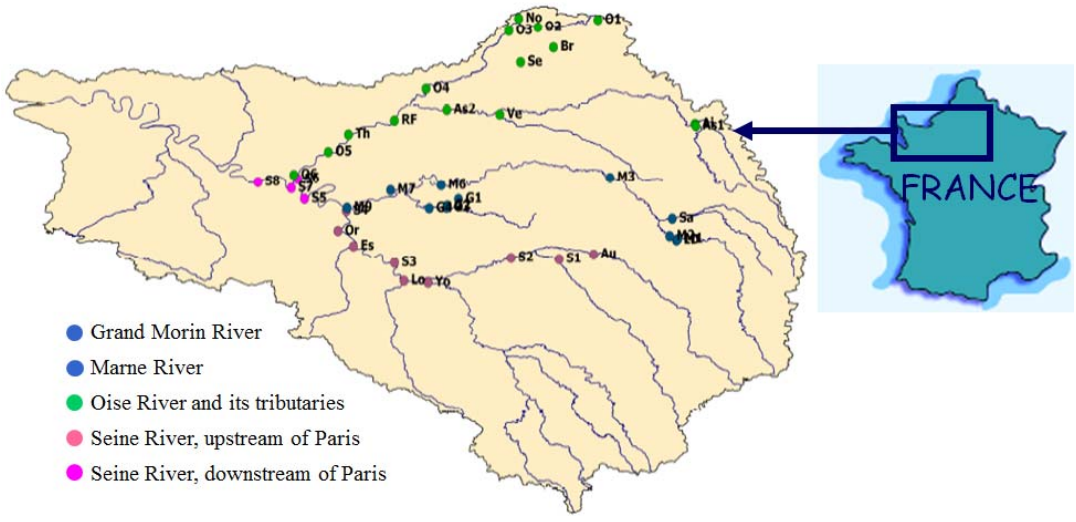

Figure 2.3 Location of sampling sites in 2013 (flood) in the Seine River catchment, France (Varrault et al., 2013)

Table 2.1 List of sampling sites and their codes

Basin	Sample name	Code	Basin	Sample name	Code	Basin	Sample name	Code
Grand Morin	Rû de Fosse Rognon (Melarchez)	G1	**Oise**	La vesle (Ciry)	Ve	**Seine**	Aube (Arcis/Aube)	Au
	Rû des Avenelles (Moulin)	G2		Aire (Termes or Grandpré)	Ai		Essone (Corbeil-Essonne)	Es
	Rû de l'Orgeval (Theil)	G3		Aisne (Senuc)	As1		Loing (Moret/Loing)	Lo
	Grand Morin (Tresmes)	G4		Aisne (Vic/Aisne)	As2		Orge (Savigny/Orge)	Or
Marne	Lac de Der (Arrigny)	LD		La rivière brune (Houry)	Br		Seine (Mery / Seine)	S1
	Marne (Larzicourt)	M1		Le Noirrieu (Tupigny)	No		Seine (Marnay /Seine)	S2
	Marne (Moncetz l'Abbaye)	M2		Oise (Forêt Hirson)	O1		Seine (Fontaine le port)	S3
	Marne (Matougues)	M3		Oise (Proisy)	O2		Seine (Alfortville)	S4
	Marne (Dormans)	M4		Oise (Macquigny)	O3		Seine (Bougival)	S5
	Marne (Saulchery)	M5		Oise (Ribécourt-Dreslincourt)	O4		Seine (Conflans St Honorine)	S6
	Marne (Sammeron)	M6		Oise (Beaumont/Oise)	O5		Seine (Poissy)	S7
	Marne (Annet/Marne)	M7		Oise (Neuville/Oise)	O6		Seine (Porcheville)	S8
	Marne (Neuilly/Marne)	M8		Ruisseau forestier Compiègne	RF		Seine (Vernon)	S9
	Marne (Saint Maurice)	M9		La serre (Crecy/Serre)	Se		Yonne (Cannes-Ecluse)	Yo
	La Saulx (Virty en Perthois)	Sa		Le Therain (Cramoisy)	Th		Seine (Maison-Laffite)	S5'

2.2 Different methods for characterisation and fractionation of DOM

2.2.1 DOC measurement

Dissolved Organic Carbon (DOC) is the major component of DOM and it is generally used to quantify the DOM present in natural waters.

Measurements of DOC were performed at the IPGP-LGE (UMR CNRS 7154, Paris) using a Shimadzu TOC-V CSN mode NPOC (non-purgeable organic carbon). The filtered samples were acidified to 0.5% with 2N HCl (prepared from 30% hydrochloric acid superpure, Merck) and sparged for 6 minutes with synthetic air 5.0 to remove dissolved inorganic carbon. The water samples were then injected onto a combustion column packed with platinum-coated alumina beads held at 680°C (standard catalyst Shimadzu). Non-purgeable organic carbon compounds are combusted and converted to CO_2, which is detected by a non dispersive infrared detector (NDIR). The quantification is achieved by external calibration with standard solutions of potassium phthalate $C_6H_4(COOK)(COOH)$ (Shimadzu) at various concentrations. Different ranges of calibration are performed according to the DOC content of the samples.

For each sample, the result is the average of at least three measurements satisfactory in terms of standard deviation and coefficient of variation. The measurement accuracy is of the order of 0.3 mg C/ L.

2.2.2 UV-visible absorption spectroscopy

2.2.2.1 The principle of UV-visible absorption

Ultraviolet visible spectrometry (UV-Vis), electron spectrometry, is based on the electrons transition when they absorb energy from photons. Normally, photons are supplied via light source (deuterium and wolfram lamp for ultraviolet and visible wavelength region, respectively). In the Perrin–Jablonski diagram below (figure 2.4), the ground state (S_0) and exciting electron states (S_1, S_2) with are shown. In general, electrons at ground state, that absorbed energy from light, jump to excited state and then return to ground state and release energy via thermal energy. However, there are only valence electrons attending in transition

steps. In addition, the life time of electron transition is long enough meanwhile vibrational and rotational transitions are very short. The UV-Vis spectra with vibrational and rotational transitions can be only observed in vapor state via high resolution UV-Vis spectrometer. Because of so many possible transitions, each differing from the other by only a slight amount, each electronic transition consist a vast number lines spaced so closely that the spectrometer cannot resolve them. What is observed from those types of combined transitions is that the UV spectrum of a molecule usually consists of a broad band of absorption centered near the wavelength of the major transition. Therefore, the UV-Vis spectrum can be only observed in the Figure 2.4.

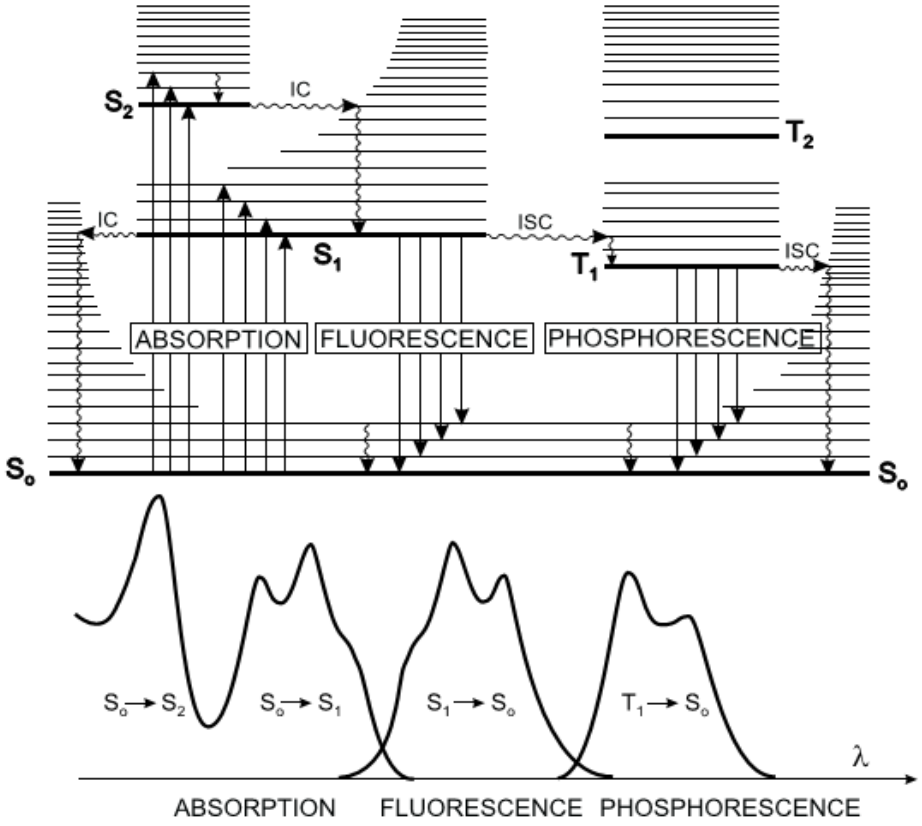

Figure 2.4 Perrin–Jablonski diagram and illustration of the relative positions of absorption, fluorescence and phosphorescence spectra (Valeur, 2001)

Chromophoric and colored dissolved organic matter (CDOM) is composed of optical active components of bulk DOM. They absorb light over a broad range of ultraviolet and visible range (200 – 900 nm). For fresh or marine waters, the intensities of DOM UV-Vis spectra generally decrease while increasing the wavelengths. A chromophore is defined as a part of an

organic molecular or functional group with or without electron-donating heteroatom such as N, O or S, as a functional group with a highly aliphatic carbon chain, or as a molecule with a structure that can hold up an electron or have conjugated π-π electron system which can absorbed light energy (photon) with significant efficiency, causing promotion from the ground state to an excited state. The key chromophores in a molecule or DOM in natural waters are: hydroxyl, aldehyde, ketone, carboxyl, methyl ester, methyl ether, primary amine, secondary amine, acetyl, S-, N-, O-containing functional groups and so on. All of these functional groups can be considered as key chromophores in fulvic and humic acids in natural water. The more chromophoric groups have a molecule, the more energy is absorbed from light, especially when the chromophores are combined together. Therefore, the light absorption efficiency is enhanced and the intensity of absorptivity is increased. In principal, the conjugation is increased in the molecule, the maximum absorbance is shifted to longer wavelength (red shift or bathochromic shift).

Photon absorption by a CDOM chromophore in aqueous solution firstly induces the excitation of an electron from its ground state to an excited one. Three types of electronic transitions occur commonly with the CDOM chromophores in natural waters due to the absorption of ultraviolet (UV) or visible (Vis) radiation:

(i) Transitions involving π, σ and n electrons

(ii) Transitions involving charge-transfer electrons between analytes, between analyte and solvent or vice versa.

(iii) Transitions involving d- and f- orbital electrons in the transition metals, especially in the complexes of natural organic matter with transitional metals e.g. complexes of fulvic acid with transition metals such as Cu(II) or Fe(III) (Voelker and Sulzberger, 1996), having unpaired electrons.

In general, the position of peaks is characteristic of a given compound or group of compounds in the solution. It strongly depends on the structure of compounds. As a result, ultraviolet visible spectra can be used to elucidate the structure and type of compounds. The determination of the structure of compounds can be based on the ground and exciting electron structures. However, the UV-Vis spectra only give information of electron structures, especially equivalent electrons of a group of compounds not of a particular component. Normally, the elucidation of the structure of compounds are performed with various

spectrometric techniques such as UV-Vis spectrophotometry, Fourier Transform Infrared spectroscopy (FTIR), Nuclear Magnetic Resonance (NMR) spectroscopy, mass spectrometry (MS). The more methods of spectrometry are used, the more information on the structure of organic targeted compound is obtained. The exact structure can then be elucidated. In summary, the UV-Vis spectra only supply the structure of the outer layer of electrons (valence electrons) in the molecule. The conjugated electron systems can be indicated by maxima wavelengths and their intensities.

For quantification of CDOM, the light absorbance in aqueous solution is directly proportional to the path length (l) in cm and CDOM concentration of absorbing species (c) in mol L^{-1}. The Beer's law states that

$$A = \varepsilon.l.c \qquad (2.1)$$

where: ε is a constant of proportionality called the molar absorption coefficient or molar extinction coefficient (L mol^{-1} cm^{-1}). The attenuation of radiation in the solution increases with increasing CDOM concentration. The classification of CDOM is based on the maximum wavelength (λ_{max}) at which the specific CDOM have highest light absorbance. In general, CDOM is classified into sub groups such as: humic substances, amino acids, sugar- and protein-like subgroups.

2.2.2.2 The UV-Vis spectrophotometer

UV-visible absorbance spectroscopy was used to determine DOM properties at natural pH. All surface water samples were allowed to warm to room temperature and the instrument was turned on 30 min before the sample analysis. The UV-visible spectrophotometer used (V-560, Jasco Corporation, Tokyo, Japan) is equipped with a deuterium discharge tube (190 to 350 nm) and an incandescent lamp with a tungsten filament (330 to 900 nm) and a double monochromator for the selection of wavelengths and a photomultiplier (which converts the received light intensity into an electric signal) as the detector. Absorbance is measured in the 200-700 nm regions with a 1 cm quartz cuvette using ultrapure water (Milli-Q, Millipore) as a reference. The measured absorbance at wavelength λ was converted to absorption coefficient a (m^{-1}) according to

$$a_\lambda = 2.303\ A_\lambda / l \qquad (2.2)$$

with A_λ, the absorbance and l, the path-length of the optical cell in meter (here 0.01 m). The wavelength dependence of absorption was parameterized with a non-linear exponential model according to

$$a_\lambda = a_{\lambda_0} . e^{-S(\lambda - \lambda_0)} \qquad (2.3)$$

where a_λ is absorption coefficient (m^{-1}), λ is wavelength (nm), λ_0 is reference wavelength (nm), and S is spectral slope (nm^{-1}) (Helms et al., 2008; Twardowski et al., 2004).

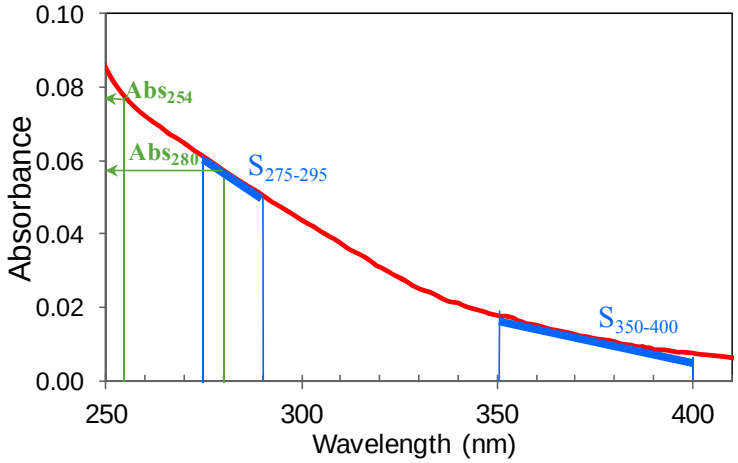

Figure 2.5 UV-visible absorption spectrum (sample Mery/ Seine-S1, 2012)

Two parameters, SUVA and percentage of aromaticity are generally used to characterize the aromaticity of a sample (Figure 2.5).

The SUVA parameter ("Specific UV Absorbance") is the ratio of UV absorbance at 254 nm on DOC concentration of sample. It is expressed in L mgC^{-1} m^{-1}. This parameter is used to assess the degree of aromaticity of the soluble organic matrix. It increases with the aromaticity and molecular weight of molecules (Chin et al. 1994). In general, a SUVA > 4 indicates mostly aquatic humic substances, relatively high hydrophobicity and high molecular weight, while SUVA in the range of 2-4 indicates a mixture of aquatic humic substances and other NOM, mixture of hydrophobic and hydrophilic NOM and a mixture of molecular weights (Edzwald and Tobiason, 1999).

$$SUVA = \frac{Abs_{254}}{[DOC]} \times 100 \qquad (2.4)$$

(with Abs_{254}, the absorbance at 254 nm and [DOC], the DOC concentration in mg C L^{-1})

The percentage of aromaticity from the absorbance at 280 nm

$$\text{Aromaticity}(\%) = 0.05 \times \frac{Abs_{280}}{[DOC]} + 6.74 \quad (2.5)$$

(with Abs_{280}, the absorbance at 280 nm and [DOC], the DOC concentration in mol L^{-1})

The absorption ratios can also be used to characterize the aromaticity of a sample. For example, the ratio called E_2/E_3 equivalent to the absorbance at 250 nm divided by the absorbance at 365 nm is often used to characterize the aromaticity of macromolecules (the E_2/E_3 ratio increases with a decrease in aromaticity). Another ratio often used is E_4/E_6 (absorbance at 465 nm divided by the absorbance at 665 nm), which decreases when the average size of macromolecules increases.

The slope parameters S are calculated over the 275–295nm ($S_{275-295}$) and 350–400nm ($S_{350-400}$) ranges, using non linear least squares fit procedures. The spectral slope ratio S_R ($S_R = S_{275-295} / S_{350-400}$) is also used to estimate the variation of the molecular weight of DOM (Guéguen et al., 2012). The molecular weight decreases when S_R increases.

2.2.3 Fluorescence spectroscopy

Fluorescence is a very sensitive technique for characterizing DOM in natural waters without pre-concentration or extraction. Excitation emission matrix (EEM) fluorescence spectroscopy has been extensively used to characterise and differentiate water masses. This technique records the fluorescence intensity of fluorophores as a function of the excitation and emission wavelengths. EEM spectra are a combination of multiple emission spectra at a range of excitations.

2.2.3.1 The principle of fluorescence

The principle of fluorescence spectroscopy

When a fluorophore or fluorescent molecule absorbs a photon with frequency ν_{ex}, which corresponds to a photon energy $h\nu_{ex}$ (h: Planck's constant), its fluorescence emission can simply be depicted by the wave function ψ as below

Excitation steps (absorption spectra):

$$\Psi_o + h\nu_{ex} \rightarrow \psi_e$$

Emission steps (fluorescence spectra):

$$\psi_e \rightarrow \psi_o + h\nu_F + \text{heat}$$

where ψ_0 is termed the ground state of the fluorophore and ψ_e is its first electronically excited state. The fluorescence emission energy, $h\nu_F$, varies depending on the return of the photon to the ground state level (ψ_0). A fluorophore in its excited state, ψ_1, can lose its energy by internal conversion such as 'non-radiative relaxation', where the excitation energy is dissipated as heat (vibrational relaxation) to the solvent.

The emission wavelengths are characteristic for a particular compound or group of compounds with similar fluorophore structures. The emission wavelength could be used for elucidation of structure of target analytes.

In the figure 2.4, S_o, S_1, and S_2 represent the ground, first and second excited states, respectively. The electrons in the ground state (S_o) absorb energy from exciting light to jump to excited states (S_1 or S_2) and release energy via thermal relaxation and return to lower states (e.g. S_2 to S_1). The lifetime of the fluorescence is shorter than that of the phosphorescence.

The fluorescence quantum yield (or efficiency) is defined as the ratio of the number of emitted fluorescence photons to the number of photons absorbed.

$$Fluorescence\ efficiency = \frac{number\ of\ photons\ emitted}{number\ of\ photons\ absorbed}$$

The fluorescence efficiency determines the effectiveness with which the absorbed energy is re-emitted. It depends on several factors such as molecular structure of the fluorescent molecule and its absorption nature, the non-radiative processes, the temperature and the wavelength used for excitation.

Fluorophores

A fluorophore is defined as a part of an organic molecule, with or without electron-donating heteroatoms such as N, O, and S or as a functional group of a highly unstaturated aliphatic molecule with structure that can hold up an excited electron, or having extensive π-electron

systems, which exhibits fluorescence with significant efficiency. The characteristics of the fluorescence spectrum of a given substance are the intensities and the position of excitation/emission peaks. The observed fluorescent bands give qualitative information about the substance or group of substances. The concentration of fluorescent compounds can be determined via internal or external calibration curves in which fluorescent intensity acts as a function of concentration of target analytes at very low concentration levels (in diluted solution). The mathematic equations expressing the fluorescent intensity as a function of concentration of analytes at given experimental conditions are presented below.

In diluted solutions, where light absorbance is small enough, the fluorescence intensity can be expressed as:

$$F = \Phi \cdot I_o \cdot \varepsilon \cdot l \cdot c \tag{2.6}$$

where F is fluorescence intensity, Φ is quantum of fluorescence or fluorescence efficiency, I_o is light intensity of excited light.

This equation predicts a linear relationship between fluorescence intensity and concentration of molecules when εlc is very small. If the concentration of the molecule is high, as a result, εlc increases, the non-linear relationship can be observed and expressed by the following equation:

$$F = \Phi I_o \left[1 - \exp\left(-\varepsilon l c\right)\right] \tag{2.7}$$

The major fluorophores in various fluorescent organic molecules in natural waters are composed of Schiff-base derivatives (–N=C–C=C–N–), –COOH, –COOCH3, –OH, –OCH3, –CH=O, –C=O, –NH2, –NH–, –CH=CH–COOH, –OCH3, –CH2–(NH2)CH–COOH, S-, O- or N-containing aromatic compounds.

According to the basic principle of fluorescence, the elements O, N, S, and P as well as their related functional groups (C–O, C=C, CH–O, COOH, and C=O) in fulvic acids can show fluorescence properties. Each of the functional groups in fulvic acids is referred to as fluorophore. All fluorophores in a mother molecule can exhibit fluorescence properties and any change in the molecule can have an effect on the overall fluorescence properties (Senesi, 1990). The molecular structures of humic substances and natural organic matter in general are

not yet known because of their complicated chemical composition and large panel of molecular sizes. However, fulvic and humic acids originating from vascular plants have allowed a partial identification of their molecular structure as benzene-containing carboxyl, methoxylate and phenolic groups, carboxyl, alcoholic OH, carbohydrate OH, –C=C–, hydroxycoumarin-like structures, fluorophores containing Schiff-base derivatives, chromone, xanthone, quinoline ones, as well as functional groups containing O, N, S, and P atoms (Malcolm, 1985; Leenheer and Croue, 2003).

2.2.3.2 The spectrofluorometer

Fluorescence spectra were recorded with a Fluorolog FL3-22 Fluorometer (Horiba-Jobin-Yvon-SPEX, France) equipped with double monochromators both at the excitation and the emission sides. Samples were contained in a 1 cm path length fused silica cell (Hellma), thermostated at 20°C. Fluorescence EEM spectroscopy involved scanning and recording of 17 individual emission spectra (260-700 nm) at sequential 10 nm increments of excitation wavelength between 250 and 410 nm (Parlanti et al., 2000). Experiments were run in ratio mode with 4 nm bandwidth for both excitation and emission, 0.5 s integration time and 1 nm emission wavelength increment. The photomultiplier voltage was set to 950V. Spectra were obtained by subtracting ultrapure water blank spectra, recorded under the same conditions, to eliminate water Raman and Rayleigh scatter bands. The 17 scans were used to generate 3-D contour plots of fluorescence intensity as a function of excitation and emission wavelengths. To make the graphs readable, the topographic and contour EEM plots are presented with excitation and emission wavelength increments of 10 and 5 nm respectively. Although the resolution in the plots is lower, the positions and intensities quoted in the manuscript correspond to the original line spectra.

The ratio mode (sample/reference) selected as the acquisition mode produced spectra corrected for variations in lamp intensity with respect to time. The spectra were electronically corrected for instrumental response (De Souza Sierra et al., 1994; Ewald et al., 1983).

Fluorescence spectra were calibrated by normalization to the integrated water Raman scattering band, yielding the Raman unit as a quantitative measure of the signal intensity (Determann et al., 1994; Nieke et al., 1997). Since signal intensities taken at specific

wavelengths are normalized to intensities integrated over a wavelength interval, data are in units of inverse wavelength (nm^{-1}), which are denoted as "Raman units" (Nieke et al., 1997). Fluorescence spectra were normalized to the integrated intensities of the Raman scattering band of ultrapure water (Milli-Q, Millipore) samples. The water Raman scatter band was integrated from 380 to 420 nm at λ_{exc} = 350 nm for 30 ultra pure water samples, the average value was used for normalization.

The analytical uncertainty associated to both measurement of fluorescence intensities and normalization to Raman units was lower than 2% (Huguet at al., 2009).

In order to avoid inner-filtering effect, the UV-visible absorbance spectrum of water samples was systematically recorded before analysis using spectrofluorometry. The fluorescence intensity is proportional to the concentration of fluorescent compounds only for low absorbance (lower than 0.1). When the maximum absorbance observed at 250 nm was higher than 0.1 for the studied natural water samples, samples were diluted with ultrapure water. The UV-visible absorbance spectrum was then recorded again to control the maximum absorbance value and define the dilution correction factor to apply to EEM spectra.

2.2.3.3 Fluorescence indices

Three fluorescence indices are proposed for studying the origin and transformation degree of DOM: the f_{450}/f_{500} index, the humification index (HIX) and the biological autochthonous input index (BIX).

The f_{450}/f_{500} index

The f_{450}/f_{500} index was introduced by McKnight et al. (2001) to discriminate the sources of DOM. It is calculated as the ratio of the fluorescence intensity at the emission wavelength 450 nm (f_{450}) to that at 500 nm (f_{500}) at λ_{exc} 370 nm (Figure 2.6). This index allows the distinction between autochthonous aquatic DOM (with a value around 1.9 for aquatic and microbial sources) and allochthonous aquatic DOM (with a value approximately 1.4 for terrestrial and soil sources).

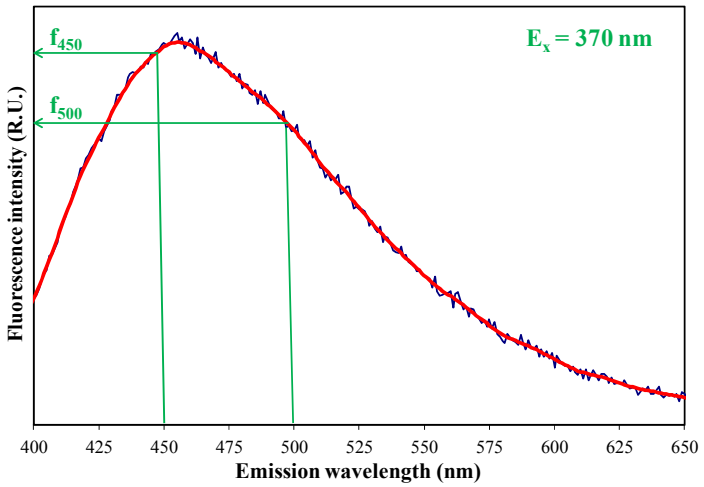

Figure 2.6 Emission spectrum at the excitation wavelength 370 nm to calculate the f_{450}/f_{500} index (sample Mery/ Seine-S1, 2012)

The HIX index

The HIX index was proposed by Zsolnay et al. (1999) to estimate the degree of condensation of DOM in soil (shift of emission spectra towards longer wavelengths in relation with lower H/C ratios). It is calculated from the ratio H/L of two integrated emission spectrum areas (between emission wavelength 300 and 345 nm for L and between 435 and 480 nm for H) at excitation wavelength 254 nm (Figure 2.7).

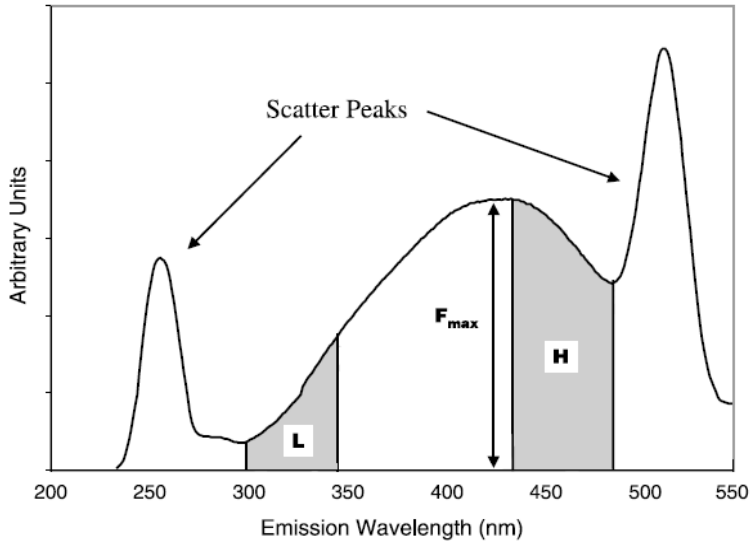

Figure 2.7 Emission spectrum at the excitation wavelength 254 nm to calculate the HIX index (Zsolnay, 2003)

According to Huguet et al. (2009), this index allows to determine DOM origin: a value less than 4 was associated with autochthonous organic matter, whereas a higher value (between 10 and 16) indicated strongly humified organic matter or a great terrestrial contribution. The HIX index values for describing the types of DOM in estuaries and coastal areas are presented in Table 2.2.

The BIX index

The BIX index was previously introduced in the laboratory to characterize the autochthonous production of DOM in water samples in relation with the presence of the β fluorophore (Huguet et al., 2009). Its calculation is based on dividing the fluorescence intensity at λ_{em} 380 nm by the intensity at λ_{em} 430 nm with an excitation wavelength of 310 nm (Figure 2.8). In estuarine waters, the BIX values have been determined to be higher than 0.8 for DOM originating from biological or aquatic bacterial activity and around 0.6 when the autochthonous production was reduced and DOM mainly from allochthonous origin (Table 2.2).

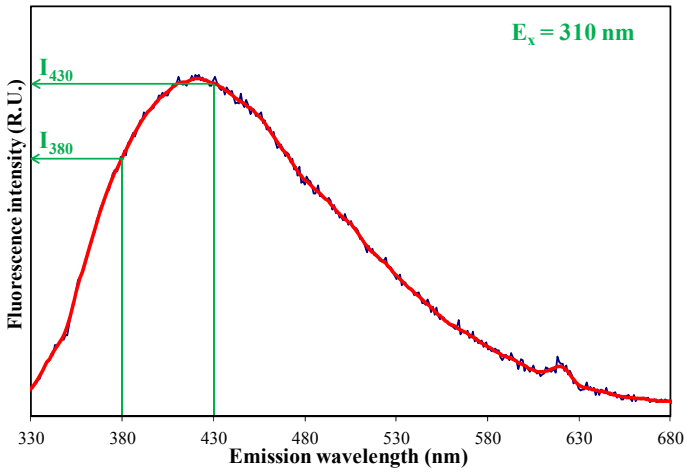

Figure 2.8 Emission spectrum at the excitation wavelength 310 nm to calculate the BIX index (sample Mery/ Seine-S1 collected in 2012)

Table 2.2 DOM characteristics associated with the range of values obtained for the HIX and BIX indices from estuarine and seawater samples (Vacher 2004, Huguet et al., 2009)

Fluorescence Indices	Value ranges	Characteristics of the DOM
HIX	16 – 10	Strongly humic character or an important terrestrial contribution
	10 - 6	Important humic component and recent autochthonous component
	6 - 4	Low humic character and important recent autochthonous component
	< 4	Biological or aquatic bacterial origin
BIX	0.6 – 0.7	Low biological activity
	0.7 – 0.8	Average biological activity
	0.8 - 1	High biological activity
	> 1	Biological or aquatic bacterial origin

The analytical uncertainty in the calculation of fluorescence indices HIX and BIX does not exceed 2% and 1% respectively (Huguet at al., 2009).

2.2.4 The asymmetrical flow field flow fractionation

Field-flow fractionation (FFF) is a chromatographic-like technique, which is used to separate and characterize macromolecular, colloidal and particulate materials according to their diffusion coefficient related to a secondary physical force.

During more or less 50 years since its inception, several techniques have been developed and applied for the separation of samples depending on the applied field, including flow FFF (FlFFF), sedimentation FFF, thermal FFF, electric FFF, gravitational FFF, dielectrophoretic FFF, acoustic FFF and magnetic FFF (Messaud et al., 2009). Though principally developed for the analysis of polymer, the dynamic range combined with the advent of commercially available equipment has greatly increased the prominence of FlFFF over the past decade, extending its application to nanoparticles and colloidal particulates (Gimbert et al., 2003). The principal benefit of FlFFF is its capacity to provide reliable size information and fractionation in complex populations with minimal interaction between the analyte particles and the separation channel, by relying on hydrodynamic forces to achieve diffusion-based separation (size and shape). The principal drawback of FlFFF is the lack of established and universal

protocols and standards for its application, and therefore the persistent burden of repeated sample-specific method development.

2.2.4.1 Principle of FlFFF

There are two forms of FlFFF, known as symmetric and asymmetric, that differ in the way that the channel is designed and cross-flow applied (Yohannes et al., 2011). For most purposes, the principles and procedures discussed in this work are equally applicable to both forms. We have used asymmetrical flow field-flow fractionation (AF4). Compared to symmetrical FlFFF, asymmetrical FlFFF has some following advantages: simpler construction, the ability to visualize the migration of samples, reducing sample dilution, better fractionation resolution.

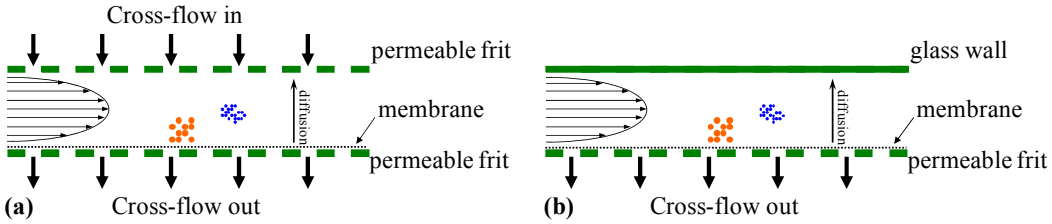

Figure 2.9 The two main types of FlFFF. (a) Symmetric FlFFF with two permeable walls. (b) Asymmetric FlFFF with only one permeable wall (Williams and Benincasa, 2006)

Two operating modes are possible in a FlFFF system: normal (Brownian) and steric/hyperlayer modes. The normal (Brownian) mode is usually applied for analyte sizes smaller than 1 μm. When the applied field drives macromolecules of analytes towards the accumulation wall, the concentration of these macromolecules builds up against the wall. This build-up constructs a concentration gradient that causes analyte diffusion away from the wall. The opposing diffusive flow increases proportionately with the concentration gradient until the transport of analytes by the field towards the wall attains a balance. The balancing of these opposing transport processes yields clouds of analytes having exponential size distributions or layers of different thicknesses. The greater the thickness of the layer, the further the distance to the accumulation wall, the deeper the penetration into the fast streamlines of the parabolic flow profile and the faster the migration of this layer is. In addition, the thickness of the distribution has inverse

relation to the applied force. As a result, the smaller size components will migrate faster and elute earlier, while the larger size components will elute later.

When the constituent sizes increase larger than >1 μm in diameter, the diffusion becomes negligible and the retention is governed by the distance of closest migration to the accumulation wall (Messaud et al., 2009). Small size constituents will migrate to the accumulation wall more closely than larger size constituents, while larger size constituents will penetrate deeper towards the centre of the parabolic profile and thus larger size constituents will elute more rapidly than smaller size constituents. This fractionation is named steric mode.

In the case of hyperlayer mode, when high flow velocities are applied, hydrodynamic lift forces drive sample constituents to higher velocity streams located more than one constituent radius from the accumulation wall. Thus, the elution in hyperlayer mode is similar to that in steric mode.

In this work, all DOM samples were filtered through a pre-combusted glass fibre filter (GF/F 0.7μm; Whatman) so the fractionation applies in the normal mode.

Under laminar flow conditions, the main flow across the channel has a parabolic profile with the highest flow velocity at the centre of the channel and slowest velocity at the walls (Figure 2.10). A secondary flow stream (cross-flow) is applied perpendicularly to the direction of the main flow as the hydrodynamic field to push the analytes toward the bottom of the channel wall (accumulation wall). In normal mode elution the diffusion of analytes creates a counteracting motion. Small molecules with higher diffusion rates tend to reach an equilibrium position higher up in the channel, where the longitudinal flow is faster. Thus, different sizes of analytes are separated by the velocity gradient flowing inside the channel.

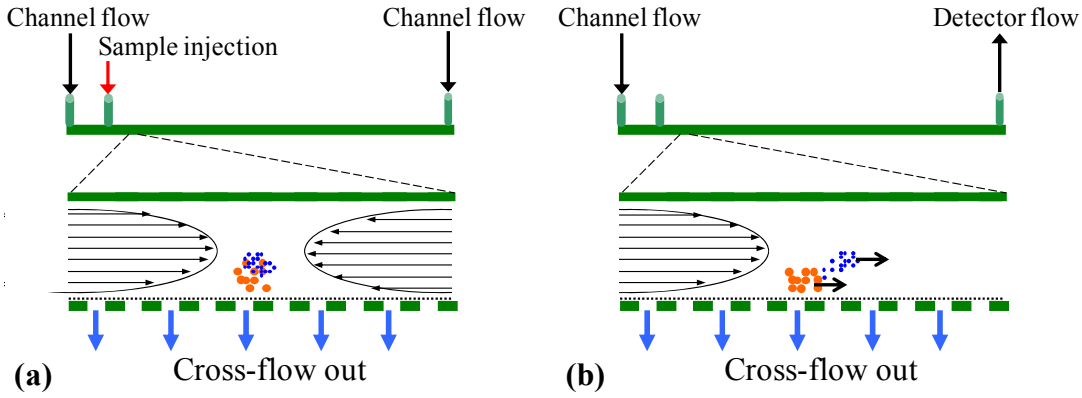

Figure 2.10 Principle of the separation of macromolecules by FlFFF. (A) Injection and focusing/relaxation step; (B) Elution step

The separation process occurs in three steps: injection, focusing/relaxation and elution (Figure 2.10). During the two first steps, the main flow is split, entering the channel from both inlet and outlet, and is balanced to meet under the injection port. At this balanced point, the flow will move only down and pass through the membrane. When the analytes are injected, they are focused in a narrow band and concentrated towards the membrane. As a result of concentration polarization, the analytes will diffuse back into the channel depending on the diffusion coefficient of the species (Figure 2.10-a). In the next step, the main flow only enters from the inlet and elutes the components towards the outlet perpendicularly to the cross-flow (Fraunhofer and Winter, 2004; Yohannes et al., 2011).

2.2.4.2 Theory

The FlFFF theory was developed mainly by Giddings in the 1960s and described in detail in a number of publications (Schimpf et al. 2000; Giddings 1977; Gimbert et al. 2003; Messaud et al. 2009) for the separation and characterization of macromolecular colloidal and particulate materials. Hence, it will be described only briefly here. The sample molecules are distributed across the channel thickness (w) after sample injection into the channel, and then they are pushed towards the bottom of the channel by applying a perpendicular hydrodynamic field to the main flow. The molecules diffusion separates them against the accumulation wall according to their size: large molecules with low diffusion coefficients are driven towards the accumulation wall while small molecules with high diffusion coefficients are still further away from the accumulation wall. As a result of interaction with parabolic laminar flow stream in the

FlFFF channel, molecules travelling nearer to the middle of the channel move faster than molecules travelling closer to the channel walls, and the smaller molecules tend to elute first.

Compared to other fractionation methods, the FlFFF presents the great advantage that the retention time of the analytes is directly proportional to their physical properties. Retention in FFF is expressed as the retention ratio (R), which refers to the retarding of analyte zones caused by its compression when applying field. The retention ratio is calculated by using the following Equation (2.8).

$$R = \frac{t_o}{t_R} \tag{2.8}$$

where t_o and t_R are the retention times corresponding to the maximum of unretained and retained peaks, respectively (Figure 2.11).

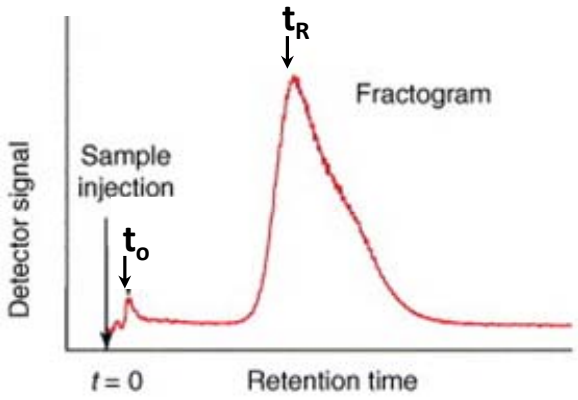

Figure 2.11 Field flow fractionation fractogram (Reschiglian et al., 2005)

In this regard, FFF retention theory is centred on the measurement of zone velocities. The parabolic flow velocity profile (v(x)) across the FFF channel can be described by an ideal equation:

$$v(x) = 6\langle v\rangle\left[\frac{x}{w} - \left(\frac{x}{w}\right)^2\right] \tag{2.9}$$

where <v> is the average velocity of the carrier liquid; w is the channel thickness; v is the velocity of the carrier liquid at distance x from the accumulation wall.

The concentration profile (c(x)) of the analytes is determined by the balance of two opposing forces: The former resulting from the applied field causes the analytes to move towards the

accumulation wall at velocity U_x and the latter is the diffusive force causing the analytes to move in the opposite direction. When these two opposing forces are in equilibrium, the net flux is zero, and

$$U_x c(x) = D\frac{dc(x)}{dx} \tag{2.10}$$

where D is the diffusion coefficient. Equation (3) can be integrated to yield

$$c(x) = c_o \exp\left(-\frac{xU_x}{D}\right) \tag{2.11}$$

where c_o is the analyte concentration at the accumulation wall (x = 0).

The transverse velocity U_x is the field force (F) on the analyte divided by the friction coefficient f of the analyte: $U_x = F/f$. Diffusion of a Brownian particle depends on the friction coefficient and can be stated by the Nernst-Einstein equation: $D = kT/f$, where k is Boltzmann's constant and T is absolute temperature. Substituting these into Equation (2.11) yields

$$c(x) = c_o \exp\left(-\frac{Fx}{kT}\right) \tag{2.12}$$

Another form for expressing the field force F is:

$$F = U_x f = kT\frac{U_x}{D} \tag{2.13}$$

The quantity kT/F is the ratio of the thermal energy to the force on a particle. This quantity is abbreviated as $l = kT/F$, where l is the mean layer thickness and l is measured by the average distance of the analyte from the accumulation wall. The parameter l is typically expressed in non-dimensional form as $\lambda = l/w$, where λ is the retention parameter basis to FFF equations. The force F exerted on an analyte by the external field is related to λ as shown in Equation (2.14).

$$\lambda = \frac{l}{w} = \frac{kT}{Fw} \tag{2.14}$$

Equation (2.14) indicates that the larger the force on the analyte, the more compressed will be the zone at the accumulation wall. The retention parameter λ has several physical meaning. λ is considered as the distance from the accumulation wall to the centre of gravity of the analyte zone relative to the channel thickness. λ is related to the characteristics of the sample that

define its interaction with the force field. λ can be related to the experimentally measured retention ratio R, and thus, it is the bridge between theory and experiment.

In FlFFF, the field comprises a cross-flow of carrier liquid with a velocity U_x, which transports all analyte materials to the accumulation wall. This velocity equals to the volumetric cross-flow rate V_c, divided by the surface area of the accumulation wall. Owing to the fact that the geometric volume of the channel V^o is equal to the surface area of the accumulation wall times the channel thickness w, it can be stated that:

$$U_x = \frac{V_c w}{V^o} \tag{2.15}$$

Substituting Equation (2.13) into the expression for force defined in Equation (2.15) results in:

$$F = \frac{V_c w}{V^o} f \tag{2.16}$$

Substituting Equation (2.16) into the expression for λ in Equation (2.14) results in:

$$\lambda = \frac{kTV^o}{fV_c w^2} = \frac{V^o D}{V_c w^2} \tag{2.17}$$

A relationship exists between the elution behavior and intrinsic physicochemical parameters contained in λ, which can be experimentally determined and is expressed by the retention ratio R, according to:

$$R = 6\lambda\left[\coth\left(\frac{1}{2\lambda}\right) - 2\lambda\right] \tag{2.18}$$

There are a number of approximations for Equation (2.18). Two of the more recognized approximations are described in Equation (2.19) and Equation (2.20). The former is accurate to within 2% when $\lambda<0.2$ and the latter is accurate to within 5% when $\lambda<0.02$

$$R = 6\lambda - 12\lambda^2 \tag{2.19}$$

$$R = 6\lambda \tag{2.20}$$

In normal mode elution, when R is in the range from 0.03 to 0.17, an approximation for λ in Eq. Equation (2.17) can be applied to account for the particle shape (Gigault et al., 2014):

$$D = \frac{\dot{V}_c \omega^2}{A V_0} R \tag{2.21}$$

where A = 6 for spheres, A = 12 for thin rods and A = 18 for thin disks.

Fractionation of analytes in FflFFF (both symmetrical and asymmetric channels) is determined by D, and therefore hydrodynamic diameter (d_H) can be calculated by applying the Stokes-Einstein relationship:

$$\mathrm{D} = \frac{\mathrm{k_B T}}{3\pi\eta \mathrm{d_H}} \tag{2.22}$$

where η is the viscosity of the mobile phase (kg m^{-1} s^{-1}), T is the temperature of the medium (at room temperature, 293 K) and k_B is the Boltzmann constant (1.38 x × 10^{-23} kg m^2 s^{-2} K^{-1}). More specifically to the channel geometries and flow profiles common for AF4, determination of D based on t_R under normal mode elution can be described by:

$$t_R = \frac{\omega_2}{6D} \ln\left(1 + \frac{V_c}{V_p}\right) \tag{2.23}$$

where V_p is the channel flow (mL min^{-1}).

2.2.4.3 Asymmetrical FlFFF system set up

Experiments were carried out with an Eclipse 3 AF4 system (Wyatt Technology, Europe) coupled online to a variable wavelength UV detector (HP 1200 series, Agilent) and a multi-angle laser light scattering detector (three measuring angles - miniDAWN TREOS, Wyatt Technology Europe). The fractionation system was equipped with a 1-kDa molecular weight cut-off polyethersulfone (PES, Pall Omega) membrane, a 1-mL injection loop and a 490-µm spacer. Before placing in the cell, the membranes were rinsed with ultrapure water. Flows were controlled with an Agilent 1200 Series isocratic pump equipped with an Agilent 1200 Series micro vacuum degasser (Agilent Technologies). The carrier solution was ultrapure water (Milli-Q, Millipore). 0.1 µm in-line polyvinylidene fluoride (PVDF) filters were placed in the carrier lines after the HPLC pump and before entering to the channel in order to remove any impure particulate coming from the pump.

2.2.5. AF4 detectors

2.2.5.1 Ultraviolet – visible (UV-Vis) detector

The UV-Vis is the molecular absorbance detector that is commonly used to hyphenate on-line to asymmetrical FlFFF system for environmental applications. Particularly, UV-Vis detector allows determining on-line the concentration of constituents having similar molar extinction (ε_λ) (Lespes and Gigault, 2011). Nevertheless, ε_λ depends on the selected wavelength. In this study, the wavelength of the UV detector is set up at 280 nm owing to the fact that π-π^* electron transitions occur in this region of the UV range for aromatic substances (such as phenolic substances, aniline derivatives, benzoic acids, polycyclic aromatic hydrocarbons) which are precursors or components of NOM, particularly those derived from terrestrial origins (Chin et al. 1994). Moreover, nitrate, a ubiquitous UV-absorbing nutrient in natural waters, does not absorb radiation at 280 nm, so it would not interfere in the analysis.

The number-average (M_n) and weight-average (M_w) molecular weight were determined according to the following equations:

$$M_n = \frac{\sum h_i}{\sum \frac{h_i}{M_i}} \tag{2.24}$$

$$M_w = \frac{\sum h_i M_i}{\sum h_i} \tag{2.25}$$

where h_i is the detector response of the sample AF4 curve eluted at retention time (R_t)i and M_i is the molecular weight at retention time i, as determined from the standard calibration curve.

The polydispersity index (PDI) was calculated as a ratio of the weight- to the number-average molar mass:

$$PDI = \frac{M_w}{M_n} \tag{2.26}$$

2.2.5.2 Multi angle laser light scattering (MALLS)

The MALLS detector allows determining molar masses and sizes of particles or colloids by analyzing the light scattered in a suspension at different angles. The light scattering theory has been described in many publications (Wyatt, 1993; Zimm, 1948a, 1948b). Following Zimm development (Zimm, 1948a), Wyatt (1993) gave the fundamental equation relating the intensity of the light scattered by particles which have smaller size than the incident light wavelength:

$$\frac{\mathrm{Kc}}{\mathrm{R}_\theta} = \frac{1}{\mathrm{M_w} P(\theta)} + 2A_2 c \tag{2.27}$$

where: c is the component concentration (g ml^{-1})

Mw is the weight-average molar mass (g mol^{-1})

A_2 is the second viral coefficient (mol ml g^{-2}), considered to be negligible due to high sample dilution occurring in FFF

θ is the angle between incident and scattered beam

R_θ is the excess Rayleigh ratio (cm^{-1})

K is the physical constant and is given by the Equation (2.25)

$$\mathrm{K} = \frac{4\pi^2 n_0^2}{\lambda_0^4 N_A}\left(\frac{dn}{dc}\right)^2 \tag{2.28}$$

with n_0 is the refractive index of the solvent at the incident radiation wavelength; λ_0 is the incident radiation wavelength (nm); N_A is the Avogadro's number, equal to 6.022×10^{23} mol^{-1}; dn/dc is the refractive index increment of the solution (g^{-1} ml).

P(θ) is the theoretically-derived form factor describing the angular dependence of scattered light and is given by the Equation (2.26)

$$\mathrm{P}(\theta) = 1 - \frac{16\pi^2 n_0^2}{3\lambda_0^2}\left\langle r_g^2 \right\rangle \sin^2\frac{\theta}{2} \tag{2.29}$$

with r_g is the radius of gyration

From the Equation (2.29), radius of gyration can be determined for each elution time.

$$\mathrm{r_{g\,w}} = \frac{\sum c_i r_i}{\sum c_i} \tag{2.30}$$

The quantities c_i and r_i in this equation are the mass concentration and the radius of gyration for a slice i of the corresponding distributions, respectively.

In this study, laser light at a wavelength of 658nm was used as the light source. The scattered light was measured at three different angles corresponding to 45°, 90° and 135°, respectively. Combining UV-visible and MALLS detectors with AF4 system is suitable for the analysis of heterogeneous and complex samples and provides additional online information about fractions.

2.3 Data processing and statistical analysis

2.3.1 Parallel Factor Analysis modelling

Parallel Factor Analysis (PARAFAC) is a statistical tool which uses an alternating least squares algorithm to minimize the sum of squared residuals in a three way model (Stedmon and Bro 2008; Stedmon et al. 2003). PARAFAC separates the data signal into a set of three linear terms and a residual array using:

$$X_{ijk} = \sum_{f=1}^{F} a_{if} b_{jf} c_{kf} + \varepsilon_{ijk} \qquad (2.31)$$

where X_{ijk} is the fluorescence intensity of the ith sample at a couple (j,k) of excitation and emission wavelengths. a_{if} is directly proportional to the concentration of the fluorophore f in the ith sample (defined as scores). b_{jf} and c_{kf} are estimates of the emission and excitation spectra respectively for the fth fluorophore (defined as loadings). F defines the number of components in the model, and ε_{ijk} is the error term representing the variability not accounted for by the model.

In this study, the PARAFAC analysis was carried out in the MATLAB 6.5 software using N-way toolbox version 2.0 according to the procedure detailed by Stedmon and Bro (2008). However, phenomena of light scattering, Raman and Rayleigh, will also influence the PARAFAC decomposition. Raman scattering lines were removed by subtracting Milli-Q water blank spectra from each sample spectrum. Rayleigh scattering lines were removed by replacing the fluorescence intensity values with missing values in the region immediately adjacent to where emission and excitation wavelengths were equal. Regions where the emission wavelength was less than the excitation wavelength were set to zero (Bahram et al., 2006; Yan et al., 2013).

The results of the PARAFAC analysis are substantially related to the number of selected components, thus determining the number of components is a critical step for the analyses. Split-half analysis and examination of residual error plots were used to find suitable components to describe the dataset in the studied excitation and emission wavelength ranges.

2.3.2 Principal component analysis (PCA)

Principal component analysis (PCA) is a statistical technique that is useful for the interpretation and explanatory of data variability (Reid and Spencer, 2009). In simple terms, PCA is a statistical tool available for reducing the dimensionality of a data set by finding a new set of variables (called principal components), smaller than the original set of variables, that nonetheless retains most of the sample's information. It allows us to identify the principal directions in which the data varies. The first principle component explains the greatest variability of the data and is followed by a number of new principle components with each accounting for less data variability than the previous one (Webster, 2001). Thus, the first few components usually represent the majority of the multidimensional variations of the data set.

PCA was performed using the R version 2.11.1 (R Foundation for Statistical Computing). PCA reduces the dimensionality of a set of variables by grouping correlated variables (e.g. proportions) into linearly-independent sets, which are ordered according to the amount of variance explained (Cuss and Guéguen, 2013). Distinct PCAs were conducted for optical indices and components determined by PARAFAC model.

2.3.3 Statistical analysis

All statistical analyses were performed using Minitab software package (version 14.12). The Shapiro-Wilk tests were performed to test whether datasets would take a normal distribution or not. Each test will report a P-value. If the P-value is lower than 0.05, the dataset cannot be drawn from normal distribution.

Student T-test analysis was performed to compare significant differences between two data with the assumption that values were normally distributed. On the other hand, Mann-Whitney

U-test was used. The statistical significance is reported (P-value < 0.05) as significant or non significant (P-value >0.05).

Analysis of variance (ANOVA) was used to compare co-variation of PARAFAC components between different locations of sampling area (different basins).

Person correlation coefficients were reported for all correlations where data were normally distributed. On the other hand, Spearman correlation coefficients were used. Similarity, P values less than 0.05 were considered statistically significant.

CHAPTER III: CHARACTERIZATION OF DISSOLVED ORGANIC MATTER (DOM) IN THE SEINE RIVER CATCHMENT

3.1. Dissolved organic carbon concentrations

Dissolved organic carbon contents were measured in the Laboratory of Water Geochemistry (LGE), Institute of Geophysics (IPGP), Université Paris Diderot, Sorbonne Paris Cité and in the Laboratory Sisyphe, University Pierre and Marie Curie, Paris, France.

For the snapshot campaign in November 2011, it can be seen in Figure 3.1 and Appendix 1 that DOC concentrations were relatively low for samples collected in the Marne basin, these values were less than 2.0 mg C L^{-1} and increased slightly to 2.1 mg C L^{-1} for sample M9, whereas DOC concentrations were higher for samples collected in the Seine basin, downstream of Paris, in the range of 2.6 to 3.9 mg C L^{-1}. The DOC concentration for sample O1 in the upstream of the Oise River (forest area) was slightly higher compared to the other samples collected in the Oise basin. In fact, this value was roughly 4.0 mg C L^{-1}, while the values of DOC concentration for samples in the Oise River ranged from 1.8 to 2.7 mg C L^{-1}. The highest DOC concentration was observed for sample G3 ([DOC] = 9.3 mg C L^{-1}), in Grand Morin River, a tributary of the Marne River, while DOC concentrations for the three other samples collected from this same river were rather low, about 2.0 mg C L^{-1}.

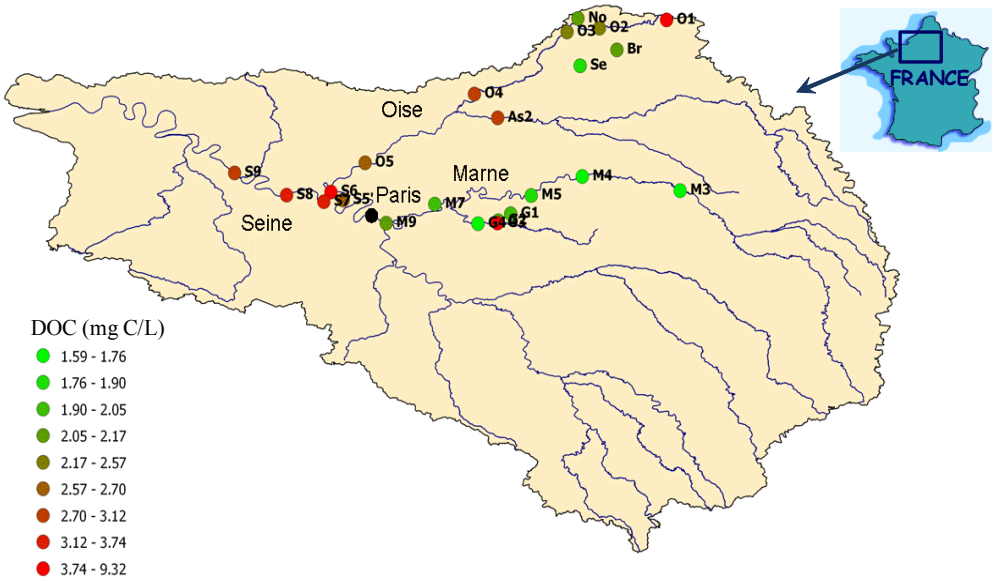

Figure 3.1 DOC concentrations for samples collected in November 2011 (Varrault et al., 2013)

For the snapshot campaign in 2012 (Figure 3.2 and Appendix 1), the DOC concentrations were generally in the range of 2.0 - 2.5 mg C L^{-1} for all the samples collected in the Seine

River catchment with slightly higher values in the Oise River (highest value for sample O1 4.1 mg C L^{-1}). In addition, the spatial distribution of DOC concentrations in the Seine basin indicated significant differences (Mann-Whitney Test , P-value < 0.05) between upstream of Paris ([DOC] = 2.25±0.49 mg C L^{-1}, n=9) and downstream of Paris ([DOC] = 2.95±0.33 mg C L^{-1}, n=5). For the Marne basin, the DOC concentrations for samples LD and M2 collected in the upstream were slightly higher than for the other samples (2.8 and 2.9 mg C L^{-1}, respectively).

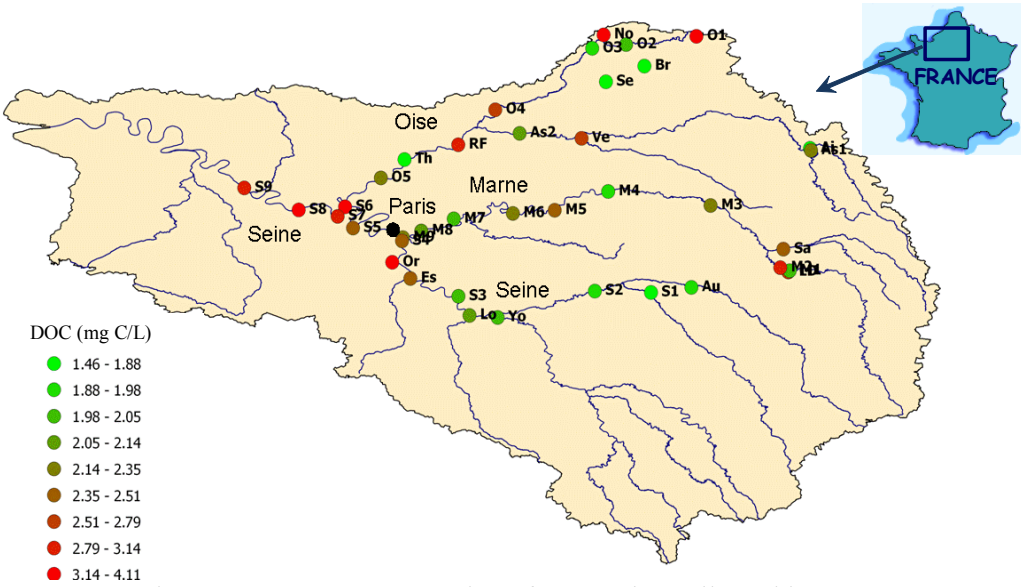

Figure 3.2 DOC concentrations for samples collected in 2012 (Varrault et al., 2013)

For the snapshot campaign in 2013 (Figure 3.3), the DOC concentrations were found to increase about two times along the Marne River from upstream ([DOC] = 1.2 mg C L^{-1} for sample M1) to downstream ([DOC] = 2.4 and 2.2 mg C L^{-1} for sample M7 and M9, respectively), while the DOC concentrations for samples collected from the Grand Morin River were rather similar ([DOC] = 2.73±0.12 mg C L^{-1}, n=4). For the Oise basin, the highest and lowest DOC concentrations were determined for sample RF ([DOC] = 6.5 mg C L^{-1}) derived from forest area and sample Br ([DOC] = 1.8 mg C L^{-1}), respectively, while the DOC concentrations for the other samples ranged from 2.2 to 4.4 mg C L^{-1}. For the Seine basin, non-significant differences (Mann-Whitney Test, P-value>0.05) were observed between upstream of Paris ([DOC] = 3.05±1.21 mg C L^{-1}, n=9) and downstream of Paris ([DOC]=2.58±0.18 mg C L^{-1}, n=4).

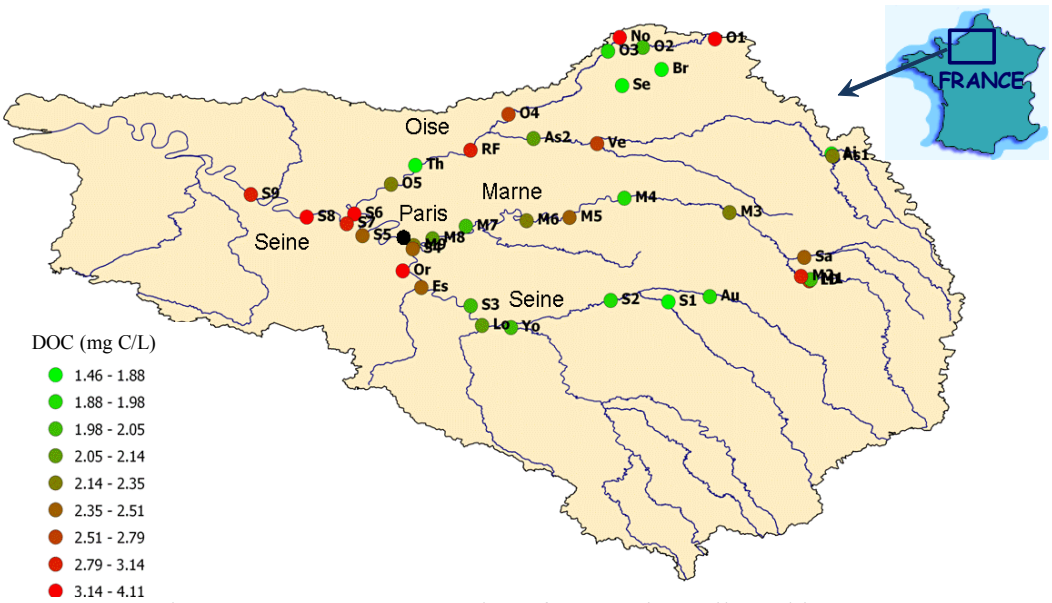

Figure 3.3 DOC concentrations for samples collected in 2013 (Varrault et al., 2013)

3.2. Absorbance spectroscopy

The UV–Visible absorbance spectra of all surface river samples decreased exponentially with increasing wavelengths. To extract information about DOM properties from these spectra, several spectral parameters have been calculated, including spectral slope ratio (S_R); specific ultraviolet absorbance ($SUVA_{254}$), aromaticity percentage. The results are given in Table 3.1.

The spectral parameters, aromaticity percentage and specific ultraviolet absorbance (SUVA) values at 254 nm derived from DOM absorbance spectra, have been interpreted as representing the aromatic content of DOM in the aquatic environment (Carstea et al., 2009). Figure 3.4 showed a strong correlation existing between the percentage of aromaticity and the $SUVA_{254}$ values (Person correlation coefficient R=0.993, P-value <0.05, n=102). During this study, we thus considered only the variations of the $SUVA_{254}$ index.

The $SUVA_{254}$ index has been utilized as an indicator to characterize and differentiate DOM from different origins. Previously, Hur et al. (2007) observed the $SUVA_{254}$ values of DOM in the surrounding Yongdam Reservoir in the range of 2.43 to 3.05 L mg^{-1} C m^{-1}, suggesting that in this reservoir, DOM was mainly constituted by allochthonous material. Generally, it is shown in the literature that natural waters with high $SUVA_{254}$ values (≥4 L $mg^{-1}C$ m^{-1}) have relatively high contents of hydrophobic, aromatic and high molecular weight DOM, whereas waters with $SUVA_{254}$ values ≤ 2-3 L $mg^{-1}C$ m^{-1}, contain a mixture of hydrophobic and hydrophilic DOM from various origins with a range of molecular weights.

Table 3.1 UV–Visible absorbance parameters of surface water samples in the Seine River catchment (the relative standard deviation (RSD) was estimated for samples collected in 2011 and applied to all samples)

Basins	Sample	Aromaticity (%) (RSD ≤ 10%)			$SUVA_{254}$ (L $m^{-1}mg^{-1}C$) (RSD ≤ 2%)			S_R (RSD ≤ 1%)		
		2011	2012	2013	2011	2012	2013	2011	2012	2013
Marne	G1	22.29		16.14	3.23		2.01	0.60		0.60
	G2	21.75		15.18	3.14		1.89	0.59		0.54
	G3	12.11		13.04	1.11		1.36	0.85		0.75
	G4	19.03		20.07	2.56		3.01	0.66		0.67
	LD		12.48	16.24		1.35	2.12		1.35	0.78
	Sa		13.02	18.53		1.36	2.45		0.97	1.14
	M1		17.25	10.94		2.36	1.00		1.20	0.39
	M2		13.05	18.39		1.48	2.68		1.29	0.59
	M3	17.17	15.30	21.46	2.30	1.93	3.21	1.04	1.25	0.64
	M4	16.26	15.23		2.13	1.94		1.11	1.18	
	M5	16.78	15.70		2.19	2.02		1.07	1.16	
	M6		17.02	23.42		2.26	3.62		1.10	0.61
	M7	17.39	17.13	21.01	2.32	2.32	3.22	1.07	1.07	0.71
	M8		21.08			3.08			1.37	
	M9	17.54	17.07	19.00	2.34	2.28	2.64	1.10	1.07	0.73
Oise	Ve		15.78	13.62		2.09	1.55		0.82	0.64
	Ai		19.74	23.09		2.79	3.64		0.86	0.70
	As1		18.30	23.82		2.59	3.82		0.87	0.76
	As2	19.55	18.52	14.18	2.82	2.63	1.66	0.84	0.90	0.72
	Br	21.08	18.95	15.54	3.00	2.68	2.33	0.74	0.63	0.76
	No	18.84	14.77	14.98	2.61	1.80	1.91	0.78	0.90	0.64
	RF		19.51	18.27		2.82	2.66		0.82	0.81
	Se	21.06	18.63	21.27	3.03	2.68	3.33	0.78	0.70	0.61
	Th		18.20	15.24		2.47	2.00		0.86	0.60
	O1	32.02	20.19	21.17	5.34	2.95	3.22	0.70	0.67	0.74
	O2	22.07	18.94	15.30	3.31	2.73	1.91	0.79	0.85	0.57
	O3	21.10	21.27	14.19	3.09	3.13	1.69	0.84	0.92	0.64
	O4	18.70	16.30	13.45	2.64	2.13	1.50	0.81	0.82	0.80
	O5	19.54	18.45	11.30	2.83	2.61	1.03	0.83	0.96	0.77
	O6			17.91			2.57			0.72
Seine	Au		14.45	17.89		1.78	2.27		1.16	0.93
	Es		21.15	18.17		3.14	2.71		1.04	0.80
	Lo		17.55	22.40		2.39	3.53		0.92	0.72
	Or		17.48	12.85		2.38	1.43		0.91	0.70
	Yo		19.42	11.80		2.87	1.14		0.92	0.55
	S1		15.79	21.93		2.04	3.29		1.05	0.60
	S2		16.77	14.55		2.25	1.55		1.29	0.39
	S3		17.27	18.78		2.40	2.73		1.06	0.70
	S4		16.95	15.23		2.30	1.81		1.00	0.77
	S5		17.64	16.61		2.42	2.29		1.02	0.70
	S5'	19.48			2.81			0.86		
	S6	19.28	17.53	20.99	2.69	2.36	3.24	0.80	0.88	0.67
	S7	19.11	17.77	15.49	2.66	2.46	1.98	0.83	0.93	0.74
	S8	18.91	17.58	15.08	2.62	2.37	1.85	0.80	0.96	0.65
	S9	18.76	16.38		2.61	2.12		0.78	0.91	

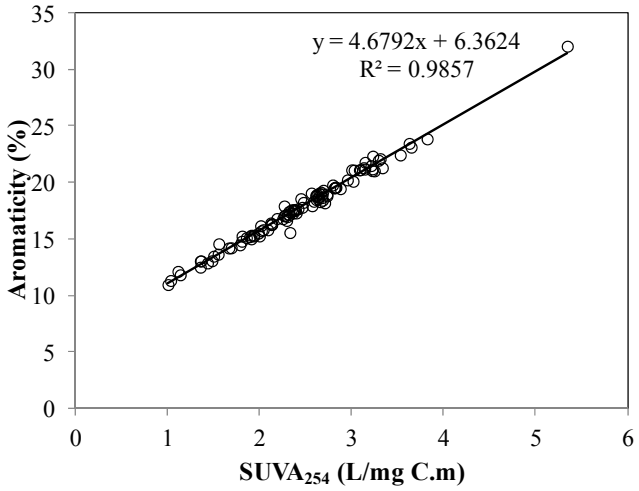

Figure 3.4 Variations of relationship between SUVA254 and Aromaticity in the Seine River catchment

In this study, the highest value of $SUVA_{254}$ was determined for sample O1 collected from the Oise River in 2011 (5.34 L $mg^{-1}C$ m^{-1}), reflecting a relatively high content of complex heterogeneous macromolecular organic compounds rich in aromatics, while DOM in all other samples exhibited lower $SUVA_{254}$ values (1.00-3.82 L $mg^{-1}C$ m^{-1}), implying a large panel of DOM characteristics and molecular weights (Table 3.2, Figure 3.5).

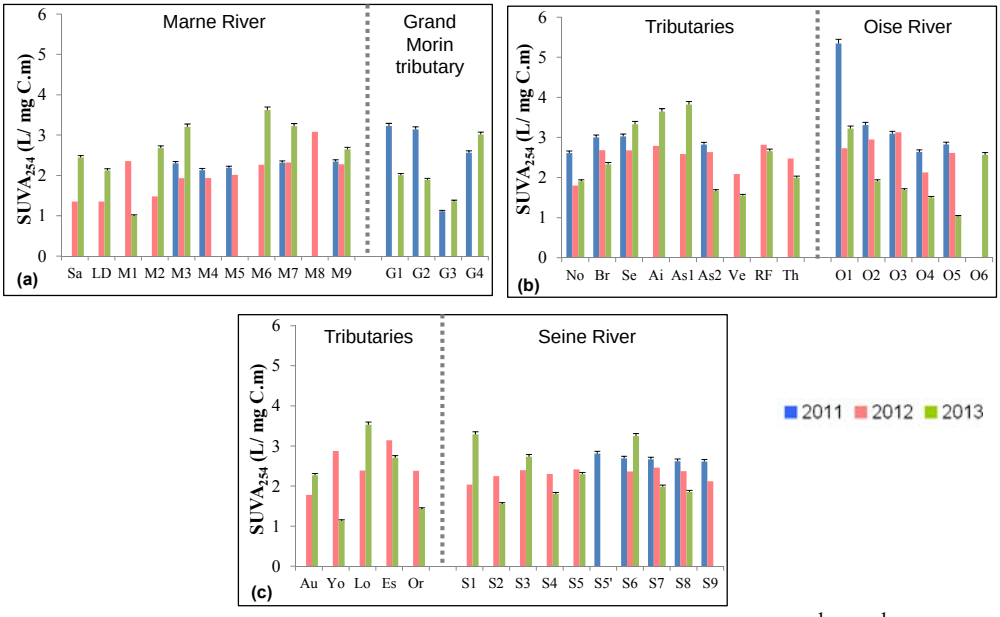

Figure 3.5 Variations of specific ultraviolet absorbance ($SUVA_{254}$) ($L.m^{-1}.mg^{-1}C$) in the three studied basins. (a) Marne River and its tributary (Grand Morin);
(b) Oise River and its tributaries; (c) Seine River and its tributaries.
Error bars indicate relative standard deviation

In addition to the above parameters, the spectral slope ratio S_R ($S_{275-290}$ / $S_{350-400}$) is applied to estimate the change in molecular weight of DOM in this study. Helms et al. (2008) showed an inverse relationship between spectral slope ratio S_R and DOM molecular weight. The spectral slope ratio parameters of DOM for samples collected in the Seine River catchment are presented in Table 3.2 and Figure 3.6. The average value of S_R was 0.84±0.20, which was smaller than that for freshwater samples collected along the Yangtze River (China) and its tributary Daning River (S_R = 0.973 ± 0.137) (Chen et al., 2011).

A negative correlation has been observed between S_R and molecular weight of DOM (Helms, 2008; Guéguen and Cuss, 2011). We can see in Figure 3.6 that the samples collected from the Marne River in 2011 and 2012 show the highest values of S_R, reflecting the presence of lower molecular weight organic material in this area, whereas we can notice, for all the sampling sites in 2013, the lowest values of S_R corresponding to higher molecular weight organic matter. The samples collected from the Grand Morin River in 2011 are also characterised by organic components of high molecular weight (HMW - low values of S_R). As for the samples of the Seine River in 2012, they are characterized by low molecular weight (LMW) DOM.

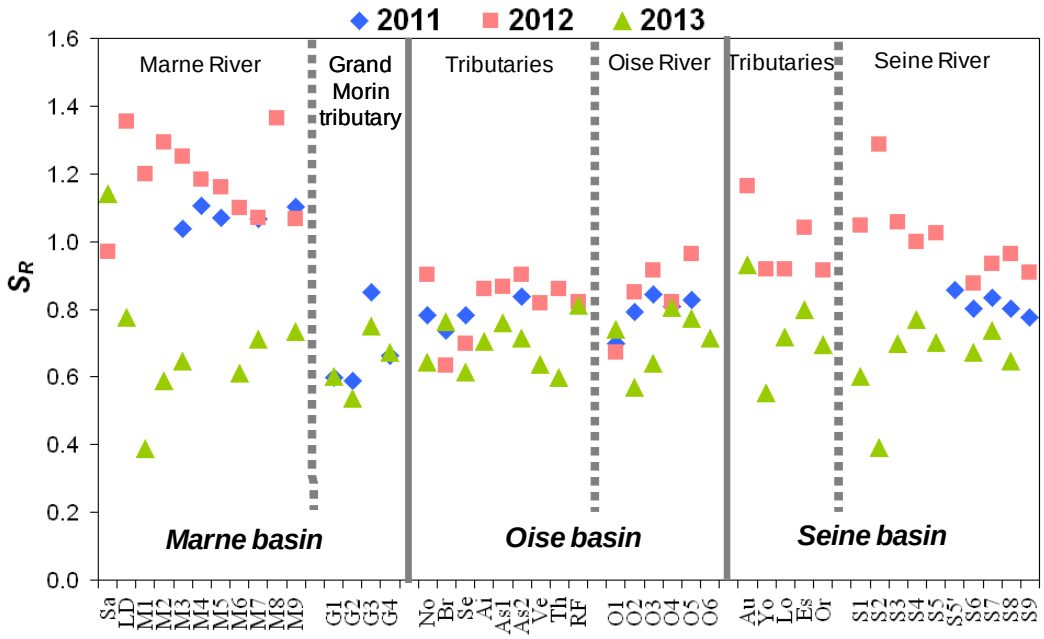

Figure 3.6 Variation of the spectral slope ratio S_R in the Seine River catchment during the three sampling periods (Relative standard deviation marks are not visible in the graph because they are less than 1%)

One interesting observation is that in this dataset there were significant differences in the spectral slope ratio S_R variation between basins in 2012 (Mann-Whitney Test, P-value < 0.05). However, non-significant differences in the S_R values were determined between basins in 2011 and in 2013 (Mann-Whitney Test, P-value > 0.05). Helms et al. (2008) indicated that S_R is dependent on the origins of DOM and the values of S_R are smaller than 1 for DOM derived from terrestrial origin. Given the values of S_R <1 for all the sampling sites in 2013, DOM for these samples should be of terrestrial origin, except for sample Sa collected from the Marne basin (S_R = 1.14).

There was no statistically significant relationship between DOC concentration and either of the two DOM quality parameters ($SUVA_{254}$ and S_R; Figure 3.7a and 3.7b). It can be noticed in Figure 3.7a, the difference in the molecular weight of DOM between the periods of low-water (2012 - characterized by LMW DOM) and of flood (2013 - characterized by HMW DOM).

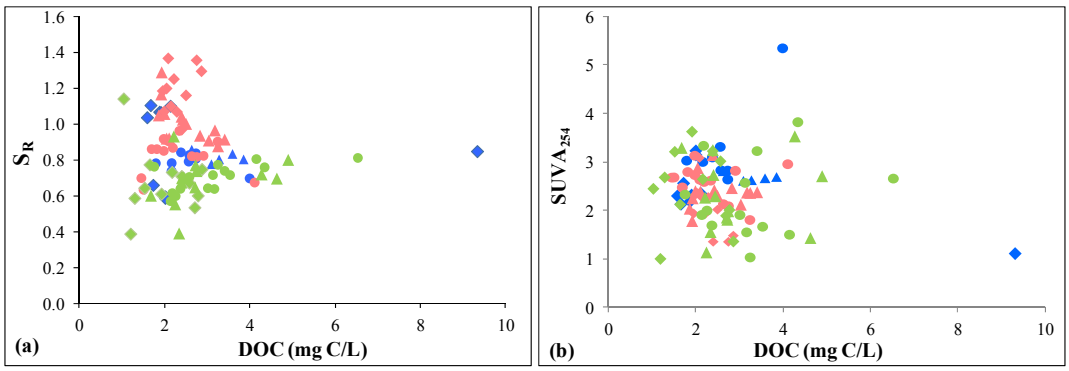

Figure 3.7 Variations of (a) spectral slope ratio S_R and (b) $SUVA_{254}$ as a function of DOC concentration. Keys: Marne basin (♦) 2011, (♦) 2012, (♦) 2013; Oise basin (●) 2011, (●) 2012, (●) 2013 and Seine basin (▲) 2011, (▲) 2012 (▲) 2013.

3.3. Fluorescence spectroscopy

In addition to absorbance spectroscopy, fluorescence spectroscopy was also used to characterize DOM properties in the aquatic environment. This technique has been utilized to identify a broad range of natural (soils and plant litter or microorganisms) or anthropogenic (wastewater, urban and agricultural runoff) DOM inputs into the aquatic ecosystems (Baker, 2002; Baker and Spencer, 2004; Chen et al., 2013).

3.3.1. Fluorescence intensities

The fluorescence intensities of the four main bands characterizing fluorescent DOM (α, α', β, and γ) were determined at fixed excitation wavelengths for all the samples in the Seine River catchment in order to remove the variability in the position of the fluorescence maxima and to produce comparable results between the different water samples (Huguet et al., 2009). Thus, the excitation wavelengths selected to determine the maximal fluorescence intensity of the α' band and that of the α band were 250 nm and 370 nm, respectively. As for β and γ bands, the fluorescence intensity of the former was measured at $\lambda_{exc}/\lambda_{em}$ 310/400 nm, while the fluorescence intensity of the latter was measured at $\lambda_{exc}/\lambda_{em}$ 280/330 nm.

The overall relationship between fluorescence intensity of the four bands (I_α, $I_{\alpha'}$, I_β, and I_γ) and DOC concentration is indicated in Figure 3.8 and showed that there was no correlation of I_γ with DOC concentration (Spearman correlation, P-value > 0.05, n=102). Our result contrasts with that of Baker et al. (2007), which showed linearity between I_γ and DOC concentration. By contrast, the overall relationships between the three other bands with DOC exhibited significantly positive correlations (Spearman correlation coefficients R = 0.48; 0.50 and 0.46 for correlation of $I_{\alpha'}$, I_α and I_β with DOC concentration, respectively, P-values < 0.05, n=102). However, relatively low Spearman correlation coefficients demonstrated that there were weak correlations between DOC concentrations and fluorescence intensities.

For our study, fluorescence intensities of the four bands (α, α', β and γ) normalized to dissolved organic carbon concentration was used to compare the fluorescence properties of DOM without the influence of DOC contents. The ratio of fluorescence intensity to DOC concentration for the four main bands was then presented in Figure 3.9. The mean ratios of the four bands normalized to DOC concentration for the three basins were significantly (Student T-Test, P-values<0.05) higher in 2011, in comparison with the two other sampling periods, reflecting the higher concentration of fluorescent materials for samples collected in 2011 compared to samples collected in 2012 and in 2013. The highest value of $I_{\alpha'}$/DOC ratio was observed in the Marne basin at M5 site (0.42 R.U. L mg^{-1} C) and the highest values for the three other ratios were obtained at S6 site in the Seine basin (0.19; 0.23 and 0.14 R.U. L mg^{-1} C for I_α/DOC; I_β/DOC and I_γ/DOC ratios, respectively). The lowest values for $I_{\alpha'}$/DOC, I_α/DOC and I_β/DOC ratios were observed at M1 site in the Marne basin in 2013 (0.056; 0.023 and 0.029 R.U. L mg^{-1} C, respectively) and the lowest I_γ/DOC ratio at S4 in the Seine basin in 2013 (9.10^{-7} R.U. L mg^{-1} C).

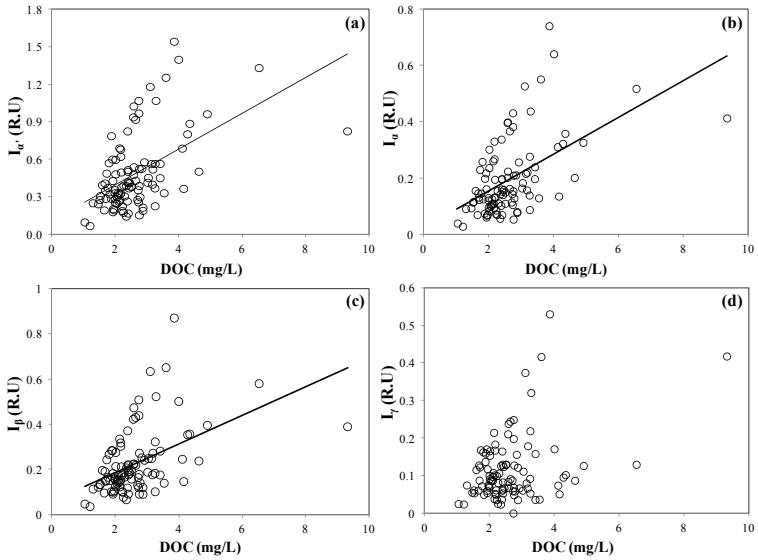

Figure 3.8 Variations of fluorescence intensities of (a) α'; (b) α; (c) β and (d) γ bands as a function of DOC concentrations in the Seine River catchment during the three campaign periods.

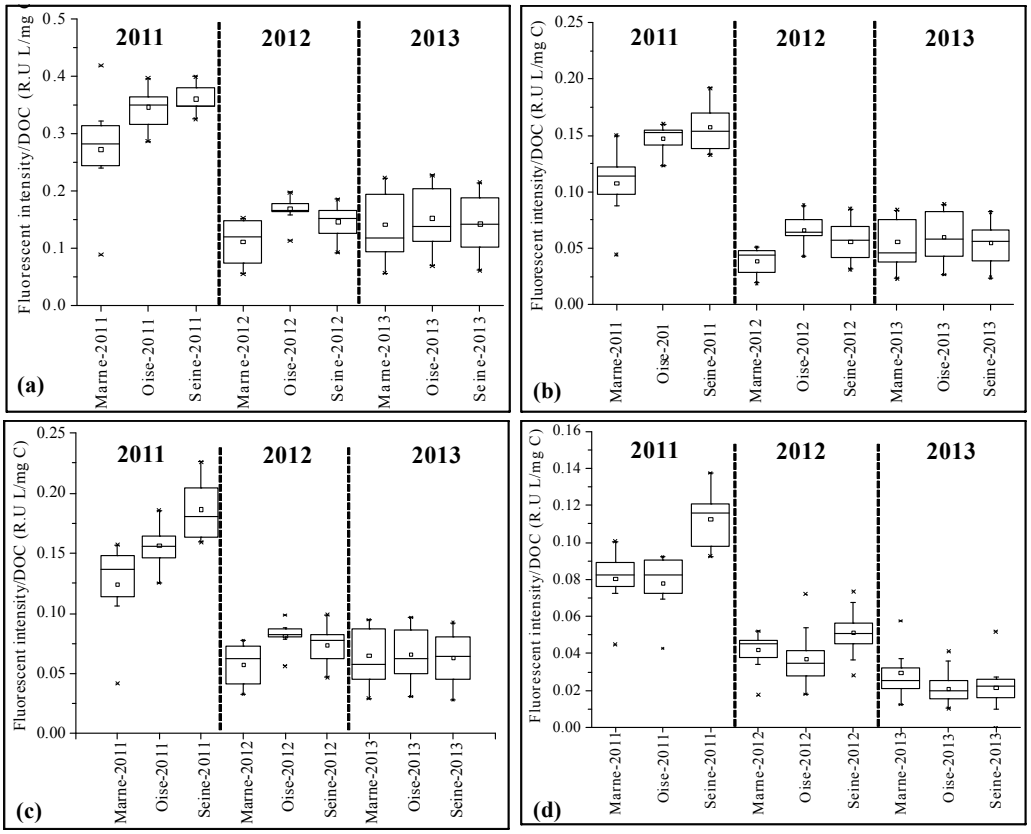

Figure 3.9 Box plots of fluorescence intensities normalized to DOC concentration. (a): $I_{\alpha'}$/DOC; (b): I_{α}/DOC; (c): I_{β}/DOC; (d): I_{γ}/DOC. Key: the square symbol in the box symbolizes the mean of data; the horizontal lines stand for the 25th, 50th and 75th percentile values; error bars denote the 5th and 95th percentile values, two symbols below the 5th and above 95th percentile error bars denote the min and max values.

An interesting observation is that in this dataset, the ratios of fluorescence intensities normalized to DOC concentration were significantly and positively correlated with each other (at 99% confidence level, n=102). The Spearmans' rank correlation coefficients for these ratios are presented in Table 3.2. We can see in this table strong correlations (Spearman correlation coefficients R > 0.95) for $I_{\alpha'}$/DOC; I_{α}/DOC and I_{β}/DOC ratios, while correlations between these ratios and I_{γ}/DOC ratio exhibited lower Spearman correlation coefficients in the range of 0.598 and 0.761, suggesting weaker correlations between I_{γ}/DOC ratio with the other ones.

Table 3.2 Spearman coefficients of correlation (P<0.01, n=102) between ratios of fluorescent intensities to DOC concentration

Parameter	$I_{\alpha'}$/DOC	I_{α}/DOC	I_{β}/DOC	I_{γ}/DOC
$I_{\alpha'}$/DOC	1	0.973	0.966	0.631
I_{α}/DOC		1	0.958	0.598
I_{β}/DOC			1	0.716

In addition to the ratio of fluorescence intensity to DOC concentration, ratios of fluorescence intensities were also calculated in order to estimate the relative contributions of the considered fluorophores in the studied area.

From a qualitative point of view, the examination of these ratios of intensities of the main characteristic bands of fluorescence of recent material (autochthonous origin - α', β, and γ) versus the band of fluorescence of more humified matter (older material - α), is interesting because it allows us to estimate the relative contributions of the various DOM components and their maturity. The Figures 3.10, 3.11 and 3.12 present the distributions of these ratios of fluorescence intensities according to the content in DOC. We observed very net variations of the quality of DOM between the three sampling periods for the Marne and Seine basins, while less discriminating results were obtained for the Oise basin. The values of these ratios of fluorescence intensities were mainly higher for the samples of the snapshot campaign of 2012. This tended to show the presence of a more recent fluorescent organic material and a stronger biologic contribution in September, 2012.

The $I_{\alpha'}/I_{\alpha}$ ratio has been commonly used to evaluate the relative contributions of α' and α fluorophores, which are both associated with humic-like substances. This ratio has been considered as an indicator of the young and mature character of humic substances in natural

waters. The α fluorophore is connected with more degraded and old material (Huguet et al., 2009). Significant differences were observed in the Marne and Seine basins for $I_{\alpha'}/I_{\alpha}$ ratio between the three sampling periods (Figure 3.10-a and 3.10-c). The highest values of this ratio were mainly determined for the samples collected during the snapshot campaign in September 2012, suggesting that the organic matter observed during this low-water period was more recent than in 2011 and 2013. On the other hand, the ratio $I_{\alpha'}/I_{\alpha}$ gave similar values for samples collected in the Oise basin whatever the sampling date (Figure 3.10-b).

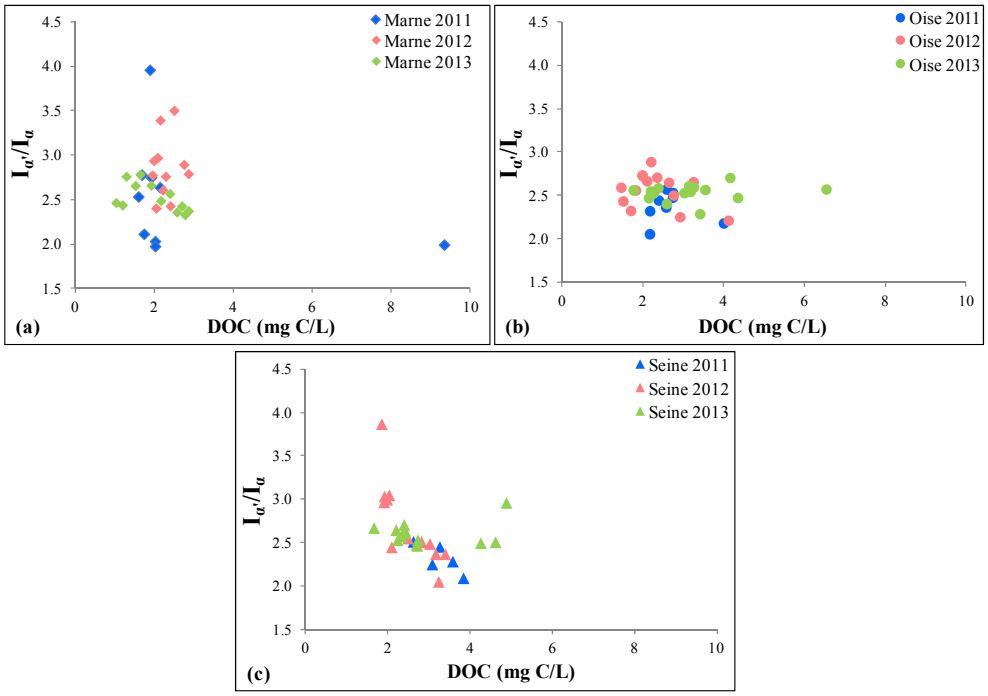

Figure 3.10 Distribution of $I_{\alpha'}/I_{\alpha}$ ratio as a function of DOC concentration in the Marne (a), Oise (b) and Seine (c) basins during the three snapshot campaigns

The I_{β}/I_{α} ratio showed the same variations as the $I_{\alpha'}/I_{\alpha}$ ratio for samples collected in the Marne and Seine basins (Figure 3.11-a and 3.11-c). However, and by contrast with the $I_{\alpha'}/I_{\alpha}$ ratio, this ratio was more discriminating in the Oise basin between the three snapshot campaigns (Figure 3.11-b). Indeed, samples collected in 2012 were characterized by higher I_{β}/I_{α} ratios in comparison with samples collected in 2011 and 2013, suggesting a slightly greater biological contribution in the Oise basin, as well as in the two other river basins, in September 2012. This confirms the previous observations with the ratio $I_{\alpha'}/I_{\alpha}$.

As well as for the ratio $I_{\alpha'}/I_{\alpha}$, the ratio I_{γ}/I_{α} presented higher values for samples taken from the Marne and Seine basins in 2012 compared to samples collected in 2013 (Figure 3.12-a and

3.12-c). This ratio was again less discriminating for samples collected in the Oise basin during the three sampling campaigns (Figure 3.12-b).

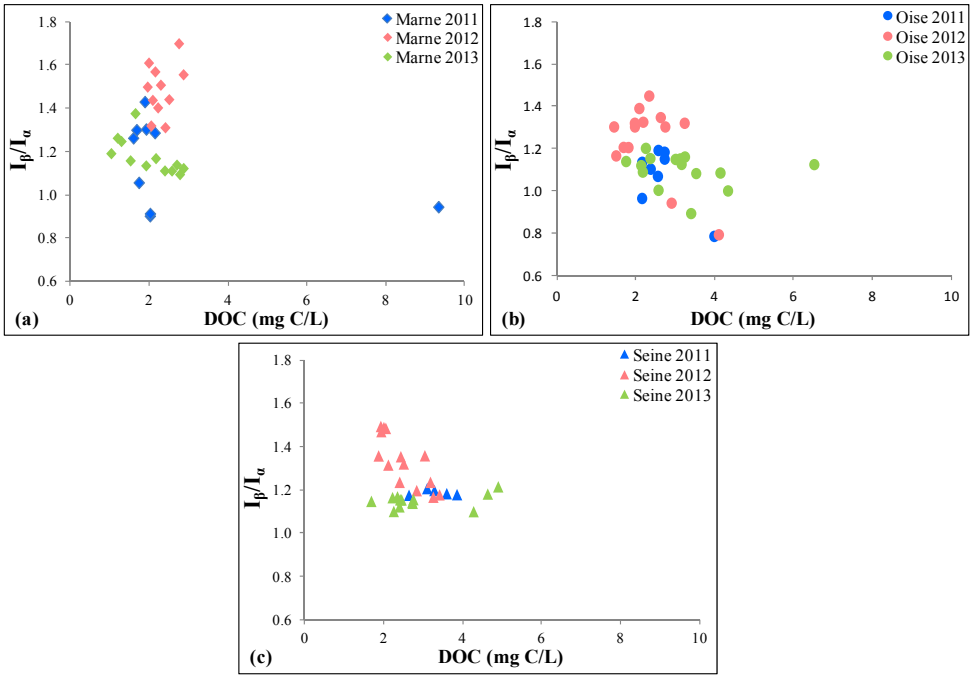

Figure 3.11 Distribution of I_β/I_α ratio as a function of DOC concentration in the Marne (a), Oise (b) and Seine (c) basins during the three snapshot campaigns

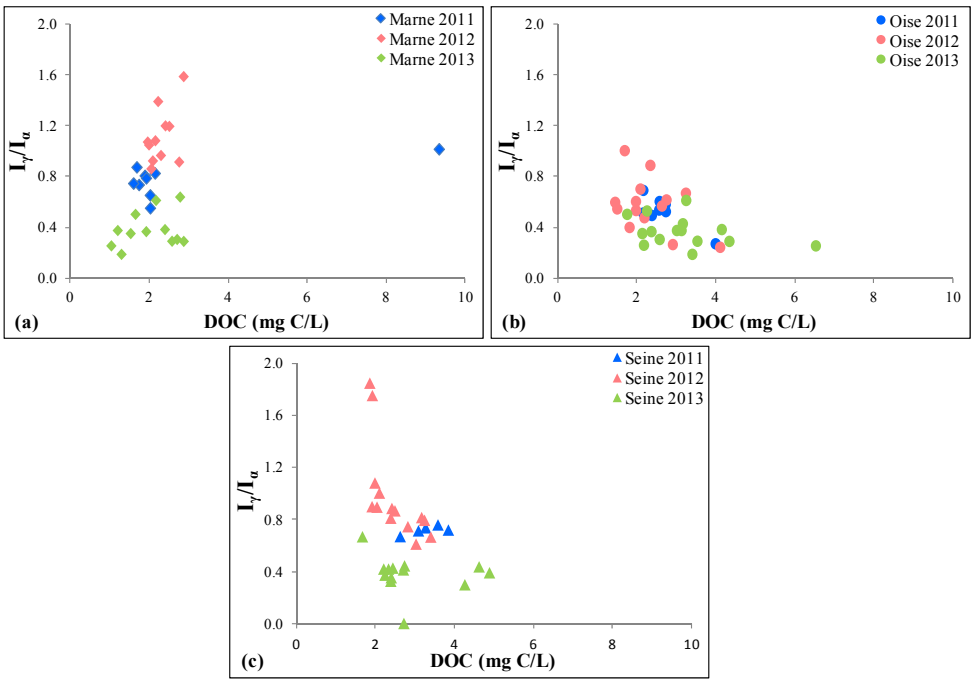

Figure 3.12 Distribution of I_γ/I_α ratios as a function of DOC concentration in the Marne (a), Oise (b) and Seine (c) basins during the three snapshot campaigns

Actually, relatively low values (<0.75) of I_γ/I_α ratio for samples in the Oise basin seem to indicate the dominance of humic material in this basin. On the other hand, higher values of the ratio I_γ/I_α were observed in 2012 for samples from the Marne and Seine basins, reflecting the presence of more labile compounds at these sites.

3.3.2. Fluorescence indices

The determination of the fluorescence intensities and the fluorescence intensity ratios allow us to trace and monitor the variations and evolutions of fluorescent DOM in the environment. Moreover, complementary information on the origin and on the transformation degree of DOM can be obtained through the calculation of fluorescence indices. Common fluorescence indices have been proposed, including the f_{450}/f_{500} index (McKnight et al., 2001), the humification index (HIX – Zsolnay et al., 1999) and the biological autochthonous input index (BIX – Huguet et al. 2009).

3.3.2.1. The f_{450}/f_{500} index

The f_{450}/f_{500} index is expected to discriminate dissolved organic matter from different sources (McKnight et al., 2001). Microbially derived DOM has values of f_{450}/f_{500} index very close to 1.9, while terrestrially derived DOM presents values of roughly 1.4. The values of f_{450}/f_{500} index are rarely lower than 1.0, and the highest values were reported less than 3.0 (McKnight et al., 2011). For our study, none of the samples had a value of f_{450}/f_{500} index higher than 1.9. Actually, almost all the values of the f_{450}/f_{500} index were lower than 1.5. Especially, three values of the f_{450}/f_{500} index were lower than 1.1, corresponding to the sample O1 collected in 2011, 2012 and 2013 (1.06, 1.05 and 1.03, respectively). This implies a predominantly terrestrial origin of DOM for this site, what is logical for a forest zone. On the other hand, the samples with the f_{450}/f_{500} values higher than 1.4 suggested the contribution of DOM derived from both terrestrial and microbial sources. Similar to $SUVA_{254}$ parameter, there was no significant correlation between the f_{450}/f_{500} index and DOC concentration (Figure 3.13).

The values of the f_{450}/f_{500} index in this study are similar to those found by Battin (1998) from the black water Surumoni river, South Venezuela and by Al-Reasi et al. (2011) for freshwater

samples collected in Norway and are higher than those obtained by Huguet (2009) for the Gironde Estuary, France.

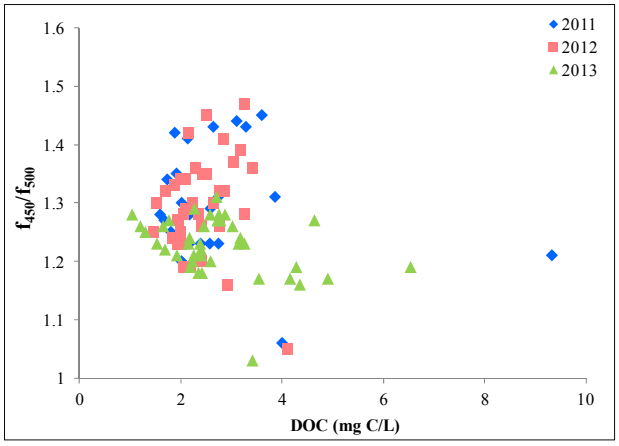

Figure 3.13 Variations of the f_{450}/f_{500} index as a function of DOC concentration

3.3.2.2. HIX and BIX indices

The humification index (HIX) is used to estimate the degree of DOM humification (Zsolnay et al., 1999) which has been considered by Birdwell and Engel (2009) an indicator of DOM bioavailability in natural system, because highly humified organic matter is thought to be less labile than lower degree humified organic material. Variations of the humification index (HIX) were shown in Figure 3.14. The higher values of HIX, reflecting the more mature and aromatic material, are observed for all sites in 2013 during flood. Especially, the highest values of the HIX index were observed in the forest sites O1 and RF. These results confirm those obtained from the I_γ/I_α ratio with relatively low values (< 0.5).

In order to compare the differences in the humification degree between basins during the three sampling periods, Mann-Whitney U-test was used and P-values were determined (Table 3.3). Comparisons in the HIX data for samples from the Marne basin during the three sampling events yielded P-values <0.05.

These results indicated that there were significant differences in HIX according to the sampling period in the Marne basin. For the Oise basin, P-values were 0.007 between 2011 and 2013 as well as between 2012 and 2013, while comparison of HIX index between 2011 and 2012 had P-values >0.05. These results suggested that there was no significant difference in HIX index between samples collected in 2011 and in 2012, but the values of HIX for samples collected

during these periods significantly differed from those for samples collected in 2013. Similar trends were observed for the Seine basin.

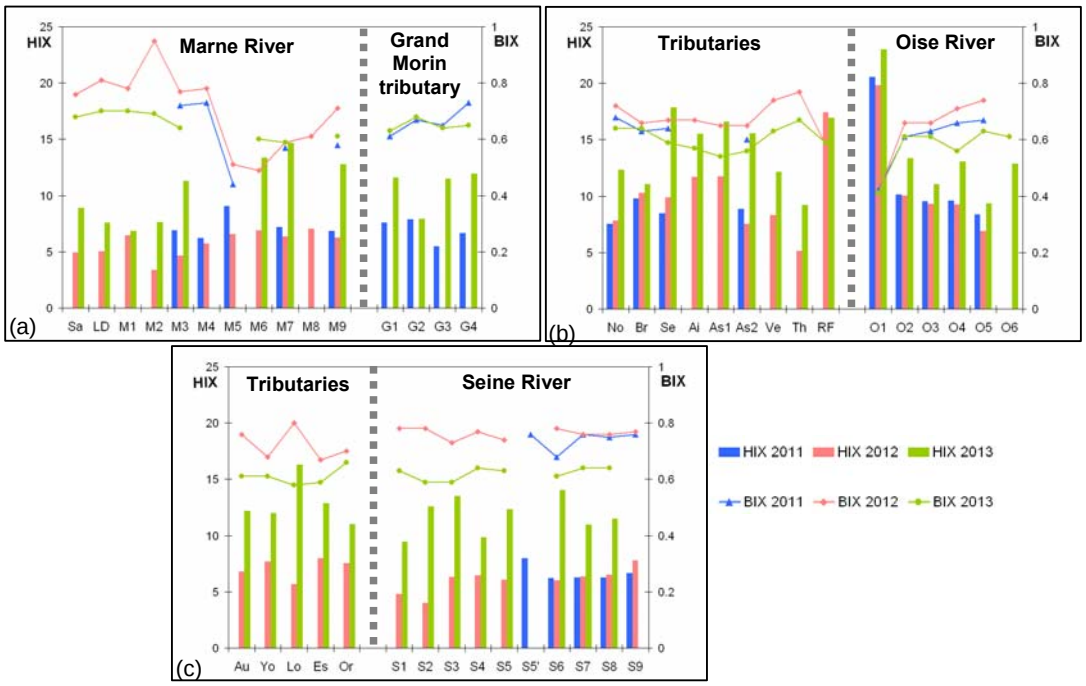

Figure 3.14 Variations of HIX and BIX for samples in the Marne (a), Oise (b) and Seine (c) basins during the three snapshot campaigns

Table 3.3 Spatial Mann-Whitney U-test analysis for comparison of HIX values during the three sampling events

Basin	U-test comparison between different sampling periods								
	Number of samples (n)			Median of HIX values			P-value		
	2011	2012	2013	2011	2012	2013	2011 and 2012	2011 and 2013	2012 and 2013
Marne	9	11	12	7.09	5.76	10.50	0.023	0.003	0.000
Oise	9	14	15	10.32	10.36	13.99	0.925	0.007	0.007
Seine	5	14	13	6.67	6.42	12.19	0.817	0.002	0.000

The BIX index was also determined for all samples and its variations are shown in Figure 3.14. The lowest BIX index values were determined for samples M5 (2011- 0.44) and O1 (in 2011, 2012 and 2013 - 0.42, 0.41 and 0.41, respectively) and combined with relatively high HIX values (9.07, 20.56, 19.82 and 22.99, respectively). These results denote an allochthonous

nature at these sites. These results also confirm those obtained for the f_{450}/f_{500} values. In contrast, all the other samples are characterized by a relatively high biological activity, the highest values being observed for samples collected in 2012 as well as for samples collected in the Seine basin in 2011.

For the BIX data, Mann-Whitney U-test was also used to investigate the differences in biological activity between the studied basins during the three sampling times. The P-values determined for the Marne basin samples were all >0.05 (Table 3.4), implying no significant difference in BIX values between three different sampling times with each other in the Marne basin.

Table 3.4 Spatial Mann-Whitney U-test analysis for comparison of BIX values during the three sampling events

Basin	U-test comparison between different sampling periods								
	Number of samples (n)			Median of BIX values			P-value		
	2011	2012	2013	2011	2012	2013	2011 and 2012	2011 and 2013	2012 and 2013
Marne	9	11	12	0.65	0.76	0.65	0.160	0.915	0.207
Oise	9	14	15	0.63	0.67	0.61	0.068	0.107	0.001
Seine	5	14	13	0.76	0.67	0.61	0.431	0.001	0.000

Comparisons of samples in the Oise basin had P-values 0.068 between 2011 and 2012; 0.107 between 2012 and 2013 and 0.001 between 2012 and 2013, respectively. These results pointed out that the values of BIX for Oise samples collected in 2011 were not significantly different from the values for samples collected in 2012 and in 2013; however, significant differences were observed between samples collected in 2012 and in 2013. For the Seine basin, the P-value determined for comparison of BIX values between samples collected in 2011 and in 2012 was > 0.05, while comparisons of those samples to the BIX values from the 2013 samples yielded again P-values < 0.05. These results indicated that BIX values in 2013 for the Seine basin samples, as already mentioned for the two other basins, were significantly different from the other sampling periods.

There was no significant correlation of the fluorescence indices HIX or BIX with DOC concentration (P-values> 0.05, n=102, Figure 3.15). However, both HIX and BIX indices

exhibited a strong negative correlation with each other (Spearmans correlation coefficient R = -0.765, P-value< 0.05, n=102, Figure 3.16-a).

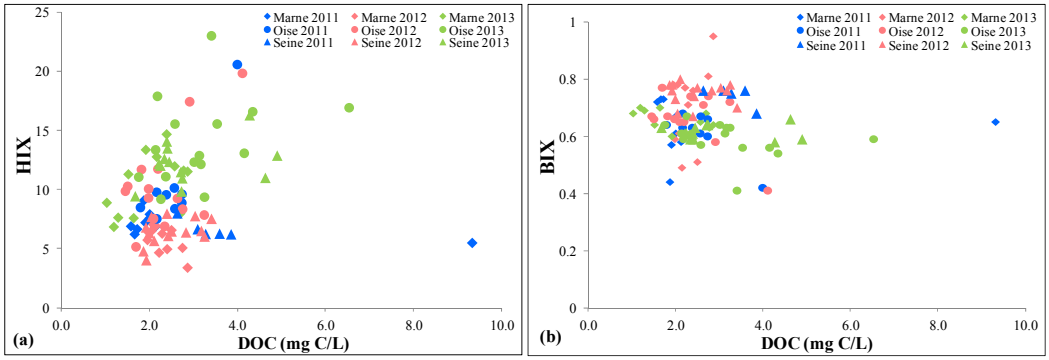

Figure 3.15 Variations of HIX (a) and BIX (b) indices as a function of DOC concentration

In addition, HIX was also negatively correlated with S_R, and the Spearman correlation coefficient R was only -0.639 (P-value < 0.05, n=102, Figure 3.16-b). This weak correlation points out that a higher HIX does not always come with a lower S_R as already observed by Chen et al. (2011) for DOM of various origins. For instance in the Oise basin in 2011, sample O2 presented simultaneously lower values of S_R and HIX than those of sample O1. For another example, for samples G2 and G3 collected in 2011, both S_R and HIX values for sample G3 were higher than those for sample G2.

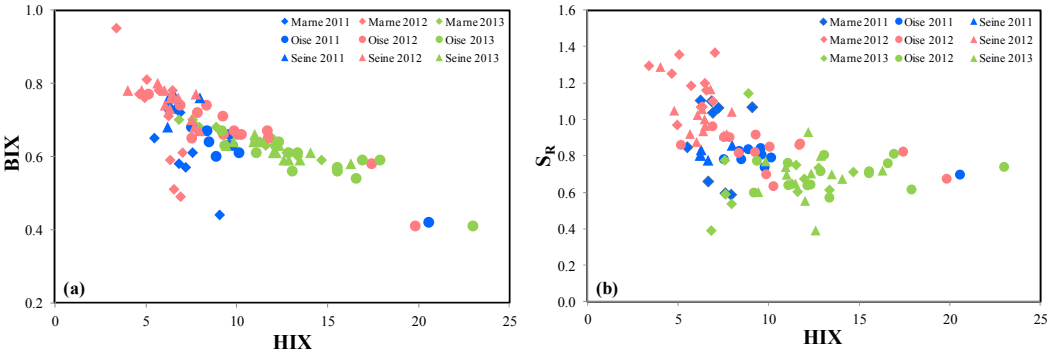

Figure 3.16 Variations of BIX index (a) and spectral slope ratio S_R (b) as a function of HIX index

To summarize, the indices of fluorescence HIX and BIX showed spatial variations of the quality of DOM. The strongest values of HIX, corresponding to aromatic and mature organic material, were observed in the Oise basin and in a logical way the maxima in forest zones (O1 and RF). Almost all the samples were characterized by a relatively high biological activity

(BIX > 0.6), the strongest values being observed for the Seine River in 2011 and 2012 and in the Marne basin in 2012.

The period of flood (2013) is characterized by strong values of HIX while the lowest values are observed in period of low-water (2012) and mainly associated with high values of BIX, indicating a strong biological activity for these samples.

3.4. EEM-PARAFAC modeling

In order to obtain more detailed information on DOM quality, the fluorescence data sets were analyzed using PARAFAC which decomposes the complex data matrix of DOM into its main components. A total of 102 EEMs of surface water samples from the Seine River catchment were used for PARAFAC analysis. The analysis was carried out in Matlab using the DOMFluor toolbox and split half analysis was used to validate the identified components. The model was constrained to non negative values.

3.4.1. EEM-PARAFAC components of DOM

A seven-component PARAFAC model was selected as most suitable for this data set with excitation and emission ranges of 250–410 nm and 300–600 nm, respectively. The contour plots of the seven components identified by PARAFAC are presented in Figure 3.17. The 7 component model, determined by PARAFAC analysis, explained 99.8 % of the total data set (102 samples) variability.
All fluorescent components had single or multiple excitation maxima and only single emission maximum.

Examples of measured, modeled and residual EEMs can be seen in Figure 3.18. The examination of residuals for each sample indicated that all the main features of the measured EEMs were reproduced in their correlative model.

The characteristics of the fluorescence components determined in this study presented many features in common with previous studies (Coble et al., 1998; Parlanti et al., 2000; Yamashita et al., 2008; Cawley et al., 2012).

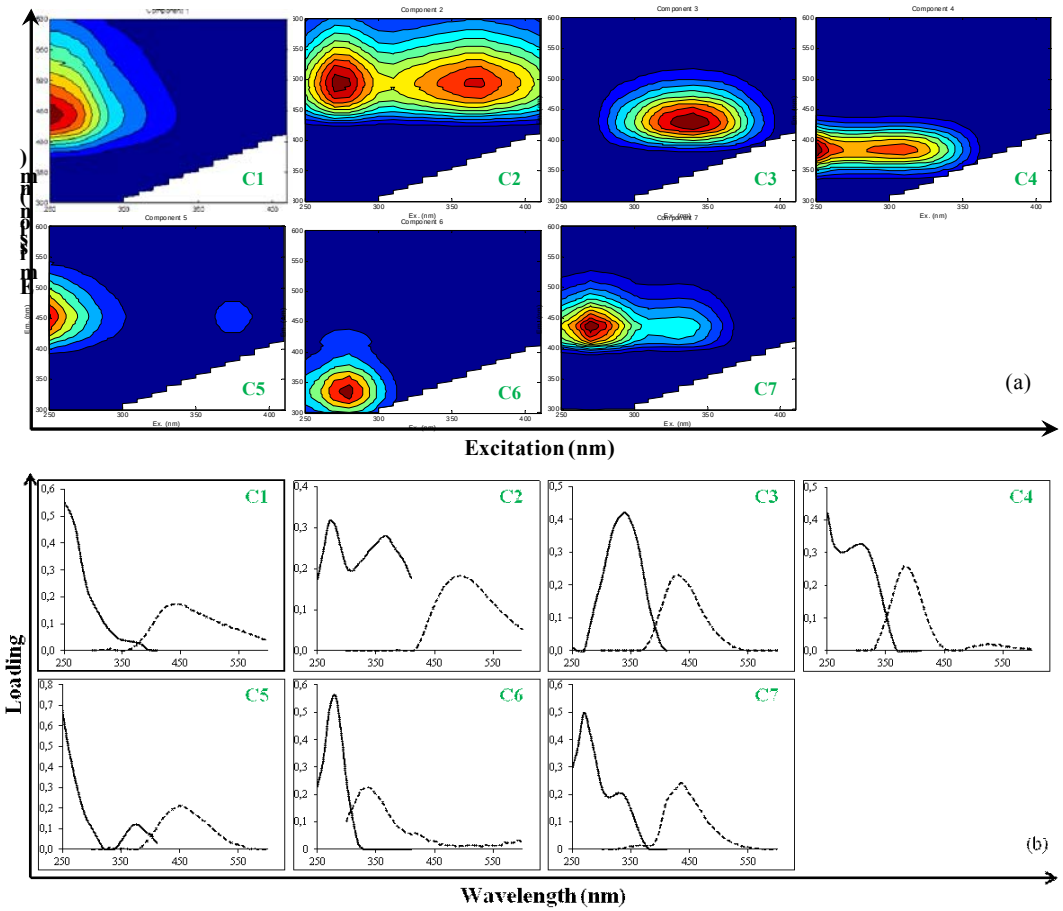

Figure 3.17 (a) Contour plots of the seven components identified by PARAFAC analysis, and (b) Excitation (solid lines) and Emission loadings (dotted lines) of each component

The position of emission and excitation maxima for each component is summarized in Table 3.5 and compared to those found in previous studies. The identified seven components could be distinguished as humic-like components (components 1, 2, 3, and 5), a component similar to fluorophore β and thus related to autochthonous production (component 4), a protein-like component (component 6), and an unknown substance (component 7).

Component 1 (C1) showed an intense excitation maximum below 250 nm at 444 nm emission (Figure 3.16; Tab. 3.6). This component is similar to the humic-like fluorophore in the ultraviolet region (peak A) as defined by Coble (1996) and Coble et al. (1998) and is associated with the terrestrial fluorescent component identified through PARAFAC model by other authors (Table 3.5).

C1 was described to be high molecular weight and aromatic humic, widespread in environments (Fellman et al., 2010). Stedmon et al. (2003) showed that this component dominated the EEMs of DOM from forested and wetlands regions.

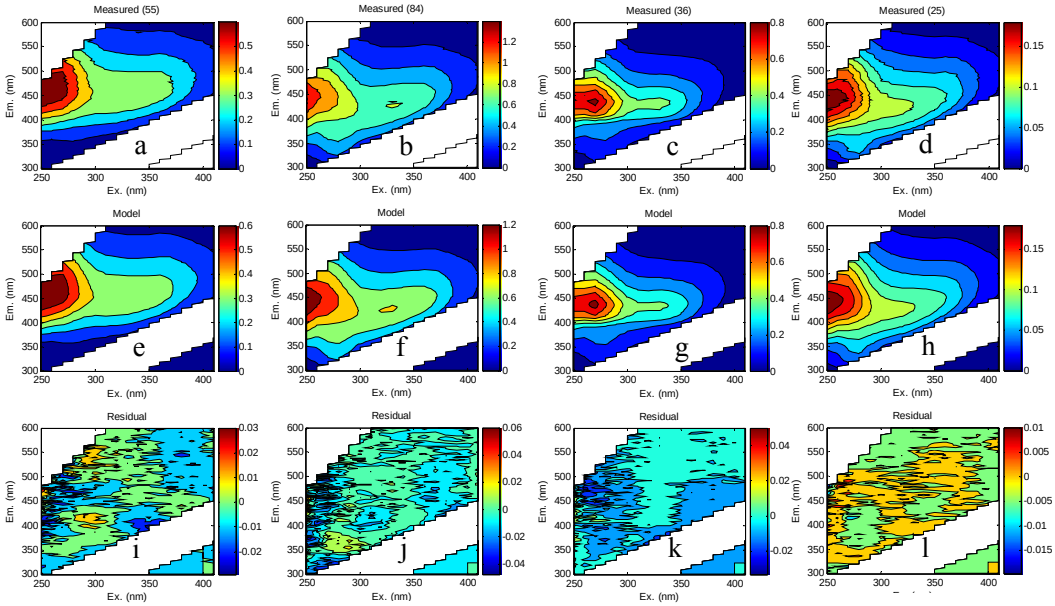

Figure 3.18 Examples of measured (a-d), modeled (e-h) and residual (i-l) EEMs for different DOM in the catchment. Fluorescence emission is in Raman units.

Table 3.5 Characteristics of the seven component model determined by PARAFAC in this work compared to previous studies

Component	Ex maximum (nm)	Em maximum (nm)	Description and probable source
C1	<250	444	Humic-like substances, Peak A[1], α' type[2], C1[3], C1[5], C1[6], C1[10], C1[11], C2[14]
C2	270 (370)	492	Humic-like substances α' and α types[2], C3[3], C3[5], C3[6], P3[8], C1[9], C4[10], C1[13], C5[14]
C3	340	429	Humic-like substances Peak C[1], α type[2], C2[5], C2[6], C1[14]
C4	310 (<250)	384	Biological and/or microbial origin ,anthropogenic activities Peak M[1], β type[2], C4[3], C3[4], C6[5], C4[6], C2[7], P2[8], C2[9], C3[10] , C5[11], C2[13], C3[14]
C5	<250 (370)	450	Humic-like substances α' type[2], P8[8], C4[11], C11[14]
C6	280	336	Protein-like material, mino acids, free or bound in proteins Peak T[1], γ type[2], C5[3], C5[5], C3[7], P6[8], C3[9], C6[10], C7[11], C3[12], C3[13], C8[14]
C7	270 (330)	438	Unknown humic-like substance, microbial origin C6[6], C6[14]

[1] Coble et al.(1998); [2] Parlanti et al. (2000); [3] Stedmon et al. (2003); [4] Stedmon et al. (2007b); [5] Yamashita et al. (2008); [6] Cawley et al. (2012); [7] Holbrook et al. (2006); [8] Murphy et al. (2008); [9] Guéguen et al. (2011); [10] Kowalczuk et al. (2009); [11] Stedmon et al. (2005a) ; [12]Sanchez et al. (2013) ; [13] Guéguen et al. (2012b) ; [14] Cory and McKnight (2005)

Component 2 (C2) comprised a double excitation maximum at 270 and 370 nm and an emission peak at 492 nm. This component represented fluorophores that had the longest excitation and emission wavelengths in the Seine River catchment model, indicating that this component may comprise large molecular size, hydrophobic compounds (Ishii and Boyer,

2012). C2 was similar to a terrestrial organic matter that is composed of high molecular weight and aromatic organic compounds (Stedmon et al., 2003), but this component had a red shift of about 10 nm in comparison with traditional α' and α types (Parlanti et al., 2000). Such a red shift has however already been observed for humic acids extracted from mangrove sediments (Sierra et al., 2005). Yamashita and Jaffé (2008) indicated an origin of this component from higher vascular plants.

The third terrestrial component in this study, component 3 (C3), had an excitation maximum at 340 nm and an emission maximum at 429 nm. These excitation-emission wavelength pair was identified within the range of wavelengths for peak C or the visible humic-like peak (Coble et al., 1998), and also called the α type according to Parlanti et al. (2000). C3 is visually similar to C2 in Yamashita et al. (2008) and Cawley et al. (2012). This component was also showed to be consistent with high-molecular-weight humic substance and widespread in the environment, especially in wetlands and forested ecosystems.
Component 4 (C4) has lower emission wavelength maximum compared to terrestrial humic-like components and is similar to fluorophore β thus related to recently autochthonous produced material and to biological activity (Parlanti et al., 2000). This component, also defined as marine humic-like peak M (Coble et al. ,1998) has also been found through PARAFAC analyses in coastal environments (Yamashita et al., 2008; Cawley et al., 2012) and from coastal to oceanic areas (Murphy et al., 2008). C4 showed similarity to component 3 found in the Stedmon and Markager (2005b) study, thus providing evidence that this component was associated with recent biological activity and that this component attributed the microbial source to autochthonous production of biologically labile organic matter.

Component 5 (C5) had an excitation maximum below 250 nm, a less intense maximum at 380 nm, and an emission maximum at 450 nm. The characteristics of C5 may resemble another humic-like fraction identified in previous studies (Stedmon et Markager, 2005a; Murphy et al., 2008).

Component 6 (C6) had a pair of excitation and emission wavelengths at 280 and 336 nm, respectively. This wavelength pair matches well with the excitation-emission spectra of protein-like compounds, specifically tryptophan which observed in both marine (Coble et al., 1998; Stedmon et al., 2003; Murphy et al., 2008; Guéguen et al., 2011; Kowalczuk et al.,

2009) and terrestrial water (Holbrook et al., 2006), and associated with biological production in surface waters as well as activity of microorganisms (Coble et al., 1998; Stedmon et al., 2003).

Component 7 (C7) had two excitation maxima at 270 and 330 nm, and an emission maximum at 438 nm. The signature of C7 is similar to component 6 as recognized by Cawley et al. (2012). Fellman et al. (2010) pointed out that this component related to unknown humic-like fluorescence group derived from microbial processing.

3.4.2. Spatial distribution of EEM-PARAFAC components

In addition to identifying fluorophore components within complex matrices, the PARAFAC model also gives us the maximum fluorescence (F_{max}), expressed in Raman units in this study, of components for both excitation and emission spectra. Therefore, a comparison of F_{max} values can reveal relative variations in the fluorophore composition. Considering that DOM fluorescence of the total data set was explained by seven components identified by PARAFAC model, the distribution of these components was presented for every site in the Figure 3.19 as well as the distribution of their relative percentages in the Figure 3.20.

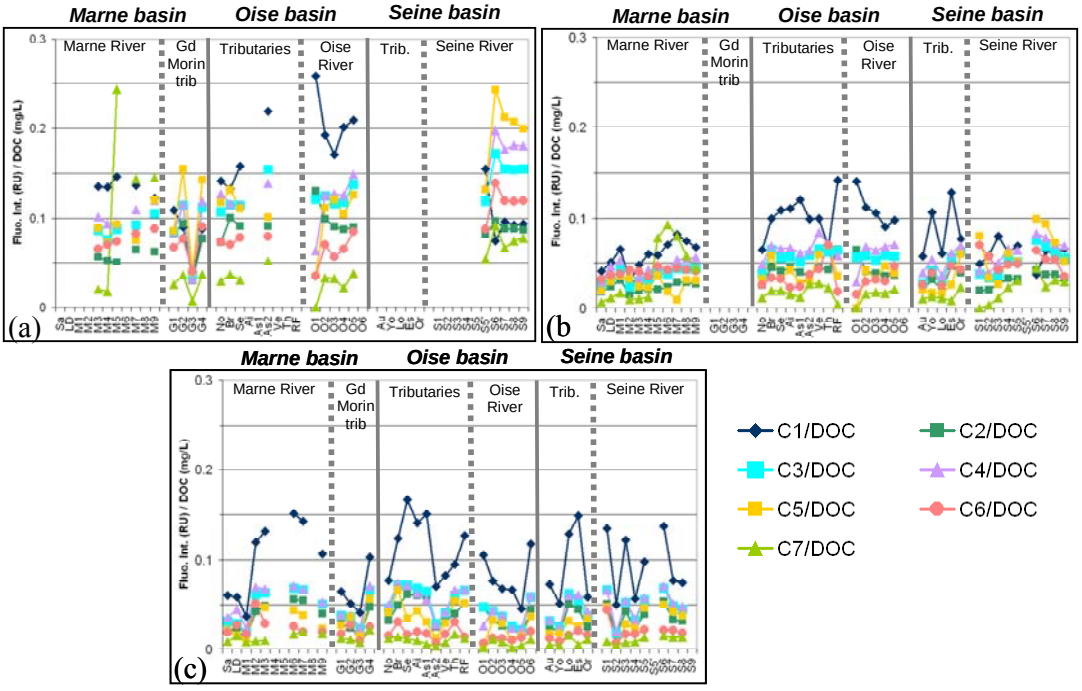

Figure 3.19 Distribution of the fluorescence intensity normalized to DOC of the 7 components identified by PARAFAC in the three studied basins in (a) 2011; (b) 2012 and (c) 2013.

As mentioned previously the intensities of the 7 components were stronger in 2011 reflecting higher fluorescent compound concentrations (Figure 3.19). For 2011 and 2012, we observed very different distributions of these 7 components from one basin to another, highlighting different and specific DOM characteristics for each zone. On the contrary, a homogeneous distribution of the 7 components was obtained for the samples collected during the flood in February 2013. For this sampling period, the component 1 was dominant for all the samples and the observed distribution reflected more humic DOM characteristics with the presence of organic material mainly from terrigenous origin.

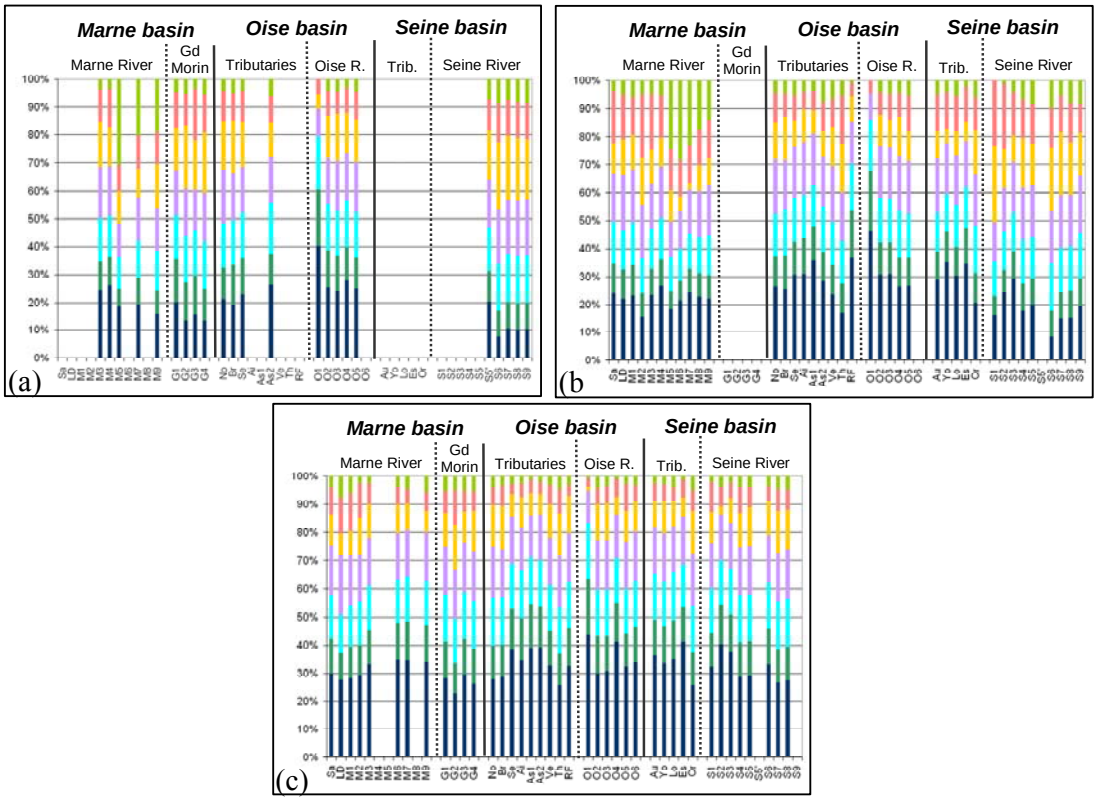

Figure 3.20 Relative percentage distributions of the 7 components identified by PARAFAC in the three studied basins in (a) 2011; (b) 2012 and (c) 2013.
Keys: ■C1; ■C2; ■C3; ■C4; ■C5; ■C6 and ■C7

The percentage of the terrestrial component C1 was found to be the highest during the three sampling periods, for the Oise basin, the tributaries of the Seine River and some samples from the Marne River (Figure 3.20). The variability in mean values of the relative percentage distribution of component C1 was observed as 18.5±4.5 (Marne 2011); 25.7±6.1 (Oise 2011); 22.1±2.9 (Marne 2012); 29.7±6.9 (Oise 2012); 22.5±8.0 (Seine 2012); 29.8±3.7 (Marne 2013);

33.9±5.2 (Oise 2013) and 32.7±5.1 (Seine 2013). For the Seine basin in 2011, the highest percentage to the total DOM fluorescence was observed for the component C5 and its mean percentage value was 21.8±2.6.

As for component C7, it was found to be the least abundant component for almost all sites in the Seine River catchment, except for the Marne River where it dominated the distribution in 2011 and 2012 for some samples (M5, M6, M7 or M9). Actually, the percentage distribution of component C7 is less than 10% for almost all samples, except for the samples previously mentioned for which the relative abundance of this component vary from 14% (M9 in 2012) to 31% (M5 in 2011).

Compared to samples collected in the Marne and Seine basins, the samples collected in the Oise basin had a relatively higher percentage of component C2, which account for a percentage of 13.1±2.9, 12.1± 3.14 and 13.5± 2.2 in the Oise basin compared to 11.0±2.9, 8.9±1.4 and 11.9±1.2 and 9.8±0.5, 9.6±1.3, 12.5±0.8 in the Marne and Seine basins during the three sampling times, respectively. Particularly, the highest percentages of component C2 were found at forest sites. They were roughly 20% for DOM fluorescence of sample O1 collected in 2011 2012 and 2013. On the other hand, the lowest relative abundance of component C2 was observed for samples collected in the Marne and Seine Rivers where component C2 just contributed less than 10% for total DOM fluorescence. For all the other samples, the relative abundance of component C2 ranged from 10% to 15%.

The component C3 corresponding to α type fluorophore had a relatively higher abundance in the forest sites in comparison with the other sampling sites and showed the lowest abundances for samples collected in the Marne River in 2011 and 2012.

In contrast to terrestrial components, the component C4 showed a lower relative abundance in the forest sites relatively to the other locations, suggesting a microbial origin for this component. Indeed, these values were approximately 10% for sample O1, while the other samples were characterized by relatively higher percentage values for this component in the range of 15% and 20%.

As for component C6, we observed the relatively highest abundance for samples S1 and S2 collected in 2012 as well as for samples from the Marne basin in 2012.

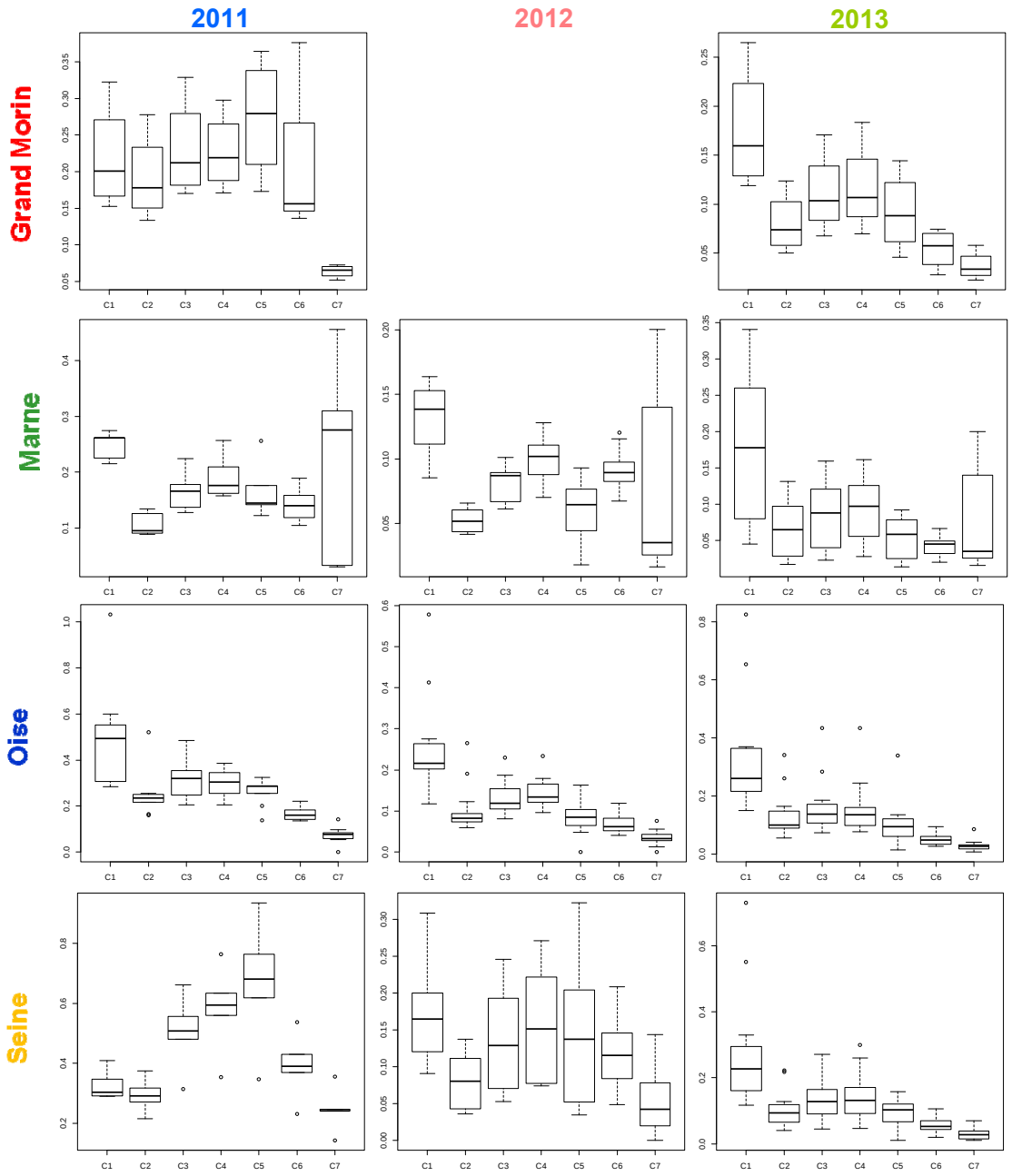

Figure 3.21 Distribution of the 7 components identified by PARAFAC by river basin and by sampling period.

The statistical analysis of the data showed a temporal variation of the distribution of the 7 identified DOM components with component 7 more represented in 2011 and highlighted again a variation of the characteristics of DOM according to the sampling sites and a differentiation of the studied basins. These spatiotemporal variations are illustrated by the box-and-whisker

plots in Figure 3.21. The component 1 was dominant for year 2013, but also for the three sampling periods for the Oise basin. Although we observed a great dispersal for component 7 for the Marne River samples, this component seems to characterize this river, in any case for samples M5 to M9 (Figure 3.20). The samples from the Seine basin (2011 and 2012) distinguished themselves with a particular signature showing as major components C3, C4 and C5.

The ratios of PARAFAC components were also used to examine the differences in composition and distribution of DOM between three basins in the Seine catchment and are presented in Figure 3.22. The data in this Figure depicted the average ratios of F_{max} of each component relative to that of component C2, as this component was considered to be a terrestrially derived component and to be present in a wide range of environments (Stedmon et al., 2003). Stedmon et al. (2003) indicated that by presented in this way, the data reflect the differences in composition rather than the considerable differences in concentration.

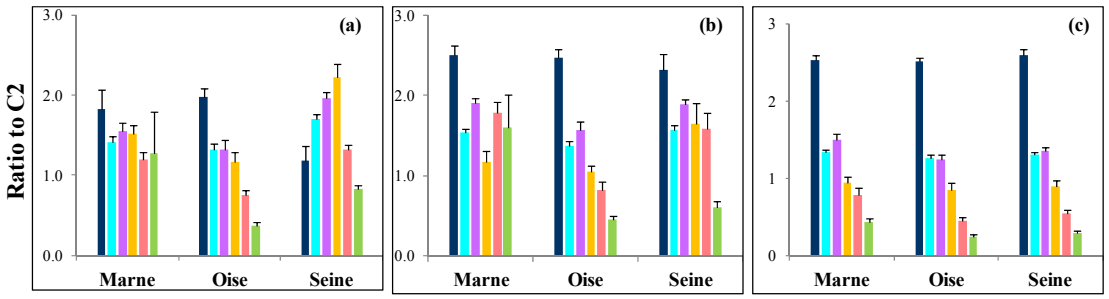

Figure 3.22 Average ratios of the fluorescence maximum of each component to the fluorescence maximum of C2 during the three sampling times.
Error bars indicate standard error.
Key: (a) 2011; (b) 2012 and (c) 2013; ■C1; ■C3; ■C4; ■C5; ■C6 and ■C7

In 2011, the average ratios of the fluorescence maximum of each component to that of C2 fluctuated substantially between the different basins, suggesting that these components were independently variable. Especially, components C5 and C7 were twice as large in the Seine basin than in the Oise basin (2.23±0.15 and 0.82±0.05 compared to 1.17±0.12 and 0.38±0.03, respectively). This might indicate that the two components were derived from autochthonous origin or/and related to anthropogenic activities. In 2012 and 2013, we observed no significant difference in the variations of ratios C1/C2 and C5/C2 between the various basins (P-values > 0.05). This lets us imagine a similar behavior of the components C1 and C5 towards the component C2. The comparisons of the ratios C3/C2 and C4/C2 in 2013 also exhibited non-

significant differences between the three basins, however, the comparisons of the ratios C6/C2 and C7/C2 gave inverse results (P-values < 0.05), meaning that significant differences in these ratios were observed between the three basins, thus, pointing out independent variations of components C6 and C7 compared to C2.

3.4.3. Correlations between EEM-PARAFAC components

In order to study the mixing and removal of fluorescent material in the surface waters from the Seine River catchment, the correlations between different the 7 fluorescent components were investigated, the whole data set being divided into three groups corresponding to the three basins of interest.

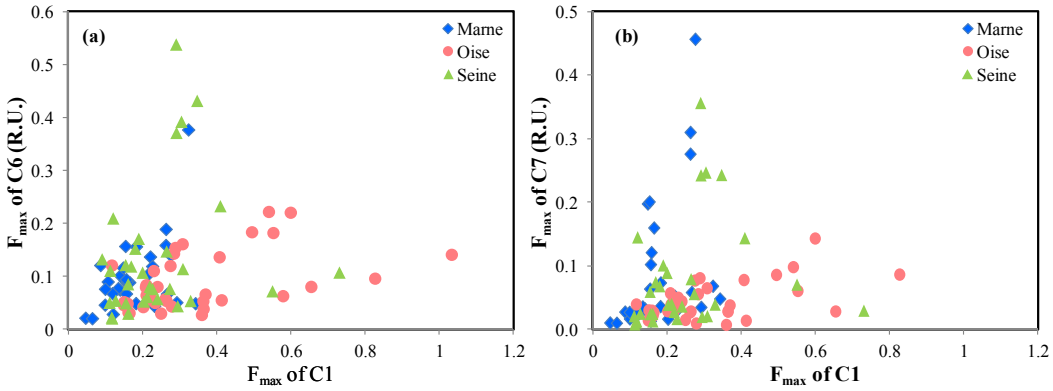

Figure 3.23 Variations of relationships between fluorescence maximum of pairs of components in the Seine River catchment. (a) Correlation between the components C6 and C1; (b) correlation between the components C7 and C1

Nonlinear correlations were seen between several of the components in single basins as well as, in some cases, for all three basins. For example, the relationships between fluorescence of components C1, C6 and C7 were shown in Figure 3.23. A logarithmic correlation was calculated between components for each basin and for all data set. However, DOM in sample O1 collected in 2011 and 2012 as well as sample S1 collected in 2012 did not contain components C5 or C7 or both C5 and C7. Thus, relationships between components C5 or C7 with other components were investigated in the data set except for the samples for which these components were not present. After log-transformation, a stronger linear correlation was found between the components (Table 3.6). Stedmon and Markager (2005a) indicated that this analysis allowed us to investigate the similarities and differences in the spatial and temporal distribution of each component and that a linear relationship will be observed between the logarithms of two components if they are both controlled by the same factor in an exponential fashion.

Table 3.6 Regression analysis of logarithmic correlation between EEM-PARAFAC components

x	y	Basin	n	R	R2	Slope		Intercept		P-value
						value	SE*	value	SE*	
C1	C2	Marne	32	0.87	0.76	1.117	0.115	-0.258	0.091	<0.001
		Oise	38	0.95	0.91	1.053	0.056	-0.342	0.032	<0.001
		Seine	32	0.80	0.64	1.105	0.146	-0.256	0.103	<0.001
		All	102	0.89	0.79	1.050	0.053	-0.317	0.037	<0.001
C1	C3	Marne	32	0.88	0.78	1.069	0.100	-0.145	0.082	<0.001
		Oise	38	0.91	0.83	0.910	0.066	-0.303	0.038	<0.001
		Seine	32	0.69	0.48	1.037	0.200	-0.134	0.141	<0.001
		All	102	0.82	0.68	0.944	0.064	-0.244	0.045	<0.001
C1	C4	Marne	32	0.94	0.88	0.806	0.052	-0.011	0.060	<0.001
		Oise	38	0.73	0.53	0.671	0.103	-0.425	0.059	<0.001
		Seine	32	0.66	0.43	0.991	0.200	-0.114	0.141	<0.001
		all	102	0.73	0.53	0.782	0.073	-0.314	0.051	<0.001
C1	C5	Marne	32	0.68	0.46	1.170	0.223	-0.171	0.182	<0.001
		Oise	37	0.48	0.23	0.692	0.203	-0.586	0.118	0.002
		Seine	32	0.41	0.17	0.935	0.344	-0.285	0.242	0.012
		all	101	0.52	0.27	0.827	0.135	-0.442	0.095	<0.001
C1	C6	Marne	32	0.49	0.24	0.694	0.212	-0.546	0.173	0.003
		Oise	38	0.44	0.19	0.546	0.174	-0.848	0.099	0.003
		Seine	32	0.30	0.09	0.583	0.292	-0.627	0.206	0.055
		all	101	0.33	0.11	0.429	0.119	-0.806	0.083	<0.001
C1	C7	Marne	32	0.52	0.275	1.174	0.329	-0.388	0.269	<0.001
		Oise	36	0.33	0.11	0.547	0.240	-1.151	0.141	0.029
		Seine	31	0.39	0.15	0.926	0.373	-0.735	0.258	0.019
		all	99	0.32	0.10	0.587	0.171	-0.987	0.119	<0.001
C2	C3	Marne	32	0.98	0.96	0.923	0.036	0.063	0.042	<0.001
		Oise	38	0.96	0.92	0.864	0.041	-0.007	0.038	<0.001
		Seine	32	0.98	0.96	1.059	0.040	0.226	0.041	<0.001
		all	102	0.97	0.94	0.942	0.023	0.084	0.024	<0.001
C2	C4	Marne	32	0.94	0.89	0.806	0.052	-0.011	0.060	<0.001
		Oise	38	0.77	0.60	0.646	0.085	-0.199	0.080	<0.001
		Seine	32	0.96	0.92	1.040	0.055	0.259	0.057	<0.001
		all	102	0.89	0.80	0.816	0.040	-0.007	0.042	<0.001
C2	C5	Marne	32	0.88	0.77	1.167	0.115	0.236	0.135	<0.001
		Oise	37	0.60	0.36	0.769	0.168	-0.259	0.158	<0.001
		Seine	32	0.82	0.68	1.280	0.157	0.366	0.163	<0.001
		all	101	0.77	0.59	1.031	0.085	0.054	0.089	<0.001
C2	C6	Marne	32	0.66	0.43	0.714	0.144	-0.280	0.168	<0.001
		Oise	38	0.57	0.32	0.616	0.145	-0.583	0.135	<0.001
		Seine	32	0.71	0.50	0.897	0.158	-0.122	0.165	<0.001
		all	102	0.58	0.34	0.633	0.087	-0.450	0.091	<0.001
C2	C7	Marne	32	0.44	0.19	0.785	0.273	-0.420	0.320	0.007
		Oise	36	0.44	0.19	0.631	0.208	-0.869	0.198	0.005
		Seine	31	0.83	0.69	1.342	0.163	-0.025	0.167	<0.001
		all	99	0.51	0.26	0.775	0.129	-0.590	0.136	<0.001

**SE means standard error*

Table 3.6 *(continued)*

x	y	Basin	n	R	R^2	Slope		Intercept		P-value
						value	SE*	value	SE*	
C3	C4	Marne	32	0.98	0.96	0.89	0.034	-0.05	0.034	<0.001
		Oise	38	0.91	0.82	0.831	0.065	-0.128	0.053	<0.001
		Seine	32	0.99	0.98	0.993	0.023	0.046	0.020	<0.001
		all	102	0.96	0.93	0.905	0.025	-0.046	0.022	<0.001
C3	C5	Marne	32	0.91	0.82	1.276	0.109	0.166	0.111	<0.001
		Oise	37	0.73	0.53	1.008	0.157	-0.163	0.129	<0.001
		Seine	32	0.92	0.84	1.313	0.102	0.179	0.090	<0.001
		all	101	0.87	0.75	1.177	0.069	0.032	0.062	<0.001
C3	C6	Marne	32	0.74	0.55	0.848	0.135	-0.256	0.138	<0.001
		Oise	38	0.72	0.52	0.866	0.135	-0.459	0.110	<0.001
		Seine	32	0.82	0.67	0.950	0.120	-0.228	0.106	<0.001
		all	102	0.71	0.51	0.796	0.077	-0.399	0.070	<0.001
C3	C7	Marne	32	0.57	0.33	1.057	0.264	-0.270	0.269	<0.001
		Oise	36	0.63	0.40	0.928	0.189	-0.709	0.156	<0.001
		Seine	31	0.89	0.80	1.300	0.118	-0.278	0.104	<0.001
		all	99	0.65	0.42	0.968	0.115	-0.534	0.105	<0.001
C4	C5	Marne	32	0.89	0.80	1.393	0.126	0.202	0.120	<0.001
		Oise	37	0.88	0.78	1.326	0.118	0.071	0.094	<0.001
		Seine	32	0.92	0.85	1.318	0.099	0.115	0.083	<0.001
		all	101	0.91	0.82	1.315	0.061	0.099	0.053	<0.001
C4	C6	Marne	32	0.80	0.64	1.000	0.135	-0.163	0.129	<0.001
		Oise	38	0.84	0.71	1.097	0.114	-0.281	0.092	<0.001
		Seine	32	0.85	0.73	0.994	0.107	-0.243	0.090	<0.001
		all	102	0.80	0.64	0.947	0.070	-0.303	0.061	<0.001
C4	C7	Marne	32	0.60	0.36	1.217	0.284	-0.183	0.272	<0.001
		Oise	36	0.80	0.64	1.194	0.150	-0.520	0.121	<0.001
		Seine	31	0.92	0.85	1.338	0.103	-0.317	0.085	<0.001
		all	99	0.71	0.51	1.122	0.110	-0.448	0.095	<0.001
C5	C6	Marne	32	0.76	0.58	0.617	0.093	-0.419	0.107	<0.001
		Oise	37	0.84	0.70	0.731	0.079	-0.435	0.080	<0.001
		Seine	32	0.89	0.79	0.723	0.067	-0.359	0.067	<0.001
		all	101	0.82	0.68	0.675	0.046	-0.419	0.048	<0.001
C5	C7	Marne	32	0.40	0.16	0.549	0.210	-0.716	0.241	0.014
		Oise	36	0.85	0.73	0.842	0.086	-0.645	0.086	<0.001
		Seine	31	0.91	0.82	0.908	0.077	-0.515	0.078	<0.001
		all	99	0.69	0.48	0.741	0.078	-0.642	0.082	<0.001
C6	C7	Marne	32	0.61	0.37	0.995	0.226	-0.228	0.256	<0.001
		Oise	36	0.85	0.72	0.979	0.102	-0.334	0.119	<0.001
		Seine	31	0.85	0.72	1.051	0.120	-0.271	0.131	<0.001
		all	99	0.77	0.59	1.011	0.085	-0.274	0.097	<0.001

**SE means standard error*

Logarithmic relationships between C1 and the components C5, C6, C7 did not exhibit significantly strong correlations for samples collected in the Marne, Oise and Seine basins. The Person correlation coefficients between C1 and these components ranged from 0.30 to 0.68 (Table 3.6). Similar trends were also observed between components C2 and C6 and between components C2 and C7. It can be concluded that these components vary in concentration independently and are not controlled by a common factor.

The slopes of regression lines between the component C1 and C2 for the samples from the basins of the rivers Marne, Oise and Seine were not significantly different from each other (F=1.65, P-value=0.197, Figure 3.24-a). This showed that the concentrations of C1 and C2 were directly proportional and that both of them have a common factor controlling their concentration. The slopes for this regression were not significantly different from 1 (z=0.94, P-value=0.349), implying that for these samples, the production rates of the two components co-vary linearly. The log(C1) intercept for Oise samples was significantly different than for the Marne and Seine samples (P-value<0.001). Stedmon and Markager (2005a) indicated that different intercepts implied that two environments had a different reference ratio of the two components. However, samples collected in the Marne and Seine basins fit on the same regression line and have an intercept common, indicating that both components have a common source and that their rates of production and of removal are controlled by a common environmental factor.

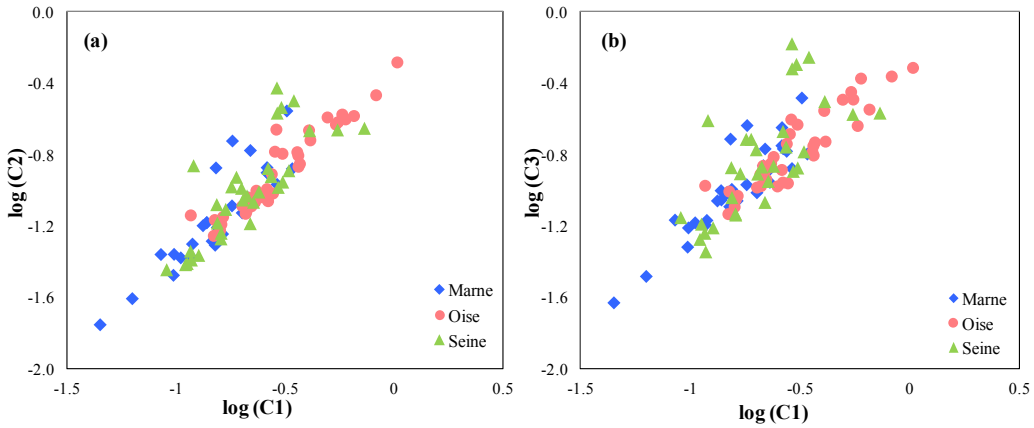

Figure 3.24 Variations of relationships between fluorescence maximum of pairs of components in the Seine River catchment. (a) Correlation between the components C2 and C1; (b) correlation between the components C3 and C1

The results in Table 3.6 and Figure 3.24-b indicated that for the samples collected in the basins of the rivers Marne and Oise, the components C1 and C3 were strongly and linearly correlated, indicating that these components have a common factor controlling their concentration. Moreover, the rates of the removal and production processes which controlled the concentration of these two components in the Marne basin are certainly similar to those occurring in the Oise basin, owing to the fact that no significant difference in the slope was observed between the regression lines of C1 and C3 in the two basins. On the other hand, the relationship for the samples from the Seine basin was weaker but significant (R^2=0.69, Table 3.6), a greater scattering was observed in the data of samples collected from the Seine basin in 2011.

In the Seine River catchment, we observed strongly linear relationships between the fluorescence of the components C2, C3 and C4, except between C2 and C4 in the basin of Oise. Nevertheless, for the regressions between the components C2, C3 and C4, the samples collected in the basin of Oise River showed different slopes and intercepts in comparison with samples collected in the basin of Seine River. These results pointed out that the production rates of these components in the Oise basin differed from those in the Seine basin. The correlations observed between these components for samples collected in the Seine basin were the same for those in the Marne basin.

We observed that the fluorescence intensity of the component C5 co-vary with that of the component C4, giving the impression that the concentration of the component C5 is linked to the concentration of the component C4. This result illustrates the fact that common processes may control their concentrations. Similarly to the relationship described between the components C1 and C2, the slopes of regression lines determined between the components C4 and C5 for samples collected from the three basins were not significantly different from each other (F=1.79, P-value=0.172). This showed that both components had a common source and were controlled by the same environmental factor. However, the values of slope were significantly higher than 1 (z=5.17, P-value < 0.05), meaning that the production rate of the component C4 was greater than that of the component C5.

The trytophan-like fluorescence (γ type fluorophore) corresponding to the component C6 in this study, has been considered to derive from autochthonous productions, associated to the

biological degradation of DOM (Coble et al. 1998). In our study, this component had a moderate correlation with the terrestrial humic-like component C3 with R^2 in the range of 0.55-0.67. These results suggested that the component C6 did not only come from autochthonous production of DOM but was also related to terrestrial inputs. This agrees with Stedmon and Markager (2005a) who reported that the fluorescence of tryptophan component co-vary with terrestrially derived components in the streams draining natural catchments and this component was associated with the degradation of terrestrial DOM in natural waters. On the other hand, Baker and Inverarity (2004) have indicated that this material was related to the labile organic matter fraction.

To sum up, the regression analysis of the humic-like components showed that there were common environmental factors controlling their concentrations, however, removal and production rates of these components were different from one basin to another. The moderate relationship of trytophan-like component with terrestrial humic-like component C3 implied the additional terrestrial origin combined to autochthonous origin.

3.4.4. Correlation between ratios of EEM-PARAFAC components with fluorescence indices

In order to evaluate the degrees of humification and the distribution of biological and/or microbial activities of each component, the correlations between the ratios of the average fluorescence maximum of components and the fluorescence indices were calculated based on the 102 EEMs samples (Table 3.7). Only correlations with both moderate and strong correlation coefficient ($-0.5>R>0.5$) and significant P-values<0.01 were presented and discussed.

The ratios of components C3, C5 and C7 versus component C1 were positively correlated with the f_{450}/f_{500} index (R^2 values ranged from 0.50 to 0.76, P-values<0.01), indicative that these components are rather microbially derived than component C1.

Table 3.7 Correlation coefficients between ratios of intensities of EEM-PARAFAC components with fluorescence indices

Correlation coefficient (R)	HIX	BIX	f_{450}/f_{500}
C3/C1	-0.618	0.505	0.785
C5/C1	-0.576	0.527	0.701
C7/C1	-0.668	ns*	0.869
C3/C2	-0.705	0.569	0.906
C4/C2	-0.791	0.717	0.802
C5/C2	-0.620	0.577	0.761
C7/C2	-0.650	ns*	0.873
C5/C3	-0.542	0.520	0.629
C7/C3	-0.627	ns*	0.807

*ns means non-significant

Moreover, there was an increase of HIX with an increase of component C2 compared to components C3, C4, C5 and C7 (R^2 values in the range of 0.42-0.50, P-values < 0.01). This proved that a relative increase of C2 considerably contributed to the humification degree or condensation of the whole DOM and that C2 seems to be more degraded than others. It is additionally observed in Table 3.7 a positive correlation of BIX with ratios of components C3, C4, C5 to C2, suggesting that C3, C4, C5 may be more derived from autochthonous origin than C2. Both ratios of intensities of components C5 and C7 to C3 showed a statistically significant and negative correlation with HIX, but positively with the f_{450}/f_{500} index, indicating that C5 as well as C7 is rather recently produced in comparison to C3.

3.5. Principal component analysis

In this study, the principal component analysis (PCA) was applied to identify the different precursors and sources of DOM in a qualitative way. PCA analysis was run on the whole data set with the following 19 variables: the seven components determined by PARAFAC analysis, nine fluorescence indices ($I_{\alpha'}$/DOC, I_{α}/DOC, I_{β}/DOC, I_{γ}/DOC, $I_{\alpha'}/I_{\alpha}$, I_{β}/I_{α}, I_{γ}/I_{α}, HIX, and BIX), three absorbance indices (SUVA, aromaticity and S_R). The PCA of these 19 parameters yielded 2 principal components (PCs) that account for 71.66% of the total variance (Figure 3.25). Figure 3.25-a demonstrated that 46.14% of the variability in the data

could be explained by the first principal component and the second principal component explained further 25.52% of the data.

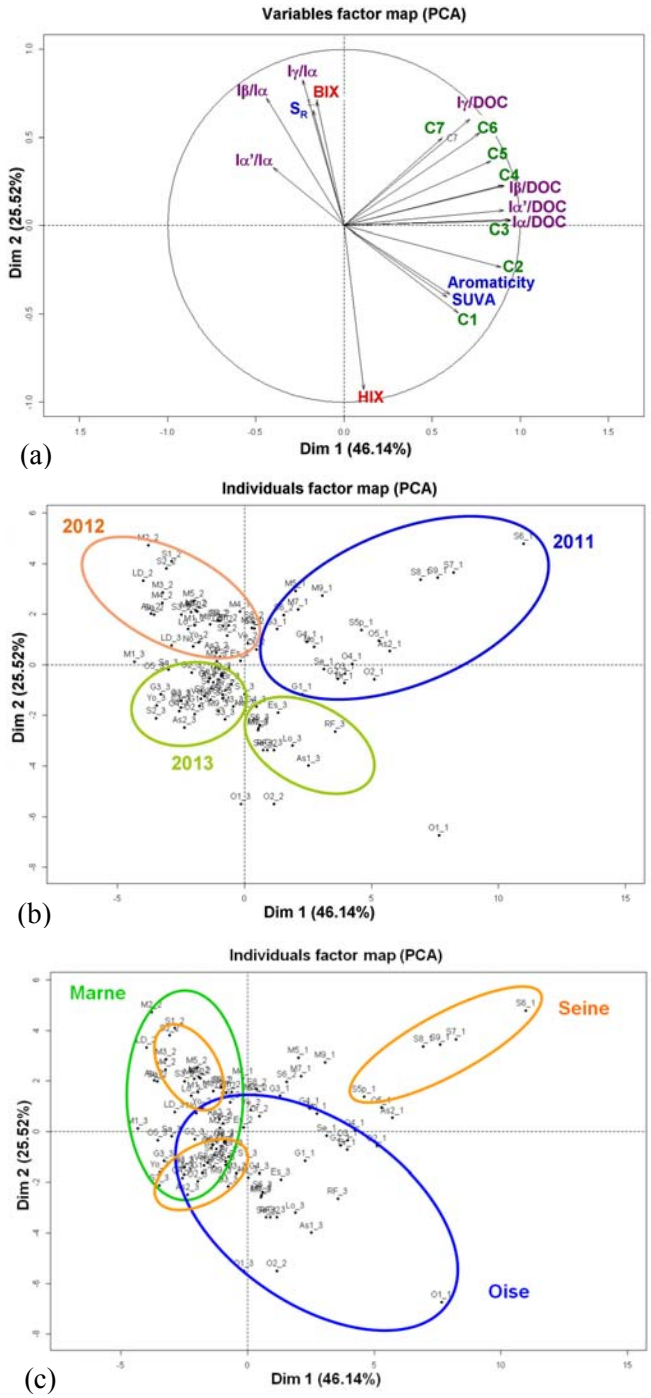

Figure 3.25 Principal component score plot of the total variance from data set. (a)-Variables factor map; (b) and (c)-Individuals factor map

The components C4 and C6 are related to the ratios of fluorescence intensity to DOC concentration I_β/DOC and I_γ/DOC, respectively. This, first, confirms that the component 4 is

similar to fluorophore β and the component 6 corresponds to protein-like material (fluorophore γ). This PCA results also indicate that C4 and C6 correspond to organic materials and substances produced from bacterial activity. The component C3 had a good relationship with $I_{\alpha'}$/DOC and I_{α}/DOC, suggesting that C3 is dominated by terrestrial humic substances (α' and α type fluorophores). The component C1 is linked to the absorbance indices (SUVA and aromaticity) and similar to humic material type, whereas HIX was negatively correlated with BIX.

The PCA analysis allowed us to observe differences among the three different sampling times. The correlation between almost all samples collected in 2012 and the fluorescence indices I_{β}/I_{α}, I_{γ}/I_{α} and BIX pointed out that for these samples DOM was linked to biological activity (Figure 3.25-b). The samples collected in 2011, especially from the Seine River, corresponded with the EEM-PARAFAC components C5, C6 and C7 as well as I_{γ}/DOC suggested that protein-like material and bacterial activity were dominant at these sites. The samples from the forest sites in the Oise basin (O1 and RF) strongly correlated with the absorbance indices (SUVA and Aromaticity) and the component C1, indicated stronger humic-like characteristics in this areas. Allmost all the samples collected in 2013 are linked with the absorbance indices aromaticity and SUVA as well as fluorescence index HIX. This result implied the more mature and aromatic DOM for samples collected during the period of flood. The differences among the three basins were also identified by PCA analysis. The Figure 3.25-c showed that samples collected in the Oise basin were characterised by more mature and aromatic DOM, whereas samples collected from the Marne and Seine basins were characterised by DOM linked to biological activity.

The PCA analysis allows us to distinguish three types of organic matter for 2011, 2012 and 2013, DOM during the flood event being more mature and aromatic. The Seine basin is characterized by the strongest biological activity (certainly in connection with the presence of the "Seine-Aval" WWTP). DOM from the Oise basin seems to have more "humic" characteristics (sample O1 presenting the strongest humic-type material). Samples collected from the Marne basin are characterized by a third specific type of organic matter.

3.6 Conclusion

The application of UV/visible absorbance and EEM fluorescence spectroscopy in combination with PARAFAC and PCA for the characteristics of DOM allowed identifying different sources of dissolved organic matter as well as variability of DOM properties in the catchment of the Seine River, the following conclusions can be drawn from this study:

1- The investigation of DOM molecular weight (MW) in the Seine River catchment showed spatio-temporal variations of this parameter. The study of S_R variations pointed out that the samples of the Marne basin (2011 and 2012) are characterized by lower molecular weight (LMW) organic material. The samples of the Seine River in 2012 are also characterized by LMW DOM. The highest molecular weights (HMW) are observed for the samples from the tributary of Marne River, Grand Morin River, and the samples collected in all the sites in 2013 (flood). The results obtained for the $SUVA_{254}$ parameter confirmed a large panel of DOM characteristics and molecular weights in the studied areas. Moreover, DOC concentration has statistically non-significant correlations with the aromatic content of DOM ($SUVA_{254}$) as well as with spectra slope ratio (S_R).

2- Spatial and temporal variations of DOM quality were highlighted according to hydrological conditions. The higher concentrations of fluorescent materials were found for waters collected in 2011 in comparison to those sampled in 2012 (low-water) and in 2013 (flood). On the other hand, higher values of fluorescence intensity ratios were observed for samples collected in 2012, reflecting the higher biological activity occurring in waters during low-water period. The samples collected in 2013 were characterised by higher HIX values, corresponding to more mature DOM compared to samples collected in 2011 and 2012.

3- A 7 components model was determined by PARAFAC on a data set of 102 samples collected from 45 sites in the Seine River catchment during three sampling periods. The seven components determined, showed similarities with peaks identified in previous studies and related in the literature. The components 4, 5, 6 and 7 seemed to be related to biological activity in these river water samples. As for components 1, 2 and 3, they seemed to be more connected to humic-like material (C1 and C2 being mainly linked to aromaticity). The component 4 is similar to fluorophore β and the

component 6 corresponds to protein-like material (fluorophore γ). Moreover, the regression analysis of the humic-like components showed that there were common factors controlling their concentrations, however, removal and production rates of these components were different from one basin to another. The moderate relationship of trytophan-like component with terrestrial humic-like component C3 implied the additional terrestrial origin in the combination with autochthonous origin. Consequently, all results supported that the combination of EEM fluorescence and Parallel Factor Analysis is an effective tool to distinguish between different sources of dissolved organic matter.

4- The separation of the samples on both axes of the PCA results showed that there were distinct differences in sources of DOM in the different basins during the three contrasting sampling periods.
5- Three types of organic matter were distinguished, the Seine River being mainly characterized by the strongest biological activity, the Oise basin by more "humic" characteristics (forest areas presenting the strongest humic-type material and a part of the Marne basin by a third specific type of organic matter.
6- Both qualitative and quantitative variations of DOM seemed to be related to hydrological conditions (floods, low water) and specific geographical locations.

In conclusion, UV/visible absorbance and EEM fluorescence spectroscopy combined to PARAFAC and PCA analyses thus appear as powerful tools to characterise DOM properties in the Seine River catchment. In order to improve the knowledge in DOM characterization and properties, it seems also of great interest to investigate its molecular size distribution. Nowadays, the size distribution of the molecules composing DOM is still remaining an open question. Dissolved organic matter is involved in numerous environmental processes (Minor et al., 2014), and its molecular size appears as a key parameter in many of these processes, such as DOM interactions with contaminants (Chin et al., 1997; Chen et al., 2010), DOM bioavailability (Amon and Benner, 1996), or DOM sorptive capacity (Sun et al., 2013).

The next chapter thus deals with the development of a semi-quantitative asymmetrical flow field-flow fractionation (AF4) methodology for characterizing and determining the size distribution of DOM from the Seine River catchment.

CHAPTER IV: DEVELOPMENT OF ASYMMETRICAL FLOW FIELD-FLOW FRACTIONATION TO CHARACTERIZE DISSOLVED ORGANIC MATTER IN NATURAL FRESHWATER ENVIRONMENTS

Development of asymmetrical flow field-flow fractionation to characterize dissolved organic matter

Keywords: Dissolved organic matter, asymmetrical flow field-flow fractionation, optimization, cross-flow rate, focusing time

Abstract:

The separation of dissolved organic matter (DOM) macromolecules by asymmetrical flow field-flow fractionation hyphenated to UV and light scattering detectors was investigated by optimising the operating conditions: programmed cross-flow form and focusing time. An off-line excitation emission matrix (EEM) fluorescence detection was performed to characterize the nature of the fractionated DOM. In order to achieve the complete separation of DOM in natural aquatic environments, the following experimental conditions were defined: a constant cross-flow rate of 2 ml min^{-1} during the focus/relaxation step with a focusing time of 2 min and an exponential gradient of cross-flow from 3.5 to 0.2 ml min^{-1} during the elution step.

4.1 Introduction

Dissolved organic matter (DOM) presents in natural freshwater environments and particularly in surface waters [1], is a highly complex mixture of organic compounds derived from both natural sources (terrestrial vegetation, soils, and microorganisms) and anthropogenic inputs (municipal and industrial wastewater discharge) [2]. DOM plays an essential role in shaping aquatic ecosystems [3] because of the number of processes in which it becomes involved. It can influence in particular the speciation, solubility, toxicity and transport of organic and inorganic pollutants [4]–[6]. Furthermore, DOM is also involved in aqueous photochemical reactions, nutrients cycling and availability [7], [8]. The mechanisms implied in the transport and transformation of contaminants and nutrients are strongly associated with the nature and in particular the size of DOM. To get a better understanding of DOM environmental role in aquatic ecosystems, it is essential to improve the knowledge on its physicochemical properties, composition as well as size distribution in the aquatic environment.

The size distributions of DOM have traditionally been determined using ultrafiltration. However, owing to DOM's heterogeneity, ultrafiltration methods provide limited information about the size spectrum [9]. Recently, flow field-flow fractionation (FlFFF), a size-fractionation technique, has been applied to characterize DOM across the size continuum. Flow field-flow fractionation is a chromatography-like elution technique allowing the separation of macromolecules in the range of 0.001 to 1 µm. The continuous size distribution of macromolecules will be obtained by on-line coupling to a multi-detector setup or by collecting sample fractions for further off-line analyses. Typically, the most commonly utilized detectors with FFF are UV-Vis and fluorescence spectroscopy, laser light scattering (MALLS), dynamic light scattering (DLS), and differential refractive index (RI)...

The objective of this work was to develop an asymmetrical flow field-flow fractionation (AF4) methodology for characterizing and determining the size distribution of DOM from natural waters without pre-concentration before injection into the channel of AF4. The optimized method was performed to characterize the DOM size properties in natural surface water samples collected from the Seine River watershed in France.

4.2 Material and methods

4.2.1 Sampling site

The Seine River catchment (75,000 km^2) in the Northern part of France is characterised by a high population of some 16 million inhabitants (28% of the total French population), mainly present in the urban area of Paris [10]. It represents an important example of regional territory strongly influenced by anthropogenic activity [11]. Among the 39 natural water samples collected in the Seine River catchment in September 2012 (during low-water period), six of them, presenting contrasted DOM characteristics on the basis of their EEM spectral signatures, were chosen to optimize the AF4 operating conditions. These samples were collected from the following sites: Moncetz l'Abbaye (M2) and Dormans (M4) in the Marne River, Beaumont (O5) in the Oise River, Mery (S1), Conflans St Honorine (S6) and Vernon (S9) in the Seine River (Figure 4.1). Immediately after sampling, all freshwater samples were filtered through a pre-combusted glass fibre filter (GF/F 0.7µm; Whatman) and stored in the dark at 4°C.

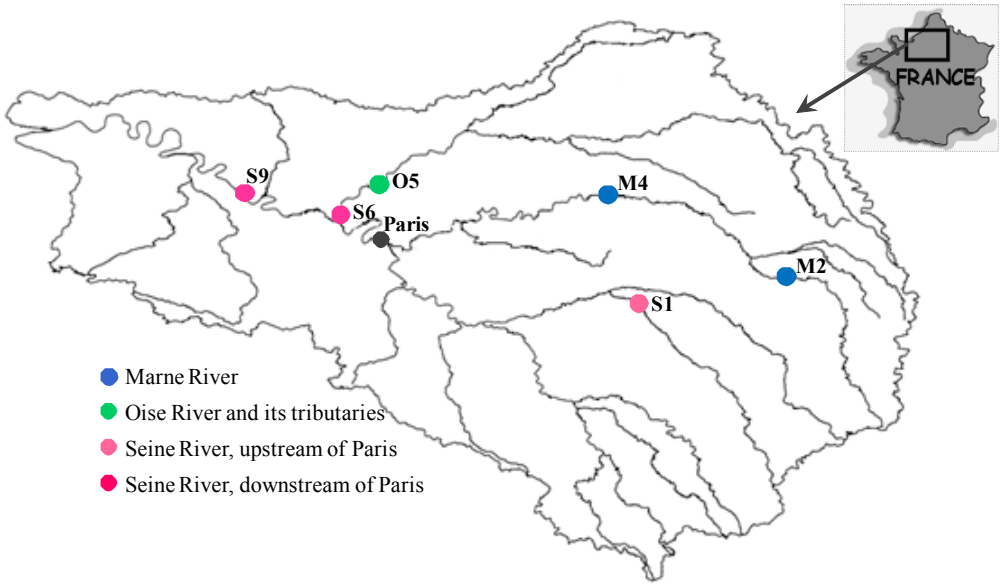

Figure 4.1 Location of the studied samples in the Seine River catchment, France [12]

4.2.2 DOC measurements

Dissolved organic carbon (DOC) concentration was measured using a total organic carbon analyser (Shimadzu TOC-V CSN). The total carbon in the sample was oxidized, by high temperature combustion catalytic oxidation method, in carbon dioxide which was detected by a non-dispersive infrared detector (NDIR). The instrument was run in non purgeable organic carbon (NPOC) mode. The apparatus was calibrated using a standard solution of potassium hydrogen phthalate $C_6H_4(COOK)(-COOH)$, diluted to different concentrations according to the estimated DOC content of the samples.

4.2.3 Fluorescence measurements

All samples were analyzed by excitation emission matrix (EEM) fluorescence spectroscopy. Fluorescence spectra were recorded using a Fluorolog FL3-22 Horiba Jobin-Yvon spectrofluorometer, equipped with double monochromators for both excitation and emission sides. The samples were placed, at natural pH, in 1 cm quartz cuvettes, thermostated at 20°C. The fluorescence spectra were generated by recording 17 emission spectra (260-700nm) at excitation wavelengths taken every 10 nm between 250 and 410 nm [13]. The EEM spectra of the samples were obtained by subtracting the EEM spectrum of ultrapure water (Milli-Q, Millipore) and were instrumentally corrected. Fluorescence spectra were normalized to the integrated intensities of the Raman scattering band of ultrapure water samples as previously

described (Huguet et al., 2009), affording the Raman unit as a quantitative measure of the signal intensity. If UV-Vis absorbance values were higher than 0.1, samples were diluted with ultrapure water before fluorescence analysis in order to avoid inner filter effects.

4.2.4 Asymmetrical flow field-flow fractionation setup

Experiments were carried out with an Eclipse 3 AF4 system (Wyatt Technology, Europe) coupled online to variable wavelength UV detector (HP 1200 series, Agilent) and a multi-angle light scattering (MALLS) detector (three measuring angles - miniDAWN TREOS, Wyatt Technology Europe). The fractionation system was equipped with a 1 kDa molecular weight cut off polyethersulfone (PES, Pall Omega) membrane, a 1-ml injection loop and a 490-µm spacer. Before placing in the cell, the membranes were rinsed with ultrapure water (Milli-Q, Millipore). Flows were controlled with an Agilent 1200 Series isocratic pump equipped with an Agilent 1200 Series micro-vacuum degasser (Agilent Technologies). The carrier solution was filtered (0.1 µm) ultrapure water (Milli-Q, Millipore). 0.1 µm on-line polyvinylidene fluoride (PVDF) filters were placed in the carrier line, after the HPLC pump and before entering to the channel, in order to remove any impure particulate coming from the pump. The injection flow rate and focus flow rate were 0.02 and 2.00 ml min^{-1}, respectively.

Absorbance wavelength was recorded at 280 nm. The measured absorbance at wavelength λ was converted to absorption coefficient a_λ according to $a_\lambda=2.303A_\lambda/l$ (A_λ the absorbance at wavelength λ; l the path-length of the optical cell in meters (here 0.01m)). Data from MALLS detector were acquired at three angles (45^o, 90^o, and 135^o) processed with Astra software, version 5.3.4.13 (Wyatt Technology).
The recovery calculations were done by injecting sample without any cross-flow (i.e., inject with elution)[14], [15].

4.3 Results and discussion

4.3.1 Optimization of cross-flow rate/cross flow mode

During both the focus and the elution steps, the cross-flow rate plays an important role on the fractionation. It is the main parameter that controls the distribution of analytes in the channel and so the efficiency of the separation.

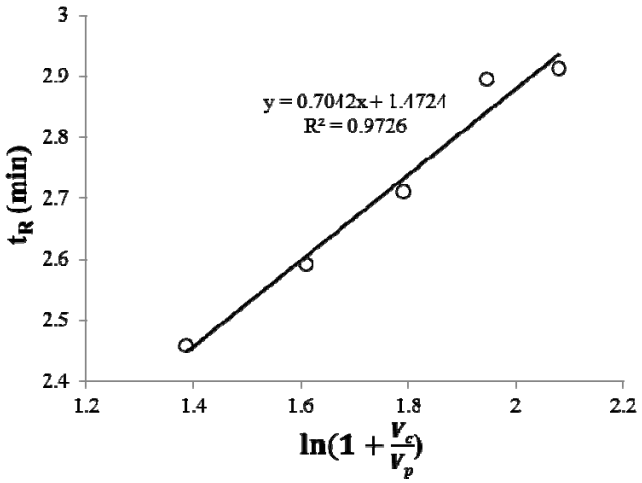

Figure 4.2 Correlation between cross-flow rate (V_c) and the retention time (t_R) of small fractions of DOM for sample Beaumont (O5) collected in 2012. V_p is detector flow.

The cross-flow rate was investigated over the range 1.5-3.5 ml min^{-1} with a corresponding detector-flow rate kept constant at 0.5 ml min^{-1}. Figure 4.2 showed the effect of changing the cross-flow rates on the retention time of small size DOM fraction. According to these results, increasing the cross flow the DOM macromolecules migrated closer to the accumulation wall and were hold longer in the channel. Thus, they eluted with a larger retention time, what resulted in a higher resolution of the low molecular weight (LMW) DOM fractionation from the void time, and the optimal cross-flow rate appears clearly to be the highest one. According to the relationship between the retention time and the cross-flow rate in AF4 (Equation 2.23 in chapter II), by plotting the change in t_R according the V_c, a linear relation appears where the slope is directly proportional to the size. By assuming the range of the effective channel spacer thickness, a surrounding size of this population can be estimated under 1nm. As this size range is centred relatively low, and owing to the fact that DOM macromolecules had a high diffusiveness [16], it is essential to apply high cross-flow rate for the separation of these macromolecules from the void peak in order to determine their diffusion coefficient, size or molar mass distribution. However, a too high cross-flow rate might lead to a very long separation time and adsorption or absorption onto the membrane or aggregation of the macromolecules [14].

The high cross-flow rate indicated a high resolution and selectivity for the LMW-DOM fractionation. On the other hand, the high molecular weight (HMW) DOM fractionation was eluted very strongly diluted and very late or even not eluted completely [17]. Figure 4.4 showed the elution of some material detected by the UV and MALLS detectors when the cross-

flow was turned off after 35 minutes. Expanding the elution time to 45 min resulted in some material eluted in the end of the analysis procedure. From these attempts it was obvious that the constant cross-flow was not satisfactory to fractionate DOM macromolecules. A cross-flow profile (exponential, gradient…) was considered as a valuable solution for the AF4 separation of samples with a wide range of molecular size.

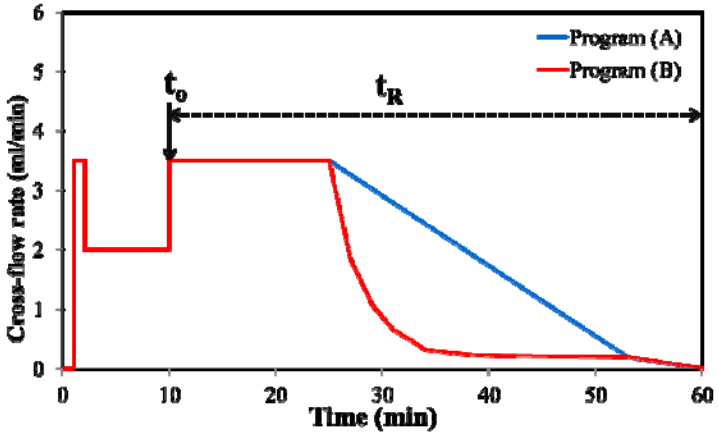

Figure 4.3 Cross-flow rate during different phases of a programmed cross-flow separation

Applying a linear gradient program seemed to be the intuitively simplest way of continuously decreasing the cross-flow rate [18]. As aquatic DOM is expected to cover a wide range of sizes with nevertheless a considerable part of molecular sizes rather low, we investigated the two following different cross-flow rate programs (Figure 4.3):

- Program (A) 3.5 ml min^{-1} for 15 min and a decrease to 0.2 ml min^{-1} within 28 min in a linear way.
- Program (B) 3.5 ml min^{-1} for 15 min and exponentially reduced to 0.2 ml min^{-1} within 28 min.

The corresponding UV and MALLS fractograms obtained are presented on Figure 4.4. By using a non-constant cross-flow program, even if some residue appears, the elution of the HMW-DOM macromolecules is improved compared to the constant one. However, by using the program (B) the largest DOM size were successively eluted with a more suitable resolution as it was shown in literature for inorganic and organic colloid [19].

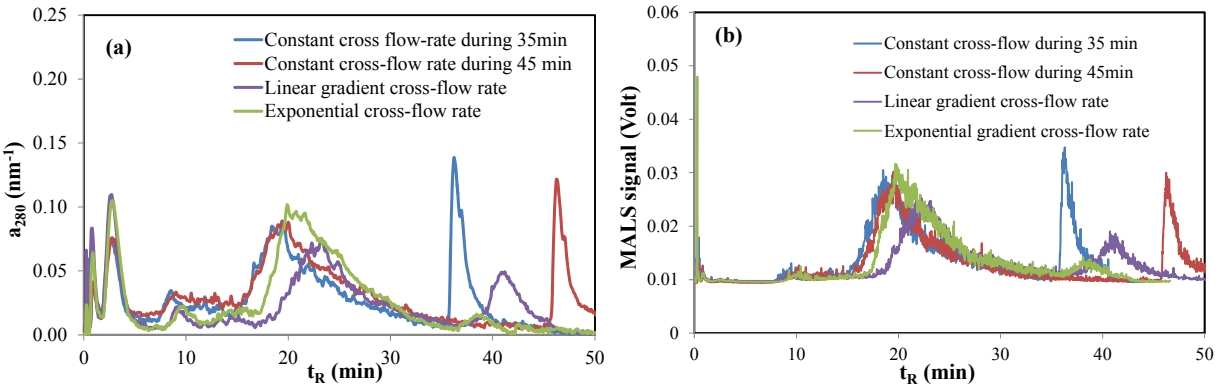

Figure 4.4 Effect of different cross-flow program form on the separation of DOM macromolecules of sample Mery (S1) collected in 2012.
(a) - UV signal at 280 nm; (b) - MALLS 90^{o} signal

To conclude, in order to fractionate natural colloids the exponential method presents other advantages compared to the constant cross-flow one, including (a) the ability to separate a large size range of colloids in a single experiment associated to a convenient time; (b) maintaining a convenient resolution on the whole fractogram; (c) the ability to identify and characterize highly retained colloidal material by using appropriate detection; and (d) a convenient baseline stability. Nevertheless, the simple AF4 equation connecting retention time and analytes size with a constant cross-flow program cannot be applied with exponential cross-flow. For this last mode, a more complicated equation exists and expressed as [19]:

$$t_R = \tau + \left(\frac{\tau}{1 + \frac{6 D \tau}{W^2}} \right) \ln \left\{ 1 + \left[\left(\frac{L - z'}{L} . \frac{V_{co}}{V_p} \right) \left(1 + \frac{W^2}{6 D \tau} \right) \right] + \left[\frac{W^2}{6 D \tau} \left(e^{-\frac{W^2}{6 D \tau}} - 1 \right) \right] \right\}$$

where τ is the time constant of the exponential decay, L is the channel length (cm), z is the sample focusing distance from the chanel inlet (cm) and V_{co} is the initial cross-flow rate (ml/min).

According to its complexity, the characterization of analyte sizes based on their retention time appears to be highly difficult without appropriate calibrants. However, for natural colloids, it is quite impossible to find accurate, efficient and identical calibrants. But by using an off-line detection, such as fluorescence, the exponential program becomes highly interesting due to its high resolution to separate and fractionate natural organic matter colloids on a wide size range.

4.3.2 Optimization of relaxation time

The relaxation time or focusing time is the time necessary for the analytes to reach the equilibrium according to Fick's law. This equilibrium leads to an exponential distribution of the analytes (Equation 2.12 in chapter II) according to their size along the channel height at the focusing point. Pitkänen et al. [20] indicated that the longer sample focusing time may improve the resolution and influence the recovery.

In this work, the duration of the focusing step was investigated for eight different values from 0 to 10 min associated to a constant cross-flow rate of 2 ml min^{-1}. For the fraction closer to the void time, the signal decreases with longer focus time (Figure 4.5). This decrease could be attributed to the loss of smallest analytes through the channel membrane and/or adsorbed on its surface. A longer focusing time could change the dispersion state of the analytes characterized by its aggregation. To understand this phenomenon, the smallest fraction was collected without focus time (t_f=0 min) and with t_f=2 min, and then analyzed by EEM fluorescence spectroscopy and illustrated on Figure 4.6. Similar EEM spectra shapes were obtained between the collected fraction with t_f=0 min and the initial sample (before injection), whereas for t_f =2 min, some differences appeared on the EEM spectrum compared to that of the raw water. Based on this observation, the fraction with t_f=0 min seems to be unfractionated compared to the t_f=2min one. This result allows verifying that a longer focusing time is necessary to insure an equilibrium and a distribution of the analytes in the channel height [16]. As it is illustrated on the UV trace of the fractogram on Figure 4.5, the area of the peak at low t_R (1 min) stayed constant after t_f= 2 min. In contrast, t_f> 3min led to a decrease of the signal area corresponding to the continuous fraction eluted between 1.5 and 5 min. Indeed, a too long focusing time may increase sample-membrane interactions or lead to aggregation, what in both cases is characterized by a decrease of the recovery level for the corresponding signal. Based on these results, a 2min focusing time was chosen as optimal value.

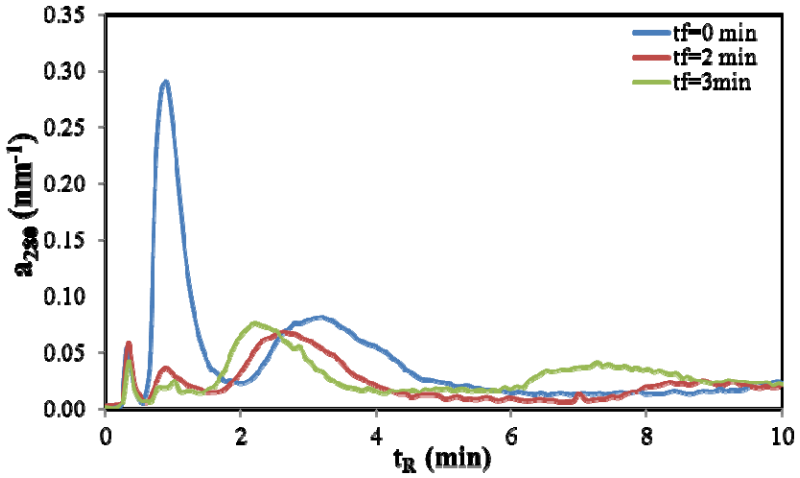

Figure 4.5 Fractograms of small fractions of DOM obtained by UV detector as a function of focus time.

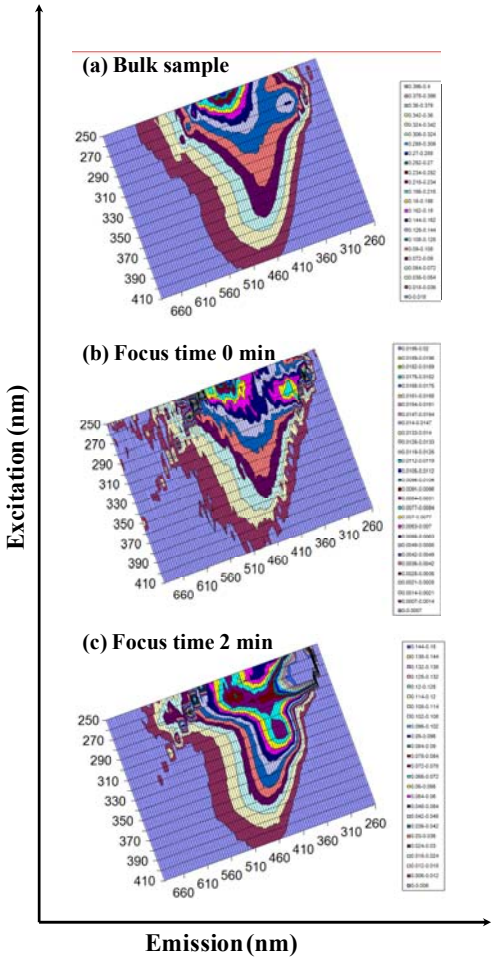

Figure 4.6 EEM spectra of (a) bulk sample Mery (S1- 2012),
(b) fraction collected for t_f =0 min, (c) fraction collected for t_f =2 min

4.4 Applicability

In order to evaluate the efficiency of the optimized parameters, the developed method was applied to analyse the natural water samples from the Seine River catchment collected in 2012. Figure 4.7 presents the corresponding UV and MALLS fractograms, in the optimized conditions previously determined, for 6 samples presenting contrasted DOM characteristics and representative trends of what we observed in the whole Seine River catchment.

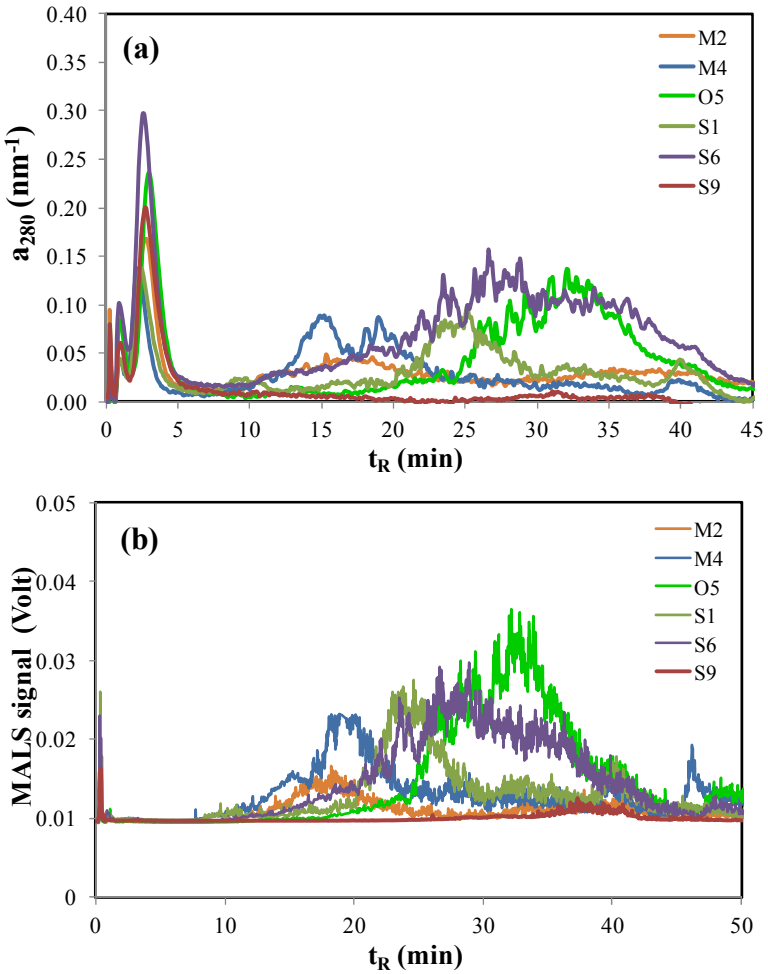

Figure 4.7 Fractograms for 6 samples from the Seine River catchment in the optimized conditions obtained by (a) UV and (b) MALLS detectors

By using a constant cross-flow rate of 3.5 ml min-1, two UV signals appear between 1 and 5 minutes, the first signal is centred at 1.0±0.1 min and the second one is centred at 2.6±0.3 min. Because MALLS detectors depends to both size and quantify of the analyte, the lack of MALLS signals at this time range indicates the presence of small size analytes (under the size

cut-off of the detector, i.e. 10 nm). On the other hand, by using an exponential cross-flow program after 15 minutes, a large MALLS signal corresponding to larger molecular weight fractions is evidenced. The relatively long broad elution of HMW-DOM fraction was also observed from the Damariscotta River estuary in previous study [21]. In this study, the fractograms of the DOM presents two peaks corresponding of distinct colloidal populations. It appears that the LMW-DOM fraction presents the identical UV abundance to the one observed in our study compared to the larger DOM fraction. These previous results confirm the accuracy and the efficiency of new method to fractionate natural colloidal samples.

According to the natural surface water samples studied, different distribution profiles were observed. Indeed, on the whole data set, three main tendencies appeared through three different types of fractogram patterns highlighting different types and/or sources of organic matter, in any case exhibiting different molecular sizes, with some similarities or peculiarities between the three studied sub-basins. These results thus demonstrated that the optimized method was applicable for the separation of DOM macromolecules in natural waters on a wide range of sizes.

4.5 Conclusion

In this study, Asymmetrical Flow Field-Flow Fractionation technique was optimized to characterize DOM macromolecules. The different cross-flow rate, relaxation time as well as cross-flow gradient were investigated in order to determine the optimal parameters and the best compromises for an efficiency of separation while minimizing material losses. Indeed, almost all the LMW DOM may be lost through the membrane during the relaxation time. To avoid this phenomenon, it would be necessary in the future to utilize smaller molecular weight cut-off membranes.

Nevertheless, AF4 has been applied in this study to the partition of constituents from natural surface water samples into a continuum of colloidal sizes. This work allowed us to discriminate between different types of DOM in the catchment of the Seine River, in France, and highlighted significant spatial variations of DOM as well as specific typologies for the different sampling sites. On the other hand, EEM fluorescence spectroscopy coupled to AF4 appeared to be a powerful tool for the study of DOM in aquatic environment and offered new perspectives in the characterization and separation of colloidal DOM.

Acknowledgements: *The Program PIREN-Seine (http://www.piren-seine.fr) is acknowledged for financial support. All the members involved in the "Organic Matter" part of PIREN Seine project are acknowledged for their help in sampling. The French Government (Embassy of France in Hanoi) is acknowledged for the PhD grant of NGUYEN Phuong Thanh.*

References

[1] Matilainen A, Gjessing ET, Lahtinen T, Hed L, Bhatnagar A and Sillanpää M (2011) An overview of the methods used in the characterisation of natural organic matter (NOM) in relation to drinking water treatment. *Chemosphere* 83(11):1431-1442

[2] Cawley KM, Butler KD, Aiken GR, Larsen LG, Huntington TG and McKnight DM (2012) Identifying fluorescent pulp mill effluent in the Gulf of Maine and its watershed. *Mar. Pollut. Bull.* 64(8):1678-1687

[3] Stedmon CA, Markager S and Bro R (2003) Tracing dissolved organic matter in aquatic environments using a new approach to fluorescence spectroscopy. *Mar. Chem.* 82(3–4):239–254

[4] Backhus DA, Golini C and Castellanos E (2003) Evaluation of Fluorescence Quenching for Assessing the Importance of Interactions between Nonpolar Organic Pollutants and Dissolved Organic Matter. *Environ. Sci. Technol.* 37(20):4717-4723

[5] Koukal B, Guéguen C, Pardos M and Dominik J (2003) Influence of humic substances on the toxic effects of cadmium and zinc to the green alga Pseudokirchneriella subcapitata. *Chemosphere* 53(8):953-961

[6] Guéguen C, Gilbin R, Pardos M and Dominik J (2004) Water toxicity and metal contamination assessment of a polluted river: the Upper Vistula River (Poland). *Appl. Geochem.*19(1):153-162

[7] Bormann FH and Likens GE (1967) Nutrient Cycling. *Science* 155(3761):424-429

[8] Nebbioso A and Piccolo A (2013) Molecular characterization of dissolved organic matter (DOM): a critical review. *Anal. Bioanal. Chem.* 405(1):109-124

[9] Stolpe B, Guo L, Shiller AM and Hassellöv M (2010) Size and composition of colloidal organic matter and trace elements in the Mississippi River, Pearl River and the northern Gulf of Mexico, as characterized by flow field-flow fractionation. *Mar. Chem.* 118(3-4):119-128

[10] Even S, Billen G, Bacq N, Théry S, Ruelland D, Garnier J, Cugier P, Poulin M, Blanc S, Lamy F and Paffoni C (2007) New tools for modelling water quality of hydrosystems: An application in the Seine River basin in the frame of the Water Framework Directive. *Sci. Total Environ.* 375(1–3):274-291

[11] Billen G, Garnier J, Mouchel J-M and Silvestre M (2007) The Seine system: Introduction to a multidisciplinary approach of the functioning of a regional river system. *Sci. Total Environ.* 375 (1-3):1-12

[12] Varrault G, Nguyen PT, Bonnot C, Soares-Pereira C, Guo Y, Parot J, Parlanti E, Benedetti M F, Garnier J, Derenne S, Gelabert A, Bressy A, Boudahmane L, Mercier B, Martinez A, Cordier M-A, Cordier L, Anquetil C, Tharaud M and Saad M (2013) Caractérisation de la variabilité spatio-temporelle des qualités et des quantités de

matière organique dans l'Oise, la Seine et la Marne. Programme PIREN-Seine - Phase 6 - Rapport 2013. http://www.sisyphe.upmc.fr/piren/?q=webfm_send/1300

[13] Parlanti E, Wörz K, Geoffroy L, and Lamotte M (2000) Dissolved organic matter fluorescence spectroscopy as a tool to estimate biological activity in a coastal zone submitted to anthropogenic inputs. *Org. Geochem.* 31(12):1765-1781

[14] Dubascoux S, Kammer FVD, Le Hécho I, Gautier MP and Lespes G (2008) Optimisation of asymmetrical flow field flow fractionation for environmental nanoparticles separation. *J. Chromatogr. A* 1206(2):160-165

[15] Hadri HE, Gigault J, Chéry P, Potin-Gautier M, and Lespes G (2014) Optimization of flow field-flow fractionation for the characterization of natural colloids. *Anal. Bioanal. Chem.* 406(6):1-11

[16] Hassellöv M, Kammer FVD, and Beckett R (2007) Characterisation of Aquatic Colloids and Macromolecules by Field-Flow Fractionation. West Sussex, England, John Wiley & Sons Ltd, 223-276.

[17] Qureshi RN and Kok WT (2011) Application of flow field-flow fractionation for the characterization of macromolecules of biological interest: a review. *Anal. Bioanal. Chem.* 399(4):1401-1411

[18] Leeman M, Wahlund K-G, and Wittgren B (2006) Programmed cross flow asymmetrical flow field-flow fractionation for the size separation of pullulans and hydroxypropyl cellulose. *J. Chromatogr. A* 1134(1–2):236-245

[19] Kirkland JJ, Dilks CH, Jr., Rementer SW, and Yau WW (1992) Asymmetric-channel flow field-flow fractionation with exponential force-field programming. *J. Chromatogr. A* 593(1-2):339-355

[20] Pitkänen L, Sontag-Strohm T, and Kanerva P (2014) Enhanced separation and characterization of gluten polymers by asymmetrical flow field-flow fractionation coupled with multiple detectors. *J. Cereal Sci.* 59(2):126-131

[21] Boehme J and Wells M (2016) Fluorescence variability of marine and terrestrial colloids: Examining size fractions of chromophoric dissolved organic matter in the Damariscotta River estuary. Mar. Chem. 101:95-103

CHAPTER V: ASYMMETRICAL FLOW FIELD-FLOW FRACTIONATION COMBINED TO OPTICAL SPECTROSCOPY FOR THE CHARACTERIZATION OF AQUATIC DISSOLVED ORGANIC MATTER FROM THE SEINE RIVER CATCHMENT (FRANCE)

In order to obtain more information on the organic matter in the Seine River catchment, asymmetrical flow field-flow fractionation, coupled on-line to UV detector and off-line to EEM fluorescence spectroscopy, was applied to characterize the different size-based fractions of colloidal DOM and determine their molecular weight (MW) distributions.

5.1. Molecular weight calibration

Organic macromolecules ranging from 960 to 66,000 Da, including Trypan blue (0.961 KDa), vitamin B12 (1.33 KDa), bovine heart cytochrome C (12.4 KDa) and bovine serum albumin (66 KDa) were used as molecular mass standards to estimate the molecular weight (MW) distributions of DOM from the Seine River catchment (Figure 5.1). Such a MW calibration was previously validated by Guéguen and Cuss (2011) by comparing the MW of Suwannee River Fulvic Acid (SRFA) and Suwannee River Humic Acid (SRHA) determined by using these macromolecular standards to those obtained by using polystyrenesulfonate (PSS) standards. These authors showed that calibration using the above organic macromolecules could be used to estimate MW of natural organic colloids.

The void time, t_o was determined by injecting 10mM ascorbic acid (MW = 0.18 KDa) into the AF4 system with the optimized parameters determined in chapter IV. The result showed that the retention time of ascorbic acid or void time was 1.08 min (Figure 5.1a).

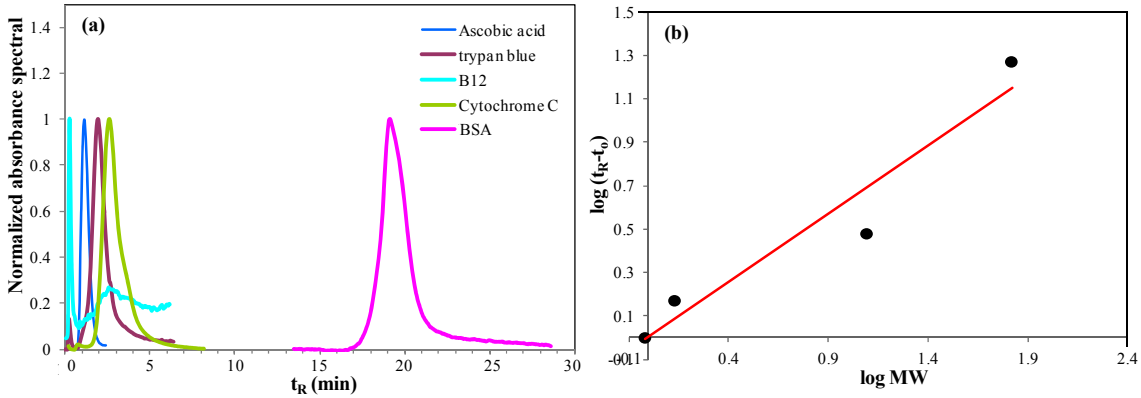

Figure 5.1 (a) UV fractogram of standards, and (b) UV calibration curve obtained between molecular weight and retention time of standards

A relationship (Figure 5.1b) between molecular weight of the organic macromolecular standards, MW and the retention time, t_R was obtained as follows.

$$\log (t_R\text{-}t_o) = 0.652 \log MW - 0.029$$

where t_o is the void time.

The recovery calculations were done by injecting sample without any cross-flow (i.e., inject with elution) (Dubascoux et al., 2008). Then, injections with an effective fractionation (i.e., with cross flow or focus time) were realized. After each different injection, peak areas were calculated and the recovery (R) was expressed as

$$R\,(\%) = \frac{S}{S_0} x100$$

Where S is peak area obtained with cross-flow, S_0 is the peak area obtained without cross-flow and focus time.

For our study, the recovery was determined by considering both the UV and MALLS signal. The relatively low recovery (less than 20%) determined by the UV signal and high recovery (more than 70%) determined by the MALLS signal showed that samples within the Seine River catchment was characterized by low molecular weight DOM which could be lost through the membrane during the relaxation time.

The lack of MALLS signals observed for small fractions eluted from 1 to 10 min (Figure 5.2) indicated the presence of small size analytes under the size cut-off of the detector. Thus, we just focus on the UV signals of samples collected in the Seine River catchment. On the other hand, for the larger size fraction eluted after 10 min exhibited relatively long broad peak. From the theory, we can estimate the hydrodynamic diameter of these fractions in the range of 4 nm to 0.7µm.

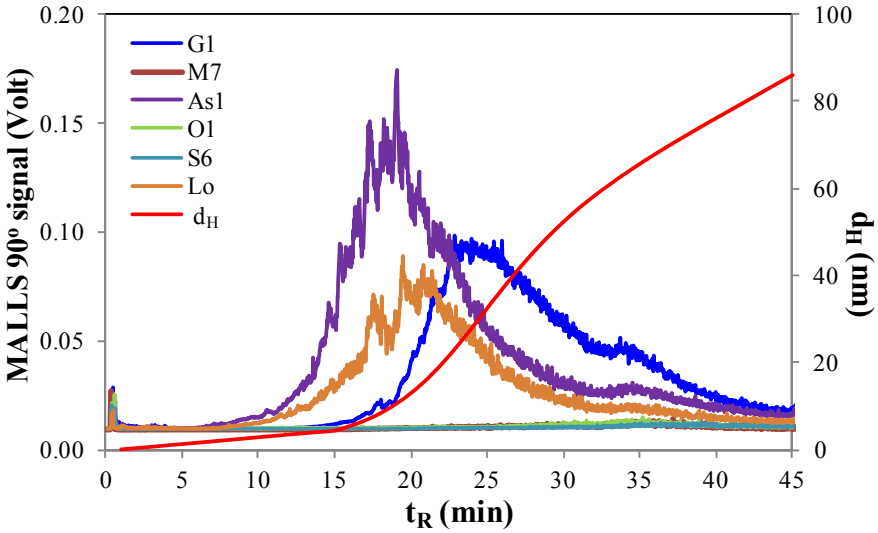

Figure 5.2 MALLS fractograms of samples collected in the Seine River catchment in 2013

5.2. Characterization of organic matter fractions

The DOM size distributions investigated for the samples collected in 2011 in the Seine River catchment are presented on Figures 5.3, 5.4 and 5.5. All other fractograms of samples collected in 2012 and 2013 are given in Appendix 3.

The UV signal observed for samples collected in forest zones such as sample O1 was much higher than the other ones, whatever the sampling date. For this sample, higher values of DOC concentrations and HIX index have already been mentioned in chapter III.

The first peak, that eluted during the first five minutes of elution period and quantified the smallest constituents, was observed in all samples with the highest UV signal intensity. The peak eluted from 5 min to 10 min corresponding to MW in the range 9000-31000 Da was just seen for some samples such as sample G3 collected in 2011 (Figure 5.3), samples M2 and Or collected in 2012 as well as sample As1 collected in 2013 (Appendix 3).

However, in comparison with the first peak, the relatively lower UV signal of this fraction indicated considerably low concentration of its constituents. The continuous elution corresponding to larger MW gave rise to a broader signal making difficult the determination of the MW distributions for these fractions. Thus, we just limited our study to the estimation of the MW distribution of the smallest DOM constituents.

The MW distributions of DOM obtained from the UV detector signal were determined by calibrating the AF4 system with a series of molecular weight-known organic macromolecules (part 5.1). Resulting values of number-average (M_n) and weight-average (M_w) molecular weights, as well as polydispersity index (PDI) corresponding to the smallest DOM constituents were indicated in Table 5.1.

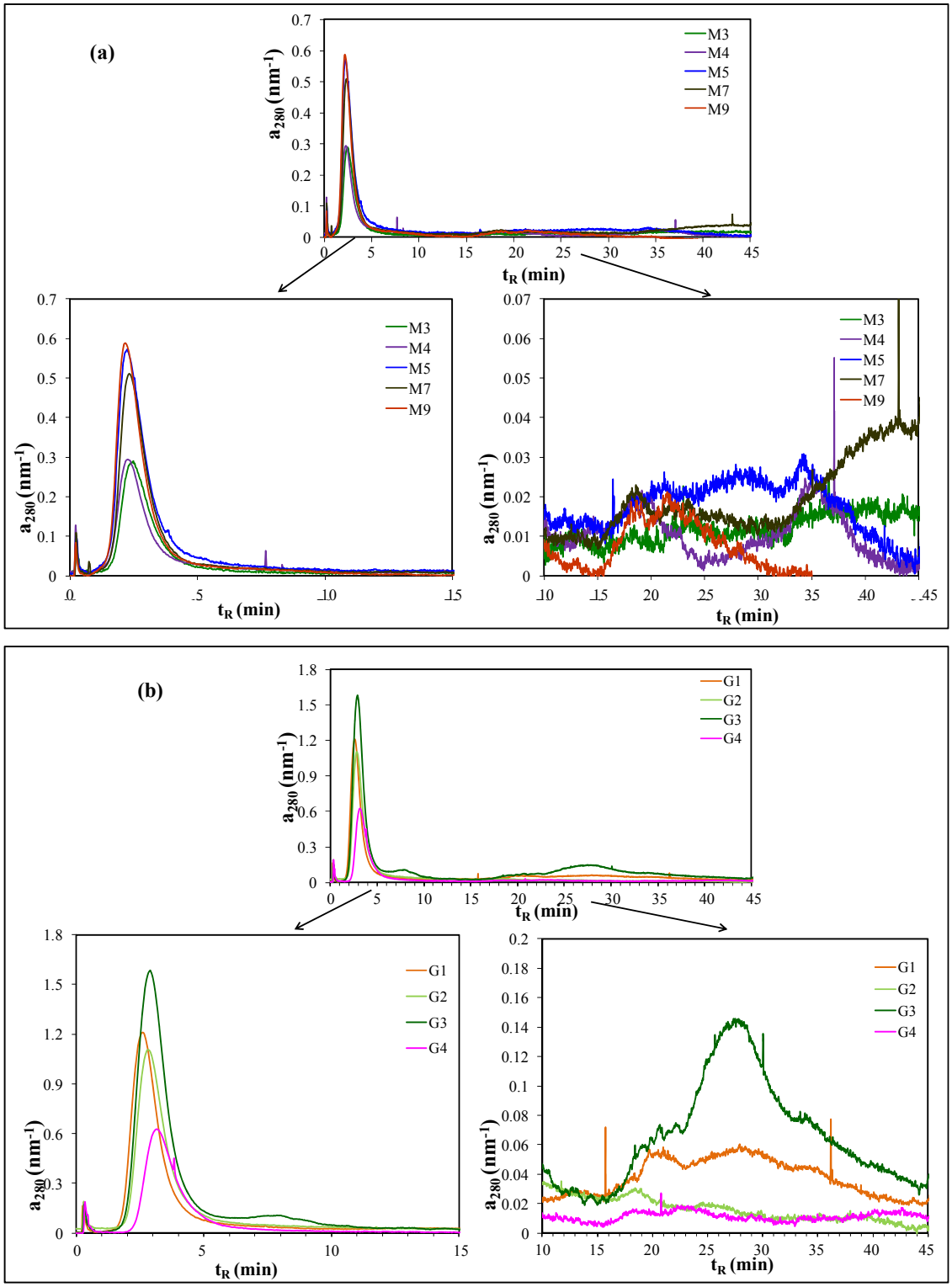

Figure 5.3 UV fractograms of samples collected in (a) Marne River and (b) Grand Morin tributary in 2011.

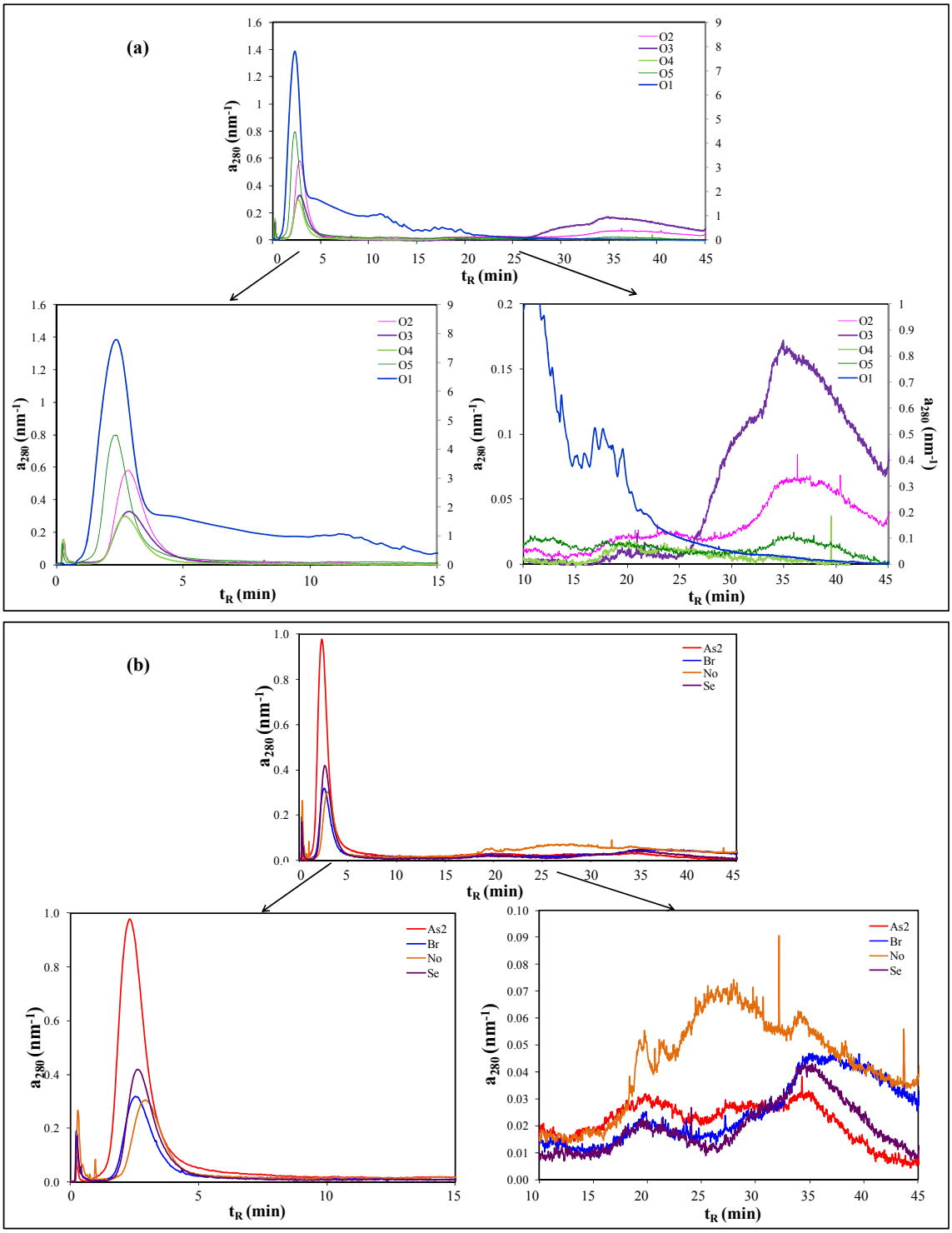

Figure 5.4 UV fractograms of samples collected in (a) Oise River and (b) its tributaries in 2011.

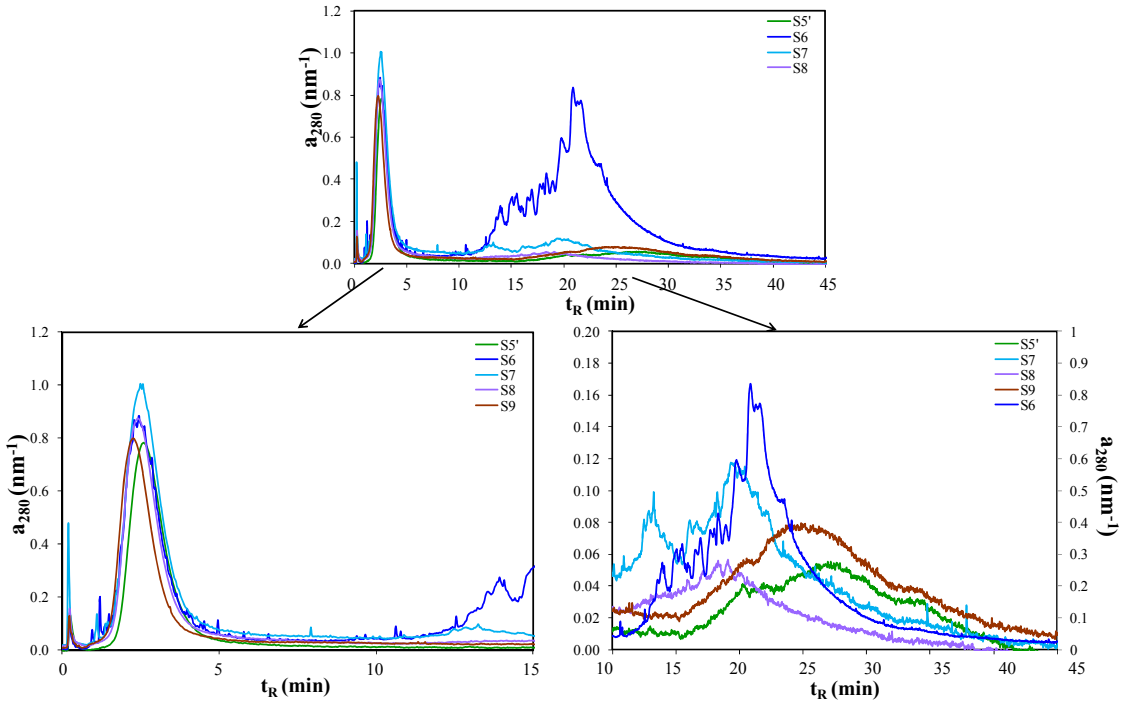

Figure 5.5 UV fractograms of samples collected in Seine River in 2011.

M_n and M_w molecular weights ranged from 674 Da to 3427 Da and from 2104 Da to 3963 Da, respectively. The obtained values were in the range generally determined by FlFFF in previously published studies (Alasonati et al., 2010; Benedetti et al., 2002; Guéguen and Cuss, 2011; Reszat and Hendry, 2005; Worms et al., 2010). On the other hand, these values were slightly lower than those obtained by Perminova et al. (2003) for aquatic humic substances extracted onto XAD resins or aquatic DOM isolated by reverse osmosis and fractionated by HPSEC. The M_n and M_w molecular weights reported by these authors ranged from 2900 Da to 4400 Da and from 5200 Da to 8010 Da, respectively.

The polydispersity values (Table 5.1) varied within the range of 1.16-3.76 with maxima observed for samples collected in 2013 and some samples mainly originating from forest zones. The range of polydispersity values determined on DOM in this study corresponds well with the determination of DOM in previous studies (Alasonati et al., 2010; Guéguen and Cuss, 2011; Reszat and Hendry, 2005).

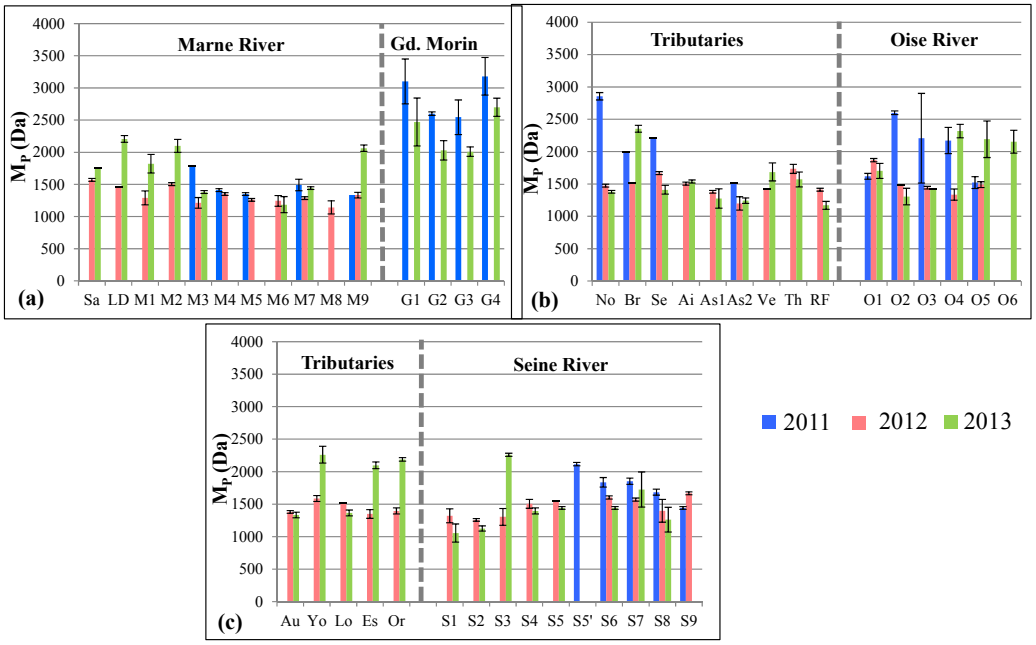

Figure 5.6 Variations of M_p in the four basins. (a) Marne River and its tributary Grand Morin; (b) Oise River and tributaries; (c) Seine River and tributaries.
Error bars indicate standard deviation

The molecular weight corresponding to the peak maximum (M_p) of the first fraction was determined for all samples and shown in Table 5.1 and Figure 5.6. The values of M_p ranged from 1057 Da to 3181 Da indicating a relatively large variation in molecular sizes of the small DOM fraction. The higher values of M_p were observed for samples in 2011, especially, the highest values were found for samples in Grand Morin River. This is in good agreement with the higher MW determined on the basis of S_R variations in chapter III (Figure 3.5) as shown on Figure 5.7 for the snapshot campaign in November 2011.

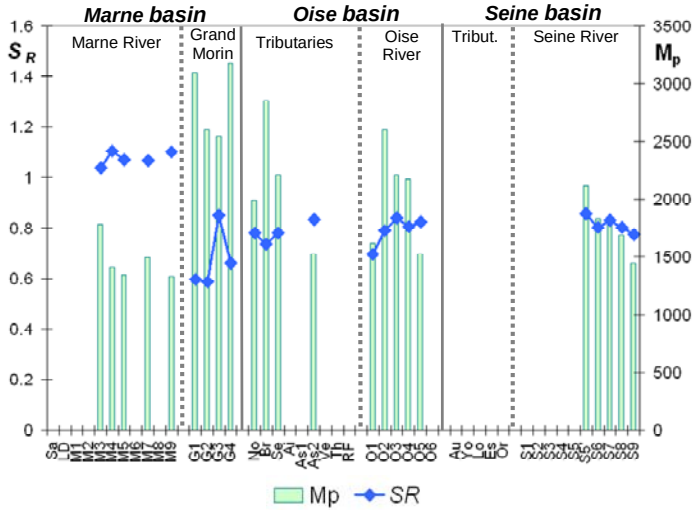

Figure 5.7 Comparison of M_p and S_R for all the samples collected in 2011

Table 5.1 Number-average (M_n), weight-average (M_w), peak (M_p) molecular weights and polydispersity index (PDI) of lower-molecular weight fraction determined at 280 nm using UV detection

Basins	Samples	M_p (±SD)			M_n (±SD)			M_w (±SD)			PDI (±SD)		
		2011	2012	2013	2011	2012	2013	2011	2012	2013	2011	2012	2013
Marne	G1	3100±348		2471±373	2820±18		1664±9	3793±19		3268±13	1,345±0.002		1,964±0.002
	G2	2600±28		2028±150	2805±1		1648±1	3788±2		3269±2	1,351±0.001		1,983±0.001
	G3	2544±270		2009±74	1877±8		1651±1	3944±10		3264±2	2,101±0.004		1,977±0.001
	G4	3181±293		2697±141	3427±6		1662±4	3963±5		3276±3	1,156±0.001		1,972±0.003
	LD		1458±0	2207±52		1895±1	2141±1		3369±1	3477±1		1,778±0.001	1,624±0.001
	Sa		1571±23	1751±0		1896±1	1897±1		3371±1	3372±1		1,778±0.001	1,777±0.001
	M1		1290±107	1820±144		1890±2	1644±1		3361±1	3272±1		1,778±0.001	1,990±0.001
	M2		1506±23	2099±100		1659±1	1374±1		2731±1	3175±1		1,646±0.001	2,310±0.001
	M3	1785±0	1214±83	1381±22	1897±1	1889±2	1371±1	3368±1	3362±2	3153±1	1,776±0.001	1,780±0.001	2,300±0.001
	M4	1412±23	1350±22		1641±1	1892±1		3264±1	3364±1		1,989±0.001	1,778±0.001	
	M5	1350±22	1259±21		1640±2	1888±1		3254±1	3355±1		1,984±0.001	1,777±0.001	
	M6		1244±83	1185±124		1887±2	1071±4		3356±1	3039±4		1,778±0.001	2,837±0.005
	M7	1491±89	1288±21	1443±21	1642±2	1889±1	1077±1	3257±1	3357±1	3039±1	1,984±0.001	1,777±0.001	2,820±0.001
	M8		1142±102			1885±3			3355±2			1,780±0.002	
	M9	1335±87	1334±44	2063±49	1639±2	1889±1	1653±1	3253±2	3358±1	3263±2	1,985±0.001	1,777±0.001	1,975±0.001
Oise	Ve		1428±0	1686±140		1890±1	2131±4		3358±1	3461±3		1,777±0.001	1,624±0.001
	Ai		1506±23	1538±23		1893±1	800±1		3361±1	2951±1		1,776±0.001	3,690±0.002
	As1		1381±22	1276±149		1883±1	790±9		3346±1	2890±14		1,777±0.001	3,658±0.023
	As2	1522±0	1200±104	1244±42	1638±1	2769±1	1354±3	3240±5	3784±1	3101±1	1,978±0.001	1,367±0.001	2,291±0.004
	Br	1992±0	1522±0	2354±53	2804±6	2134±1	2807±0	3803±1	3472±1	3805±1	1,356±0.001	1,627±0.001	1,356±0.001
	No	2855±57	1474±22	1381±22	2809±1	1889±1	1631±1	3807±1	3355±1	3232±1	1,355±0.001	1,776±0.001	1,982±0.001
	RF		1412±23	1170±62		1370±1	787±2		3140±1	2958±1		2,292±0.001	3,757±0.006
	Se	2207±0	1668±23	1412±66	2801±1	2136±1	1635±3	3798±3	3474±1	3235±1	1,356±0.001	1,627±0.001	1,979±0.002
	Th		1735±71	1570±115		2134±1	2132±1		3467±1	3467±1		1,624±0.001	1,626±0.001
	O1	1619±45	1870±25	1703±117	731±1	674±1	2131±4	2267±7	2104±1	3461±3	3,103±0.011	3,121±0.022	1,620±0.004
	O2	2600±28	1489±0	1305±129	2804±1	1889±7	1630±5	3796±2	3353±6	3231±4	1,354±0.001	1,776±0.001	1,983±0.004
	O3	2208±692	1443±21	1428±0	2800±9	1891±1	1635±1	3799±8	3360±1	3235±1	1,357±0.002	1,778±0.001	1,978±0.001
	O4	2172±204	1335±87	2318±104	2802±2	1890±2	2146±7	3800±2	3360±1	3441±7	1,356±0.001	1,778±0.001	1,603±0.002
	O5	1523±91	1490±45	2192±282	1638±1	1891±1	2142±8	3245±1	3357±1	3464±7	1,981±0.001	1,776±0.001	1,617±0.003
	O6			2153±177			2139±6			3457±5			1,616±0.002
Seine	Au		1381±22	1334±44		1893±1	1636±1		3366±1	3245±1		1,778±0.001	1,983±0.001
	Es		1350±66	2098±52		1367±2	1659±1		3140±1	3244±3		2,296±0.002	1,956±0.001
	Lo		1522±0	1365±44		1894±1	796±1		3365±1	2931±1		1,777±0.001	3,683±0.004
	Or		1397±45	2189±26		1369±1	2794±1		3148±1	3786±1		2,299±0.001	1,355±0.001
	Yo		1587±47	2262±129		1889±1	2142±3		3349±1	3464±4		1,778±0.001	1,617±0.001
	S1		1320±107	1057±139		1892±2	1632±3		3364±2	3252±2		1,780±0.001	1,992±0.003
	S2		1259±21	1126±41		2799±1	1629±1		3802±1	3242±1		1,358±0.001	1,990±0.001
	S3		1305±129	2261±24		1637±3	2145±1		3254±3	3459±1		1,987±0.002	1,613±0.001
	S4		1506±68	1397±45		1891±1	1631±2		3357±1	3227±2		1,775±0.001	1,978±0.001
	S5		1554±0	1443±21		1893±1	1636±2		3359±1	3238±2		1,775±0.001	1,979±0.001
	S5'	2116±26			2138±1			3460±3			1,619±0.001		
	S6	1836±72	1603±23	1443±21	1377±1	1891±1	1630±1	3153±1	3354±1	3220±3	2,290±0.001	1,773±0.001	1,975±0.001
	S7	1854±47	1571±23	1724±270	1380±1	1891±1	1894±7	3152±1	3354±1	3352±6	2,284±0.001	1,776±0.002	1,769±0.004
	S8	1685±47	1398±176	1261±191	1376±1	1887±4	1632±6	3152±1	3353±2	3242±4	2,290±0.002	1,772±0.001	1,986±0.005
	S9	1443±21	1668±23		2775±1	1894±1		3775±1	3356±1		1,361±0.001	1,773±0.001	

**SD: Standard deviation*

We however did not find correlations between these two parameters for all the samples collected during the 3 sampling periods.

Samples, from different locations as well as sampling periods, were selected both on the basis of their fractogram patterns and their optical properties. The selected samples were: G1 (2011 and 2013) – Marne tributary Grand Morin; M7 (2011, 2012 and 2013) – Marne River; O1 (2011, 2012 and 2013) – Oise River, forest zone; S5 (2012 and 2013) and S6 (2011, 2012 and 2013) – Seine River downstream of Paris. The main parameters determined for these samples are summarized on Figure 5.8.

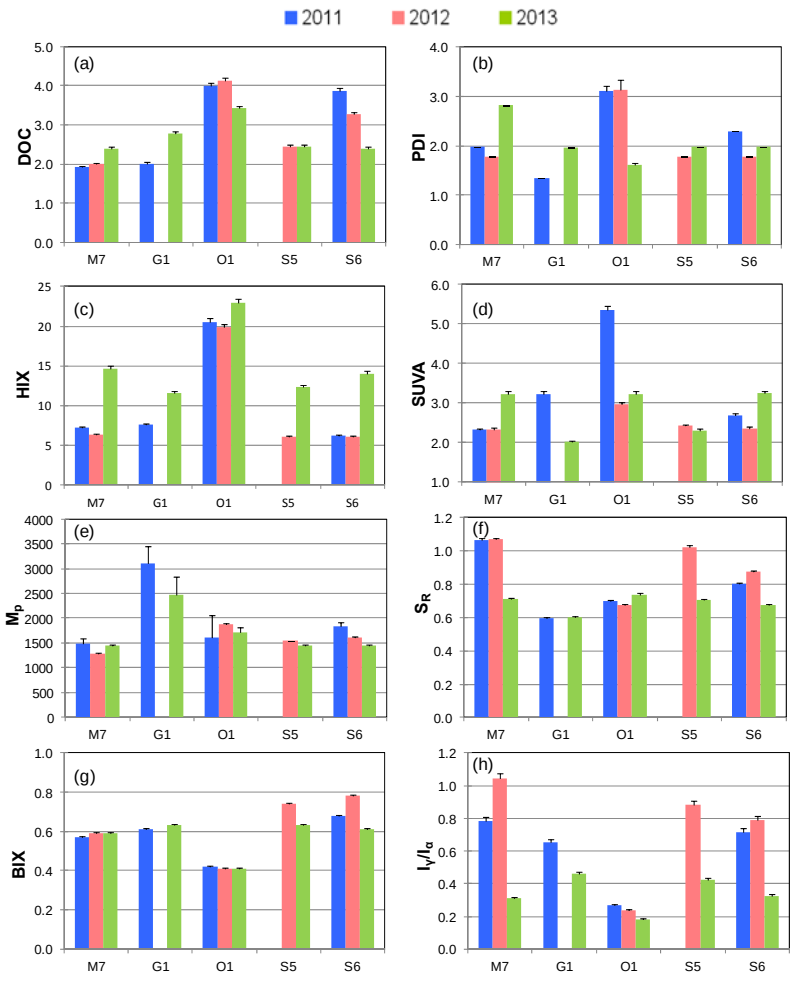

Figure 5.8 Distributions of (a) DOC, (b) PDI, (c) HIX, (d) SUVA, (e) M_p, (f) S_R, (g) BIX and (h) Iγ/Iα for the 13 samples selected for fractionation

O1 is characterized by the highest DOC contents and HIX values (Figure 5.8 (a) and (c)) for the three sampling dates but also by the highest polydispersity and SUVA in 2011 (Figure 5.8

(b) and (d)). The highest MW are observed for G1 as the lowest ones for M7 (Figure 5.8 (e) and (f)). The highest biological activity characterized the low-water period (2012) and especially the samples S5, S6 and M7 (Figure 5.8 (g) and (h)), which also presented relatively low MW (Figure 5.8 (e) and (f)).

The fractions of these 13 samples were thus isolated, as detailed below, for further EEM fluorescence analyses. Each sample was injected 3 times successively in order to provide a sufficient volume for each of the collected fractions.

Samples M7 collected during the three sampling periods were fractionated by AF4 into nine fractions as shown on Figure 5.9.

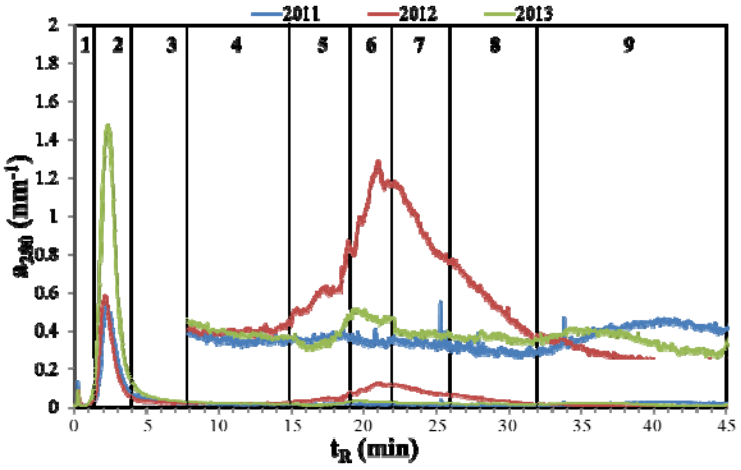

Figure 5.9 AF4 fractograms of the samples M7 collected both in 2011, 2012 and 2013

Samples G1 collected in 2011 and 2013 were fractionated by AF4 into eight fractions (Figure 5.10) and then, the fluorescence properties of each fraction were off-line determined by EEM fluorescence spectroscopy.

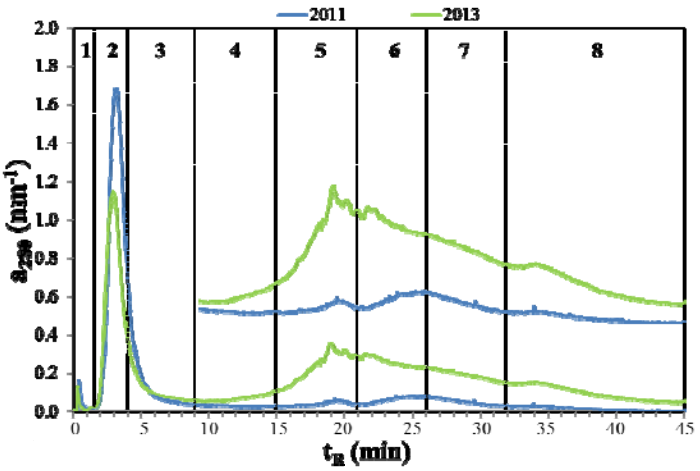

Figure 5.10 AF4 fractograms of the samples G1 collected both in 2011 and 2013

The Figure 5.11 gives the AF4 fractograms for the samples O1 collected both in 2011, 2012 and 2013 from the Oise River and shows the nine fractions which were isolated.

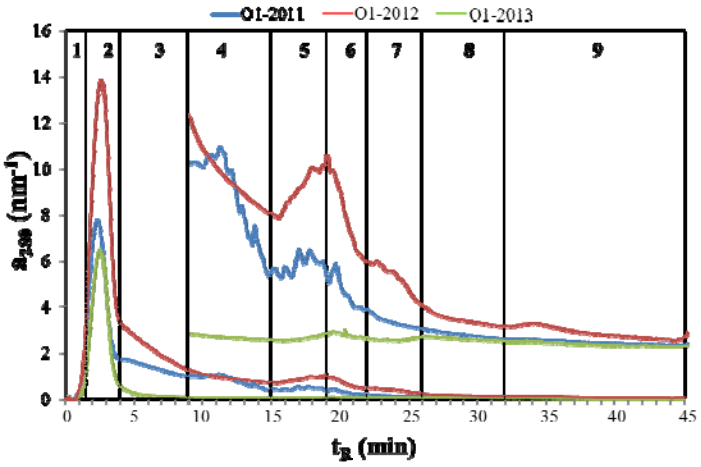

Figure 5.11 AF4 fractograms of the samples O1 collected both in 2011, 2012 and 2013

The AF4 fractograms obtained for the samples from the Seine River S5 (2012 and 2013) and S6 (2011, 2012 and 2013) are given on the Figures 5.12 (a) and (b) respectively. Nine fractions were collected for each sample.

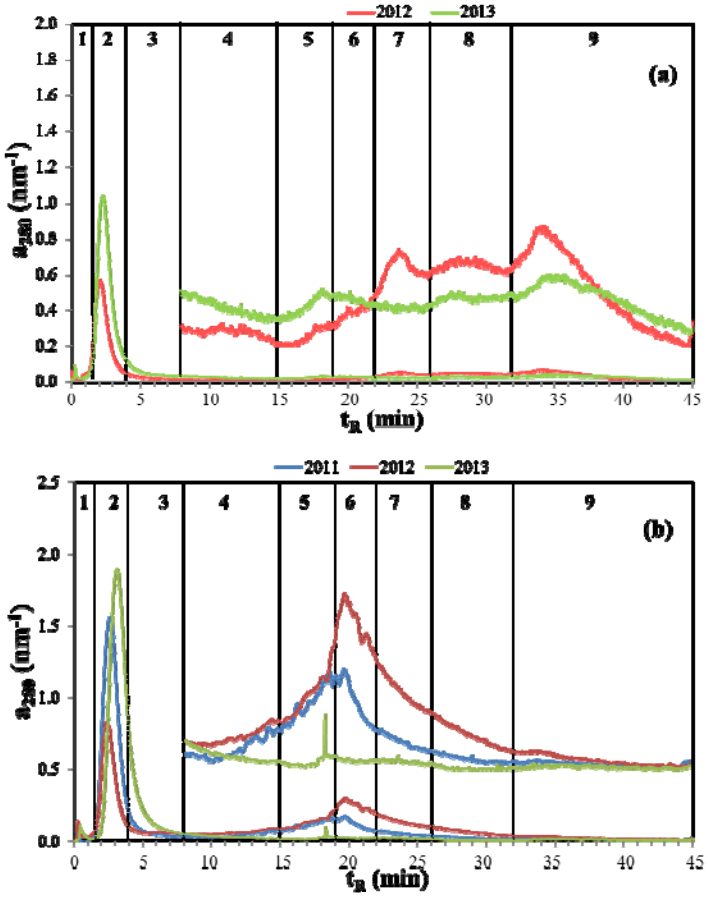

Figure 5.12 AF4 fractograms of samples S5 (a) and S6 (b) fractionated for the Seine River

5.2. Fluorescence properties of DOM fractions

The fluorescence properties of the different size-based fractions of DOM colloids were then investigated. For that purpose, every AF4 fraction of DOM, which was isolated as described previously, was analysed by EEM fluorescence spectroscopy. The Figure 5.13 pointed out, in the EEM spectra of all fractions, the presence of an intense peak at excitation and emission wavelengths ranging from 260 nm to 290 nm and from 290 nm to 340 nm, respectively. This peak overlapped the band γ, thus making it impossible to evaluate whether the fluorophore γ contributed to any DOM fractions or not. Due to this contamination, the spectral region mentioned just above will not be then considered in the following paragraphs for the interpretation of the EEM spectra of the isolated AF4 fractions.

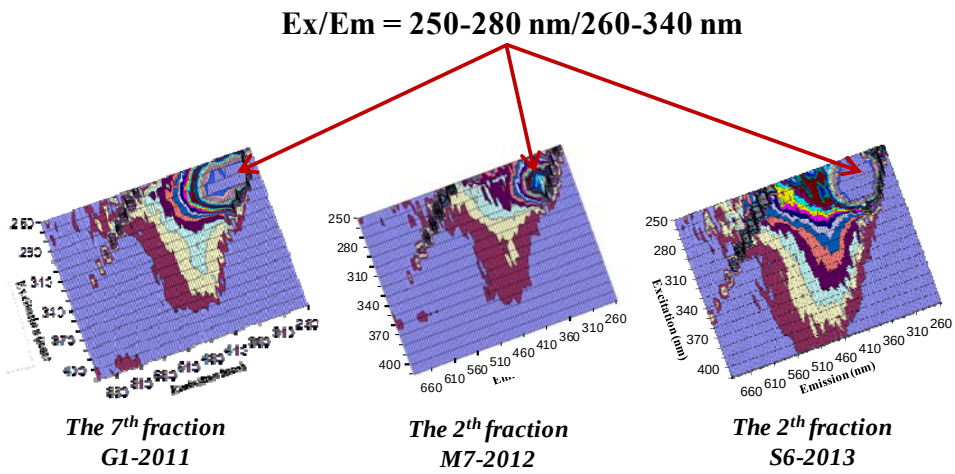

Figure 5.13 Examples of EEM spectra of DOM in the Seine River catchment

5.2.1. Oise River

The EEM spectra of the nine fractions isolated by AF4 (Figure 5.11) for samples O1 collected in 2011, 2012 and 2013 are given in Table 5.2.

In order to facilitate the comparison of the spectral shape between the various fractions, different scales were used for the contour plots. The intensities are not thus comparable from one spectrum to another.

A peak corresponding to excitation wavelength maximum at 400 nm and emission wavelength maximum at 470 nm could be clearly observed in the spectrum of the 1st fraction of sample O1 collected in 2011 as well as in the spectrum of the 2nd fraction of sample O1 collected in 2013 (Table 5.2 and Figure 5.14). This band could not be distinguished for the bulk samples. In comparison with the position of fluorophore α, this peak was shifted towards longer excitation and emission wavelengths.

Moreover, the 4th fraction of the three samples O1 presented EEM spectra similar to the 3rd fraction, suggesting the same type of fluorescent DOM in the two factions. For sample O1-2012, the fluorescence peaks of the 3rd fraction have been identified at longer emission wavelength than for samples O1-2011 and -2013. These results suggested a higher hydrophobic degree of this DOM fraction during the low-water conditions.

Table 5.2 EEM contour plots (intensity scales different) of the bulk samples and the nine AF4 fractions isolated for O1 (2011, 2012 and 2013) in the Oise River

Fraction number	O1 collected in 2011	O1 collected in 2012	O1 collected in 2013
Bulk sample	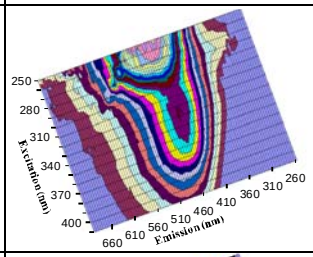	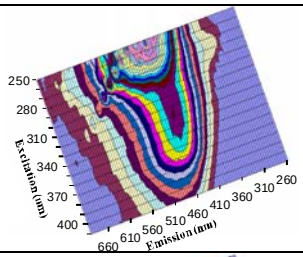	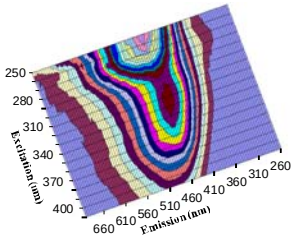
The 1st fraction	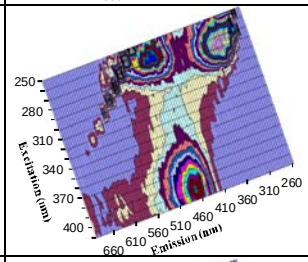	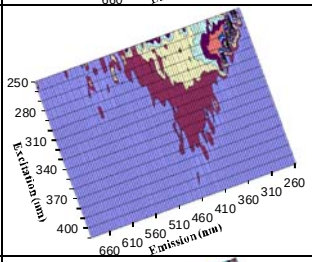	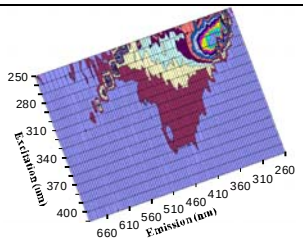
The 2nd fraction	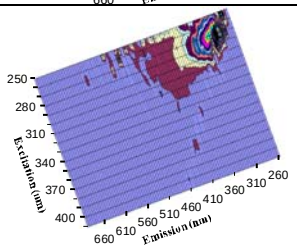	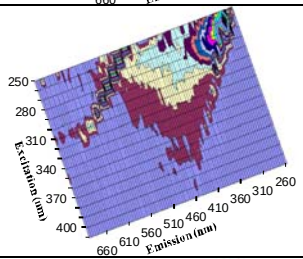	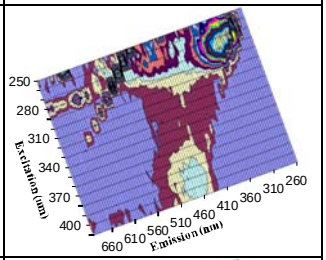
The 3rd fraction	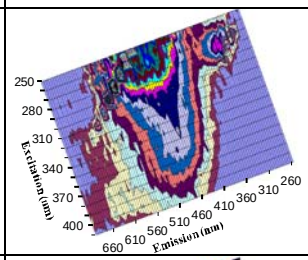	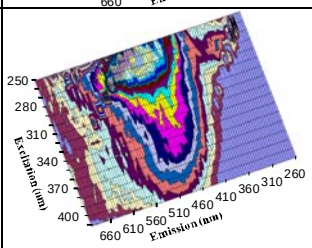	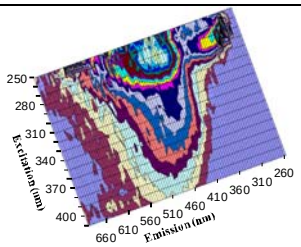
The 4th fraction	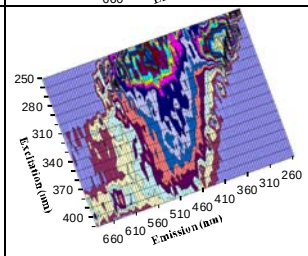	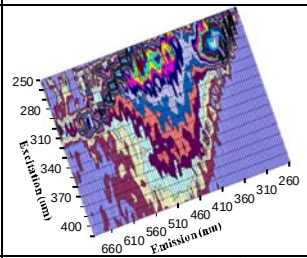	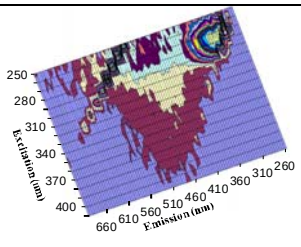
The 5th fraction	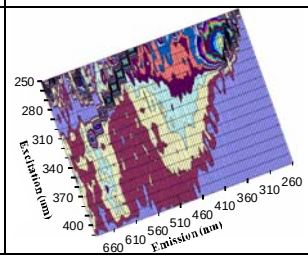	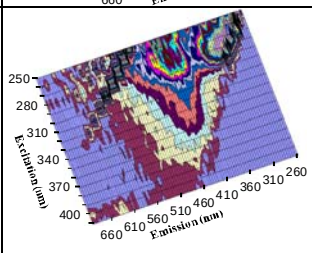	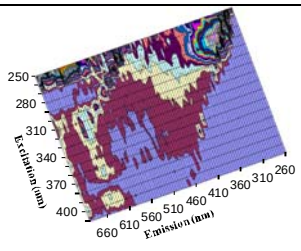

Table 5.3 *(continued)*

Fraction number	O1 collected in 2011	O1 collected in 2012	O1 collected in 2013
The 6th fraction	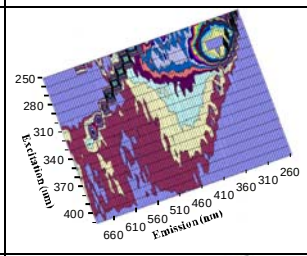	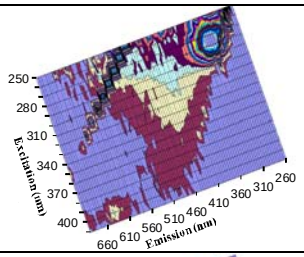	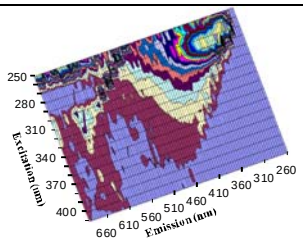
The 7th fraction	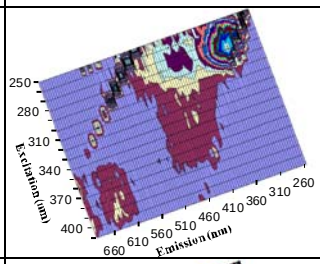	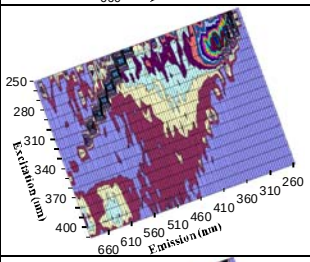	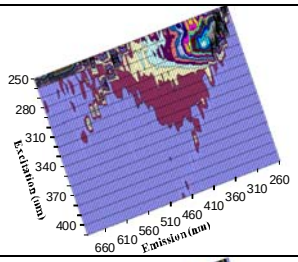
The 8th fraction	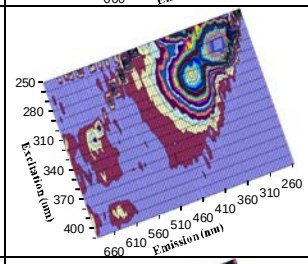	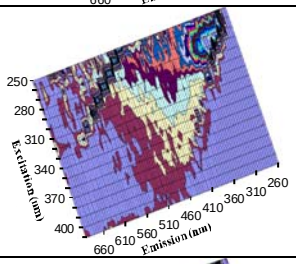	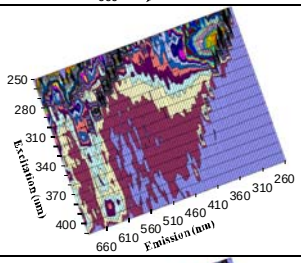
The 9th fraction	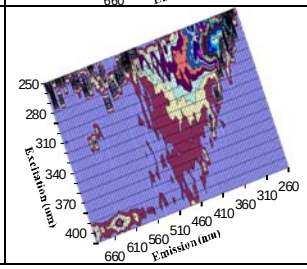	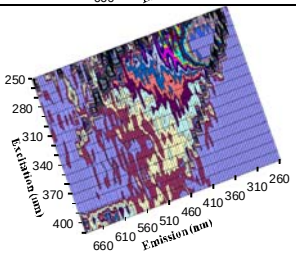	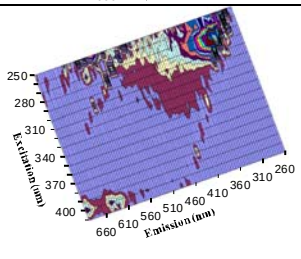

The Figure 5.14 pointed out the presence of a component in EEM spectra at 400-410 nm/640-670 nm (E_x/E_m). A similar peak was attributed by Coble et al. (1998) to the fluorescence of chlorophyll *a* or its degradation products (Peak P, 410 nm/680 nm). Rottgers and Koch (2012) reported that a fluorophore at 415 nm/650 nm (E_x/E_m) do not support that the molecule is an early chlorophyll *a* degradation product, but match in absorption and fluorescence to that of a non-chlorin porphyrin molecule. They suggested that the detection of this fluorophore could be used as a tracer for bacterial production, or POM and DOM remineralization. However, these works concerned only marine waters, and to our knowledge, no specific EEM fluorescence of pigment was related for freshwater samples in the literature. This fluorescence peak we observed might thus correspond to a pigment molecule or a group of similar

molecules. The slight wavelength shift in both the emission and excitation maximum within our EEM spectra might be due to pigments specific of the freshwater environments we studied.

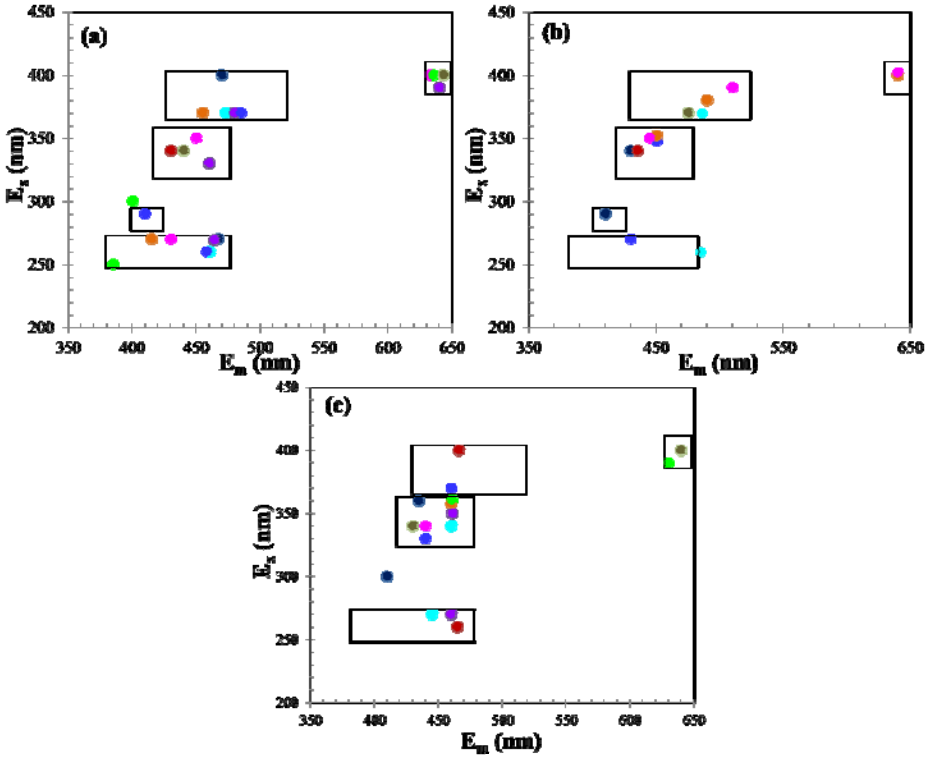

Figure 5.14 Positions of all fluorescence intensity maxima identified within EEM spectra for all fractions of samples O1 collected in the Oise River
(a) in 2011 (b) in 2012 and (c) in 2013.
Keys: (●) 1st fraction; (●) 2nd fraction; (●) 3rd fraction; (●) 4th fraction; (●) 5th fraction; (●) 6th fraction; (●) 7th fraction; (●) 8th fraction; (●) 9th fraction

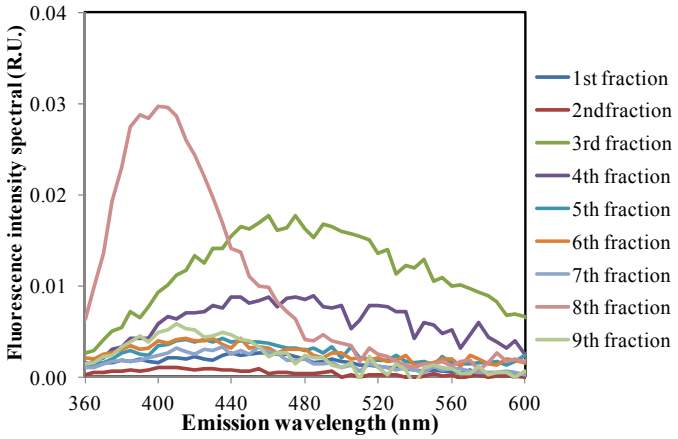

Figure 5.15 Emission spectra, at E_x = 310 nm, of the nine fractions isolated from sample O1 collected in 2011

The emission spectra at excitation wavelength 310 nm of all fractions from sample O1 collected in 2011 are plotted on Figure 5.15. This Figure highlighted the shift towards shorter wavelengths observed for the EEM spectrum of the 8th fraction. This blue shift could be related to the fluorophore β in this fraction, however the maximum at excitation is observed at shorter wavelength (290-300nm). The band β is attributed to autochthonous production and is often observed as a shoulder of the band α for excitation wavelength of 310-320 nm. The main band in the 8th fraction of sample O1-2011, is a well-defined peak, distinct from the band α and slightly shifted towards shorter excitation wavelength compared to the traditional fluorophore β.

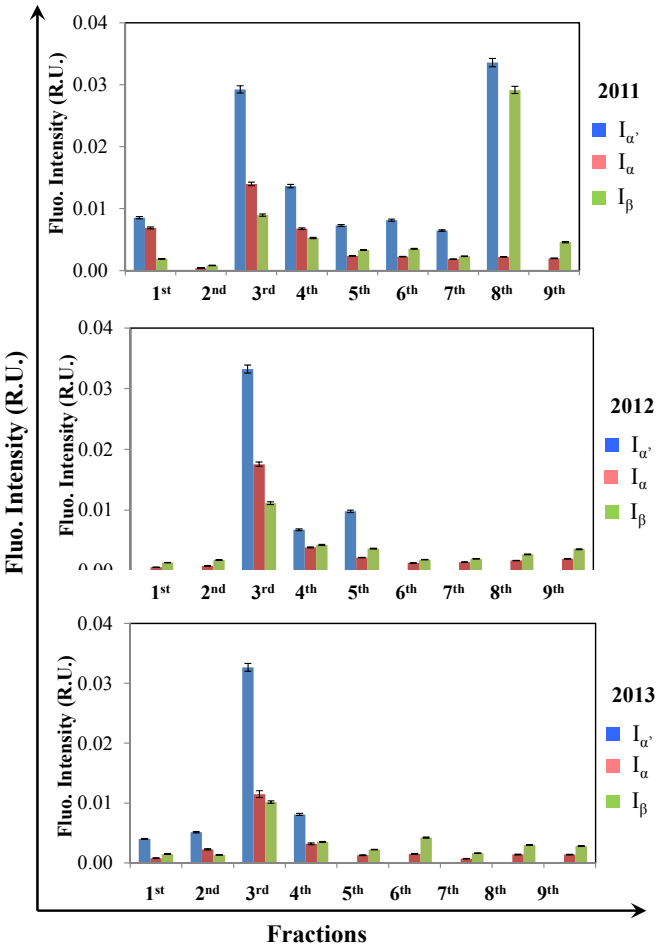

Figure 5.16 Variations of the fluorescence intensity of the bands α', α and β between the nine fractions and the three sampling dates for O1 in the Oise River.
Error bars indicate standard deviation

For sample O1 taken in 2011, the fluorescence intensity of the three bands α', α and β, decreased from the 3rd fraction to the 7th fraction, and then sharply increased in the 8th fraction, except for the band α (Figure 5.16). The fluorescence intensities reported in this

Figure were corrected for the dilution factor applied to each fraction during elution. These intensities are thus comparable between fractions. The highest fluorescence intensities of these three bands for O1-2012 and -2013, were determined for the 3rd fraction and decreased then significantly in the 6th fraction to the last one. These results pointed out that the fluorescent DOM components were separated and mainly eluted during the first five fractions, especially in the 3rd fraction.

BIX values determined for all fractions of samples O1 are presented on Figure 5.17. The lowest values were determined for the 3rd fraction, suggesting the presence in this fraction of DOM constituents from mainly terrestrial origin.

On the other hand, the highest values of BIX were obtained for the two first fractions what is in good agreement with previous studies on the size distribution of fluorescent DOM, obtained by tangential ultrafiltration, in both the Gironde and Seine estuaries (Huguet at al., 2010). Indeed, in that work, the fluorophore β was mainly isolated in the smallest molecular size fraction (<1000Da) of all samples, wherever they were collected (i.e. upstream or downstream parts of the estuaries). We showed in chapter III, that the period of low-water (2012) was mainly associated with high values of BIX. For sample O1-2012, the 1st fraction showed the strongest BIX value, suggesting that the constituents of DOM related to biological activity during this period of low-water are mainly characterized by LMW.

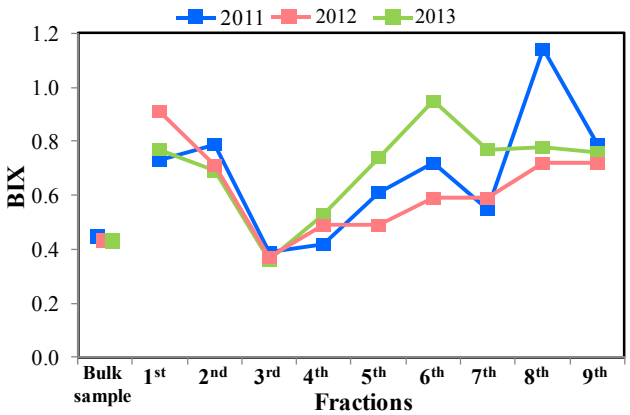

Figure 5.17 Variations of BIX between fractions compared to bulk samples for site O1 in 2011, 2012 and 2013.

However, the strongest BIX values were not only determined for the small molecular sizes but also from the fraction 5 (O1-2013) or 6 (O1-2011 and -2012) and till the end of the elution, with a maximum for fraction 6 in 2011 and 2013. Huguet et al. (2010) reported high

values of BIX in all the size fractions of marine samples. We can observe on Figure 5.17 that, for the freshwater samples O1, the fluorophore β is also distributed in HMW fractions.
For O1 taken in 2011, the highest BIX value was nevertheless obtained for the 8th fraction, but as described above, the peak at 290-300 nm/390-400 nm (E_x/E_m) certainly corresponds to another fluorophore than β. These results showed that DOM constituents of autochthonous origin are characterized by either low or high molecular weights.

5.2.2. Grand Morin River

The EEM spectra of each of the eight fractions (Figure 5.10) isolated for samples G1 (2011 and 2013) are given in Table 5.3. The Figure 5.18 showed the positions of fluorescence peaks identified within EEM spectra of all the fractions of the samples G1-2011 and G1-2013 in Grand Morin River (a tributary of Marne River). For sample G1 collected in 2011, three regions of fluorescent DOM were identifiable from EEM spectra of all fractions, as indicated on Figure 5.18-a.

Firstly, the fluorophore α', observed in the wavelength region of excitation 250-260 nm and emission 380-480 nm, was identified in the 1st, 4th and 8th fractions. Compared to the 1st fraction, its fluorescence intensity maximum in the 4th fraction was shifted to longer emission wavelength. This result agrees with Guéguen and Cuss (2011) who showed that HMW DOM was characterized by a red-shift in emission and excitation wavelength, which was attributed to an increase of hydrophobicity, aromaticity and oxidized forms in higher molecular weight components. The red shift of this fluorophore was also observed in the 3rd and 4th fractions of samples O1.

Secondly, the region of the fluorophore α was attributed to visible-humic fluorescence and it can be further divided into two different zones, identified at excitation 330-350 nm and 370-400 nm. The first one corresponds to excitation and emission wavelengths ranging from 320 to 360 nm and from 420 to 480 nm, respectively. For sample G1-2011, the EEM spectra of all fractions exhibited a peak within this region (Figure 5.18-a). Moreover, the 2nd fraction exhibited a fluorescence maximum at lower emission wavelengths (425 nm) compared to the 1st and 3rd fractions (435 and 450 nm, respectively). The 4th fraction had the longest peak emission wavelength (455 nm), whereas the 5th fraction showed the lowest peak emission wavelength (420 nm).

Table 5.3 EEM contour plots (intensity scales different) of the bulk samples and the eight AF4 fractions isolated for G1 (2011 and 2013) in the Grand Morin tributary

Fraction number	G1 collected in 2011	G1 collected in 2013
Bulk sample	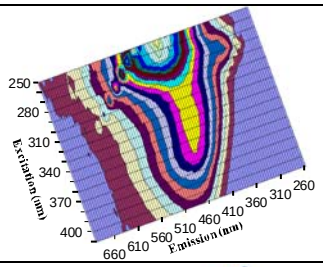	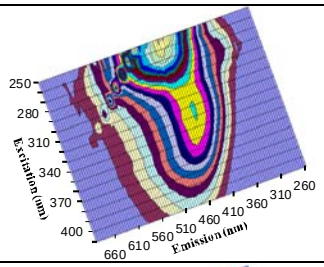
The 1st fraction	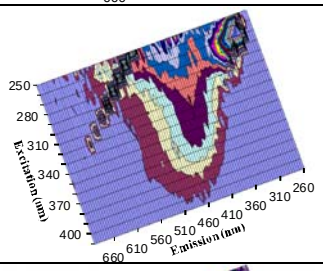	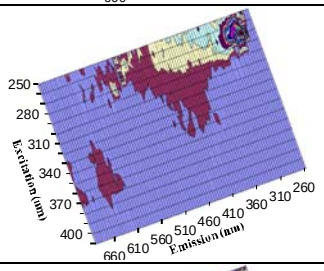
The 2nd fraction	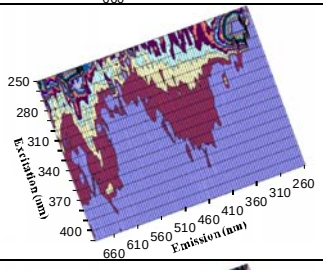	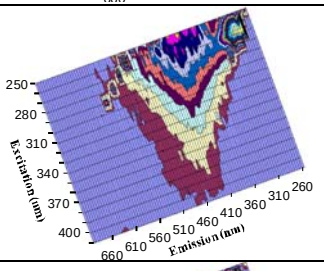
The 3rd fraction	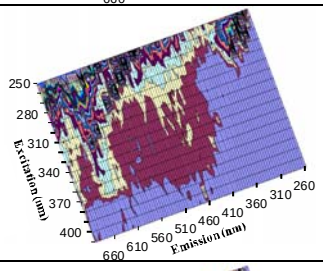	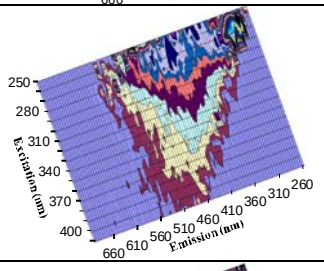
The 4th fraction	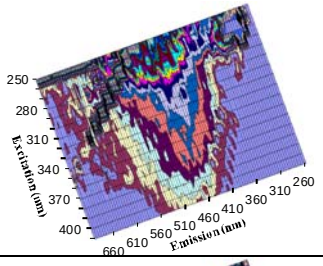	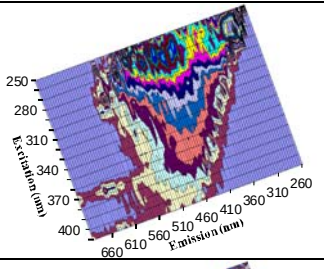
The 5th fraction	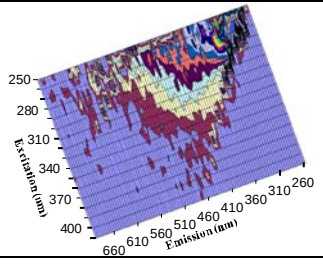	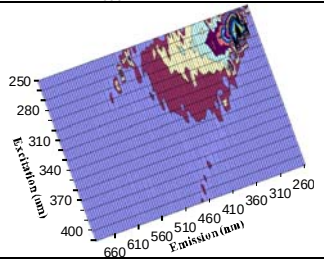

Fraction number	G1 collected in 2011	G1 collected in 2013
The 6th fraction	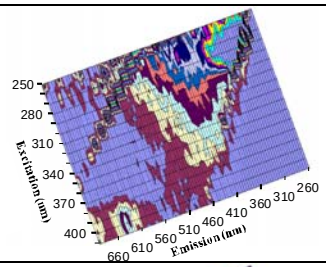	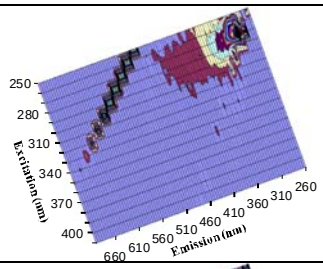
The 7th fraction	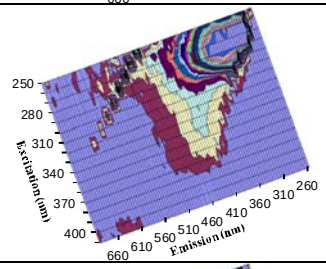	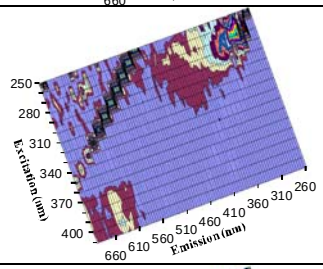
The 8th fraction	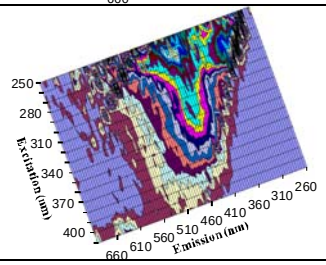	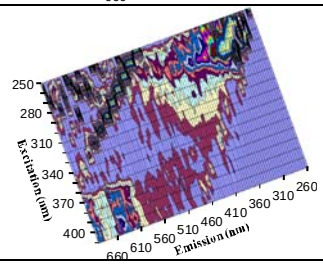

On the other hand, compared to the first region of fluorophore α, the second one has been identified at longer wavelengths for both excitation and emission (370-400 nm and 420-520 nm, respectively). It can be seen on Figure 5.18-a, that all the fractions, except the 1st and 2nd ones, exhibited a α-type fluorophore in both regions.

Thirdly, a peak at ~400 nm/640 nm (E_x/E_m) was observed in the spectra of some fractions such as the 6th and 8th fractions. This band could not be seen in the EEM spectrum of the bulk sample G1-2011, as described above for the samples O1, this peak position could correspond to a pigment-like fluorescence component associated with biological processes.

For the sample G1-2013, we did not observe the fluorophores α' and α within the EEM spectra of the 5th, 6th and 7th fractions. However, we observed a peak at 280-290nm/400-420nm (E_x/E_m) within the EEM spectra of the 6th and 7th fractions. A pigment-like fluorescence component at 400nm/640nm (E_x/E_m) was detected in the 7th and 8th fractions as already observed for the G1-2011 sample.

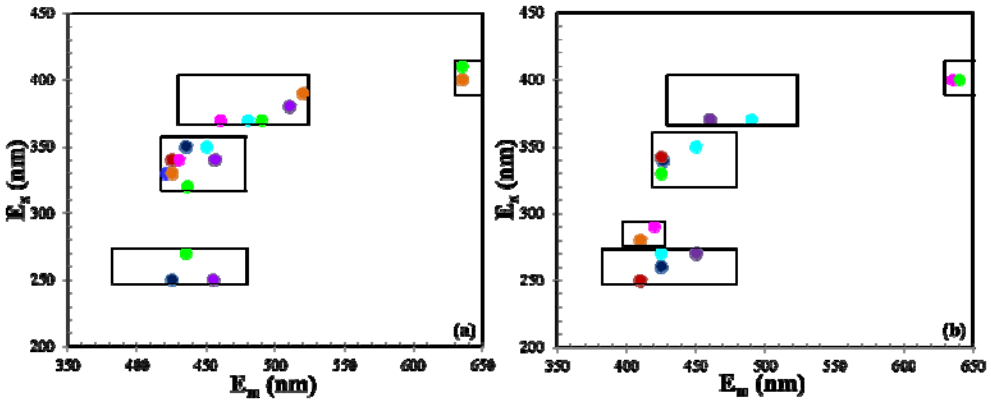

Figure 5.18 Positions of all fluorescence intensity maxima identified within EEM spectra for all fractions of samples G1 collected in the Grand Morin River
(a) in 2011 and (b) in 2013.
Keys: (●) 1st fraction; (●) 2nd fraction; (●) 3rd fraction; (●) 4th fraction; (●) 5th fraction; (●) 6th fraction; (●) 7th fraction; (●) 8th fraction

The fluorescence intensity of the three main flourophores (α', α and β) were determined for all fractions of samples G1 collected in 2011 and 2013 (Figure 5.19). For sample G1-2013, the fluorescence signals were higher for the 2nd, the 3rd and the 4th fractions than for the other fractions. Particularly the highest intensities of the three bands were determined for the 4th fraction. For sample G1-2011, the fluorescence intensities were lower than for sample G1-2013. However, the highest fluorescence intensities were still observed for the 4th fraction, but also for the first fraction. Considering that the 1st fraction exhibited an EEM spectrum with a similar shape to that of the raw sample (Table 5.3), we can think that this fraction corresponds to a portion of the bulk constituents unretained on the membrane and eluted without size separation.

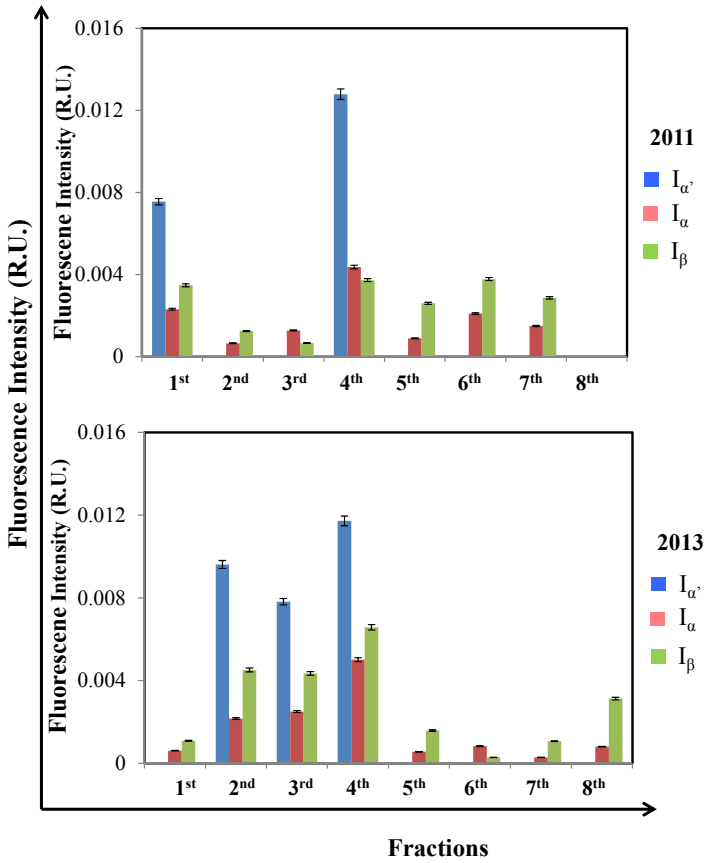

Figure 5.19 Variations of the fluorescence intensity of the bands α', α and β between the eight fractions and the sampling dates 2011 and 2013 for sample G1.
Error bars indicate standard deviation

5.2.3. Marne River

Samples M7 collected during three time periods was fractionated by AF4 and collected into nine fractionsand then, the fluorescence properties of each fraction were determined. The EEM spectra of each of the nine fractions (Figure 5.9) isolated for samples M7 (2011, 2012 and 2013) are reported in the Table 5.4.

The Figure 5.20 summarized the fluorescence peak maxima determined within the EEM spectra for all the fractions of samples M7 collected during the three sampling periods in the Marne River.

Table 5.4 EEM contour plots (intensity scales different) of the bulk samples and the nine AF4 fractions isolated for M7 (2011, 2012 and 2013) in the Marne River

Fraction number	M7 collected in 2011	M7 collected in 2012	M7 collected in 2013
Bulk sample	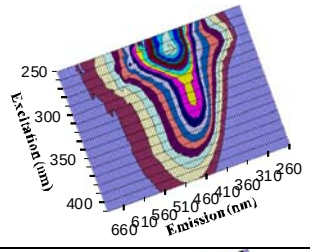	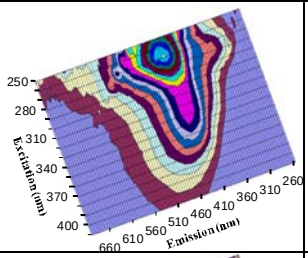	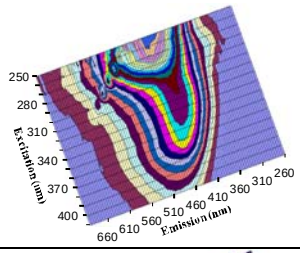
The 1st fraction	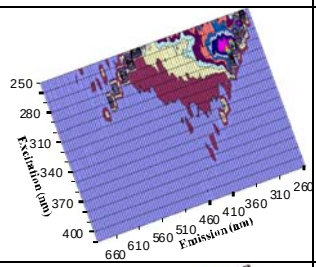	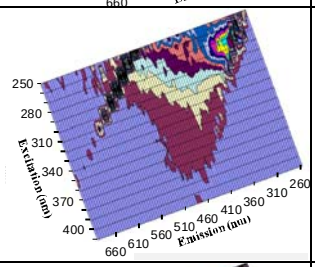	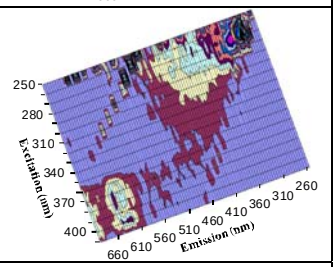
The 2nd fraction	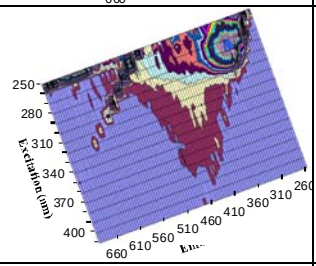	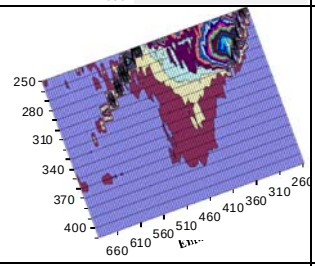	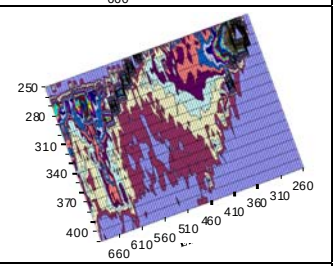
The 3rd fraction	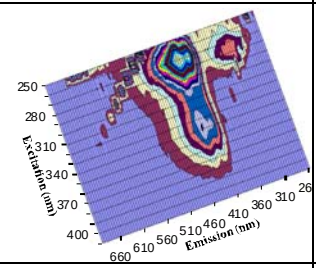	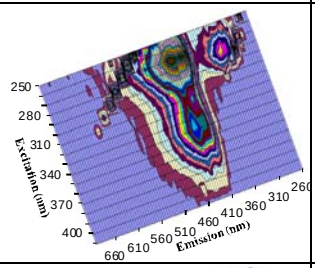	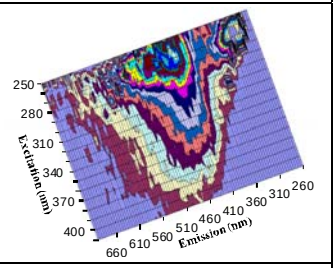
The 4th fraction	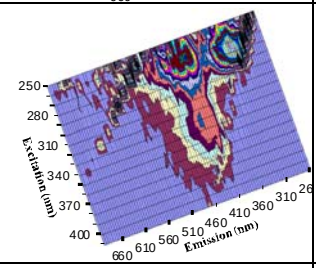	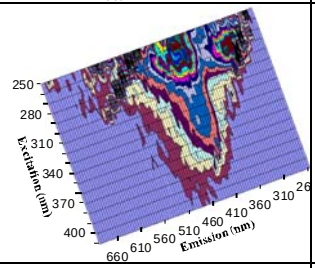	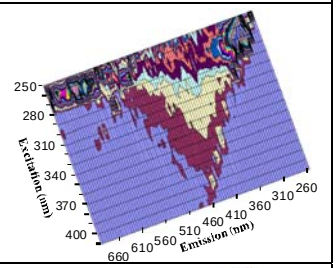
The 5th fraction	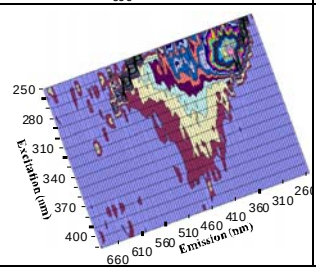	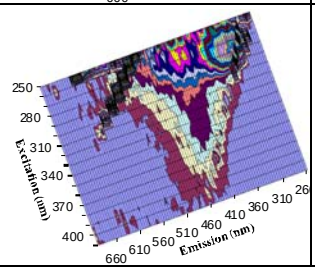	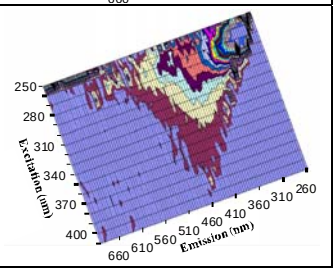

Fraction number	M7 collected in 2011	M7 collected in 2012	M7 collected in 2013
The 6th fraction	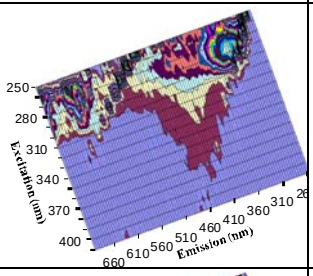	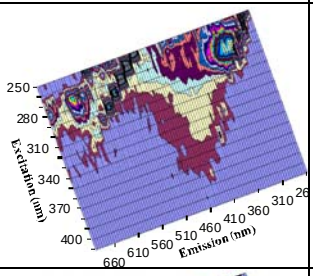	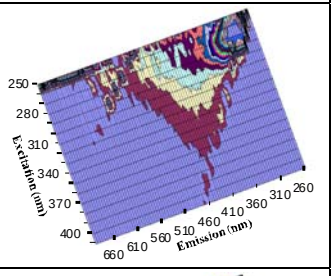
The 7th fraction	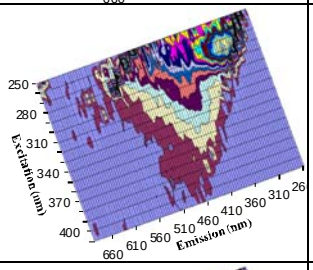	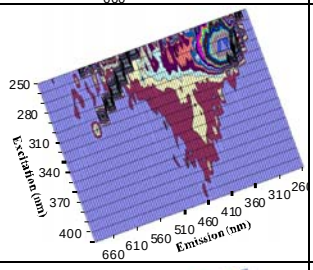	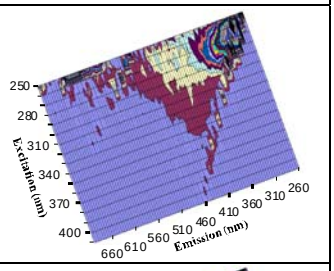
The 8th fraction	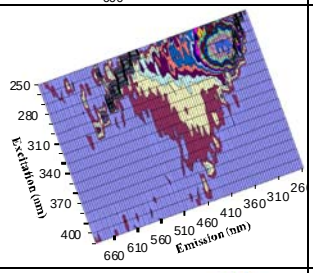	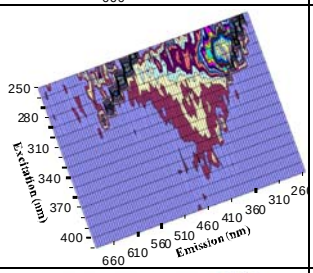	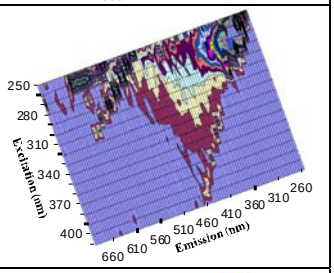
The 9th fraction	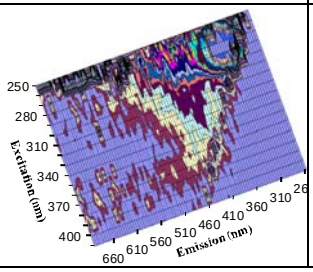	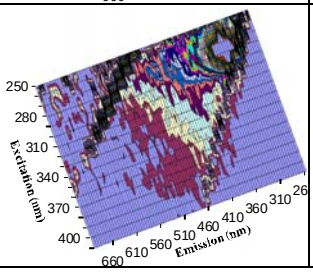	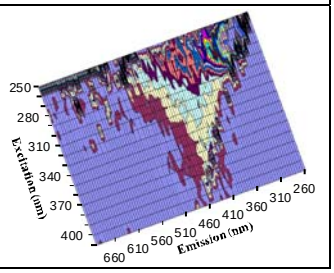

For the samples of 2011 and 2012, three major regions of fluorescent DOM were drawn from the EEM spectra of the AF4 fractions (Figures 5.20-a and 5.20-b). The region 1 was associated to excitation wavelength at 250-270 nm and emission wavelength at 380-480 nm. The regions 2 and 3 corresponded to E_x/E_m = 320-360/420-480 nm and 370-400/430-520 nm, respectively. Similar fluorescence peak positions between the 3rd and 4th fractions as well as the 5th and 6th fractions suggested, in each case, the same type of DOM fluorophores for both fractions.

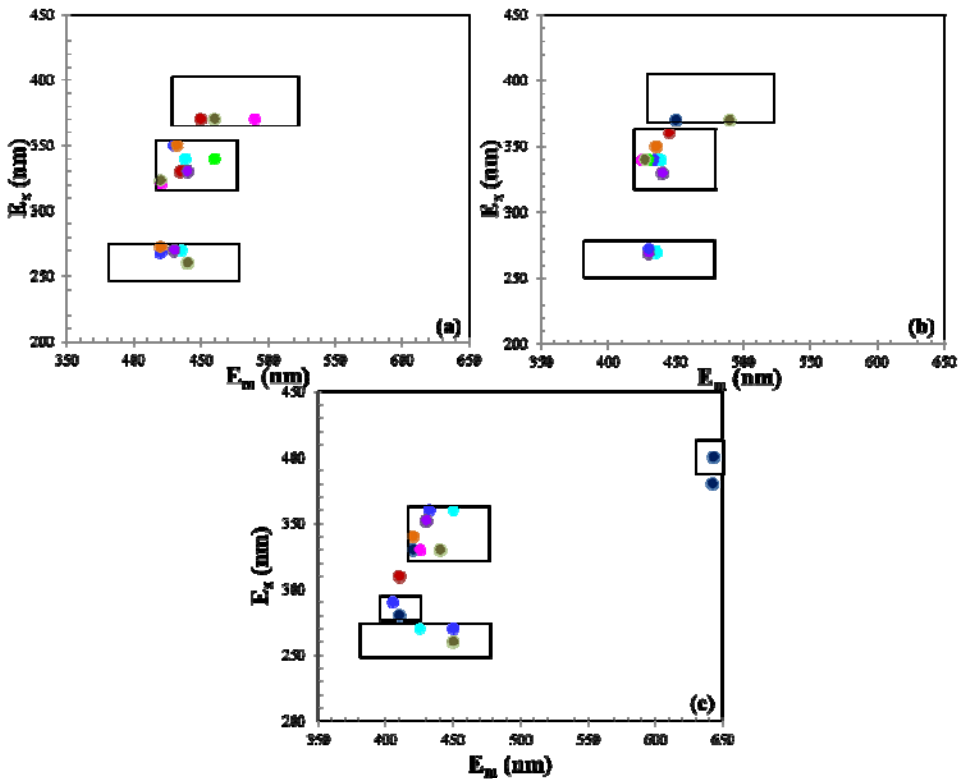

Figure 5.20 Positions of all fluorescence intensity maxima identified within EEM spectra for all fractions of samples M7 collected in the Marne River
(a) in 2011, (b) in 2012 and (c) in 2013
Keys: (●) 1st fraction; (●) 2nd fraction; (●) 3rd fraction; (●) 4th fraction
(●) 5th fraction; (●) 6th fraction; (●) 7th fraction; (●) 8th fraction; (●) 9th fraction

For sample M7-2013, the position of the fluorophore α observed in the region 2 for the 3rd fraction was shifted to longer wavelengths compared to the other fractions (Figure 5.20-c). One potential explanation for this red shift is the increase in the hydrophobic degree of DOM in this fraction. On the other hand, the position of the maximum fluorescence peak for the 2nd fraction is observed at 310 nm/410 nm (E_x/E_m). This peak suggested the presence of another type of DOM in the 2nd fraction.

Another peak was observed, within the EEM spectrum of the 1st fraction of M7-2013, in the spectral region previously identified as pigment-like fluorophore for the samples O1 and G1. However, compared to those samples, the excitation wavelength for M7-2013 ranged from 370 nm to 400 nm and was then shifted towards shorter wavelength, suggesting another type of pigment or compound in this fraction. The hypothesis of another type of component is strengthened by the fact that the molecular weight determined for this compound is smaller for M7 (fraction 2) than for O1 and G1 (fractions 6 and 7).

For the samples M7 (2011 and 2012), a specific fluorescence signature was observed for the 3rd fraction, and to a lesser extent for the 4th one, with an emission maximum at 435 nm for both excitation wavelengths 270 nm and 340 nm, pointing out the presence of another specific DOM component for this sampling site, which was not detected during the flood period in 2013.

The Figure 5.21 indicated the variations of fluorescence intensity of the three bands α', α and β determined for all the AF4 fractions of the samples M7. The fluorescence intensities of these bands were much higher for the 3rd fraction compared to the other ones. This result confirmed that fluorescent DOM constituents were mainly eluted in the 3rd fraction. On the other hand, the significantly low fluorescence intensities determined from the 6th fraction to the last one verified the fact that these samples M7 are characterised by relatively low molecular weights confirming what was observed on Figures 5.8 (e) and (f) for the raw samples.

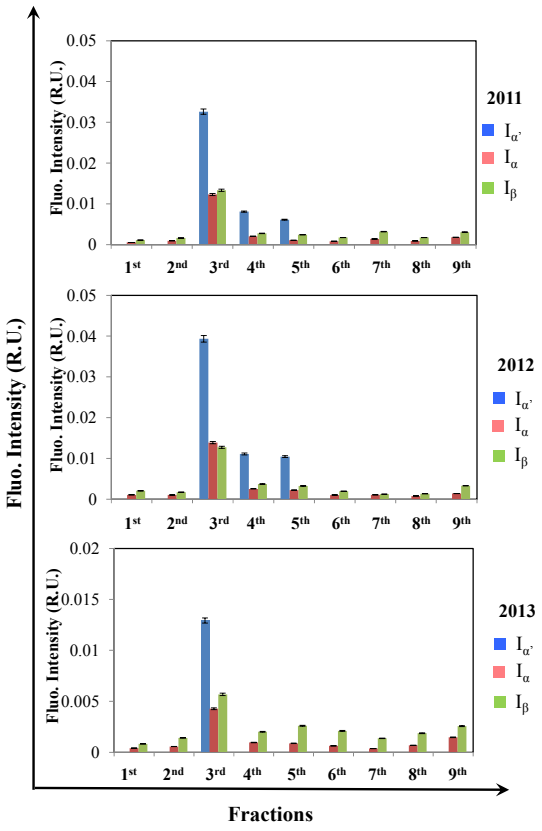

Figure 5.21 Variations of the fluorescence intensity of the bands α', α and β between the nine fractions and the three sampling dates for M7 in the Marne River.
Error bars indicate standard deviation

The fluorescence index, BIX, calculated for the bulk sample and all the fractions isolated by AF4 for samples M7 are shown on Figure 5.22. The BIX values for the raw samples M7 were about 0.6. The lowest BIX values were determined in the 3rd fraction for the three sampling periods, what suggested a predominantly allochthonous origin of DOM in the 3rd fraction.

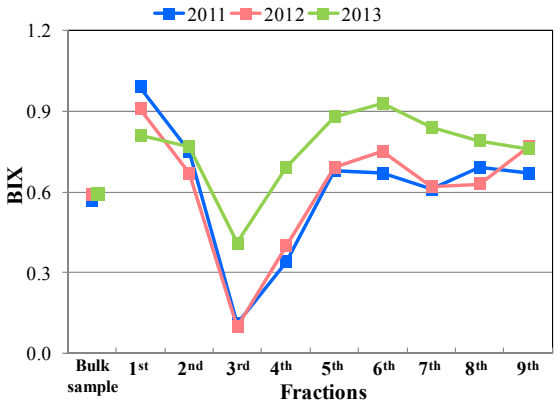

Figure 5.22 Variations of BIX between fractions compared to bulk samples for site M7 in 2011, 2012 and 2013.

As we already observed for the site O1 in the Oise River, the highest values of BIX were determined in both LMW and HMW fractions for the site M7 in the Marne River.

5.2.4. Seine River

The EEM spectra of the nine fractions isolated by AF4 (Figure 5.12) for sample S5 collected in 2012 and 2013 are given in Table 5.5. The positions of fluorescence peaks identified within the EEM spectra of all the fractions of the samples S5 taken in 2012 and 2013 (Table 5.5) are presented on Figure 5.23.

Table 5.5 EEM contour plots (intensity scales different) of the bulk samples and the nine AF4 fractions isolated for S5 (2012 and 2013) in the Seine River

Fraction number	S5 collected in 2012	S5 collected in 2013
Bulk sample	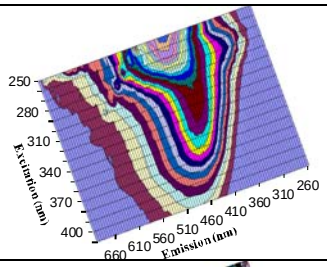	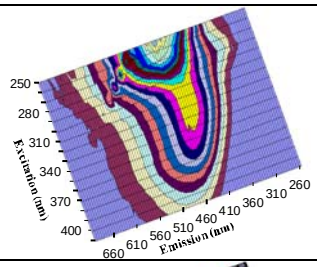
The 1st fraction	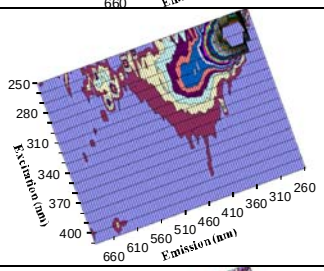	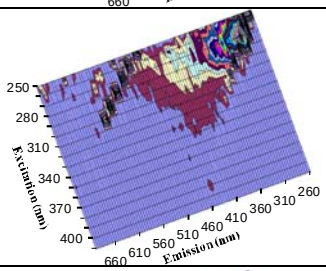
The 2nd fraction	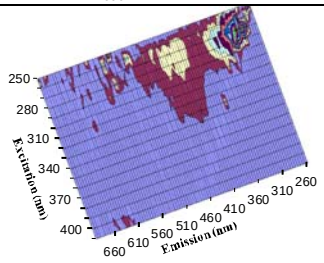	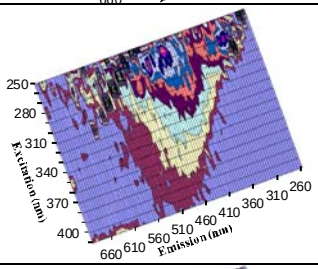
The 3rd fraction	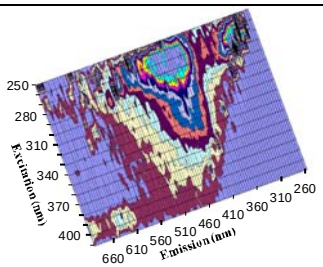	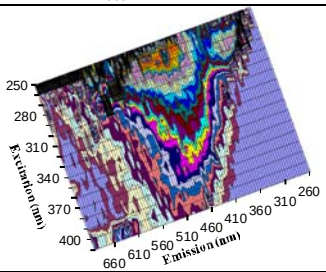
The 4th fraction	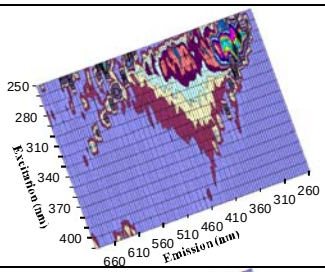	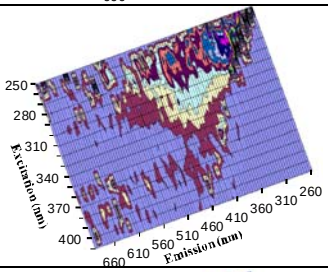
The 5th fraction	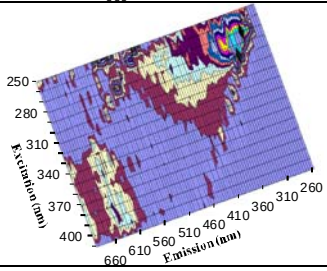	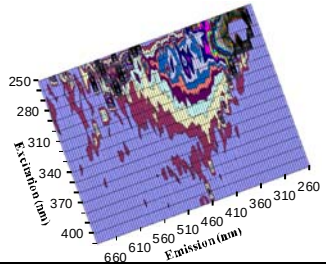

Fraction number	S5 collected in 2012	S5 collected in 2013
The 6th fraction	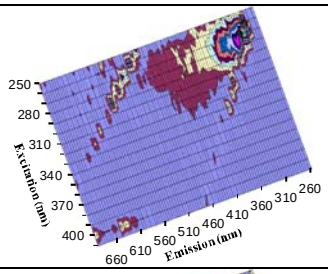	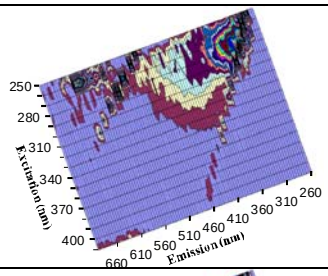
The 7th fraction	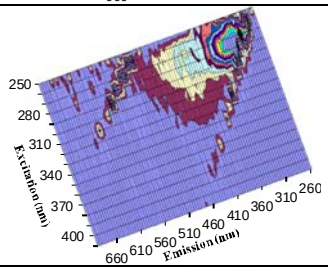	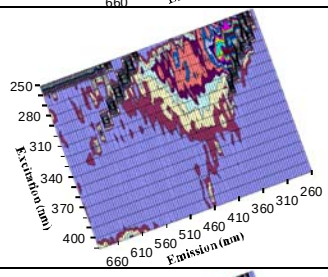
The 8th fraction	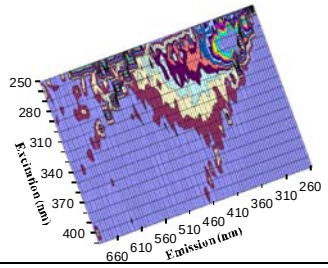	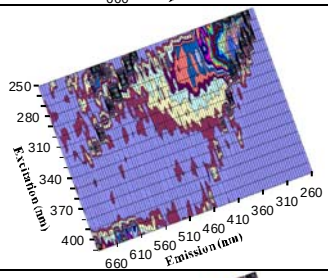
The 9th fraction	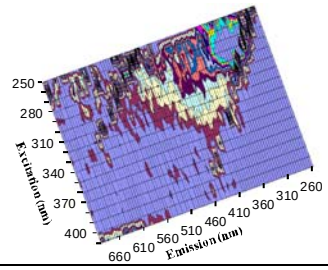	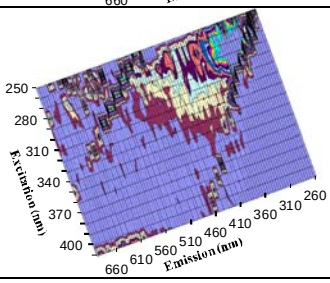

For sample S5-2012, the 1st fraction EEM spectrum exhibited a band at 290 nm / 410 nm (Ex/Em) which was difficult to discern in the EEM spectrum of the bulk sample.

We observed also, for the 3rd fraction of this sample, a specific fluorescence signature with an emission maximum at ~440 nm for both excitation wavelengths 270 nm and 320 nm, pointing out the presence of another specific DOM component. This fluorophore is distributed from the fractions 2 till 4, with the maximum in fraction 3. Another fluorescence peak at 370nm/470-475 nm (E_x/E_m) is overlaid with this specific fluorophore of the 3rd fraction as well as a pigment-like fluorophore at 400-410nm/640 nm (E_x/E_m), similar to the one observed

for O1 in the Oise River. As for sample S5-2013, a similar shape of the EEM spectra were observed for the 3rd fraction and at a lesser extent for the 2nd one.

This specific fluorophore of the fraction 3 is similar to the component C7 determined by PARAFAC (Figure 3.17) for S5 and similar to a combination of the components C3 and C7 for M7.

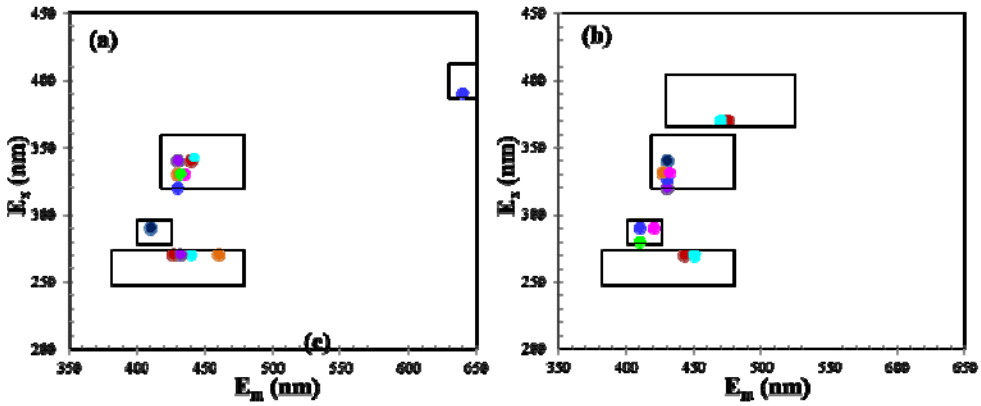

Figure 5.23 Positions of all fluorescence intensity maxima identified within EEM spectra for all fractions of samples S5 collected in the Seine River
(a) in 2012 and (b) in 2013.
Keys: (●) 1st fraction; (●) 2nd fraction; (●) 3rd fraction; (●) 4th fraction; (●) 5th fraction; (●) 6th fraction; (●) 7th fraction; (●) 8th fraction; (●) 9th fraction

The fluorescence intensities of the three bands α', α and β, for each fraction of the samples S5 collected in 2012 and 2013 are given in Figure 5.24. The higher fluorescence intensities observed for the 3rd fraction confirmed that DOM fluorophores were mainly eluted in the 3rd fraction.

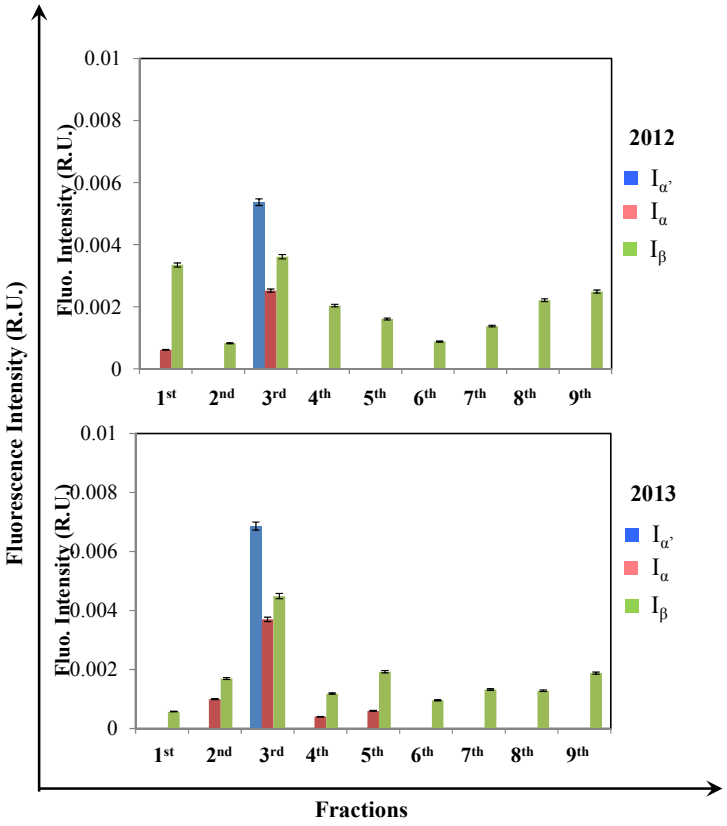

Figure 5.24 Variations of the fluorescence intensity of the bands α', α and β between the nine fractions isolated by AF4 for samples S5 collected in 2012 and in 2013 in the Seine River. Error bars indicate standard deviation

The EEM spectra of the nine fractions isolated by AF4 (Figure 5.12) for sample S6 collected in 2011, 2012 and 2013 are given in Table 5.6.

The positions of the fluorescence peaks identified within the EEM spectra of all the fractions of the samples S6 taken in 2011, 2012 and 2013 (Table 5.6) are reported on Figure 5.25.

For samples S6-2011 and S6-2012, the fluorescent DOM components of the 3rd fraction exhibited excitation and emission characteristics similar to those observed for S5 with a lower relative contribution of the fluorescence maximum at 270nm/430nm (E_x/E_m) (Figure 5.25-a and Table 5.6). As we already observed for samples S5, these compounds are distributed from fractions 2 till 4. However, the emission peaks of fluorescent DOM components of the 4th fraction indicated a slight red shift of maxima in comparison with the 2nd fraction.

Table 5.6 EEM contour plots (intensity scales different) of the bulk samples and the nine AF4 fractions isolated for S6 (2011, 2012 and 2013) in the Seine River

Fraction number	S6 collected in 2011	S6 collected in 2012	S6 collected in 2013
Bulk sample	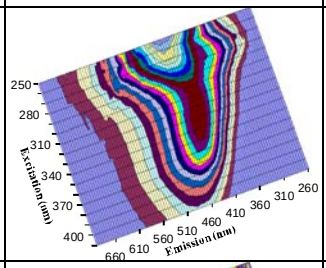	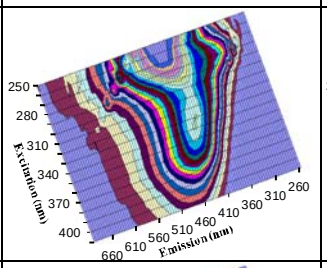	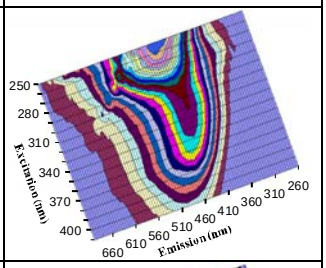
The 1st fraction	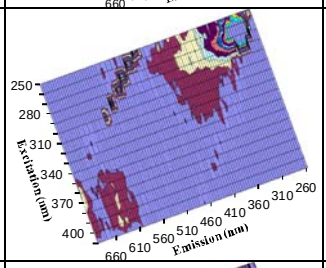	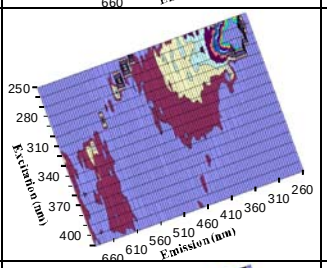	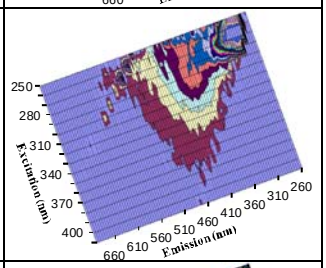
The 2nd fraction	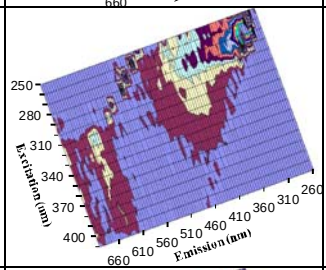	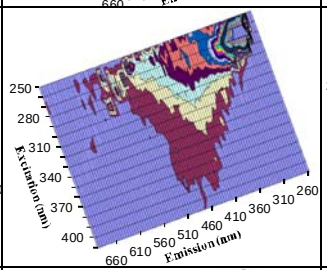	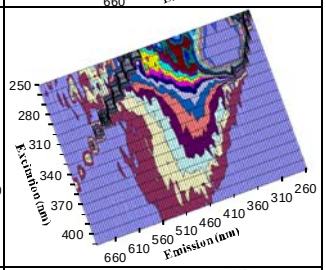
The 3rd fraction	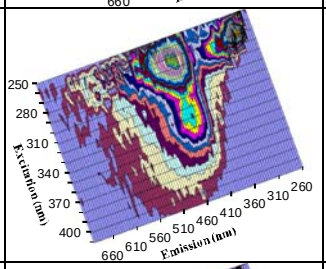	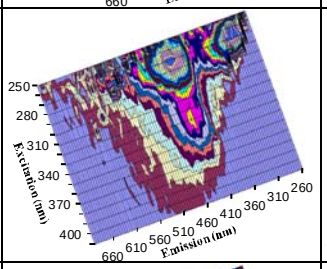	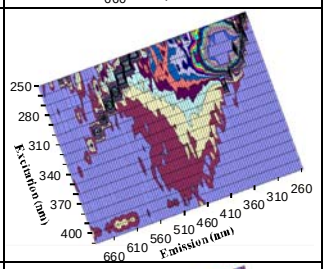
The 4th fraction	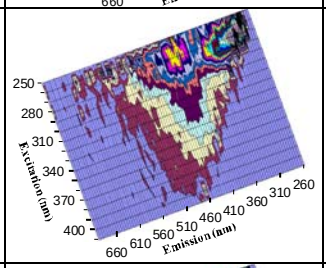	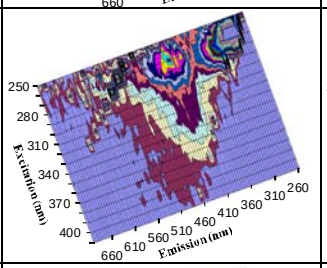	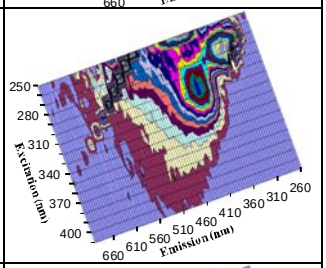
The 5th fraction	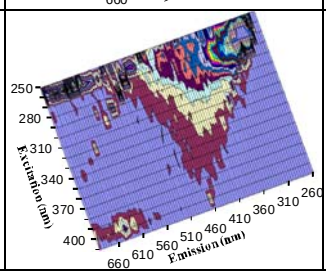	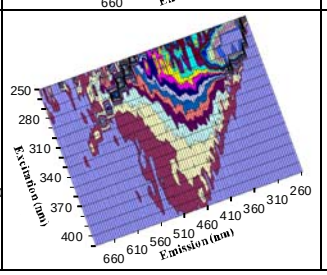	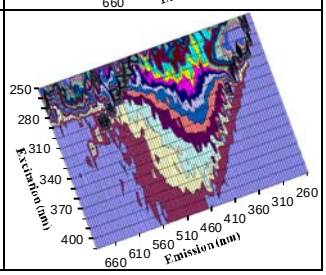

Fraction number	S6 collected in 2011	S6 collected in 2012	S6 collected in 2013
The 6th fraction	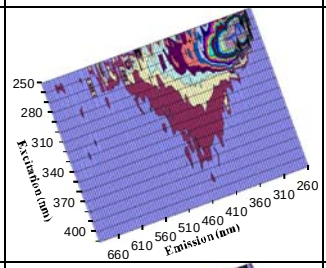	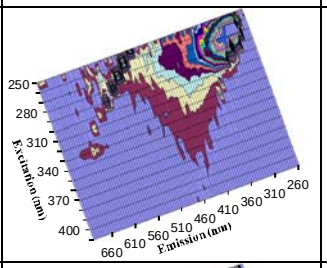	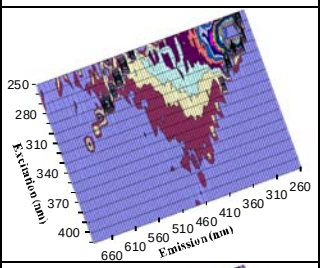
The 7th fraction	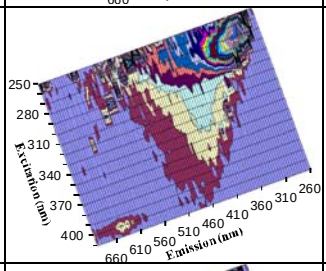	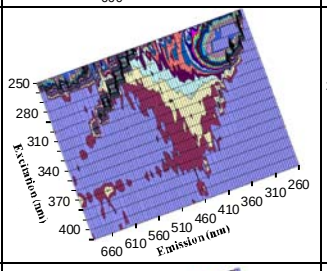	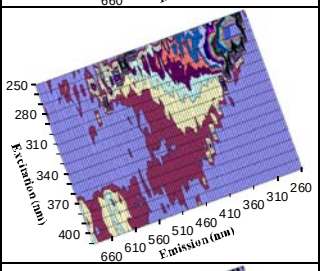
The 8th fraction	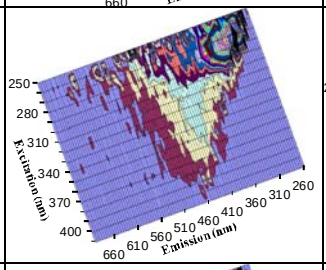	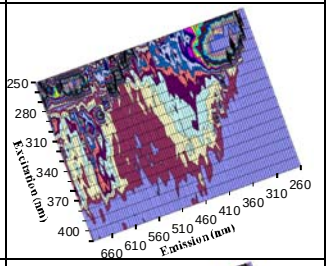	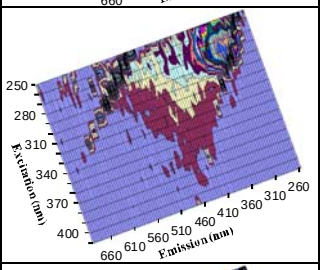
The 9th fraction	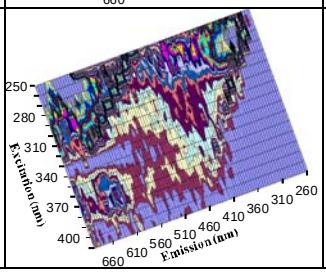	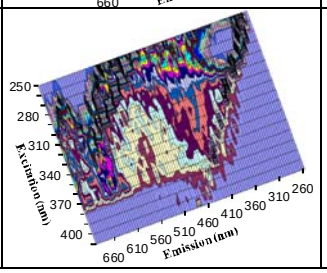	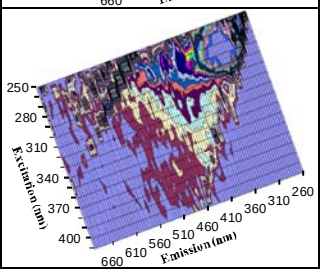

For sample S6-2012, we observed, compared to the other fractions, that the 2nd fraction presented higher values of wavelengths for both excitation and emission in the range of 330-360 nm and 420-480 nm, respectively. This result suggested a higher hydrophobic degree of the fluorophore α for this fraction.

As for sample S6-2013, we observed a peak at 300 nm / 400 nm (E_x/E_m). This peak was closer to the component C4 determined by PARAFAC. In addition, the excitation and emission maxima of the 5th fraction were shifted towards longer wavelengths than those of the 4th fraction, thus predicting more aromatic chemical nature and higher molecular weight. Furthermore, a pigment-like fluorescence was also observed within the EEM spectrum of the 7th fraction.

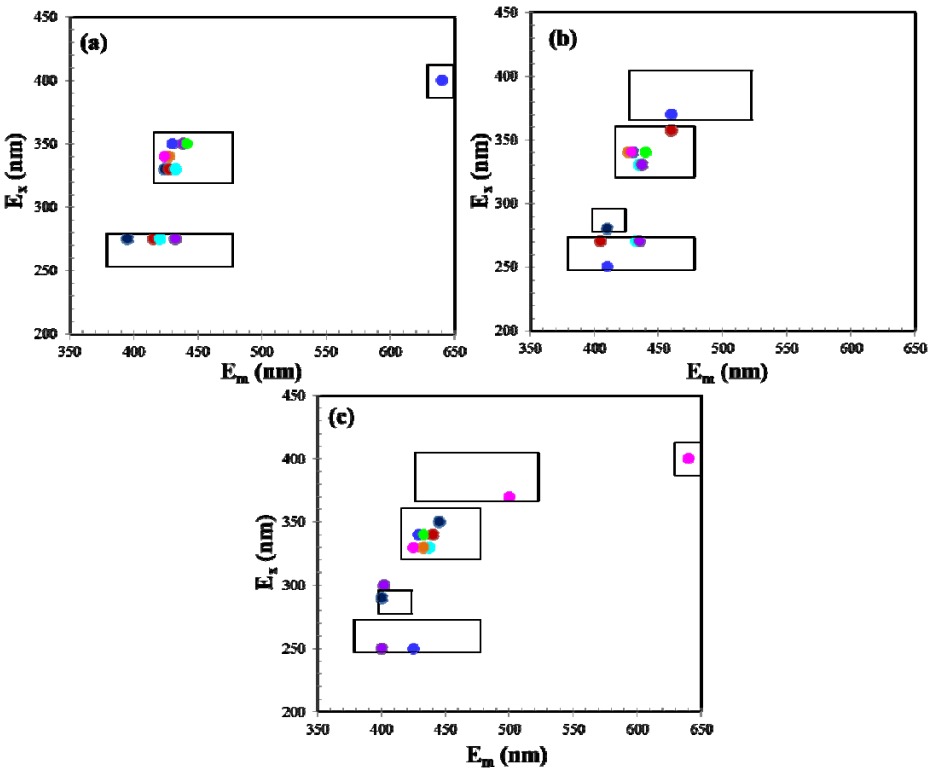

Figure 5.25 Positions of all fluorescence intensity maxima within EEM, identified in all fractions of sample S6 collected in the Seine River (a) in 2012, (b) in 2012 and (c) in 2013. Key: (●) 1st fraction; (●) 2nd fraction; (●) 3rd fraction; (●) 4th fraction; (●) 5th fraction; (●) 6th fraction; (●) 7th fraction; (●) 8th fraction; (●) 9th fraction

The Figure 5.26 showed the variations of the fluorescence intensity of the three bands α', α and β determined for all the AF4 fractions of the samples S6 collected during the three sampling periods.

For sample S6-2011, the 3rd fraction was characterised by higher fluorescence intensities of the three bands in comparison with the other fractions.

For sample S6-2012, the fluorescence intensity of the band α' was slightly more intense for the 5th fraction than for the 3rd. This is due to the fact that the position of the band α' for the 3rd fraction was shifted to longer excitation wavelength with a maximum centred at E_x=270 nm instead of 250nm for the 5th fraction.

For sample S6-2013, the highest intensity of peak β was observed for the 4th fraction at a position slightly shifted towards shorter excitation wavelengths (E_x=300 nm) than usual.

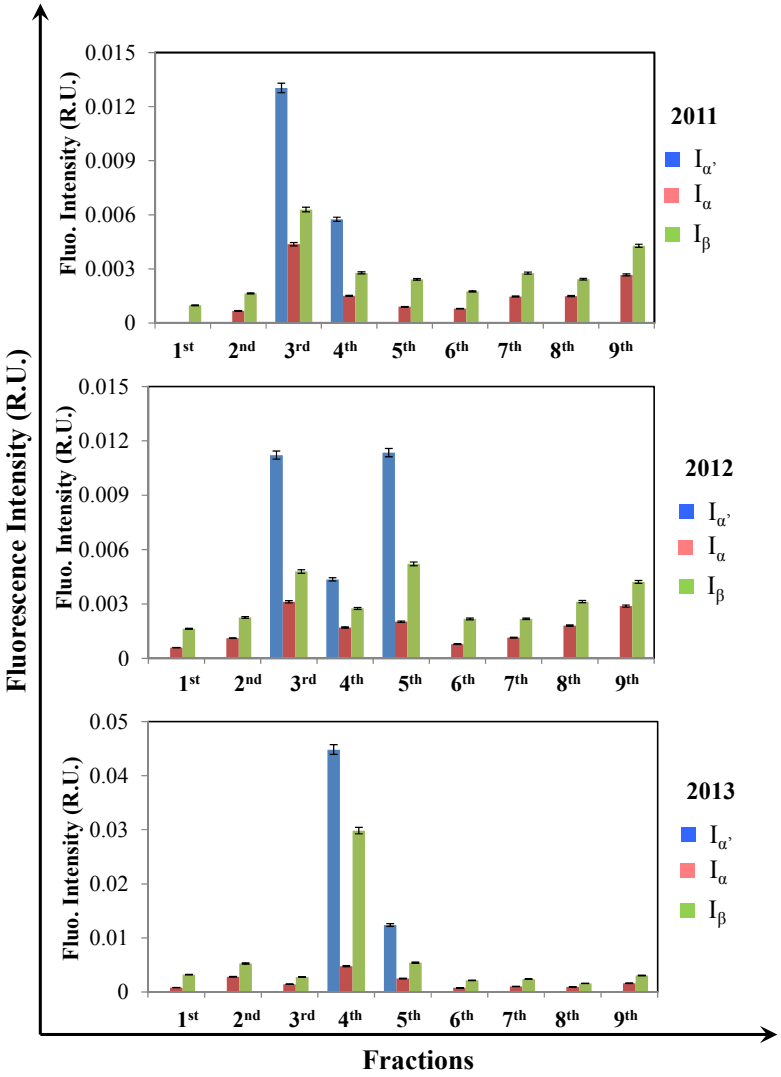

Figure 5.26 Variations of the fluorescence intensity of the bands α', α and β between the nine fractions and the three sampling dates for S6 collected in the Seine River.
Error bars indicate standard deviation

For the low-water conditions in 2012 and to a lesser extent in 2011, corresponding to a late low-water event, the highest intensities were mainly detected for the 3rd fraction, whereas they were observed for the 4th one during the flood event.

The fluorescence index, BIX, was also calculated for all the fractions of the samples S5 and S6 and its variations presented on Figure 5.27. The BIX values for the raw samples S5 and S6 taken in 2013 were lower than for the bulk samples collected in 2011 and 2012. In contrast, we observed the strongest values of BIX for the 3rd fraction in 2013 in comparison with 2011 and 2012.

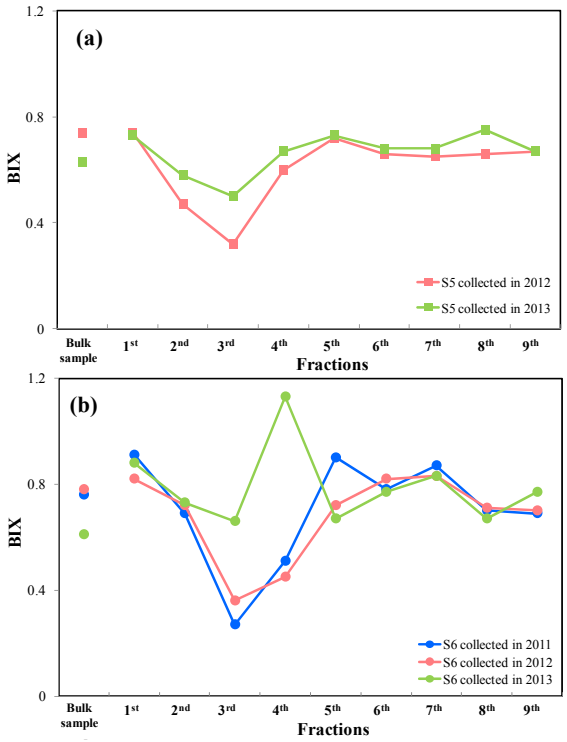

Figure 5.27 Variations of BIX between fractions compared to bulk samples for the sites (a) S5 (2011 and 2012) and (b) S6 (2011, 2012 and 2013) in the Seine River

The highest BIX value was determined for the 4th fraction of sample S6 collected in 2013 (BIX=1.13). Nevertheless, this result was probably influenced by the intense peak detected at 300nm/400nm (E_x/E_m) which differs slightly of β and which may bias the calculation of BIX.

5.3. Conclusions

In this chapter, samples collected within the Seine River catchment were fractionated by asymmetrical flow field-flow fractionation hyphenated to UV detector. AF4 was used to partition constituents from surface water samples into a continuum of colloidal sizes. We observed significant different distribution profiles for all the studied surface water samples. The AF4 fractograms of the samples indicated that the smaller molecular weight fraction exhibited a much higher UV signal than the larger molecular weight fractions. These results suggested that the samples taken from the Seine River catchment are mainly constituted by DOM molecules of small-size. However, the wide-range variation of both the number-average MW and weight-average MW implied a heterogenous distribution of DOM in this river catchment.

Thirteen samples, selected from the three sub-basins, were fractionated by AF4 leading to the isolation of eight or nine fractions per sample to be further analyzed by EEM fluorescence spectroscopy. The combination of AF4 and EEM fluorescence spectroscopy highlighted significant spatial and temporal variations of DOM as well as specific typologies for the different sampling sites.

A huge peak appeared at 250-280 nm/260-340 nm (E_x/E_m) within the EEM spectra of all fractions due to a contamination certainly related to a bacterial evolution in the AF4 system. This very unfortunately prevented us from interpreting the distribution of the band γ in the various fractions. Thus, in order to estimate the distribution of this fluorophore, it would be necessary to add in the future a suitable anti-bacterial constituent into the elution solution to prevent this contamination while avoiding a modification of the samples and respecting the environmental protection and the human health.

The lowest values of BIX were systematically determined for the 3rd fraction, whatever the considered samples, suggesting thus the presence in this fraction of the DOM constituents from mainly terrestrial origin. Again for all the considered samples, the strongest values of BIX were not observed only for the small molecular sizes, showing that DOM constituents of autochthonous origin are characterized by either low or high molecular weights. Pigment-like fluorophores were detected in some fractions of the Oise and Marne sub-basins.

The distributions of fluorescence intensities of the three main detected bands showed that fluorescent DOM was mainly eluted from 4 min to 10 min, this time period corresponding to low UV signal. These results highlighted differences in absorption and fluorescence characteristics in general. It was interesting to notice that the higher fluorescence intensities of the isolated AF4 fractions were often observed for higher MW fractions than absorbance. Considering that different molecular size distributions were observed for FDOM and CDOM, it would be thus interesting to investigate these differences of optical properties by using asymmetrical flow field-flow fractionation system hyphenated online to both UV and EEM fluorescence detectors.

GENERAL CONCLUSIONS AND PERSPECTIVES

The aim of this PhD thesis was to characterize DOM as well as to identify the sources of DOM within the Seine River catchment in the Northern part of France. To achieve these goals, three sampling campaigns were carried out in November 2011 (late low-water), September 2012 (low-water) and February 2013 (flood) from the three main sub-basins: the Oise basin, the Seine basin and the Marne basin. A large number of sites located mainly in the upstream parts of the Seine basin were sampled in order to estimate the spatio-temporal variability of DOM within the Seine River catchment.

In this study, three main objectives were pursued.

First of all, the optical properties of DOM in the bulk samples were investigated by using UV/visible absorbance and EEM fluorescence spectroscopy. The water samples collected in 2012 showed significantly high S_R values, indicative of lower organic material molecular weight while the higher molecular weights were observed for the samples collected in 2013. The ratios of fluorescence intensities ($I_{\alpha'}/I_{\alpha}$, I_{β}/I_{α} and I_{γ}/I_{α}) highlighted these temporal variations. The fluorescence indices, HIX and BIX, also showed spatial and temporal variations in the quality of DOM. The strongest values of the HIX index were observed in forest sites. Moreover, the most humified, aromatic material (high HIX) was observed for the samples collected in 2013 as the highest BIX values were mainly determined for samples collected in 2012. The water samples of the Seine River catchment were mainly characterized by a relatively high biological activity, the strongest values being observed for the samples collected from the Seine River and over half of samples from the Marne basin.

PARAFAC and PCA analyses provided further understanding of the composition of DOM as well as its sources. PARAFAC decomposed the EEM spectra of the water samples into seven discrete components. The PCA analysis helped to discriminate the variations of DOM between the three studied basins and the three sampling periods in the Seine River catchment. The PCA analysis allowed us to distinguish three types of organic matter for 2011 and 2012. The Seine basin was characterized by the strongest biological activity (certainly in connection with the presence of the "Seine-Aval" WWTP). DOM from the Oise basin seemed to have more "humic" characteristics (sample O1, forest zone, presenting the strongest humic-type material). The samples collected from the Marne basin are characterized by a third specific type of organic matter. Moreover, the samples collected during the flood period in 2013 were

characterized by more mature DOM, while samples collected during low-water period (2011 and 2012) were characterised by higher biological activities. On the other hand, during the period of flood, a similar distribution of components was observed for all the samples, whatever the river or the sub-basin considered, leading to a smoothing of the specificities observed in 2011 and 2012 for the sampling sites. This implied that both qualitative and quantitative variations of DOM, within the studied ecosystem, seem to be related to hydrological conditions (floods or low-water) and/or to specific geographical locations.

In the second part of this study, we developed a semi-quantitative asymmetrical flow field-flow fractionation technique (AF4) to fractionate and characterize DOM in the Seine River catchment. The cross-flow rate was found to be the important factor governing the efficiency of the AF4 fractionation of DOM colloids. Moreover, the AF4 technique using an exponential gradient program of cross-flow rate with initial cross-flow 3.5 ml min^{-1} period showed noticeable advantages over an isocratic cross-flow rate or linear gradient program of cross-flow rate. Additionally, a relaxation time of 2 min was shown to be necessary to achieve the complete separation of DOM macromolecules in the natural aquatic environments. However, the relatively low recoveries for the UV signals and relatively high for the MALLS signals indicated that the samples in the Seine River catchment are represented by DOM macromolecules of low-molecular-weight, a part of which must be lost through the membrane during the relaxation time.

Thirdly, AF4 was used to partition the DOM constituents from all the 102 surface water samples into a continuum of colloidal sizes. We observed different kinds of distribution profiles for all these samples, highlighting three main types of organic matter, what was in good agreement with PCA results. The size distribution of DOM macromolecules, including number-average (M_n) and weight-average (M_w) molecular weights, and the molecular weight corresponding to the peak maximum (M_p) as well as polydispersity index (PDI), was estimated on the basis of a series of organic macromolecules (Trypan blue (0.96 KDa), vitamin B12 (1.33 KDa), bovine heart cytochrome C (12.4 KDa) and bovine serum albumin (66 KDa). However, the results of the DOM molecular size distribution in this study were also limited to the determination of the smallest DOM constituents which eluted during the twenty first minutes.

A more advanced investigation in DOM molecular size distribution was addressed in this work, in regard to the fluorescence properties of various size-based fractions of DOM. The optimized AF4 methodology was thus applied to the fractionation of 13 samples, selected from the three sub-basins, into eight or nine fractions, depended on their UV signals. Then, EEM fluorescence spectroscopy was used to characterize the fluorescence properties of each isolated fraction.

The combination of AF4 and EEM fluorescence spectroscopy highlighted significant spatial and temporal variations of DOM as well as specific typologies for the different sampling sites. Different types of fluorescent organic matter were isolated in the various fractions. Some specific spectral signatures were observed while it was not possible to distinguish these maxima of fluorescence from the bulk sample EEM spectra. It was also very interesting to detect fluorophores similar to some components that had been determined by PARAFAC analysis.

The highest fluorescence intensities of the three main bands, α', α and β, were determined, for almost all samples, in the 3rd fraction (from 4 min to 10 min), indicating that fluorescent DOM was mainly eluted in this fraction. Moreover, the optical properties of these constituents allowed us to conclude to a main terrestrial origin of DOM in this fraction. As for DOM constituents of autochthonous origin, they were characterized by either low or high molecular weights.

For all the sampling sites considered for AF4 separation, it was systematically observed differences in the spectral signatures of the isolated fractions in 2013 (period of flood) in comparison with those obtained for samples collected in 2011 and 2012 (low-water conditions).

The application of AF4, UV/visible absorbance and EEM fluorescence spectroscopy coupled to PARAFAC and PCA analyses allowed us to discriminate between different sources of dissolved organic matter in the catchment of the Seine River and highlighted significant spatial and temporal variations of DOM as well as specific typologies for the different sampling sites.

Fluorescence coupled to AF4 appears to be a powerful tool for the study of DOM in aquatic environment and offers new perspectives in the characterization and separation of colloidal DOM.

The outlooks in conjunction with each chapter, describing the potential areas of future research on DOM, are listed below:

- It would be interesting to pursue the observation of the temporal and spatial variations of the characteristics of DOM within the Seine River catchment. Indeed, although DOM plays a key role in environmental processes, there is clearly a lack in DOM characterization and especially in long-term monitoring. Climate change expressed as changes in runoff, primary productivity, flood or low-water events, solar irradiation, temperature, etc. will likely result in changes in aquatic DOM quality and concentration. The key controls on DOM quality, quantity, and catchment export in response to global change are still not fully understood. More detailed knowledge of these processes is required so that changes in DOM and its interactions with contaminants can be better predicted.

- With regards to AF4 system, it would be interesting to continue the optimization of the experimental parameters. Especially, it is essential to focus on the membrane in order to increase the recovery of DOM colloids and to minimize the loss of samples. In particular, it would be necessary to test various membrane materials as well as lower molecular weight cut-offs than 1KDa. Moreover, it would be also necessary to study the effect of the ionic strengths of the mobile phase onto the efficiency of the separation of natural DOM macromolecules.

- Further research needs to be conducted to compare the molecular weight distribution between fluorescent DOM and the chromophoric DOM by hyphenating online asymmetrical flow field-flow fractionation system to both UV and EEM fluorescence detectors.

- Last but not least, it would be also essential for the investigation of the interactions of DOM with contaminants to hyphenate asymmetrical flow field-flow fractionation system to mass spectrometry. From a general point of view, a multi-dimensional detection approach could be the most efficient and informative, taking into account the complexity of both the organic matter, the environmental ecosystems, and the processes of interactions DOM/contaminants.

APPENDICES

Appendix 1

Physical-chemical parameters of surface samples in the Seine River catchment (Cond.: conductivity; DOC: Dissolved organic carbon concentration)

Rivers	Code	pH			Cond. (µS cm^{-1})			DOC (mg C L^{-1})		
		2011	2012	2013	2011	2012	2013	2011	2012	2013
Marne	G1	8.00		7.55	395		410	2.01		2.78
	G2	7.17		8.01	778		580	2.01		2.70
	G3	7.38		8.02	825		570	9.32		2.87
	G4	7.73		7.91	694		570	1.73		2.58
	LD			8.21			520		2.76	1.65
	Sa			8.31			550		2.41	1.04
	M1								2.05	1.20
	M2			8.30			510		2.87	1.30
	M3	7.48		8.16	459		510	1.59	2.22	1.53
	M4	7.87		7.92	455		520	1.67	1.96	
	M5	8.04		8.09	467		520	1.88	2.51	
	M6			8.13			520		2.15	1.92
	M7	7.80		8.10	544		530	1.91	1.99	2.40
	M8		8.11			530			2.09	
	M9	7.79		8.10	558		530	2.13	2.29	2.17
Oise	Ve		8.21	8.04		765	670		2.76	3.17
	Ai		7.92	8.09		553	500		1.82	2.58
	As1		8.07	7.90		482	440		2.20	4.35
	As2	7.35	8.18	7.80	655	599	290	2.74	2.10	3.54
	Br	7.77	8.08	8.00	650	440	1630	2.17	1.51	1.76
	No	7.72	8.27	7.70	738	591	670	2.17	3.25	3.02
	RF		8.23	7.20		242	860		2.92	6.53
	Se	7.30	8.00	7.80	514	632	850	1.80	1.46	2.19
	Th		8.15	8.02		1592	710		1.70	2.26
	O1	5.90	6.33	8.10	84	65	93	4.00	4.11	3.41
	O2	7.63	8.28	7.97	646	495	520	2.57	1.99	2.15
	O3	7.48	8.17	7.85	561	527	960	2.39	1.98	2.38
	O4	7.80	8.20	7.84	733	695	510	2.74	2.64	4.16
	O5	7.39	8.01	8.02	731	1502	610	2.58	2.35	3.25
	O6									3.14

Appendix 1 *(continued)*

Rivers	Code	pH			Cond. (µS cm^{-1})			DOC (mg C L^{-1})		
		2011	2012	2013	2011	2012	2013	2011	2012	2013
Seine	Au		8.15	8.30		386	510		1.93	2.22
	Es		7.85	8.04		530	700		2.40	4.90
	Lo		8.37	8.15		540	530		2.11	4.28
	Or		8.11	8.10		686	740		3.41	4.64
	Yo		8.12	8.29		426	420		2.05	2.25
	S1		8.01	8.22		368	530		1.87	1.68
	S2		8.24	8.29		383	520		1.94	2.35
	S3		8.14	8.30		438	510		2.00	2.41
	S4		7.90			533			2.51	2.73
	S5			8.02			530		2.43	2.45
	S5'	7.66			547			2.64		
	S6	7.49		8.08	632		530	3.86	3.26	2.40
	S7	7.71		7.97	670		560	3.60	2.83	2.75
	S8	7.59		8.00	658		550	3.28	3.18	2.72
	S9	7.72		7.97	643		550	3.10	3.04	

Appendix 2

Fluorescence indices of surface water samples in the Seine River catchment

Rivers	Code	f_{450}/f_{500} (RSD ≤ 2%)			HIX (RSD ≤ 2%)			BIX (RSD ≤ 2%)		
		2011	2012	2013	2011	2012	2013	2011	2012	2013
Marne	G1	1.20		1.27	7.58		11.6	0.61		0.63
	G2	1.30		1.31	7.90		7.95	0.67		0.68
	G3	1.21		1.28	5.48		11.51	0.65		0.64
	G4	1.34		1.28	6.64		11.96	0.73		0.65
	LD		1.26	1.26		5.06	7.58		0.81	0.70
	Sa		1.26	1.28		4.95	8.88		0.76	0.68
	M1		1.28	1.26		6.48	6.83		0.78	0.70
	M2		1.32	1.25		3.39	7.62		0.95	0.69
	M3	1.28	1.30	1.23	6.89	4.65	11.28	0.72	0.77	0.64
	M4	1.27	1.27		6.21	5.72		0.73	0.78	
	M5	1.42	1.45		9.07	6.56		0.44	0.51	
	M6		1.42	1.21		6.92	13.36		0.49	0.60
	M7	1.35	1.34	1.22	7.20	6.35	14.67	0.57	0.59	0.59
	M8		1.34			7.03			0.61	
	M9	1.41	1.36	1.24	6.83	6.26	12.76	0.58	0.71	0.61
Oise	Ve		1.32	1.24		8.34	12.13		0.74	0.63
	Ai		1.24	1.2		11.69	15.53		0.67	0.57
	As1		1.19	1.16		11.73	16.57		0.65	0.54
	As2	1.31	1.29	1.17	8.87	7.53	15.54	0.60	0.65	0.56
	Br	1.23	1.3	1.27	9.77	10.26	11.05	0.63	0.66	0.64
	No	1.28	1.28	1.26	7.52	7.84	12.31	0.68	0.72	0.64
	RF		1.16	1.19		17.42	16.91		0.58	0.59
	Se	1.25	1.25	1.19	8.48	9.86	17.88	0.64	0.67	0.59
	Th		1.32	1.29		5.15	9.18		0.77	0.67
	O1	1.06	1.05	1.03	20.56	19.82	22.99	0.42	0.41	0.41
	O2	1.23	1.24	1.23	10.13	10.05	13.35	0.61	0.66	0.61
	O3	1.23	1.25	1.23	9.55	9.28	11.08	0.63	0.66	0.61
	O4	1.23	1.3	1.17	9.60	9.24	13.06	0.66	0.71	0.56
	O5	1.29	1.28	1.23	8.37	6.89	9.35	0.67	0.74	0.63
	O6			1.23			12.86			0.61

Appendix 2 *(continued)*

Rivers	Code	f_{450}/f_{500} (RSD ≤ 2%)			HIX (RSD ≤ 2%)			BIX (RSD ≤ 2%)		
		2011	2012	2013	2011	2012	2013	2011	2012	2013
Seine	Au		1.23	1.20		6.79	12.18		0.76	0.61
	Es		1.20	1.17		7.96	12.87		0.67	0.59
	Lo		1.29	1.19		5.66	16.28		0.80	0.58
	Or		1.36	1.27		7.53	10.99		0.70	0.66
	Yo		1.19	1.21		7.68	12.01		0.68	0.61
	S1		1.33	1.22		4.78	9.43		0.78	0.63
	S2		1.27	1.18		4.02	12.59		0.78	0.59
	S3		1.23	1.18		6.32	13.48		0.73	0.59
	S4		1.35	1.27		6.46	9.83		0.77	0.64
	S5		1.35	1.26		6.07	12.34		0.74	0.63
	S5'	1.43			7.98			0.76		
	S6	1.31	1.47	1.21	6.21	6.02	14.06	0.68	0.78	0.61
	S7	1.45	1.41	1.28	6.27	6.38	10.94	0.76	0.76	0.64
	S8	1.43	1.39	1.27	6.24	6.49	11.48	0.75	0.76	0.64
	S9	1.44	1.37		6.65	7.76		0.76	0.77	

Appendix 3

Fractogram of samples collected within the Seine River catchment obtained by AF4

Appendix 3-a: Fractogram of samples collected in 2012 within the Seine River catchment obtained by AF4. (a) Marne River; (b-1) Oise River and (b-2) its tributaries; (c-1) Seine River and (c-2) its tributaries

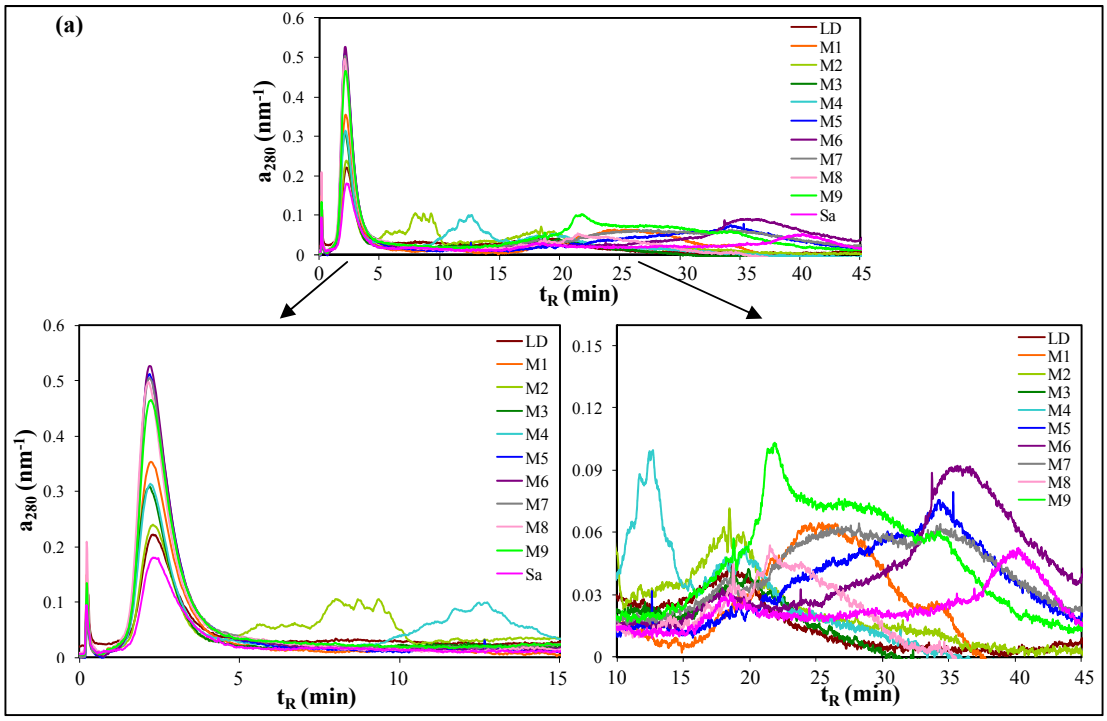

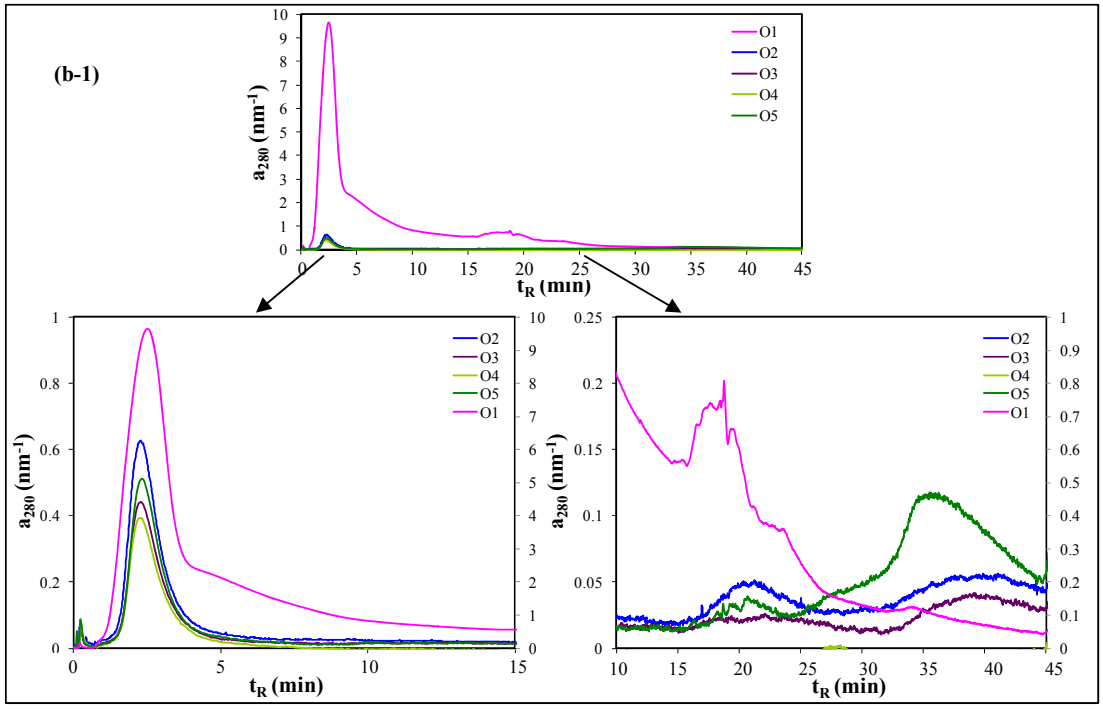

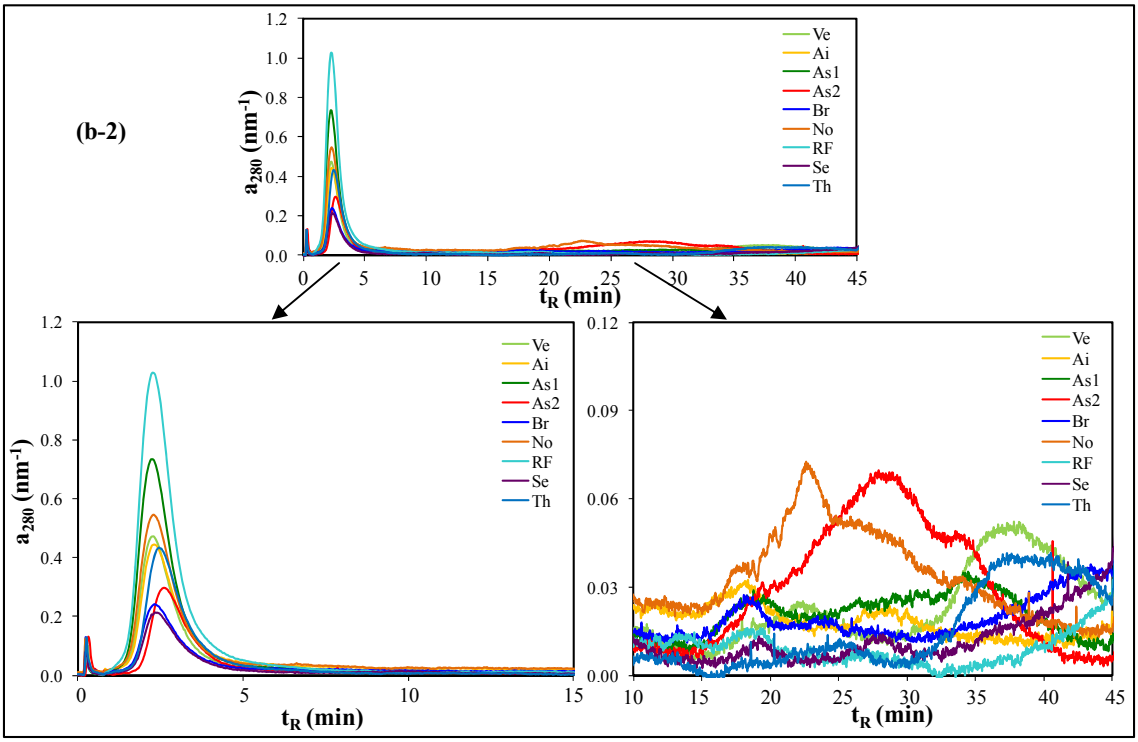
(b-2)
a_{280} (nm^{-1})
t_R (min)
Ve
Ai
As1
As2
Br
No
RF
Se
Th

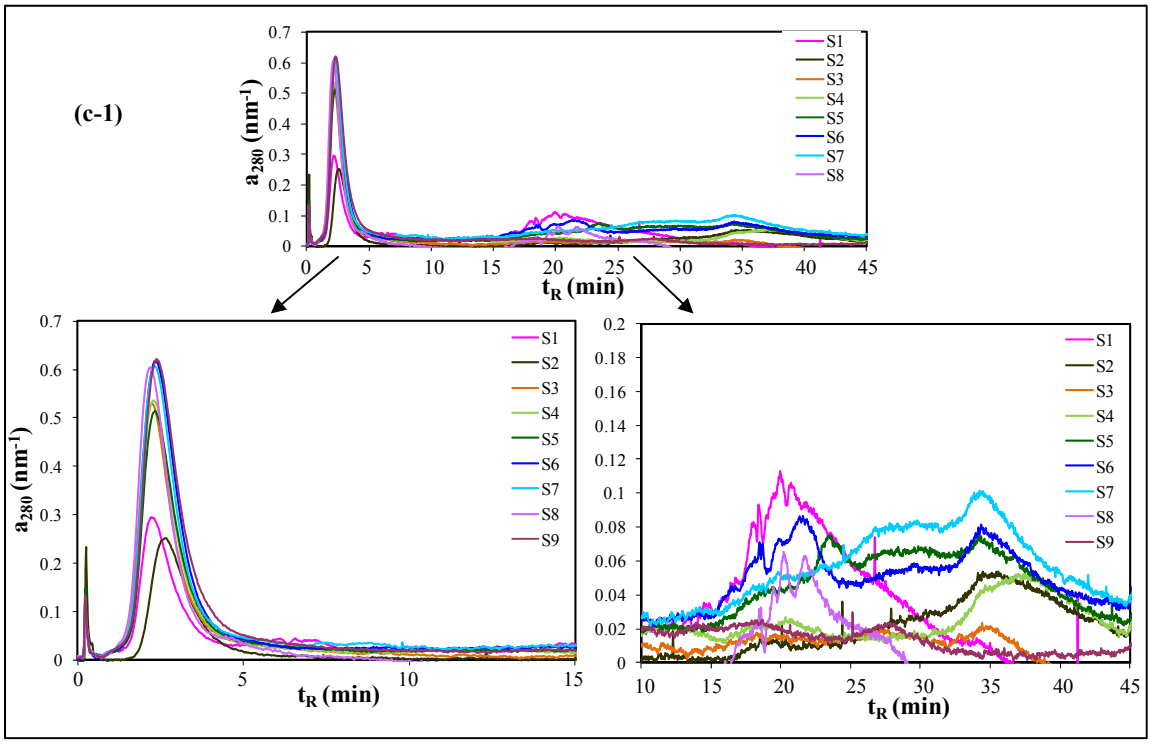
(c-1)
a_{280} (nm^{-1})
t_R (min)
S1
S2
S3
S4
S5
S6
S7
S8
S9

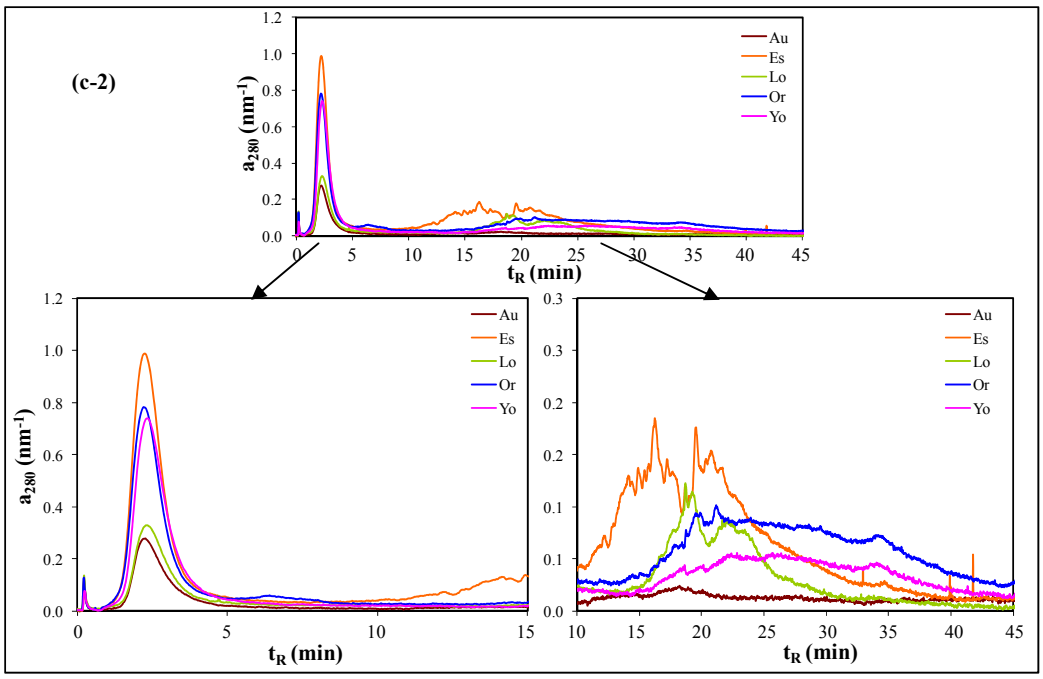
(c-2)
a_{280} (nm^{-1})
t_R (min)
Au
Es
Lo
Or
Yo

Appendix 3-b: Fractogram of samples collected in 2013 within the Seine River catchment obtained by AF4. (a-1) Marne River and (a-2) Grand Morin tributary; (b-1) Oise River and (b-2) its tributaries; (c-1) Seine River and (c-2) its tributaries

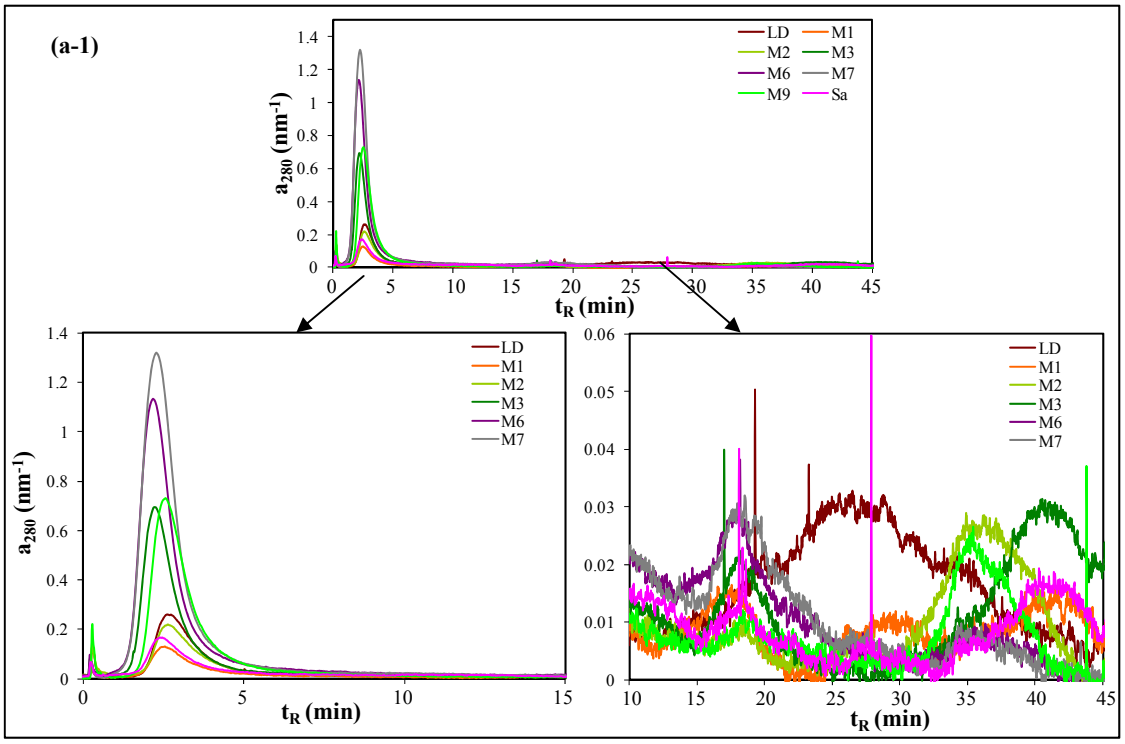

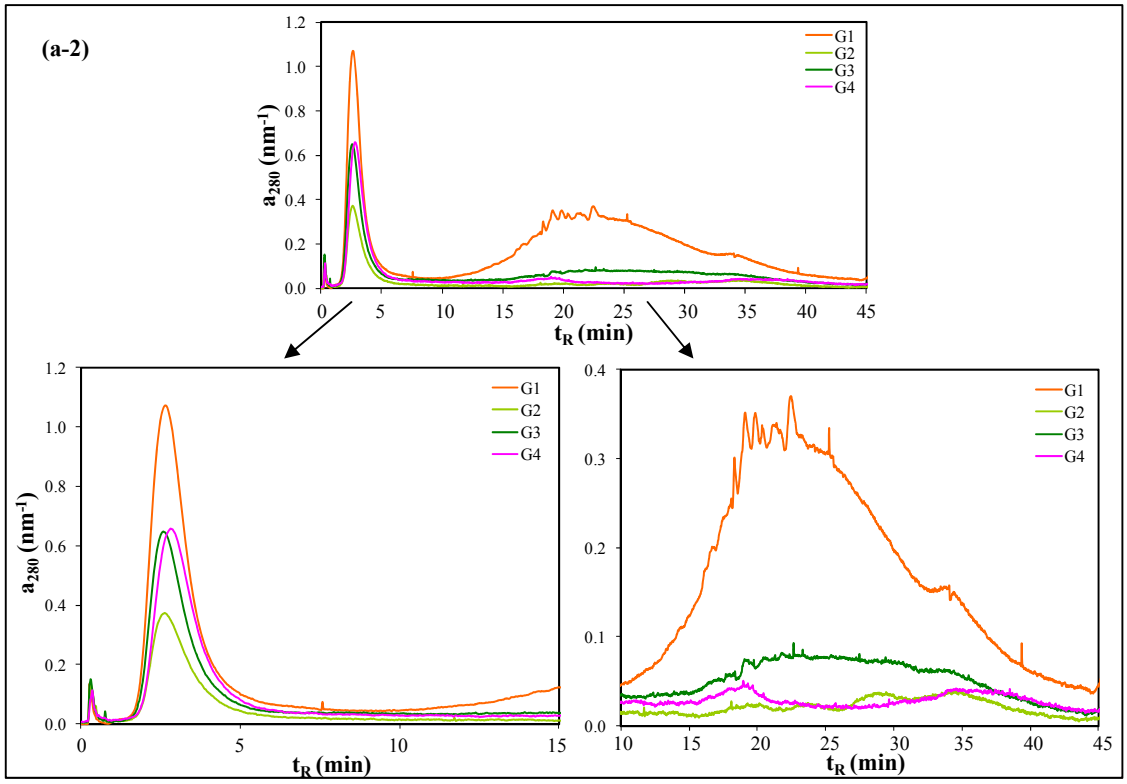

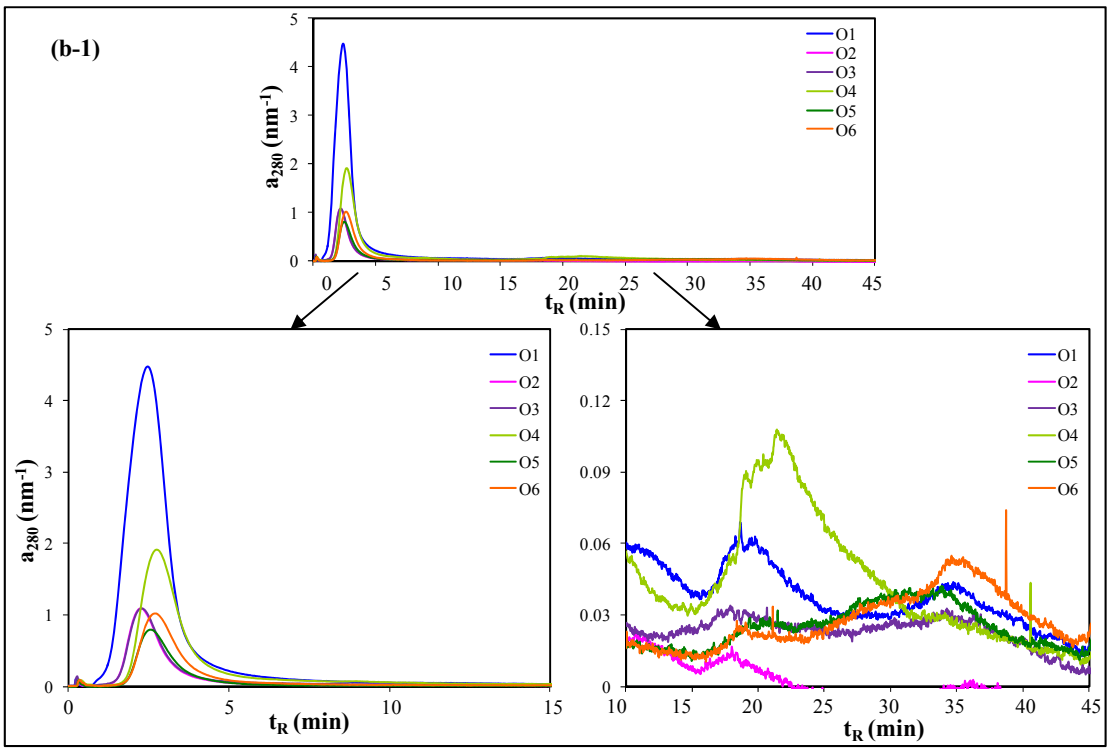
(b-1)
O1
O2
O3
O4
O5
O6
a_{280} (nm^{-1})
t_R (min)

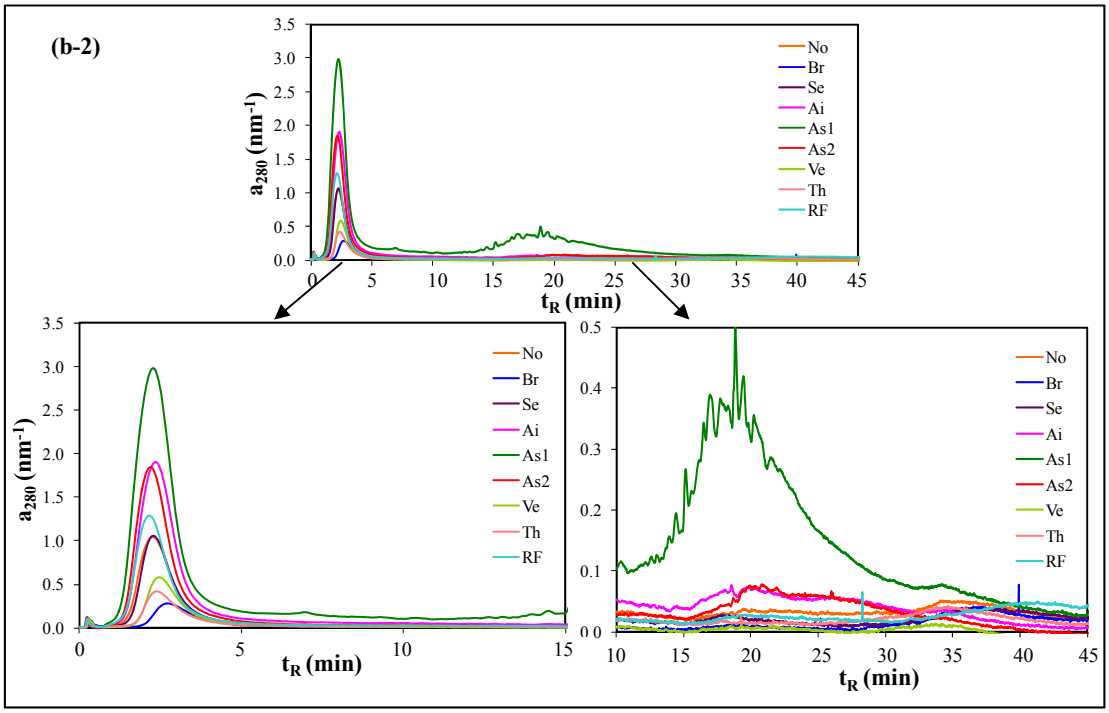
(b-2)
No
Br
Se
Ai
As1
As2
Ve
Th
RF
a_{280} (nm^{-1})
t_R (min)

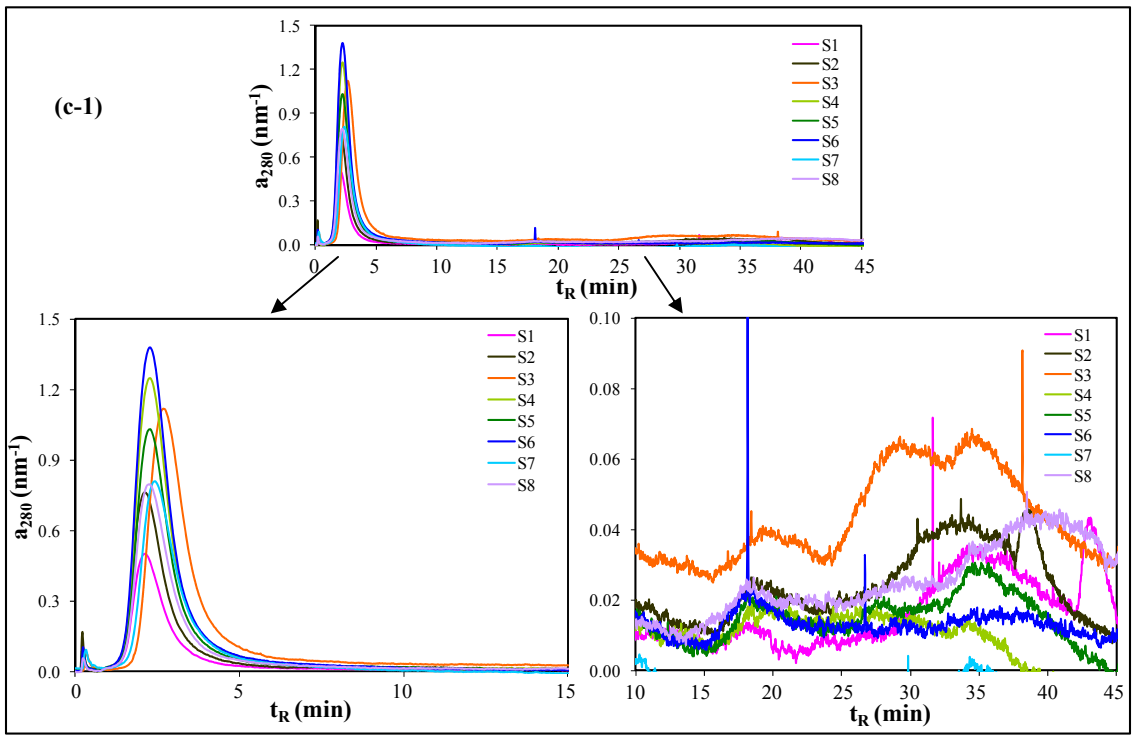
(c-1)
a_{280} (nm^{-1})
t_R (min)
S1
S2
S3
S4
S5
S6
S7
S8

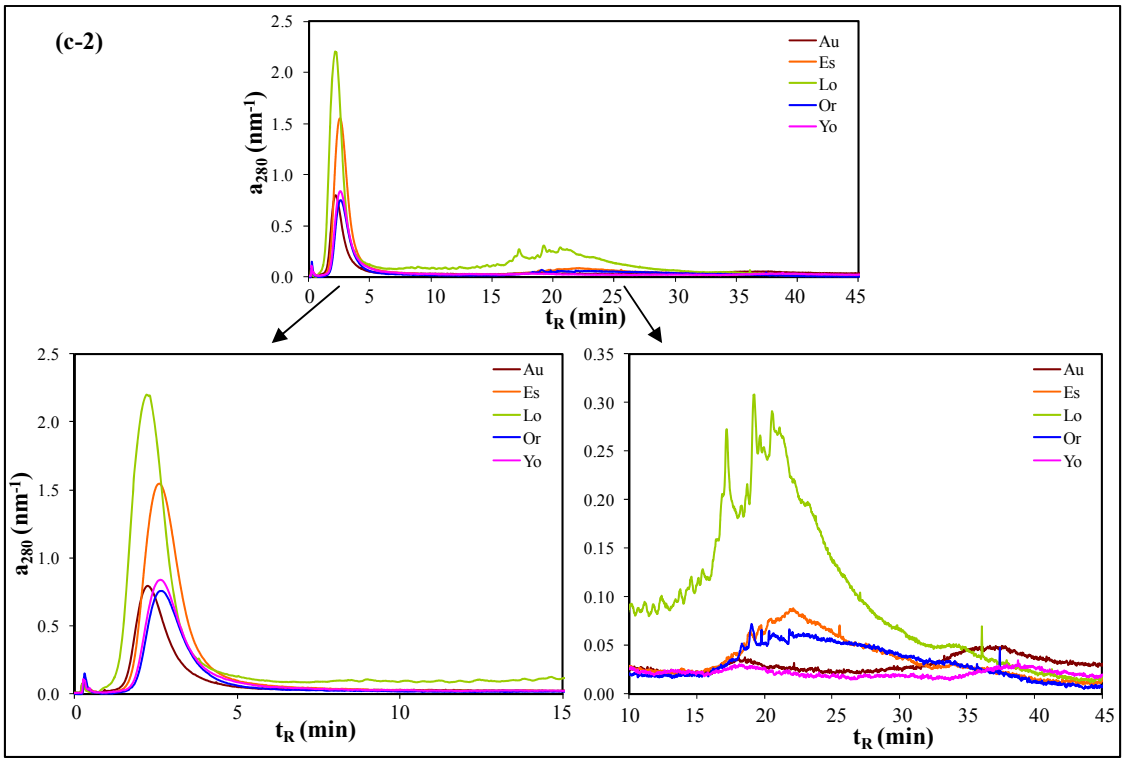
(c-2)
a_{280} (nm^{-1})
t_R (min)
Au
Es
Lo
Or
Yo

REFERENCES

Abbt-Braun, G., Lankes, U., Frimmel, F.H., 2004. Structural characterization of aquatic humic substances – The need for a multiple method approach. *Aquat. Sci.* 66, 151–170.

Aiken, G.R., 1985. Isolation and concentration techniques for aquatic humic substances, in: Aiken, G.R., McKnight, D.M., Wershaw, R.L., McCarthy, P. (Eds.), *Humic Substances in Soil, Sediment and Water: geochemistry, isolation and characterization*. John Wiley, New York, pp 363-385.

Aiken, G.R., Gilmour, C.C., Krabbenhoft, D.P., Orem, W., 2011. Dissolved Organic Matter in the Florida Everglades: Implications for Ecosystem Restoration. *Crit. Rev. Environ. Sci. Technol.* 41, 217–248.

Aiken, G.R., McKnight, D.M., Wershaw, R.L., MacCarthy, P., 1985. Humic substances in soil, sediment, and water: geochemistry, isolation and characterization, *John Wiley*, New York.

Akagi, J., Zsolnay, Á., Bastida, F., 2007. Quantity and spectroscopic properties of soil dissolved organic matter (DOM) as a function of soil sample treatments: Air-drying and pre-incubation. *Chemosphere* 69, 1040–1046.

Akkanen, J., Lyytikäinen, M., Tuikka, A., Kukkonen, J.V.K., 2005. Dissolved organic matter in pore water of freshwater sediments: Effects of separation procedure on quantity, quality and functionality. *Chemosphere* 60, 1608–1615.

Alasonati, E., Slaveykova, V.I., Gallard, H., Croué, J.-P., Benedetti, M.F., 2010. Characterization of the colloidal organic matter from the Amazonian basin by asymmetrical flow field-flow fractionation and size exclusion chromatography. *Water Res.* 44, 223–231.

Almgren, T., Josefsson, B., Nyquist, G., 1975. A Fluorescence method for studies of spent sulfite liquor and humic substances in sea water. *Anal. Chim. Acta* 78, 411–422.

Al-Reasi, H.A., Wood, C.M. and Smith, D.S., 2011. Physicochemical and Spectroscopic Properties of Natural Organic Matter (NOM) from Various Sources and Implications for Ameliorative Effects on Metal Toxicity to Aquatic Biota. *Aquatic Toxicology* 103, 179-190.

Alvarez-Puebla, R.A., Valenzuela-Calahorro, C., Garrido, J.J., 2006. Theoretical study on fulvic acid structure, conformation and aggregation: A molecular modelling approach. *Sci. Total Environ.* 358, 243–254.

Amon, R.M., Benner, R., 1996. Bacterial utilization of different size classes of dissolved organic matter. *Limnol. Oceanogr.* 41, 41–51.

Anderson, S., Zepp, R., Machula, J., Santavy, D., Hansen, L., Mueller, E., 2001. Indicators of UV Exposure in Corals and Their Relevance to Global Climate Change and Coral Bleaching. *Hum. Ecol. Risk Assess. Int. J.* 7, 1271–1282.

Aoki, S., Ohara, S., Kimura, K., Mizuguchi, H., Fuse, Y., Yamada, E., 2008. Characterization of dissolved organic matter released from Microcystis aeruginosa. *Anal. Sci.* 24, 389–394.

Arrigo, K., Brown, C., 1996. Impact of chromophoric dissolved organic matter on UV inhibition of primary productivity in the sea. *Mar. Ecol. Prog. Ser.* 140, 207–216.

Asmala, E., Autio, R., Kaartokallio, H., Pitkänen, L., Stedmon, C.A., Thomas, D.N., 2013. Bioavailability of riverine dissolved organic matter in three Baltic Sea estuaries and the effect of catchment land-use. *Biogeosciences Discuss* 10, 9819–9865.

Assemi, S., Newcombe, G., Hepplewhite, C., Beckett, R., 2004. Characterization of natural organic matter fractions separated by ultrafiltration using flow field-flow fractionation. *Water Res.* 38, 1467–1476.

Backhus, D.A., Golini, C., Castellanos, E., 2003. Evaluation of Fluorescence Quenching for Assessing the Importance of Interactions between Nonpolar Organic Pollutants and Dissolved Organic Matter. *Environ. Sci. Technol.* 37, 4717–4723.

Baghoth, S.A., 2012. Characterizing natural organic matter in drinking water treatment processes and trains. UNESCO-IHE PhD *Thesis*.

Baghoth, S.A., Sharma, S.K., Amy, G.L., 2011. Tracking natural organic matter (NOM) in a drinking water treatment plant using fluorescence excitation–emission matrices and PARAFAC. *Water Res.* 45, 797–809.

Bahram, M., Bro, R., Stedmon, C., Afkhami, A., 2006. Handling of Rayleigh and Raman scatter for PARAFAC modeling of fluorescence data using interpolation. *J. Chemom.* 20, 99–105.

Baker, A., 2002. Fluorescence Excitation-Emission Matrix Characterization of River Waters Impacted by a Tissue Mill Effluent. *Environ. Sci. Technol.* 36, 1377-1382.

Baker, A., Curry, M., 2004. Fluorescence of leachates from three contrasting landfills. *Water Res.* 38, 2605–2613.

Baker, A., Elliott, S., Lead, J.R., 2007. Effects of filtration and pH perturbation on freshwater organic matter fluorescence. *Chemosphere* 67, 2035–2043.

Baker, A., Inverarity, R., 2004. Protein-like fluorescence intensity as a possible tool for determining river water quality. *Hydrol. Process.* 18, 2927–2945.

Baker, A., Inverarity, R., Charlton, M., Richmond, S., 2003. Detecting river pollution using fluorescence spectrophotometry: case studies from the Ouseburn, NE England. *Environ. Pollut.* 124, 57–70.

Baker, A., Spencer, R.G.M., 2004. Characterization of dissolved organic matter from source to sea using fluorescence and absorbance spectroscopy. *Sci. Total Environ.* 333, 217–232.

Baker, A., Ward, D., Lieten, S.H., Periera, R., Simpson, E.C., Slater, M., 2004. Measurement of protein-like fluorescence in river and waste water using a handheld spectrophotometer. *Water Res.* 38, 2934–2938.

Banaitis, M.R., Waldrip-Dail, H., Diehl, M.S., Holmes, B.C., Hunt, J.F., Lynch, R.P., Ohno, T., 2006. Investigating sorption-driven dissolved organic matter fractionation by multidimensional fluorescence spectroscopy and PARAFAC. *J. Colloid Interface Sci.* 304, 271–276.

Barrett Sylvia E., Krasner Stuart W., Amy Gary L., 2000. Natural Organic Matter and Disinfection By-Products: Characterization and Control in Drinking Water-An Overview, in: *Natural Organic Matter and Disinfection By-Products*, ACS Symposium Series. American Chemical Society, pp. 2–14.

Battin, T.J., 1998. Dissolved organic matter and its optical properties in a blackwater tributary of the upper Orinoco River, Venezuela. *Org. Geochem.* 28, 561-569.

Beckett, R., Jue, Z., Giddings, J.C., 1987. Determination of molecular weight distributions of fulvic and humic acids using flow field-flow fractionation. *Environ. Sci. Technol.* 21, 289–295.

Benedettia, M., Ranville, J.F., Ponthieua, M., Pinheiroc, J.P., 2002. Field-flow fractionation characterization and binding properties of paniculate and colloidal organic matter from the Rio Amazon and Rio Negro. *Org. Geochem* 33, 269–279.

Benner, R., 2002. Chapter 3 - Chemical Composition and Reactivity, in: Hansell, D.A., Carlson, C.A. (Eds.), *Biogeochemistry of Marine Dissolved Organic Matter*. Academic Press, San Diego, pp. 59–90.

Benner, R., Kaiser, K., 2003. Abundance of amino sugars and peptidoglycan in marine particulate and dissolved organic matter. *Limnol. Oceanogr.* 48, 118–128.

Benner, R., Pakulski, J.D., Mccarthy, M., Hedges, J.I., Hatcher, P.G., 1992. Bulk Chemical Characteristics of Dissolved Organic Matter in the Ocean. *Science* 255, 1561–1564.

Billen, G., Garnier, J., Mouchel, J.-M., Silvestre, M., 2007. The Seine system: Introduction to a multidisciplinary approach of the functioning of a regional river system. *Sci. Total Environ.*, Human activity and material fluxes in a regional river basin: the Seine River watershed Seine Special Issue 375, 1–12.

Birdwell, J.E., Engel, A.S., 2009. Variability in terrestrial and microbial contributions to dissolved organic matter fluorescence in the Edwards Aquifer, Central Texas. *J. Cave Karst Stud.* 71, 144–156.

Blough, N.V., Del Vecchio, R., 2002. Chapter 10 - Chromophoric DOM in the Coastal Environment, in: Hansell, D.A., Carlson, C.A. (Eds.), *Biogeochemistry of Marine Dissolved Organic Matter*. Academic Press, San Diego, pp. 509–546.

Blough, N.V., Zafiriou, O.C., Bonilla, J., 1993. Optical absorption spectra of waters from the Orinoco River outflow: Terrestrial input of colored organic matter to the Caribbean. J. Geophys. Res. Oceans 98, 2271–2278.

Boehme, J., Wells, M., 2006. Fluorescence variability of marine and terrestrial colloids: Examining size fractions of chromophoric dissolved organic matter in the Damariscotta River estuary. *Mar. Chem.* 101, 95–103.

Boehme, J.R., Coble, P.G., 2000. Characterization of Colored Dissolved Organic Matter Using High-Energy Laser Fragmentation. *Environ. Sci. Technol.* 34, 3283–3290.

Borisover, M., Laor, Y., Parparov, A., Bukhanovsky, N., Lado, M., 2009. Spatial and seasonal patterns of fluorescent organic matter in Lake Kinneret (Sea of Galilee) and its catchment basin. *Water Res.* 43, 3104–3116.

Bormann, F.H., Likens, G.E., 1967. Nutrient Cycling. *Science* 155, 424–429.

Boyd, T.J., Osburn, C.L., 2004. Changes in CDOM fluorescence from allochthonous and autochthonous sources during tidal mixing and bacterial degradation in two coastal estuaries. *Mar. Chem.* 89, 189–210.

Bro, R., 1997. PARAFAC. Tutorial and applications. *Chemom. Intell. Lab. Syst.* 38, 149–171.

Bro, R., 1999. Exploratory study of sugar production using fluorescence spectroscopy and multi-way analysis. *Chemom. Intell. Lab. Syst.* 46, 133–147.

Brooks, M.L., McKnight, D.M., Clements, W.H., 2007. Photochemical control of copper complexation by dissolved organic matter in Rocky Mountain streams, Colorado. *Limnol. Oceanogr.* 52, 766–779.

Burdige, D.J., 2001. Dissolved organic matter in Chesapeake Bay sediment pore waters. *Org. Geochem.* 32, 487–505.

Burdige, D.J., 2005. Burial of terrestrial organic matter in marine sediments: A re-assessment. *Glob. Biogeochem. Cycles* 19, GB4011.

Burdige, D.J., Kline, S.W., Chen, W., 2004. Fluorescent dissolved organic matter in marine sediment pore waters. *Mar. Chem.* 89, 289–311.

Cammack, W.L., Kalff, J., Prairie, Y.T., Smith, E.M., 2004. Fluorescent dissolved organic matter in lakes: relationships with heterotrophic metabolism. *Limnol. Oceanogr.* 49, 2034–2045.

Carstea, E.M., Baker, A., Pavelescu, G., Boomer, I., 2009. Continuous fluorescence assessment of organic matter variability on the Bournbrook River, Birmingham, UK. *Hydrol. Process.* 23, 1937–1946.

Cawley, K.M., Butler, K.D., Aiken, G.R., Larsen, L.G., Huntington, T.G., McKnight, D.M., 2012. Identifying fluorescent pulp mill effluent in the Gulf of Maine and its watershed. *Mar. Pollut. Bull.* 64, 1678–1687.

Chari, N.V.H.K., Sarma, N.S., Pandi, S.R., Murthy, K.N., 2012. Seasonal and spatial constraints of fluorophores in the midwestern Bay of Bengal by PARAFAC analysis of excitation emission matrix spectra. *Estuar. Coast. Shelf Sci.* 100, 162–171.

Chen, G.; Lin, C.; Chen, L.; Yang, H., 2010. Effect of size-fractionation dissolved organic matter on the mobility of prometryne in soil. *Chemosphere* 79, 1046-1055.

Chen, H., Kenny, J.E., 2007. A study of pH effects on humic substances using chemometric analysis of excitation-emission matrices. *Ann. Environ. Sci.* 1,1-9.

Chen, H., Zheng, B., Song, Y., Qin, Y., 2011. Correlation between molecular absorption spectral slope ratios and fluorescence humification indices in characterizing CDOM. *Aquat. Sci.* 73, 103–112.

Chen, H., Zheng, B., Zhang, L., 2013. Linking fluorescence spectroscopy to diffuse soil source for dissolved humic substances in the Daning River, China. Environ. *Sci. Process. Impacts* 15, 485–493.

Chen, J., Gu, B., LeBoeuf, E.J., Pan, H., Dai, S., 2002. Spectroscopic characterization of the structural and functional properties of natural organic matter fractions. *Chemosphere* 48, 59–68.

Chen, M., Price, R.M., Yamashita, Y., Jaffé, R., 2010. Comparative study of dissolved organic matter from groundwater and surface water in the Florida coastal Everglades using multi-dimensional spectrofluorometry combined with multivariate statistics. *Appl. Geochem.* 25, 872–880.

Chen, Y., Senesi, N., Schnitzer, M., 1977. Information Provided on Humic Substances by E4/E6 Ratios. *Soil Sci. Soc. Am. J.* 41, 352-358.

Chin, Y.-P.; Aiken, G. R.; Danielsen, K. M., 1997. Binding of pyrene to aquatic and commercial humic substances: The role of molecular weight and aromaticity. *Environ. Sci. Technol.* 31, 1630-1635.

Chin, Y.-P., Aiken, G., O'Loughlin, E., 1994. Molecular Weight, Polydispersity, and Spectroscopic Properties of Aquatic Humic Substances. *Environ. Sci. Technol.* 28, 1853–1858.

Chin, Y.-P., Traina, S.J., Swank, C.R., Backhus, D., 1998. Abundance and properties of dissolved organic matter in pore waters of a freshwater wetland. *Limnol. Oceanogr.* 43, 1287–1296.

Chow, A.T., Dai, J., Conner, W.H., Hitchcock, D.R., Wang, J.-J., 2013. Dissolved organic matter and nutrient dynamics of a coastal freshwater forested wetland in Winyah Bay, South Carolina. *Biogeochemistry* 112, 571–587.

Coble, P.G., 1996. Characterization of marine and terrestrial DOM in seawater using excitation-emission matrix spectroscopy. *Mar. Chem.* 51, 325–346.

Coble, P.G., 2007. Marine Optical Biogeochemistry: The Chemistry of Ocean Color. *Chem. Rev.* 107, 402–418.

Coble, P.G., Del Castillo, C.E., Avril, B., 1998. Distribution and optical properties of CDOM in the Arabian Sea during the 1995 Southwest Moonsoon. *Deep Sea Res. II* 45, 2195-2223.

Coble, P.G., Green, S.A., Blough, N.V., Gagosian, R.B., 1990. Characterization of dissolved organic matter in the Black Sea by fluorescence spectroscopy. *Nature* 348, 432–435.

Conmy, R., 2008. Temporal and spatial patterns in optical properties of colored dissolved organic matter on florida's gulf coast: Shelf to stream to aquifer. *Thesis*: University of South Florida.

Conmy, R.N., Coble, P.G., Castillo, C.E.D., 2004. Calibration and performance of a new in situ multi-channel fluorometer for measurement of colored dissolved organic matter in the ocean. *Cont. Shelf Res.* 24, 431–442.

Cory, R.M., Green, S.A., Pregitzer, K.S., 2004. Dissolved Organic Matter concentration and composition in the forests and streams of Olympic National Park, WA. *Biogeochemistry* 67, 269–288.

Cory, R.M., McKnight, D.M., 2005. Fluorescence Spectroscopy Reveals Ubiquitous Presence of Oxidized and Reduced Quinones in Dissolved Organic Matter. *Environ. Sci. Technol.* 39, 8142–8149.

Cory, R.M., McKnight, D.M., Chin, Y.-P., Miller, P., Jaros, C.L., 2007. Chemical characteristics of fulvic acids from Arctic surface waters: Microbial contributions and photochemical transformations. *J. Geophys. Res. Biogeosciences* 112, G04S51.

Cowie, G.L., Hedges, J.I., 1984. Carbohydrate sources in a coastal marine environment. Geochim. *Cosmochim. Acta* 48, 2075–2087.

Cowie, G.L., Hedges, J.I., 1992. Sources and reactivities of amino acids in a coastal marine environment. *Limnol. Oceanogr.* 37, 703–724.

Croué, J.-P., 2004. Isolation of Humic and Non-Humic NOM Fractions: Structural Characterization. *Environ. Monit. Assess.* 92, 193–207.

Cuss, C. W. and Guéguen, C., 2012. Determination of relative molecular weights of fluorescent components in dissolved organic matter using asymmetrical flow field-flow fractionation and parallel factor analysis. *Anal. Chim. Acta* 733, 98–102.

Cuss, C.W., Guéguen, C., 2013. Distinguishing dissolved organic matter at its origin: Size and optical properties of leaf-litter leachates. *Chemosphere* 92, 1483–1489.

Dalzell, B.J., Minor, E.C., Mopper, K.M., 2009. Photodegradation of estuarine dissolved organic matter: a multi-method assessment of DOM transformation. *Org. Geochem.* 40, 243–257.

De Haan, H., De Boer, T., 1987. Applicability of light absorbance and fluorescence as measures of concentration and molecular size of dissolved organic carbon in humic Lake Tjeukemeer. *Water Res.* 21, 731–734.

De Souza Sierra, M.M., Donard, O.F.X., Lamotte, M., Belin, C., Ewald, M., 1994. Fluorescence spectroscopy of coastal and marine waters. *Mar. Chem.* 47, 127–144.

Determann, S., Lobbes, J.M., Reuter, R., Rullkötter, J., 1998. Ultraviolet fluorescence excitation and emission spectroscopy of marine algae and bacteria. *Mar. Chem.* 62, 137–156.

Determann, S., Reuter, R., Wagner, P., Willkomm, R., 1994. Fluorescent matter in the eastern Atlantic Ocean. Part 1: method of measurement and near-surface distribution. *Deep Sea Res. Part Oceanogr. Res. Pap.* 41, 659–675.

Determann, S., Reuter, R., Willkomm, R., 1996. Fluorescent matter in the eastern Atlantic Ocean. Part 2: vertical profiles and relation to water masses. *Deep Sea Res. Part Oceanogr. Res. Pap.* 43, 345–360.

Duan, S., Bianchi, T.S., 2007. Particulate and dissolved amino acids in the lower Mississippi and Pearl Rivers (USA). *Mar. Chem.* 107, 214–229.

Dubascoux, S., Von Der Kammer, F., Le Hécho, I., Gautier, M.P., Lespes, G., 2008. Optimisation of asymmetrical flow field flow fractionation for environmental nanoparticles separation. *J. Chromatogr. A* 1206, 160–165.

Dupouy, C., Neveux, J., Ouillon, S., Frouin, R., Murakami, H., Hochard, S., Dirberg, G., 2010. Inherent optical properties and satellite retrieval of chlorophyll concentration in the lagoon and open ocean waters of New Caledonia. *Mar. Pollut. Bull.* 61, 503–518.

Duursma, E.K., 1974. The fluorescence of dissolved organic matter in the sea, in: Jerlov, N.G., Nielsen, E.S. (Eds.), *Optical Aspects of Oceanography*, 237–256.

Duursma, E.K., Dawson, R., 1981. Marine organic chemistry: evolution, composition, interactions, and chemistry of organic matter in seawater. *Elsevier Oceanogr. Series*, 31 New York.

Edzwald, J.K., Tobiason, J.E., 1999. Enhanced coagulation: US requirements and a broader view. *Water Sci. Technol.* 40, 63–70.

Even, S., Billen, G., Bacq, N., Théry, S., Ruelland, D., Garnier, J., Cugier, P., Poulin, M., Blanc, S., Lamy, F., Paffoni, C., 2007. New tools for modelling water quality of hydrosystems: An application in the Seine River basin in the frame of the Water Framework Directive. *Sci. Total Environ.* 375, 274–291.

Ewald, M., Belin, C., Berger, P., Weber, J.H., 1983. Corrected fluorescence spectra of fulvic acids isolated from soil and water. *Environ. Sci. Technol.* 17, 501–504.

Fellman, J.B., D'Amore, D.V., Hood, E., 2008a. An evaluation of freezing as a preservation technique for analyzing dissolved organic C, N and P in surface water samples. *Sci. Total Environ.* 392, 305–312.

Fellman, J.B., D'Amore, D.V., Hood, E., Boone, R.D., 2008b. Fluorescence characteristics and biodegradability of dissolved organic matter in forest and wetland soils from coastal temperate watersheds in southeast Alaska. *Biogeochemistry* 88, 169–184.

Fellman, J.B., Hood, E., Spencer, R.G.M., 2010. Fluorescence spectroscopy opens new windows into dissolved organic matter dynamics in freshwater ecosystems: A review. *Limnol. Oceanogr.* 55, 2452–2462.

Fellman, J.B., Miller, M.P., Cory, R.M., D'Amore, D.V., White, D., 2009. Characterizing Dissolved Organic Matter Using PARAFAC Modeling of Fluorescence Spectroscopy: A Comparison of Two Models. *Environ. Sci. Technol.* 43, 6228–6234.

Fichot, C.G., Benner, R., 2011. A novel method to estimate DOC concentrations from CDOM absorption coefficients in coastal waters. *Geophys. Res. Lett.* 38,

Fichot, C.G., Benner, R., 2012. The spectral slope coefficient of chromophoric dissolved organic matter (S 275-295) as a tracer of terrigenous dissolved organic carbon in river-influenced ocean margins. *Limnol. Oceanogr.* 57, 1453–1466.

Franke, D., Hamilton, M.W., Ziegler, S.E., 2012. Variation in the photochemical lability of dissolved organic matter in a large boreal watershed. *Aquat. Sci.* 74, 751–768.

Fraunhofer, W., Winter, G., 2004. The use of asymmetrical flow field-flow fractionation in pharmaceutics and biopharmaceutics. *Eur. J. Pharm. Biopharm.* 58, 369–383.

Fu, P., Mostofa, K.M., Wu, F., Liu, C.-Q., Li, W., Liao, H., Wang, L., Wang, J., Mei, Y., 2010. Excitation-emission matrix characterization of dissolved organic matter sources in two eutrophic lakes (Southwestern China Plateau). *Geochem. J.* 44, 99-112.

Fu, P., Wu, F., Liu, C., Wang, F., Li, W., Yue, L., Guo, Q., 2007. Fluorescence characterization of dissolved organic matter in an urban river and its complexation with Hg(II). *Appl. Geochem.* 22, 1668–1679.

Giddings, J. C., Yang, F.J., Myers, M. N., 1977. Flow field-flow fractionation: new method for separating, purifying, and characterizing the diffusivity of viruses. *J. Virol.* 21, 131–8.

Gigault, J., Pettibone, J.M., Schmitt, C., Hackley, V.A., 2014. Rational strategy for characterization of nanoscale particles by asymmetric-flow field flow fractionation: A tutorial. *Anal. Chim. Acta* 809, 9-24.

Gimbert, L.J., Andrew, K.N., Haygarth, P.M., Worsfold, P.J., 2003. Environmental applications of flow field-flow fractionation (FIFFF). *TrAC Trends Anal. Chem.* 22, 615–633.

Gobler, C.J., Deonarine, S., Leigh-Bell, J., Gastrich, M.D., Anderson, O.R., Wilhelm, S.W., 2004. Ecology of phytoplankton communities dominated by Aureococcus anophagefferens: the role of viruses, nutrients, and microzooplankton grazing. *Harmful Algae* 3, 471–483.

Griffith, D.R., McNichol, A.P., Xu, L., McLaughlin, F.A., Macdonald, R.W., Brown, K.A., Eglinton, T.I., 2012. Carbon dynamics in the western Arctic Ocean: insights from full-depth carbon isotope profiles of DIC, DOC, and POC. *Biogeosciences* 9, 1217–1224.

Guéguen C., McLaughlin F.A., Carmack E.C., Itoh M., Narita H., Nishino S., 2012b. The nature of colored dissolved organic matter in the southern Canada Basin and East Siberian Sea. *Deep Sea Res. Part II* 81–84, 102–113.

Guéguen, C., Belin, C., Dominik, J., 2002. Organic colloid separation in contrasting aquatic environments with tangential flow filtration. *Water Res.* 36, 1677–1684.

Guéguen, C., Burns, D.C., McDonald, A., Ring, B., 2012a. Structural and optical characterization of dissolved organic matter from the lower Athabasca River, Canada. *Chemosphere* 87, 932–937.

Guéguen, C., Cuss, C.W., 2011. Characterization of aquatic dissolved organic matter by asymmetrical flow field-flow fractionation coupled to UV–Visible diode array and excitation emission matrix fluorescence. *J. Chromatogr. A* 1218, 4188–4198.

Guéguen, C., Gilbin, R., Pardos, M., Dominik, J., 2004. Water toxicity and metal contamination assessment of a polluted river: the Upper Vistula River (Poland). *Appl. Geochem.* 19, 153–162.

Guéguen, C., Granskog, M.A., McCullough, G., Barber, D.G., 2011. Characterisation of colored dissolved organic matter in Hudson Bay and Hudson Strait using parallel factor analysis. *J. Mar. Syst.* 88, 423–433.

Guggenberger, G., Zech, W., 1994. Composition and dynamics of dissolved carbohydrates and lignin-degradation products in two coniferous forests, N.E. Bavaria, Germany. *Soil Biol. Biochem.* 26, 19–27.

Guo, W., Xu, J., Wang, J., Wen, Y., Zhuo, J., Yan, Y., 2010. Characterization of dissolved organic matter in urban sewage using excitation emission matrix fluorescence spectroscopy and parallel factor analysis. *J. Environ. Sci.* 22, 1728–1734.

Guo, W., Yang, L., Hong, H., Stedmon, C.A., Wang, F., Xu, J., Xie, Y., 2011. Assessing the dynamics of chromophoric dissolved organic matter in a subtropical estuary using parallel factor analysis. *Mar. Chem.* 124, 125–133.

Guo, X., He, X., Zhang, H., Deng, Y., Chen, L., Jiang, J., 2012. Characterization of dissolved organic matter extracted from fermentation effluent of swine manure slurry using spectroscopic techniques and parallel factor analysis (PARAFAC). *Microchem. J.* 102, 115–122.

Hadri, H.E., Gigault, J., Chéry, P., Potin-Gautier, M., Lespes, G., 2013. Optimization of flow field-flow fractionation for the characterization of natural colloids. *Anal. Bioanal. Chem.* 1–11.

Hansell, D., 2001. Marine Dissolved Organic Matter and the Carbon Cycle. *Oceanography* 14, 41–49.

Hassellöv, M., 2005. Relative molar mass distributions of chromophoric colloidal organic matter in coastal seawater determined by Flow Field-Flow Fractionation with UV absorbance and fluorescence detection. *Mar. Chem.* 94, 111–123.

Hassellöv, M., der Kammer, F. von, Beckett, R., 2007. Characterisation of Aquatic Colloids and Macromolecules by Field-Flow Fractionation, in: Associateessor, K.J.W.P.D., Lecturer, J.R.L.P.D. postdoctoral research S. (Eds.), *Environmental Colloids and Particles*. John Wiley & Sons, Ltd, pp. 223–276.

Hassler, C.S., Schoemann, V., Nichols, C.M., Butler, E.C.V., Boyd, P.W., 2011. Saccharides enhance iron bioavailability to Southern Ocean phytoplankton. *Proc. Natl. Acad. Sci.* 108, 1076–1081.

Hedges, J.I., Cowie, G.L., Richey, J.E., Quay, P.D., Benner, R., Strom, M., Forsberg, B.R., 1994. Origins and processing of organic matter in the Amazon River as indicated by carbohydrates and amino acids. *Limnol. Oceanogr.* 39, 743–761.

Helms, J.R., Stubbins, A., Ritchie, J.D., Minor, E.C., Kieber, D.J., Mopper, K., 2008. Absorption spectral slopes and slope ratios as indicators of molecular weight, source, and photobleaching of chromophoric dissolved organic matter. *Limnol. Oceanogr.* 53, 955-969.

Henderson, R.K., Baker, A., Murphy, K.R., Hambly, A., Stuetz, R.M., Khan, S.J., 2009. Fluorescence as a potential monitoring tool for recycled water systems: A review. *Water Res.* 43, 863–881.

Henderson, R.K., Baker, A., Parsons, S.A., Jefferson, B., 2008. Characterisation of algogenic organic matter extracted from cyanobacteria, green algae and diatoms. *Water Res.* 42, 3435–3445.

Her, N., Amy, G., McKnight, D., Sohn, J., Yoon, Y., 2003. Characterization of DOM as a function of MW by fluorescence EEM and HPLC-SEC using UVA, DOC, and fluorescence detection. *Water Res.* 37, 4295–4303.

Hernes, P.J., 2003. Photochemical and microbial degradation of dissolved lignin phenols: Implications for the fate of terrigenous dissolved organic matter in marine environments. *J. Geophys. Res.* 108, 3291.

Hertkorn, N., Claus, H., Schmitt-Kopplin, P., Perdue, E.M., Filip, Z., 2002. Utilization and Transformation of Aquatic Humic Substances by Autochthonous Microorganisms. *Environ. Sci. Technol.* 36, 4334–4345.

Holbrook, R.D., Yen, J.H., Grizzard, T.J., 2006. Characterizing natural organic material from the Occoquan Watershed (Northern Virginia, US) using fluorescence spectroscopy and PARAFAC. *Sci. Total Environ.* 361, 249–266.

Hongve, D., Baann, J., Becher, G., Lømo, S., 1996. Characterization of humic substances by means of high-performance size exclusion chromatography. *Environ. Int.* 22, 489–494.

Hood, E., Gooseff, M.N., Johnson, S.L., 2006. Changes in the character of stream water dissolved organic carbon during flushing in three small watersheds, Oregon. *J. Geophys. Res. Biogeosciences* 111, G01007

Hood, E., Williams, M.W., McKnight, D.M., 2005. Sources of dissolved organic matter (DOM) in a Rocky Mountain stream using chemical fractionation and stable isotopes. *Biogeochemistry* 74, 231–255.

Hua, B., Veum, K., Yang, J., Jones, J., Deng, B., 2010. Parallel factor analysis of fluorescence EEM spectra to identify THM precursors in lake waters. *Environ. Monit. Assess.* 161, 71–81.

Huang, D.-Y., Peng, P., Xu, Y.-G., Sun, C.-X., Deng, H.-M., Deng, Y.-Y., 2010. Distribution, regional sources and deposition fluxes of organochlorine pesticides in precipitation in Guangzhou, South China. *Atmospheric Res.* 97, 115–123.

Hudson, N., Baker, A., Reynolds, D., 2007. Fluorescence analysis of dissolved organic matter in natural, waste and polluted waters—a review. *River Res. Appl.* 23, 631–649.

Huguet, A., 2007. Mise au point de procédés membranaires pour l'étude de la matière organique dissoute en milieux côtiers. *Thèse* no 3504: Université Bordeaux 1.

Huguet, A., Vacher, L., Relexans, S., Saubusse, S., Froidefond, J.M., Parlanti, E., 2009. Properties of fluorescent dissolved organic matter in the Gironde Estuary. *Org. Geochem.* 40, 706–719.

Huguet, A., Vacher, L., Saubusse, S., Etcheber, H., Abril, G., Relexans, S., Ibalot, F., Parlanti, E., 2010. New insights into the size distribution of fluorescent dissolved organic matter in estuarine waters. *Org. Geochem.* 41, 595–610.

Hur, J., Jung, N.-C., Shin, J.-K., 2007. Spectroscopic Distribution of Dissolved Organic Matter in a Dam Reservoir Impacted by Turbid Storm Runoff . *Environ. Monit. Assess.* 133, 53–67.

Ishii, S.K.L., Boyer, T.H., 2012. Behavior of Reoccurring PARAFAC Components in Fluorescent Dissolved Organic Matter in Natural and Engineered Systems: A Critical Review. *Environ. Sci. Technol.* 46, 2006–2017.

Ishiwatari, R., 1973. Chemical characterization of fractionated humic acids from lake and marine sediments. *Chem. Geol.* 12, 113–126.

Ittekkot, V., Zhang, S., 1989. Pattern of particulate nitrogen transport in world rivers. *Glob. Biogeochem. Cycles* 3, 383–391.

Jacobson, M.M.F., 2012. Biological and Photochemical Degradation of Dissolved Organic Carbon in Peatland Ecosystems. *Thesis*: University of Minnesota.

Jahnke, R.A., 1996. The global ocean flux of particulate organic carbon: Areal distribution and magnitude. *Glob. Biogeochem. Cycles* 10, 71–88.

Jiang, F., Lee, F.S.-C., Wang, X., Dai, D., 2008. The application of Excitation/Emission Matrix spectroscopy combined with multivariate analysis for the characterization and source identification of dissolved organic matter in seawater of Bohai Sea, China. *Mar. Chem.* 110, 109–119.

JiJi, R.D., Andersson, G.G., Booksh, K.S., 2000. Application of PARAFAC for calibration with excitation–emission matrix fluorescence spectra of three classes of environmental pollutants. *J. Chemom.* 14, 171–185.

Kalle, K., 1949. Fluoreszenz und Gelbstoff im Bottnischem und Finnishchen Meerbusen. *Dtsch Hydrogr Z* 2, 9–124.

Keller, D.P., Hood, R.R., 2011. Modeling the seasonal autochthonous sources of dissolved organic carbon and nitrogen in the upper Chesapeake Bay. *Ecol. Model.* 222, 1139–1162.

Kirkland, J.J., Dilks Jr., C.H., Rementer, S.W., Yau, W.W., 1992. Asymmetric-channel flow field-flow fractionation with exponential force-field programming. *J. Chromatogr. A* 593, 339–355.

Korshin, G.V., Li, C.-W., Benjamin, M.M., 1997. Monitoring the properties of natural organic matter through UV spectroscopy: A consistent theory. *Water Res.* 31, 1787–1795.

Kothawala, D.N., von Wachenfeldt, E., Koehler, B., Tranvik, L.J., 2012. Selective loss and preservation of lake water dissolved organic matter fluorescence during long-term dark incubations. *Sci. Total Environ.* 433, 238–246.

Koukal, B., Guéguen, C., Pardos, M., Dominik, J., 2003. Influence of humic substances on the toxic effects of cadmium and zinc to the green alga Pseudokirchneriella subcapitata. *Chemosphere* 53, 953–961.

Kowalczuk, P., Cooper, W.J., Durako, M.J., Kahn, A.E., Gonsior, M., Young, H., 2010. Characterization of dissolved organic matter fluorescence in the South Atlantic Bight with use of PARAFAC model: Relationships between fluorescence and its components, absorption coefficients and organic carbon concentrations. *Mar. Chem.* 118, 22–36.

Kowalczuk, P., Durako, M.J., Young, H., Kahn, A.E., Cooper, W.J., Gonsior, M., 2009. Characterization of dissolved organic matter fluorescence in the South Atlantic Bight with use of PARAFAC model: Interannual variability. *Mar. Chem.* 113, 182–196.

Kramer, J.B., Canonica, S., Hoigné, J., Kaschig, J., 1996. Degradation of Fluorescent Whitening Agents in Sunlit Natural Waters. *Environ. Sci. Technol.* 30, 2227–2234.

Kraus, T.E.C., Bergamaschi, B.A., Hernes, P.J., Spencer, R.G.M., Stepanauskas, R., Kendall, C., Losee, R.F., Fujii, R., 2008. Assessing the contribution of wetlands and subsided islands to dissolved organic matter and disinfection byproduct precursors in the Sacramento–San Joaquin River Delta: A geochemical approach. *Org. Geochem.* 39, 1302–1318.

Laane, R.W.P.M., Kramer, K.J.M., 1990. Natural fluorescence in the North Sea and its major estuaries. *Neth. J. Sea Res.* 26, 1–9.

Lam, B., Baer, A., Alaee, M., Lefebvre, B., Moser, A., Williams, A., Simpson, A.J., 2007. Major Structural Components in Freshwater Dissolved Organic Matter. *Environ. Sci. Technol.* 41, 8240–8247.

Lanxiu, Y., Fengchang, W., Congqiang, L., Wen, L., Jing, W., Yi, M., 2004. Molecular weight distribution of dissolved organic matter in Lake Hongfeng determined by high performance size exclusion chromatography (HPSEC) with on-line UV-vis absorbance and fluorescence detection. *Chin. J. Geochem.* 23, 275–283.

Lara, R.J., Rachold, V., Kattner, G., Hubberten, H.W., Guggenberger, G., Skoog, A., Thomas, D.N., 1998. Dissolved organic matter and nutrients in the Lena River, Siberian Arctic: Characteristics and distribution. *Mar. Chem.* 59, 301–309.

Lawrence, J., 1980. Semi-quantitative determination of fulvic acid, tannin and lignin in natural waters. *Water Res.* 14, 373–377.

Leeman, M., Wahlund, K.-G., Wittgren, B., 2006. Programmed cross flow asymmetrical flow field-flow fractionation for the size separation of pullulans and hydroxypropyl cellulose. *J. Chromatogr. A* 1134, 236–245.

Leenheer, J.A., 1981. Comprehensive approach to preparative isolation and fractionation of dissolved organic carbon from natural waters and wastewaters. *Environ. Sci. Technol.* 15, 578–587.

Leenheer, J.A., Croué, J.-P., 2003. Peer Reviewed: Characterizing Aquatic Dissolved Organic Matter. *Environ. Sci. Technol.* 37, 18A–26A.

Leenheer, J.A., Noyes, T.I., 1984. A filtration and column-adsorption system for onsite concentration and fractionation of organic substances from large volumes of water (No. WSP - 2230). *United States Geological Survey*.

Lenheer, J.A., Huffman, E.W.D., 1976. Classification of Organic Solutes in Water by Using Macroreticular Resin. *J R Stat Soc U. S.* 4:6.

Lepane, V., Leeben, A., Malashenko, O., 2004. Characterization of sediment pore-water dissolved organic matter of lakes by high-performance size exclusion chromatography. *Aquat. Sci.* 66, 185–194.

Lespes, G., Gigault, J., 2011. Hyphenated analytical techniques for multidimensional characterisation of submicron particles: A review. *Anal. Chim. Acta* 692, 26–41.

Lyvén, B., Hassellöv, M., Haraldsson, C., Turner, D.R., 1997. Optimisation of on-channel preconcentration in flow field-flow fractionation for the determination of size distributions of low molecular weight colloidal material in natural waters. *Anal. Chim. Acta* 357, 187–196.

Ma, X., Green, S.A., 2004. Photochemical Transformation of Dissolved Organic Carbon in Lake Superior—An In-situ Experiment. *J. Gt. Lakes Res.* 30, Supplement 1, 97–112.

Macko, S.A., Engel, M.H., Hartley, G., Hatcher, P., Helleur, R., Jackman, P., Silfer, J.A., 1991. Isotopic compositions of individual carbohydrates as indicators of early diagenesis of organic matter in peat. *Chem. Geol.* 93, 147–161.

Malcolm, R.L., 1985. Geochemistry of stream fulvic and humic substances, in: Aiken, G.R., Mcknight, D.M., Wershaw, R.L., MacCarthy, P. (Eds.), *Humic Substances in Soil, Sediment, and Water: Geochemistry, Isolation, and Characterization*. pp. 181–209.

Marhaba, T.F., Lippincott, R.L., 2000. Application of Fluorescence Technique for Rapid Identification of DOM Fractions in Source Waters. *J. Environ. Eng.* 126, 1039–1044.

Marhaba, T.F., Van, D., Lippincott, R.L., 2000. Rapid identification of dissolved organic matter fractions in water by spectral fluorescent signatures. *Water Res.* 34, 3543–3550.

Matar, Z., 2012. Influence de la matière organique dissoute d'origine urbaine sur la spéciation et la biodisponibilité des métaux dans les milieux récepteurs anthropisés. *Thèse* no 00806323: Université Paris-Est.

Matilainen, A., 2007. Removal of the Natural Organic Matter in the Different Stages of the Drinking Water Treatment Process. *Thesis* no 651: Tampere University of Technology.

Matilainen, A., Gjessing, E.T., Lahtinen, T., Hed, L., Bhatnagar, A., Sillanpää, M., 2011. An overview of the methods used in the characterisation of natural organic matter (NOM) in relation to drinking water treatment. *Chemosphere* 83, 1431–1442.

Mayer, L.M., Schick, L.L., Skorko, K., Boss, E., 2006. Photodissolution of particulate organic matter from sediments. *Limnol. Oceanogr.* 51, 1064–1071.

McKnight, D., Thurman, E.M., Wershaw, R.L., Hemond, H., 1985. Biogeochemistry of Aquatic Humic Substances in Thoreau's Bog, Concord, Massachusetts. *Ecology* 66, 1339.

McKnight, D.M., Aiken, G.R., 1998. Sources and Age of Aquatic Humus, in: Hessen, P.D.D.O., Tranvik, D.L.J. (Eds.), *Aquatic Humic Substances, Ecological Studies*. Springer Berlin Heidelberg, pp. 9–39.

McKnight, D.M., Alger, A.S., Tate, C.M., Shupe, G., Spaulding, S., 1998. Longitudinal patterns in algal abundance and species distribution in meltwater streams in Taylor Valley, southern Victoria Land, Antarctica, in Ecosystem Processes in a Polar Desert, Antarct. *Res. Ser.,* vol. 72, edited J. Priscu, pp. 109 – 127.

McKnight, D.M., Andrews, E.D., Spaulding, S.A., Aiken, G.R., 1994. Aquatic fulvic acids in algal-rich Antarctic ponds. *Limnol Ocean.* 39, 1972–1979.

McKnight, D.M., Boyer, E.W., Westerhoff, P.K., Doran, P.T., Kulbe, T., Andersen, D.T., 2001. Spectrofluorometric characterization of dissolved organic matter for indication of precursor organic material and aromaticity. *Limnol. Oceanogr.* 46, 38–48.

Meng, F., Huang, G., Yang, X., Li, Z., Li, J., Cao, J., Wang, Z., Sun, L., 2013. Identifying the sources and fate of anthropogenically impacted dissolved organic matter (DOM) in urbanized rivers. *Water Res.* 47, 5027–5039.

Messaud, F.A., Sanderson, R.D., Runyon, J.R., Otte, T., Pasch, H., Williams, S.K.R., 2009. An overview on field-flow fractionation techniques and their applications in the separation and characterization of polymers. *Prog. Polym. Sci.* 34, 351–368.

Miller, M.P., McKnight, D.M., Chapra, S.C., 2009. Production of microbially-derived fulvic acid from photolysis of quinone-containing extracellular products of phytoplankton. *Aquat. Sci.* 71, 170–178.

Minero, C., Lauri, V., Falletti, G., Maurino, V., Pelizzetti, E., Vione, D., 2007. Spectrophotometric characterisation of surface lakewater samples: implications for the quantification of nitrate and the properties of dissolved organic matter. *Ann. Chim.* 97, 1107–1116.

Minor, E.C., Swenson, M.M., Mattson, B.M. and Oyler, A.R., 2014. Structural characterization of dissolved organic matter: a review of current techniques for isolation and analysis. *Environ. Sci.: Processes Impacts* 16, 2064-2079.

Moberg, L., Robertsson, G., Karlberg, B., 2001. Spectrofluorimetric determination of chlorophylls and pheopigments using parallel factor analysis. *Talanta* 54, 161–170.

Moon, J., Kim, S.-H., Cho, J., 2006. Characterizations of natural organic matter as nano particle using flow field-flow fractionation. *Colloids Surf. Physicochem. Eng. Asp.* 287, 232–236.

Moran, M.A., Sheldon, W.M., Zepp, R.G., 2000. Carbon loss and optical property changes during long-term photochemical and biological degradation of estuarine dissolved organic matter. *Limnol. Oceanogr.* 45, 1254–1264.

Morvan, X., Mouvet, C., Baran, N., Gutierrez, A., 2006. Pesticides in the groundwater of a spring draining a sandy aquifer: Temporal variability of concentrations and fluxes. J. Contam. *Hydrol.* 87, 176–190.

Mostofa, K.M., Wu, F., Liu, C.-Q., Fang, W.L., Yuan, J., Ying, W.L., Wen, L., Yi, M., 2010. Characterization of Nanming River (southwestern China) sewerage-impacted pollution using an excitation-emission matrix and PARAFAC. *Limnology* 11, 217–231.

Mostofa, K.M.G., Liu, C., Mottaleb, M.A., Wan, G., Ogawa, H., Vione, D., Yoshioka, T., Wu, F., 2013. Dissolved Organic Matter in Natural Waters, in: Mostofa, K.M.G., Yoshioka, T., Mottaleb, A., Vione, D. (Eds.), *Photobiogeochemistry of Organic Matter, Environmental Science and Engineering*. Springer Berlin Heidelberg, pp. 1–137.

Mostofa, K.M.G., Liu, C.-Q., Vione, D., Gao, K., Ogawa, H., 2013. Sources, factors, mechanisms and possible solutions to pollutants in marine ecosystems. *Environ. Pollut.* 182, 461–478.

Mostofa, K.M.G., Wu, F., Liu, C.-Q., Fang, W.L., Yuan, J., Ying, W.L., Wen, L., Yi, M., 2009. Characterization of Nanming River (southwestern China) sewerage-impacted pollution using an excitation-emission matrix and PARAFAC. *Limnology* 11, 217–231.

Mostofa, K.M.G., Yoshioka, T., Konohira, E., Tanoue, E., 2007. Dynamics and Characteristics of Fluorescent Dissolved Organic Matter in the Groundwater, River and Lake Water. *Water. Air. Soil Pollut.* 184, 157–176.

Mounier, S., Patel, N., Quilici, L., Benaim, J.Y., Benamou, C., 1999. Fluorescence 3D de la matière organique dissoute du fleuve amazone: (Three-dimensional fluorescence of the dissolved organic carbon in the Amazon river). *Water Res.* 33, 1523–1533.

Münster, U., 1999. Amino acid profiling in natural organic matter isolated by reverse osmosis from eight different boreal freshwaters. *Environ. Int.* 25, 209–224.

Münster, U., Chróst, R.J., 1990. Origin, Composition, and Microbial Utilization of Dissolved Organic Matter, in: Overbeck, J., Chróst, R.J. (Eds.), *Aquatic Microbial Ecology, Brock/Springer Series in Contemporary Bioscience*. Springer New York, pp. 8–46.

Murphy, K.R., Stedmon, C.A., Waite, T.D., Ruiz, G.M., 2008. Distinguishing between terrestrial and autochthonous organic matter sources in marine environments using fluorescence spectroscopy. *Mar. Chem.* 108, 40–58.

Nebbioso, A., Piccolo, A., 2013. Molecular characterization of dissolved organic matter (DOM): a critical review. *Anal. Bioanal. Chem.* 405, 109–124.

Ngo, M.T., Geckeis, H., Kim, J.., Beck, H.., 2001. Application of the flow field flow fractionation (FFFF) to the characterization of aquatic humic colloids: evaluation and optimization of the method. Colloids Surf. *Physicochem. Eng. Asp.* 181, 289–301.

Nieke, B., Reuter, R., Heuermann, R., Wang, H., Babin, M., Therriault, J.C., 1997. Light absorption and fluorescence properties of chromophoric dissolved organic matter (CDOM), in the St. Lawrence Estuary (Case 2 waters). *Cont. Shelf Res.* 17, 235–252.

Nilsson, L., 2013. Separation and characterization of food macromolecules using field-flow fractionation: A review. *Food Hydrocoll.* 30, 1–11.

Owen, D.M., Amy, G.L., Chowdhury, Z.K., Rajendra, P., Mccoy, G., Viscosil, K., 1995. NOM : characterization and treatability : Natural organic matter. *J. - Am. Water Works Assoc.* 87, 46–63.

Pakulski, J.D., Benner, R., 1994. Abundance and distribution of carbohydrates in the ocean. *Limnol. Oceanogr.* 930–940.

Parinos, C., Gogou, A., Bouloubassi, I., Stavrakakis, S., Plakidi, E., Hatzianestis, I., 2013. Sources and downward fluxes of polycyclic aromatic hydrocarbons in the open southwestern Black Sea. *Org. Geochem.* 57, 65–75.

Parlanti, E., Wörz, K., Geoffroy, L., Lamotte, M., 2000. Dissolved organic matter fluorescence spectroscopy as a tool to estimate biological activity in a coastal zone submitted to anthropogenic inputs. *Org. Geochem.* 31, 1765–1781.

Penru, Y., Simon, F.X., Guastalli, A.R., Esplugas, S., Llorens, J., Baig, S., 2013. Characterization of natural organic matter from Mediterranean coastal seawater. *J. Water Supply Res. Technol.* 62, 42.

Perminova, I.V., Frimmel, F.H., Kudryavtsev, A.V., Kulikova, N.A., Abbt-Braun, G., Hesse S., Petrosyant, VS., 2003. Molecular weight characteristics of humic substances from different environments as determined by size exclusion chromatography and their statistical evaluation. *Environ Sci Technol* 37, 2477-2485.

Pete, R., Davidson, K., Hart, M.C., Gutierrez, T., Miller, A.E.J., 2010. Diatom derived dissolved organic matter as a driver of bacterial productivity: The role of nutrient limitation. *J. Exp. Mar. Biol. Ecol.* 391, 20–26.

Peuravuori, J., 1992. Isolation, Fractionation and Characterization of Aquatic Humic Substances: Does a Distinct Humic Molecule Exist. *Thesis*: University of Turku.

Peuravuori, J., Pihlaja, K., 1997. Molecular size distribution and spectroscopic properties of aquatic humic substances. *Anal. Chim. Acta* 337, 133–149.

Piccolo, A., 2001. The supramolecular structure of humic substances. *Soil Sicence* 166, 810-832.

Pifer, A.D., Fairey, J.L., 2012. Improving on SUVA254 using fluorescence-PARAFAC analysis and asymmetric flow-field flow fractionation for assessing disinfection byproduct formation and control. *Water Res.* 46, 2927–2936.

Pifer, A.D., Miskin, D.R., Cousins, S.L., Fairey, J.L., 2011. Coupling asymmetric flow-field flow fractionation and fluorescence parallel factor analysis reveals stratification of dissolved organic matter in a drinking water reservoir. *J. Chromatogr. A* 1218, 4167–4178.

Pitkänen, L., Sontag-Strohm, T., Kanerva, P., n.d. Enhanced separation and characterization of gluten polymers by asymmetrical flow field-flow fractionation coupled with multiple detectors. *J. Cereal Sci.* 59, 126-131

Puddu, A., Zoppini, A., Fazi, S., Rosati, M., Amalfitano, S., Magaletti, E., 2003. Bacterial uptake of DOM released from P-limited phytoplankton. *FEMS Microbiol. Ecol.* 46, 257–268.

Qureshi, R.N., Kok, W.T., 2011. Application of flow field-flow fractionation for the characterization of macromolecules of biological interest: a review. *Anal. Bioanal. Chem.* 399, 1401–1411.

Rawn, D.F.., Lockhart, W.L., Wilkinson, P., Savoie, D.A., Rosenberg, G.B., Muir, D.C.., 2001. Historical contamination of Yukon Lake sediments by PCBs and organochlorine pesticides: influence of local sources and watershed characteristics. *Sci. Total Environ.* 280, 17–37.

Reid, M.K., Spencer, K.L., 2009. Use of principal components analysis (PCA) on estuarine

sediment datasets: The effect of data pre-treatment. *Environ. Pollut.* 157, 2275–2281.

Repeta, D.J., Quan, T.M., Aluwihare, L.I., Accardi, A., 2002. Chemical characterization of high molecular weight dissolved organic matter in fresh and marine waters. *Geochim. Cosmochim. Acta* 66, 955–962.

Reszat, T.N., Hendry, M.J., 2005. Characterizing Dissolved Organic Carbon Using Asymmetrical Flow Field-Flow Fractionation with On-Line UV and DOC Detection. *Anal. Chem.* 77, 4194–4200.

Rochelle-Newall, E.., Fisher, T.., 2002. Chromophoric dissolved organic matter and dissolved organic carbon in Chesapeake Bay. *Mar. Chem.* 77, 23–41.

Rochelle-Newall, E.J., Chu, V.T., Pringault, O., Amouroux, D., Arfi, R., Bettarel, Y., Bouvier, T., Bouvier, C., Got, P., Nguyen, T.M.H., Mari, X., Navarro, P., Duong, T.N., Cao, T.T.T., Pham, T.T., Ouillon, S., Torréton, J.-P., 2011. Phytoplankton distribution and productivity in a highly turbid, tropical coastal system (Bach Dang Estuary, Vietnam). *Mar. Pollut. Bull.* 62, 2317–2329.

Romankevich, D.E.A., 1984. Carbohydrates, in: *Geochemistry of Organic Matter in the Ocean*. Springer Berlin Heidelberg, pp. 199–231.

Rosario-Ortiz, F.L., Snyder, S.A., Suffet, I.H. (Mel), 2007. Characterization of dissolved organic matter in drinking water sources impacted by multiple tributaries. *Water Res.* 41, 4115–4128.

Rottgers, R. and Koch, B.P., 2012. Spectroscopic detection of a ubiquitous dissolved pigment degradation product in subsurface waters of the global ocean. *Biogeosciences* 9, 2585–2596.

Sanchez N. P., Skeriotis A. T., Miller C. M., 2013. Assessment of dissolved organic matter fluorescence PARAFAC components before and after coagulationefiltration in a full scale water treatment plant. *Water Research* 47, 11679-1690.

Schäfer, A.I., Mauch, R., Waite, T.D., Fane, A.G., 2002. Charge Effects in the Fractionation of Natural Organics Using Ultrafiltration. *Environ. Sci. Technol.* 36, 2572–2580.

Schimpf, M.E., Caldwell, K., Giddings, J.C., 2000. Field-Flow Fractionation Handbook. Wiley.

Schimpf, M.E., Wahlund, K.-G., 1997. Asymmetrical flow field-flow fractionation as a method to study the behavior of humic acids in solution. *J. Microcolumn Sep.* 9, 535–543.

Schlesinger, W.H., Melack, J.M., 1981. Transport of organic carbon in the world's rivers. *Tellus* 33, 172–187.

Schwede-Thomas, S.B., Chin, Y.-P., Dria, K.J., Hatcher, P., Kaiser, E., Sulzberger, B., 2005. Characterizing the properties of dissolved organic matter isolated by XAD and C-18 solid phase extraction and ultrafiltration. *Aquat. Sci.* 67, 61–71.

Semenov, V.M., Tulina, A.S., Semenova, N.A., Ivannikova, L.A., 2013. Humification and nonhumification pathways of the organic matter stabilization in soil: A review. *Eurasian Soil Sci.* 46, 355–368.

Senesi, N., 1990. Molecular and quantitative aspects of the chemistry of fulvic acid and its interactions with metal ions and organic chemicals. Part II: The fluorescence

spectroscopy approach. *Anal Chim Acta* 232, 77–106.

Senesi, N., Miano, T.M., Provenzano, M.R., Brunetti, G., 1989. Spectroscopic and compositional comparative characterization of I.H.S.S. reference and standard fulvic and humic acids of various origin. *Sci. Total Environ.* 81–82, 143–156.

Senior, W., Chevolot, L., 1991. Studies of dissolved carbohydrates (or carbohydrate-like substances) in an estuarine environment. Mar. Chem. 32, 19–35.

Sharma, R.V., Edwards, R.T., Beckett, R., 1993. Physical characterization and quantification of bacteria by sedimentation field-flow fractionation. *Appl. Environ. Microbiol.* 59, 1864–1875.

Shon, H.-K., Kim, S.-H., Erdei, L., Vigneswaran, S., 2006. Analytical methods of size distribution for organic matter in water and wastewater. *Korean J. Chem. Eng.* 23, 581–591.

Sierra, M.M.D., Giovanela, M., Parlanti, E., Soriano-Sierra, E.J., 2005. Fluorescence fingerprint of fulvic and humic acids from varied origins as viewed by single-scan and excitation/emission matrix techniques. *Chemosphere* 58, 715–733.

Singh, S., D'Sa, E., Swenson, E., 2010a. Seasonal variability in CDOM absorption and fluorescence properties in the Barataria Basin, Louisiana, USA. *J. Environ. Sci.* 22, 1481–1490.

Singh, S., D'Sa, E.J., Swenson, E.M., 2010b. Chromophoric dissolved organic matter (CDOM) variability in Barataria Basin using excitation–emission matrix (EEM) fluorescence and parallel factor analysis (PARAFAC). *Sci. Total Environ.* 408, 3211–3222.

Søndergaard, M., Thomas, D.N., 2004. Dissolved organic matter (DOM) in aquatic ecosystems: a study of European catchments and coastal waters. *EU Domaine project* (EVK3-CT-2000-00034).

Spencer, R.G.M., Aiken, G.R., Butler, K.D., Dornblaser, M.M., Striegl, R.G., Hernes, P.J., 2009. Utilizing chromophoric dissolved organic matter measurements to derive export and reactivity of dissolved organic carbon exported to the Arctic Ocean: A case study of the Yukon River, Alaska. *Geophys. Res. Lett.* 36, L06401.

Spencer, R.G.M., Bolton, L., Baker, A., 2007. Freeze/thaw and pH effects on freshwater dissolved organic matter fluorescence and absorbance properties from a number of UK locations. *Water Res.* 41, 2941–2950.

Stedmon, C.A., Bro, R., 2008. Characterizing dissolved organic matter fluorescence with parallel factor analysis: a tutorial. *Limnol. Oceanogr.* 6, 572–579.

Stedmon, C.A., Markager, S., 2005a. Resolving the variability in dissolved organic matter fluorescence in a temperate estuary and its catchment using PARAFAC analysis. *Limnol. Oceanogr.* 50, 686–697.

Stedmon, C.A., Markager, S., 2005b. Tracing the production and degradation of autochthonous fractions of dissolved organic matter by fluorescence analysis. *Limnol. Oceanogr.* 50, 1415-1426.

Stedmon, C.A., Markager, S., Bro, R., 2003. Tracing dissolved organic matter in aquatic environments using a new approach to fluorescence spectroscopy. *Mar. Chem.* 82, 239–

254.

Stedmon, C.A., Markager, S., Tranvik, L., Kronberg, L., Slätis, T., Martinsen, W., 2007a. Photochemical production of ammonium and transformation of dissolved organic matter in the Baltic Sea. *Mar. Chem.* 104, 227–240.

Stedmon, C.A., Seredyńska-Sobecka, B., Boe-Hansen, R., Le Tallec, N., Waul, C.K., Arvin, E., 2011. A potential approach for monitoring drinking water quality from groundwater systems using organic matter fluorescence as an early warning for contamination events. *Water Res.* 45, 6030–6038.

Stedmon, C.A., Thomas, D.N., Granskog, M., Kaartokallio, H., Papadimitriou, S., Kuosa, H., 2007b. Characteristics of dissolved organic matter in Baltic coastal sea ice: allochthonous or autochthonous origins? *Environ. Sci. Technol.* 41, 7273–7279.

Stolpe, B., Guo, L., Shiller, A.M., Aiken, G.R., 2013. Abundance, size distributions and trace-element binding of organic and iron-rich nanocolloids in Alaskan rivers, as revealed by field-flow fractionation and ICP-MS. *Geochim. Cosmochim. Acta* 105, 221–239.

Stolpe, B., Guo, L., Shiller, A.M., Hassellöv, M., 2010. Size and composition of colloidal organic matter and trace elements in the Mississippi River, Pearl River and the northern Gulf of Mexico, as characterized by flow field-flow fractionation. *Mar. Chem.* 118, 119–128.

Summers, R.S., Cornel, P.K., Roberts, P.V., 1987. Molecular size distribution and spectroscopic characterization of humic substances. *Sci. Total Environ.* 62, 27–37.

Sun, H.; Song, Q.; Luo, P.; Wu, W.; Wu, J., 2013. Sorption of phenanthrene on single-walled carbon nanotubes modified by DOM: effects of DOM molecular weight and contact time. *Env. Sci. Process. Impacts* 15, 307-314.

Sutton, R., Sposito, G., 2005. Molecular Structure in Soil Humic Substances: The New View. *Environ. Sci. Technol.* 39, 9009–9015.

Swietlik, J., Sikorska, E., 2006. Characterization of natural organic matter fractions by high pressure size-exclusion chromatography, specific UV absorbance and total luminescence spectroscopy. *Pol. J. Environ. Stud.* 15, 145-153.

Tadanier, C.J., Berry, D.F., Knocke, W.R., 2000. Dissolved Organic Matter Apparent Molecular Weight Distribution and Number-Average Apparent Molecular Weight by Batch Ultrafiltration. *Environ. Sci. Technol.* 34, 2348–2353.

Thomas, J.D., 1997. The role of dissolved organic matter, particularly free amino acids and humic substances, in freshwater ecosystems. *Freshw. Biol.* 38, 1–36.

Thomsen, M., Dobel, S., Lassen, P., Carlsen, L., Bügel Mogensen, B., Erik Hansen, P., 2002. Reverse quantitative structure–activity relationship for modelling the sorption of esfenvalerate to dissolved organic matter: A multivariate approach. *Chemosphere* 49, 1317–1325.

Thurman, E.M., 1985a. Aquatic Humic Substances, in: *Organic Geochemistry of Natural Waters, Developments in Biogeochemistry*. Springer Netherlands, pp. 273–361.

Thurman, E.M., 1985b. Amino Acids, in: *Organic Geochemistry of Natural Waters, Developments in Biogeochemistry*. Springer Netherlands, pp. 151–180.

Thurman, E.M., Malcolm, R.L., 1981. Preparative isolation of aquatic humic substances. *Environ. Sci. Technol.* 15, 463–466.

Twardowski, M.S., Boss, E., Sullivan, J.M., Donaghay, P.L., 2004. Modeling the spectral shape of absorption by chromophoric dissolved organic matter. *Mar. Chem.* 89, 69–88.

Vacher, L., 2004. Étude par fluorescence des propriétés de la matière organique dissoute dans les systèmes estuariens : cas des estuaires de la Gironde et de la Seine. *Thèse* no 2923: Université Bordeaux 1.

Vähätalo, A.V., Wetzel, R.G., 2004. Photochemical and microbial decomposition of chromophoric dissolved organic matter during long (months–years) exposures. *Mar. Chem.* 89, 313–326.

Valeur, B., 2001. Molecular Fluorescence: Principles and Applications. Wiley-VCH Verlag GmbH.

Varrault, G., Nguyen, P.T., Bonnot, C., Soares-Pereira, C., Guo, Y., Parot, J., Parlanti, E., Benedetti, M.F., Garnier, J., Derenne, S., Gelabert, A., Bressy, A., Boudahmane, L., Mercier, B., Martinez, A., Cordier, M.-A., Cordier, L., Anquetil, C., Tharaud, M., Saad, M., 2013. Caractérisation de la variabilité spatio-temporelle des qualités et des quantités de matière organique dans l'Oise, la Seine et la Marne. *Programme PIREN-Seine – Phase 6 – Rapport 2013*. http://www.sisyphe.upmc.fr/piren/?q=webfm_send/1300

Vidon, P., Wagner, L.E., Soyeux, E., 2008. Changes in the character of DOC in streams during storms in two Midwestern watersheds with contrasting land uses. *Biogeochemistry* 88, 257–270.

Voelker, B.M., Sulzberger, B., 1996. Effects of Fulvic Acid on Fe(II) Oxidation by Hydrogen Peroxide. *Environ. Sci. Technol.* 30, 1106–1114.

Wada, S., Aoki, M.N., Tsuchiya, Y., Sato, T., Shinagawa, H., Hama, T., 2007. Quantitative and qualitative analyses of dissolved organic matter released from Ecklonia cava Kjellman, in Oura Bay, Shimoda, Izu Peninsula, Japan. *J. Exp. Mar. Biol. Ecol.* 349, 344–358.

Wahlund, K.-G., 2013. Flow field-flow fractionation: Critical overview. *J. Chromatogr. A* 1287, 97–112.

Wang, S., Mulligan, C.N., 2006. Effect of natural organic matter on arsenic release from soils and sediments into groundwater. *Environ. Geochem. Health* 28, 197–214.

Wang, X.-C., Litz, L., Chen, R.F., Huang, W., Feng, P., Altabet, M.A., 2007. Release of dissolved organic matter during oxic and anoxic decomposition of salt marsh cordgrass. *Mar. Chem.* 105, 309–321.

Webster, R., 2001. Statistiques pour soutenir la recherche du sol et leur présentation. *Eur. J. Soil Sci.* 52, 331–340.

Weishaar, J.L., Aiken, G.R., Bergamaschi, B.A., Fram, M.S., Fujii, R., Mopper, K., 2003. Evaluation of Specific Ultraviolet Absorbance as an Indicator of the Chemical Composition and Reactivity of Dissolved Organic Carbon. *Environ. Sci. Technol.* 37, 4702–4708.

Wells, M.L., 2004. The colloidal size spectrum of CDOM in the coastal region of the

Mississippi Plume using flow field-flow fractionation. *Mar. Chem.* 89, 89–102.

Westerhoff, P., Aiken, G., Amy, G., Debroux, J., 1999. Relationships between the structure of natural organic matter and its reactivity towards molecular ozone and hydroxyl radicals. *Water Res.* 33, 2265–2276.

Westerhoff, P., Chen, W., Esparza, M., 2001. Fluorescence analysis of a standard fulvic acid and tertiary treated wastewater. *J. Environ. Qual.* 30, 2037–2046.

Williams, S.K.R., Benincasa, M.-A., 2006. Field Flow Fractionation in Analysis of Polymers and Rubbers, in: Meyers, R.A. (Ed.), *Encyclopedia of Analytical Chemistry*. John Wiley & Sons, Ltd, Chichester, UK.

Worms, I.A.M., Al-Gorani Szigeti, Z., Dubascoux, S., Lespes, G., Traber, J., Sigg, L., Slaveykova, V.I., 2010. Colloidal organic matter from wastewater treatment plant effluents: Characterization and role in metal distribution. *Water Res.* 44, 340–350.

Wu, F.C., Cai, Y., Evans, D., Dillon, P., 2004a. Complexation between Hg(II) and dissolved organic matter in stream waters: an application of fluorescence spectroscopy. *Biogeochemistry* 71, 339–351.

Wu, F.C., Evans, D., Dillon, P., Schiff, S., 2004b. Molecular size distribution characteristics of the metal–DOM complexes in stream waters by high-performance size-exclusion chromatography (HPSEC) and high-resolution inductively coupled plasma mass spectrometry (ICP-MS). *J. Anal. At. Spectrom.* 19, 979–983.

Wu, F.C., Mills, R.B., Evans, R.D., Dillon, P.J., 2004. Kinetics of Metal−Fulvic Acid Complexation Using a Stopped-Flow Technique and Three-Dimensional Excitation Emission Fluorescence Spectrophotometer. *Anal. Chem.* 76, 110–113.

Wu, F.C., Tanoue, E., 2002. Tryptophan in the sediments of lakes from Southwestern China Plateau. *Chem. Geol.* 184, 139–149.

Wu, J., Zhang, H., He, P.-J., Shao, L.-M., 2011. Insight into the heavy metal binding potential of dissolved organic matter in MSW leachate using EEM quenching combined with PARAFAC analysis. *Water Res.* 45, 1711–1719.

Wyatt, P.J., 1993. Light scattering and the absolute characterization of macromolecules. *Anal. Chim. Acta* 272, 1–40.

Yamaji, N., Hayakawa, K., Takada, H., 2010. Role of Photodegradation in the Fate of Fluorescent Whitening Agents (FWAs) in Lacustrine Environments. *Environ. Sci. Technol.* 44, 7796–7801.

Yamashita, Y., Cory, R.M., Nishioka, J., Kuma, K., Tanoue, E., Jaffé, R., 2010. Fluorescence characteristics of dissolved organic matter in the deep waters of the Okhotsk Sea and the northwestern North Pacific Ocean. *Deep Sea Res. Part II Top. Stud. Oceanogr.* 57, 1478–1485.

Yamashita, Y., Jaffé, R., 2008. Characterizing the Interactions between Trace Metals and Dissolved Organic Matter Using Excitation−Emission Matrix and Parallel Factor Analysis. *Environ. Sci. Technol.* 42, 7374–7379.

Yamashita, Y., Jaffé, R., Maie, N., Tanoue, E., 2008. Assessing the dynamics of dissolved organic matter (DOM) in coastal environments by excitation emission matrix fluorescence and parallel factor analysis (EEM-PARAFAC). *Limnol. Oceanogr.* 53,

1900–1908.

Yamashita, Y., Tanoue, E., 2003. Chemical characterization of protein-like fluorophores in DOM in relation to aromatic amino acids. *Mar. Chem.* 82, 255–271.

Yamashita, Y., Tanoue, E., 2004. In situ production of chromophoric dissolved organic matter in coastal environments. *Geophys. Res. Lett.* 31, L14302.

Yan, M., Dryer, D., Korshin, G.V., Benedetti, M.F., 2013. In situ study of binding of copper by fulvic acid: Comparison of differential absorbance data and model predictions. *Water Research* 47, 588-596.

Yan, M., Fu, Q., Li, D., Gao, G., Wang, D., 2013. Study of the pH influence on the optical properties of dissolved organic matter using fluorescence excitation–emission matrix and parallel factor analysis. *J. Lumin.* 142, 103–109.

Yohannes, G., Jussila, M., Hartonen, K., Riekkola, M.-L., 2011. Asymmetrical flow field-flow fractionation technique for separation and characterization of biopolymers and bioparticles. *J. Chromatogr. A* 1218, 4104–4116.

Yohannes, G., Wiedmer, S.K., Jussila, M., Riekkola, M.-L., 2005. Fractionation of Humic Substances by Asymmetrical Flow Field-Flow Fractionation. *Chromatographia* 61, 359–364.

Yoshioka, T., Mostofa, K.M.G., Konohira, E., Tanoue, E., Hayakawa, K., Takahashi, M., Ueda, S., Katsuyama, M., Khodzher, T., Bashenkhaeva, N., Korovyakova, I., Sorokovikova, L., Gorbunova, L., 2007. Distribution and characteristics of molecular size fractions of freshwater-dissolved organic matter in watershed environments: its implication to degradation. *Limnology* 8, 29–44.

You, S.-J., Yin, Y., Allen, H.E., 1999. Partitioning of organic matter in soils: effects of pH and water/soil ratio. *Sci. Total Environ.* 227, 155–160.

Zanardi-Lamardo, E., Clark, C.D., Zika, R.G., 2001. Frit inlet/frit outlet flow field-flow fractionation: methodology for colored dissolved organic material in natural waters. *Anal. Chim. Acta* 443, 171–181.

Zanardi-Lamardo, E., Moore, C.A., Zika, R.G., 2004. Seasonal variation in molecular mass and optical properties of chromophoric dissolved organic material in coastal waters of southwest Florida. *Mar. Chem.* 89, 37–54.

Zepp, R.G., Baughman, G.L., Schlotzhauer, P.F., 1981. Comparison of photochemical behavior of various humic substances in water: II. Photosensitized oxygenations. *Chemosphere* 10, 119–126.

Zhang, Yunlin, van Dijk, M.A., Liu, M., Zhu, G., Qin, B., 2009. The contribution of phytoplankton degradation to chromophoric dissolved organic matter (CDOM) in eutrophic shallow lakes: Field and experimental evidence. *Water Res.* 43, 4685–4697.

Zhang, Yanping, Yang, G., Chen, Y., 2009. Chemical characterization and composition of dissolved organic matter in Jiaozhou Bay. *Chin. J. Oceanol. Limnol.* 27, 851–858.

Zhang, Y., Yin, Y., Liu, X., Shi, Z., Feng, L., Liu, M., Zhu, G., Gong, Z., Qin, B., 2011. Spatial-seasonal dynamics of chromophoric dissolved organic matter in Lake Taihu, a large eutrophic, shallow lake in China. *Org. Geochem.* 42, 510–519.

Zhang, Y., Zhang, E., Yin, Y., Van Dijk, M.A., Feng, L., Shi, Z., Liu, M., Qin, B., 2010. Characteristics and sources of chromophoric dissolved organic matter in lakes of the Yungui Plateau, China, differing in trophic state and altitude. *Limnol. Oceanogr.* 55, 2645–2659.

Zhao, Z.-Y., Gu, J.-D., Fan, X.-J., Li, H.-B., 2006. Molecular size distribution of dissolved organic matter in water of the Pearl River and trihalomethane formation characteristics with chlorine and chlorine dioxide treatments. *J. Hazard. Mater.* 134, 60–66.

Zimm, B.H., 1948a. The Scattering of Light and the Radial Distribution Function of High Polymer Solutions. *J. Chem. Phys.* 16, 1093–1099.

Zimm, B.H., 1948b. Apparatus and Methods for Measurement and Interpretation of the Angular Variation of Light Scattering; Preliminary Results on Polystyrene Solutions. *J. Chem. Phys.* 16, 1099–1116.

Zsolnay, A., 2003. Dissolved organic matter: artefacts, definitions, and functions. *Geoderma* 113, 187–209.

Zsolnay, A., Baigar, E., Jimenez, M., Steinweg, B., Saccomandi, F., 1999. Differentiating with fluorescence spectroscopy the sources of dissolved organic matter in soils subjected to drying. *Chemosphere* 38, 45–50.